

T-4115

**FORWARD MODELING AND INVERSION
OF RESPONSES FOR THE LATEROLOG 7**

by

Jungwhan Kim

ProQuest Number: 10796489

All rights reserved

INFORMATION TO ALL USERS

The quality of this reproduction is dependent upon the quality of the copy submitted.

In the unlikely event that the author did not send a complete manuscript and there are missing pages, these will be noted. Also, if material had to be removed, a note will indicate the deletion.



ProQuest 10796489

Published by ProQuest LLC (2019). Copyright of the Dissertation is held by the Author.

All rights reserved.

This work is protected against unauthorized copying under Title 17, United States Code
Microform Edition © ProQuest LLC.

ProQuest LLC.
789 East Eisenhower Parkway
P.O. Box 1346
Ann Arbor, MI 48106 – 1346

T-4115

A thesis submitted to the Faculty and the Board of Trustees of the Colorado School of Mines in partial fulfillment of the requirements for the degree of Doctor of Philosophy (Geophysical Engineering).

Golden, Colorado

Date Oct. 23, 1991

Signed: Kim Jungwan
Jungwhan Kim

Approved: Guy H. Towle
Dr. Guy H. Towle
Thesis Advisor

Golden, Colorado

Date 24 October 1991

P R Romig
Dr. Phillip R. Romig
Professor and Head,
Geophysics Department

Abstract

The finite difference method is used to solve the forward problems which simulate the Laterolog 7 tool configuration for a two dimensional earth model which has both horizontal and cylindrical boundaries. The apparent resistivity values in the presence of borehole mud, invaded zone and horizontal bed boundaries can be obtained from an earth geometry provided that the model is symmetric about the borehole axis. The quick and accurate calculations of forward modeling are achieved both by using an exponentially expanding grid system and by using a two dimensional average resistivity scheme in a grid block. More efficient forward modeling is also developed for the faster calculation of apparent resistivity. The finite difference solutions are verified against both analytical solutions and physical scale modeling for limiting cases, and good agreements are obtained. This finite difference forward modeling method also can be used alone for the investigation of the effects of earth parameter variations on the apparent resistivities of the Laterolog 7.

The Marquardt inversion scheme is applied to solve the inverse problems which determine the earth parameters such as bed boundaries and true resistivities from the Laterolog 7 log data. The Marquardt inversion scheme is also tested on the

T-4115

hypothetical and field log data of the Laterolog 7 tool. Because a two dimensional inversion scheme of the Laterolog 7 response is considered in this study, it is possible to determine the true resistivity and the bed boundary positions of each layer assuming that there is no invasion. Inversion of hypothetical logs show good agreement with the original hypothetical earth model. Inversion of field log data provides a seemingly realistic earth models.

Table of Contents

Abstract		iii
List of Figures		vii
List of Tables		xi
Acknowledgements		xii
1 INTRODUCTION		1
1.1 Current Focusing Logs		2
1.2 Forward Modeling of the Laterolog 7		3
1.3 Inverse Modeling of the Laterolog 7		5
2 CURRENT FOCUSING PRINCIPLES		7
2.1 Current Focusing in the Guard Electrode		8
2.2 Current Focusing in the Laterolog 7 Electrode		14
3 FORWARD MODELING OF THE LATEROLOG 7 AND GUARD LOG		18
3.1 Potential Equation		19
3.2 General Considerations for FD Algorithm of the Laterolog 7		21
3.3 Development of the Basic FD Equation of the Laterolog 7		24
3.4 Theory of Current Focusing in the Laterolog 7 Tool		28
3.5 Calculations of the Apparent Resistivity of the Laterolog 7		31
3.6 Investigations of Optimal Laterolog 7 Tool Configuration		32
3.7 Computational Accuracy		37
3.8 Faster FD Algorithm of the Laterolog 7		39
3.9 Verifications of Current Focusing		43
3.10 Verifications of the Results		51
3.10.1 Comparisons with the Analytical Solutions		51
3.10.2 Comparisons with the Physical Scale Modeling		53

3.11	Response of Synthetic Laterolog 7 for Various Earth Models	59
3.11.1	The Responses of the Laterolog 7 Tool in a Conductive Bed	61
3.11.2	The Responses of the Laterolog 7 Tool in a Resistive Bed	72
3.11.3	Multiple Invaded Layers	84
3.12	Basis of Forward Modeling of the Guard Log	93
4	INVERSION OF THE LATEROLOG 7	98
4.1	Ridge Regression Estimator	101
4.2	Parameter Resolution and Statistics	105
4.3	Particulars for the Log Inversion	107
4.4	Test Results	108
4.4.1	Two Dimensional Inversion of Hypothetical Log Data	110
4.4.2	Two Dimensional Inversion of Field Log Data	124
5	CONCLUSIONS	129
6	FURTHER STUDIES	132
	References	134
A	Synthetic Laterolog 7 for Conductive Bed	139
B	Synthetic Laterolog 7 for Resistive Bed	155
C	Inversion of Laterolog 7	171

List of Figures

2.1	Approximate measurement of resistivity of a sheet of material using facing disc electrodes applied to two sides of sheet	9
2.2	Better measurement of resistivity using guard-ring principle. This is a simple example of measure-current focusing.	9
2.3	Approximate measurement of resistivity of an annular piece of material between two concentric cylindrical electrode (Cross-sectional view)	12
2.4	Illustration of current focusing in cylindrical geometry	12
2.5	Current flow of the Guard Log	14
2.6	The Laterolog 7 electrode array (Schematic)	16
2.7	Current flow of the Laterolog 7	16
3.1	An axially symmetric logging environment	19
3.2	An exponentially expanding rectangular grid system in cylindrical coordinates	23
3.3	Principle of current focusing	29
3.4	Three layer earth model for testing electrode configuration and apparent resistivity variations	36
3.5	The Laterolog 7 electrode configuration in this study	37
3.6	Principle of faster finite difference algorithm of the Laterolog 7	42
3.7	Homogeneous earth model without borehole	45
3.8	Equipotential lines of homogeneous earth model without borehole . .	45
3.9	Homogeneous earth model with borehole	46
3.10	Equipotential lines of homogeneous earth model with borehole	46
3.11	Three layer earth model when the central current electrode is in the middle of the resistive layer	47
3.12	Equipotential lines of three layer earth model when the central current electrode is in the middle of the resistive layer	47

3.13	Three layer earth model when central current electrode is at the boundary between resistive and conductive beds	48
3.14	Equipotential lines of three layer earth model when central current electrode is at the boundary between resistive and conductive beds	48
3.15	Five layer earth model when the central current source is at depth 1015 feet	49
3.16	Equipotential lines of five layer earth model	49
3.17	Nine layer earth model when the central current source is at depth 1095 feet	50
3.18	Equipotential lines of nine layer earth model	50
3.19	Comparison of finite difference solution with analytical solution for the Laterolog 7 (Thick beds)	54
3.20	Comparison of finite difference solution with analytical solution for the Laterolog 7 (Thin beds)	55
3.21	Comparison of finite difference solution with analytical solution for the Laterolog 7 (Thin-invaded beds, $D_i/d = 4.375$)	56
3.22	Comparison of finite difference solution with analytical solution for the Laterolog 7 (Thin-invaded beds, $D_i/d = 17.5$)	57
3.23	Comparison of finite difference solution with physical scale modeling for the Laterolog 7	60
3.24	Variations in R_m (Thick - Conductive)	63
3.25	Variations in d (Thick - Conductive)	65
3.26	Variations in D_i (Thick - Conductive)	67
3.27	Variations in R_i (Thick - Conductive)	69
3.28	Variations in R_t (Thick - Conductive)	71
3.29	Variations in R_m (Thick - Resistive)	74
3.30	Variations in d (Thick - Resistive)	76
3.31	Variations in D_i (Thick - Resistive)	78
3.32	Variations in R_i (Thick - Resistive)	80
3.33	Variations in R_t (Thick - Resistive)	82
3.34	Five layer earth model	86
3.35	The synthetic Laterolog 7 in five layer earth model	87
3.36	Nine layer earth model	88
3.37	The synthetic Laterolog 7 in nine layer earth model	89
3.38	A synthetic 6FF40 in 27 layer earth model (from Center for Well-Logging, University of Houston)	90
3.39	The synthetic Laterolog 7 in 27 layer earth model	91
3.40	Comparison of apparent resistivity curves from 6FF40 tool and the Laterolog 7 tool in this study for Oklahoma benchmark	92

3.41	Approximation guard electrode by $2n + 1$ electrodes. (In this figure $n = 3$, ratio of diameter to length is exaggerated)	95
3.42	Potential distribution caused by I_i	96
3.43	Total potential distribution caused by I_0, I_1, \dots, I_n	96
4.1	Comparison of hypothetical earth model, initial guess earth model, and best fit earth model (Thick - Conductive Case)	113
4.2	Comparison of hypothetical earth model, initial guess earth model, and best fit earth model (Critically Thick - Conductive Case)	115
4.3	Comparison of hypothetical earth model, initial guess earth model, and best fit earth model (Thin - Conductive Case)	117
4.4	Comparison of hypothetical earth model, initial guess earth model, and best fit earth model (Thick - Resistive Case)	119
4.5	Comparison of hypothetical earth model, initial guess earth model, and best fit earth model (Critically Thick - Resistive Case)	121
4.6	Comparison of hypothetical earth model, initial guess earth model, and best fit earth model (Thin - Resistive Case)	123
4.7	A segment of the Laterolog 7 log to be inverted to a one dimensional model (after George Asquith, 1983)	126
4.8	Comparison of observed data, initial guess earth model, and best fit earth model	127
4.9	Comparison of observed data with best fit log	128
A.1	Variation in R_m (Thick - Conductive)	140
A.2	Variation in R_m (Critically Thick - Conductive)	141
A.3	Variation in R_m (Thin - Conductive)	142
A.4	Variation in d (Thick - Conductive)	143
A.5	Variation in d (Critically Thick - Conductive)	144
A.6	Variation in d (Thin - Conductive)	145
A.7	Variation in D_i (Thick - Conductive)	146
A.8	Variation in D_i (Critically Thick - Conductive)	147
A.9	Variation in D_i (Thin - Conductive)	148
A.10	Variation in R_i (Thick - Conductive)	149
A.11	Variation in R_i (Critically Thick - Conductive)	150
A.12	Variation in R_i (Thin - Conductive)	151
A.13	Variation in R_t (Thick - Conductive)	152
A.14	Variation in R_t (Critically Thick - Conductive)	153
A.15	Variation in R_t (Thin - Conductive)	154
B.1	Variation in R_m (Thick - Resistive)	156

B.2	Variation in R_m (Critically Thick - Resistive)	157
B.3	Variation in R_m (Thin - Resistive)	158
B.4	Variation in d (Thick - Resistive)	159
B.5	Variation in d (Critically Thick - Resistive)	160
B.6	Variation in d (Thin - Resistive)	161
B.7	Variation in D_i (Thick - Resistive)	162
B.8	Variation in D_i (Critically Thick - Resistive)	163
B.9	Variation in D_i (Thin - Resistive)	164
B.10	Variation in R_i (Thick - Resistive)	165
B.11	Variation in R_i (Critically Thick - Resistive)	166
B.12	Variation in R_i (Thin - Resistive)	167
B.13	Variation in R_t (Thick - Resistive)	168
B.14	Variation in R_t (Critically Thick - Resistive)	169
B.15	Variation in R_t (Thin - Resistive)	170
C.1	Comparison of hypothetical earth model, initial guess earth model, and best fit earth model (Thick - Conductive Case)	172
C.2	Comparison of hypothetical log data with best fit log data (Thick - Conductive Case)	173
C.3	Comparison of hypothetical earth model, initial guess earth model, and best fit earth model (Critically Thick - Conductive Case)	174
C.4	Comparison of hypothetical log data with best fit log data (Critically Thick - Conductive Case)	175
C.5	Comparison of hypothetical earth model, initial guess earth model, and best fit earth model (Thin - Conductive Case)	176
C.6	Comparison of hypothetical log data with best fit log data (Thin - Conductive Case)	177
C.7	Comparison of hypothetical earth model, initial guess earth model, and best fit earth model (Thick - Resistive Case)	178
C.8	Comparison of hypothetical log data with best fit log data (Thick - Resistive Case)	179
C.9	Comparison of hypothetical earth model, initial guess earth model, and best fit earth model (Critically Thick - Resistive Case)	180
C.10	Comparison of hypothetical log data with best fit log data (Critically Thick - Resistive Case)	181
C.11	Comparison of hypothetical earth model, initial guess earth model, and best fit earth model (Thin - Resistive Case)	182
C.12	Comparison of hypothetical log data with best fit log data (Thin - Resistive Case)	183

List of Tables

3.1	Apparent resistivity variations with the changes of the lengths A_0M_1 and A_0M_1' in a homogeneous earth model with $d = 8$ inches, $R_t = 100.0$ ohm-m, and $R_m = 0.1$ ohm-m	34
3.2	Apparent resistivity variations with the changes of the lengths A_0M_1 and A_0M_1' in a three layer earth model with $d = 8$ inches, $R_t = 100.0$ ohm-m, $R_s = 3.0$ ohm-m, $R_m = 0.1$ ohm-m, and target bed thickness = 10 feet	35
4.1	The change of depth and resistivity at each iteration in the inversion process (Thick - Conductive Case)	112
4.2	The change of depth and resistivity at each iteration in the inversion process (Critically Thick - Conductive Case)	114
4.3	The change of depth and resistivity at each iteration in the inversion process (Thin - Conductive Case)	116
4.4	The change of depth and resistivity at each iteration in the inversion process (Thick - Resistive Case)	118
4.5	The change of depth and resistivity at each iteration in the inversion process (Critically Thick - Resistive Case)	120
4.6	The change of depth and resistivity at each iteration in the inversion process (Thin - Resistive Case)	122

Acknowledgements

Many individuals have given me their time and support during my studies at *Colorado School of Mines*. First of all, I would like to thank my thesis advisor, *Dr. Guy H. Towle*, who was always open to discussions and suggestions. Without his constant guidance and encouragement, the work presented in this thesis could not have been completed. My deepest gratitude to *Dr. Walter W. Whitman*, Director of the *Center for Well Logging and Petrophysics*, for suggestions and corrections, and - especially - for solving my financial problems. I also want to thank my other committee members for their support: *Dr. Abdelwahid A. Ibrahim*, *Dr. Steven A. Pruess*, and *Prof. Donald I. Dickinson*.

I thank the *Gas Research Institute* for providing funds to the *Center for Well Logging and Petrophysics* of the *Geophysics Department* in the *Colorado School of Mines*. These funds helped support my graduate work.

I also would like to express my deepest gratitude to my mother, *Myungsook Choi*, for giving me the best educational opportunity available and for devoting herself to making me an effective scholar.

I thank my father, *Wooyoung Kim*, and step-mother, *Sungja Kang*; my sister

T-4115

Yongkyung Kim; and my brother *Jinwhan Kim*, - for their concern and support.

My wife, *Seonghey Kim*, has stood by me and assisted me in many ways which enabled me to complete my studies successfully. Moreover, my lovely daughter *Eunjai Kim* has always raised my spirits whenever I felt blue and depressed. My wife and daughter are my inspiration.

My office mates, *Gerardo García B.* and *Zhonglin Wang*, gave me their constant support.

I am grateful to *Dr. Byungkoo Hyun*, the advisor of my undergraduate and graduate study in *Seoul*, and *Dr. Junghee Suh* - both of *Seoul National University, Seoul, Republic of Korea* - for giving me the opportunity to study at *Colorado School of Mines*.

Chapter 1

INTRODUCTION

Quantitative analysis of conventional electric logging implies a determination of the true resistivity of the formations. However, the "apparent resistivity", recorded in a given layer by electric logs which were used prior to the middle 1950's was frequently quite different from the true resistivity of the given layer. This is due to the combined influences of the mud column, adjacent formations both above and below the given layer, and of the invaded zone, in which the original fluid has been mostly replaced by mud filtrate.

When the beds are thick, and, as are frequently the cases in sand and shale formations, and when their resistivities are not much different from mud resistivity, it is generally possible to obtain their true resistivities directly on conventional electric logs, or at least to obtain approximate values which can be corrected without undue difficulty by means of departure curves.

However, when the beds are thin, and particularly when, in addition, their resistivities are substantially greater than mud resistivity, the apparent resistivities

recorded on the conventional logs are seriously affected, and it is generally very difficult to estimate their true resistivities with much accuracy. In the most severe cases, such as are encountered in the holes drilled through hard formations with muds of high salinity, the conventional logs are so distorted and rounded that they do not even show clearly the boundaries of the different beds.

1.1 Current Focusing Logs

In order to overcome these combined influences, two types of current focusing methods were introduced in 1951: Guard Log and Laterolog 7. The Guard Log electrode system (Owen and Greer, 1951) measures the resistivities of formations by employing a thin disk of current which is caused to flow perpendicularly to the borehole. The control of this current disk is obtained through the use of relatively long equipotential electrodes above and below the measuring electrode (Figure 2.5). The Laterolog 7 electrode system (Doll, 1951) is an electrical method which makes use of a sheet of current of constant intensity and known thickness, focused by means of an automatic control device using three point electrodes (two are potential electrodes and one is a current electrode) above the central current electrode and another three point electrodes (two are potential electrodes and one is a current electrode) below the central current electrode (Figure 2.6).

With the current focusing electrode arrangements, the effect of the mud col-

umn will be shown to be small, and the effect of the adjacent formations is practically eliminated in all beds whose thickness is greater than that of the focused sheet of current. The investigation and development of the Laterolog 7 tool have been continued by Moran and Chemali (1979) and others.

1.2 Forward Modeling of the Laterolog 7

Forward modeling is the simulation of a log response from given earth parameters. Forward modeling of the Laterolog 7 tool can be accomplished for different earth models. A one dimensional finite element algorithm was developed by Chemali, Gianzero, and Strickland (1983). For this model, it is assumed that there is neither borehole nor invaded zone. Each layer is also assumed to be homogeneous and to have isotropic resistivity. A few numerical solutions for a two dimensional model were developed and investigated by Chemali et al. (1983), Shattuck, Bittar, and Shen (1987), and Bittar, Shattuck, and Shen (1990) using the finite element method. A two dimensional model consists of an arbitrary number of horizontal and cylindrical layers. This is the most commonly used model to represent the practical well logging environment. This model allows analyses of the effects caused by the two dimensional variations in earth parameters, which are the variations in the bed thickness, the formation resistivity, and hole diameter, and the variations in the extent and the nature of the invasion. Moreover, a three dimensional modeling using the finite element

method was developed by Chemali, Gianzero, and Su (1988). A three dimensional finite element method is useful in cases where the earth layers are asymmetrical about the borehole axis and that the earth layers are dipping. The numerical evaluation of an integral equation solution and an integral transform solution were also developed by Gianzero and Anderson (1982).

In this study, a finite difference algorithm with exponentially expanding grid spacings is developed to simulate the Laterolog 7 electrode arrangements in a two dimensional model. A large, sparse, linear system generated by the finite difference approximation is solved by the Jacobian conjugate gradient method in the ITPACK 2C software package (Kincaid, Grimes, and John, 1982). Feasibility and efficiency of this approach for the Laterolog 7 electrode arrangements are demonstrated by comparing the test results with those obtained by the analytical method of Gianzero and Anderson (1982), and with those obtained by a physical scale modeling method by Bittar et al. (1990) for limiting cases. Then, the forward modeling program is applied to the general earth models. A set of synthetic resistivity logs for the Laterolog 7 tool is illustrated in Appendix A and Appendix B, where the conductive and resistive beds which have different bed thicknesses with the variations in the earth parameters (mud resistivity, borehole diameter, depth of invaded zone, resistivity of the invaded zone, and true resistivity), respectively, are considered.

1.3 Inverse Modeling of the Laterolog 7

Forward modeling is the simulation of a log response from given earth parameters. On the other hand, inverse modeling is the determination of earth parameters from the log data. The significant earth parameters to be determined from the Laterolog 7 log responses are the thickness (or depth) and the true resistivity of the target bed. These parameters as well as the invasion diameter, the resistivity of the invaded zone, and mud resistivity play a great role in formation evaluations. At the present time, an inversion scheme of the Laterolog 7 tool has not been published. It is considered to be very expensive and time consuming to invert the coefficient matrix.

In this investigation, a Marquardt inversion scheme is used for the direct interpretation of the Laterolog 7 log responses. This scheme minimizes the root-mean-squares error between observed data and calculated data from the best fit earth model. Since a solution of the inverse problem is generally non-unique, it is important that meaningful earth parameters can be obtained by restricting the complexity of the earth model or reducing the size of the problem.

In order to obtain the resistivities of the invaded zone and depths of invasion as well as the true resistivities and depths of bed boundaries, at least two more focused logs are required in this study. One is the shallow-focused tool, and the other is the intermediate-focused tool, for the Laterolog 7 is the deep-focused tool. In reality, Dual Laterolog-MicroSFL tool is commonly used in the field. Because a two dimensional

inversion scheme of the Laterolog 7 response is considered in this study, it is possible to determine the true resistivity and the bed boundary of each layer assuming that there is no invasion. Two dimensional hypothetical and field log data are tested in Appendix C.

The principles of current focusing for the Guard Log and the Laterolog 7 will be considered in Chapter 2. Forward modeling of the Laterolog 7 tool will be considered in Chapter 3. The basis of forward modeling of the Guard Log will also be considered in Chapter 3. Inversion of the Laterolog 7 log will be considered in Chapter 4.

Chapter 2

CURRENT FOCUSING PRINCIPLES

There are several types of current focusing tools: Guard Log (Laterolog 3 or LL3), Laterolog 7 (LL7), Laterolog 8 (LL8), and Dual Laterolog (DLL), and so on. In this study, the Laterolog 7 tool as well as the Guard Log will be investigated. However, the major emphasis will be on the Laterolog 7. It is better to consider both the Laterolog 7 tool and the Guard Log tool simultaneously in order to understand how to focus the central measuring current. In 1951, Owen and Greer (1951) published the paper for the Guard Log tool, and Doll (1951) also published the paper for the Laterolog 7 tool. The difference between the above two tools is that in the Guard Log tool two relatively long metallic electrodes are used to focus the central measuring current, while in the Laterolog 7 tool two point current electrodes which are located above and below the central current electrode are used to focus the central measuring current.

2.1 Current Focusing in the Guard Electrode

Suppose an experimental setup, as shown in Figure 2.1 (Moran and Chemali, 1979), intended to measure the resistivity of a sheet of material of thickness L . Disc electrodes A and B , both of area S , are placed in contact with opposite sides of the sheet. A voltage V applied to the disc electrodes causes a current I to flow through the sheet between them. If $S \gg L^2$, Ohm's law can be approximated in the form

$$V \approx \frac{IRL}{S}, \quad (2.1)$$

or

$$R \approx \frac{SV}{LI} = K \frac{V}{I}. \quad (2.2)$$

To obtain an approximate value of the resistivity R , the measured values of V and I are inserted into equation 2.2. The constant K , which is called the "cell constant", relates the value of ratio V/I to the desired resistivity. Defined here as S/L , K has the dimension of length.

Equation 2.1 and equation 2.2, as applied to Figure 2.1, are approximate, because with such an arrangement the current density will not be uniform at all locations in the sheet between the disc electrodes, and there will be outward fringing of the current lines in the sheet material near and beyond the edges of the disc

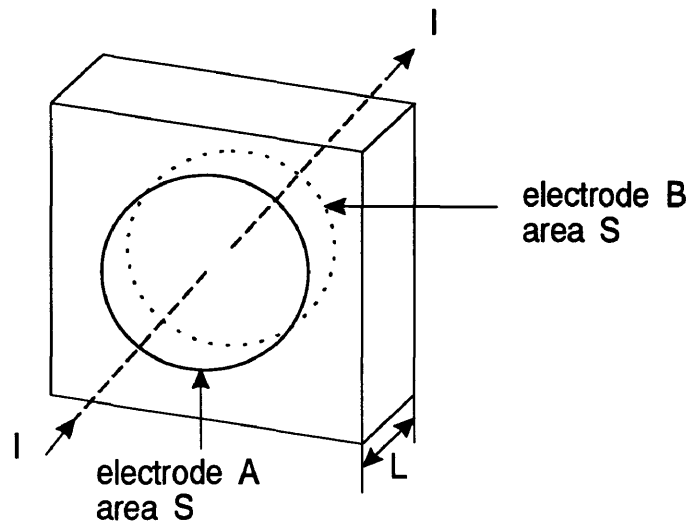


Figure 2.1: Approximate measurement of resistivity of a sheet of material using facing disc electrodes applied to two sides of sheet

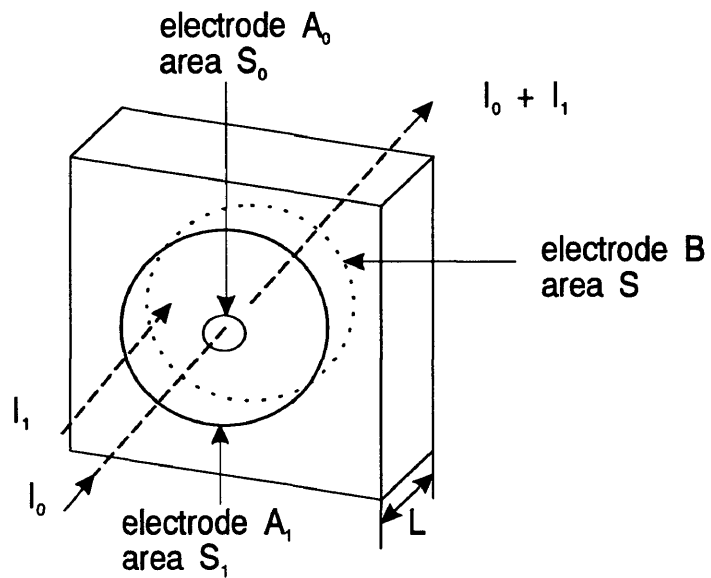


Figure 2.2: Better measurement of resistivity using guard-ring principle. This is a simple example of measure-current focusing.

electrodes.

The accuracy of the measurement can be improved by splitting the area S of one of the electrodes into a small central disc electrode of area S_0 and a surrounding annular guard electrode of area S_1 (Figure 2.2). Both electrodes A_0 and A_1 are kept at the same potential V , but only the current I_0 from the central A_0 electrode is considered in computing the resistivity. Then to a much closer approximation

$$R \approx \frac{S_0 V}{L I_0} = K_0 \frac{V}{I_0}. \quad (2.3)$$

This use of an annular guard electrode to “focus” the current lines from the central electrode is similar to the technique used with a parallel-plate guard-ring capacitor with a dielectric between the plates. The presence of the guard ring serves to make the electric field lines between the guarded small central disc electrode and the opposite plate more nearly parallel to their common axis. Thus, the electric field lines from the guarded plate conform better to the ideal geometry assumed by equation 2.1. This results in a more accurate determination of the resistivities.

The geometries of Figure 2.1 and Figure 2.2 have been used first for utmost simplicity. Figure 2.3 shows a geometry corresponding better to that of a real Guard Log. Sketched in cross section is a cylindrical electrode A of diameter d_A and of vertical length D . At a diameter d_B and coaxial with electrode A a second cylindrical electrode B extends over the same depth interval. Filling the space between

cylindrical electrodes A and B and extending beyond the ends of the electrodes is an annulus-shaped homogeneous conductive material whose resistivity is to be measured. Taking into account the cylindrical geometry, an approximate expression for the voltage drop produced between the electrodes by the radial flow of a current I between electrodes A and B can be written as

$$V \approx \frac{IR}{2\pi D} \ln\left(\frac{d_B}{d_A}\right), \quad (2.4)$$

As before, the approximation value of formation resistivity R determined from measured values of V and I would be

$$R \approx \frac{2\pi D}{\ln\left(\frac{d_B}{d_A}\right)} \frac{V}{I} = K \frac{V}{I}, \quad (2.5)$$

where $K = 2\pi D / \ln(d_B/d_A)$.

The effect of current fringing at the upper and lower ends of the electrodes on the measurement can again be diminished by using a current-focusing procedure. The inner electrode is split into a small cylindrical electrode A_0 at the middle, and two focusing electrodes A_1 and A_2 above and below A_0 (Figure 2.4). Electrode A_0 is of length D_0 and emits current I_0 . The upper electrode A_1 emits current I_1 and the lower electrode A_2 emits current I_2 . In making the resistivity measurement, all these electrodes are maintained at the same potential V by adjustment of the currents I_1 and I_2 . Then the densities of the currents being emitted from differently located areas

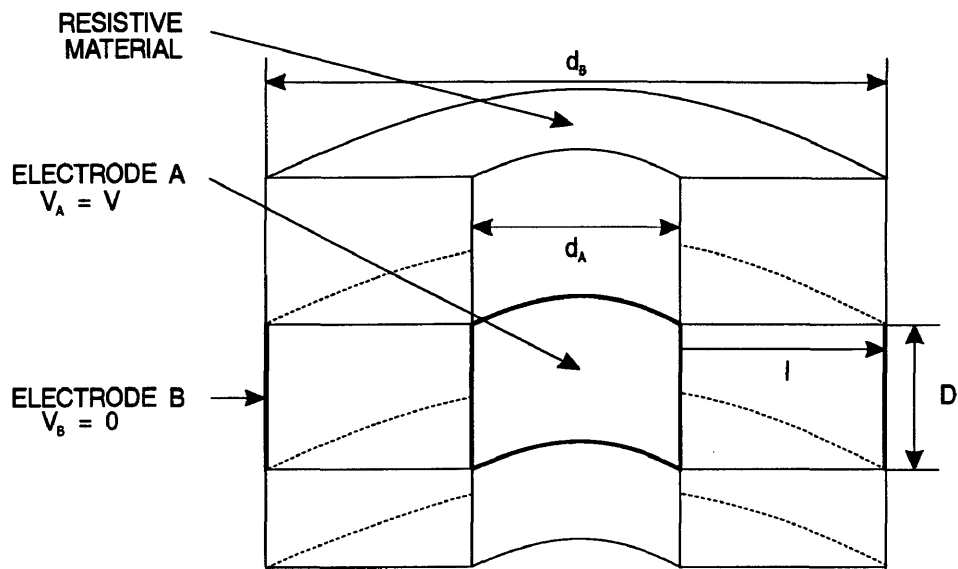


Figure 2.3: Approximate measurement of resistivity of an annular piece of material between two concentric cylindrical electrode (Cross-sectional view)

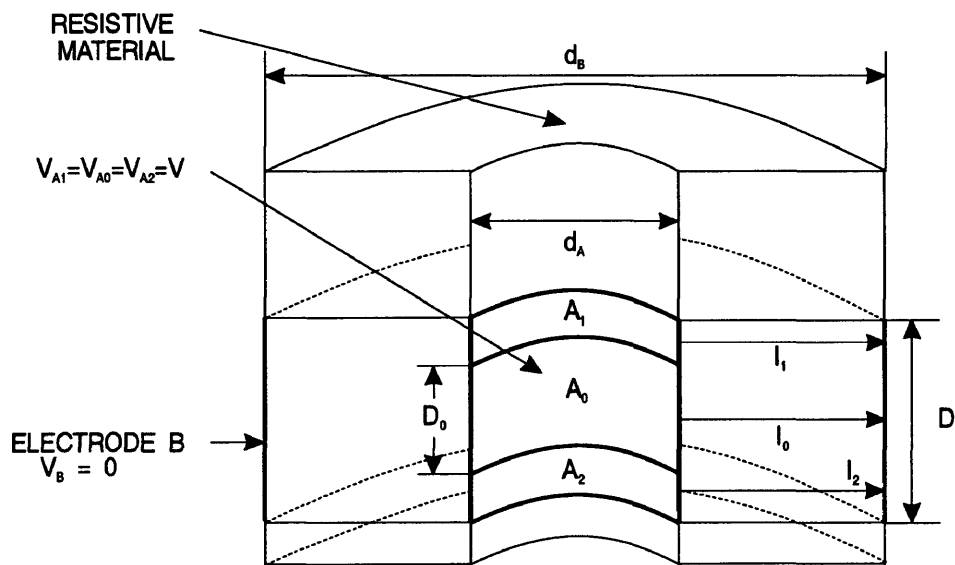


Figure 2.4: Illustration of current focusing in cylindrical geometry

of the inner electrodes in Figure 2.4 are substantially the same as those emitted from each corresponding area on the inner electrode in Figure 2.3. However, in making the resistivity measurement only the measure current I_0 , from the electrode A_0 is considered. Thus, to a closer approximation,

$$R \approx \frac{2\pi D_0}{\ln\left(\frac{d_B}{d_A}\right)} \frac{V}{I_0} = K_0 \frac{V}{I_0}, \quad (2.6)$$

where $K_0 = 2\pi D_0 / \ln(d_B/d_A)$.

The Guard tool uses currents from bucking current electrodes to focus the central measuring current into a horizontal sheet penetrating into the formation (Figure 2.5). Symmetrically placed on either of the central A_0 electrode are two very long (about 5 feet) electrodes, A_1 and A_2 , which are shorted to each other. A current, I_0 , flows from the A_0 electrode, whose potential is fixed. From A_1 and A_2 flows a bucking current, which is automatically adjusted by a short circuit to maintain A_1 and A_2 at the potential of A_0 . All electrodes of the sonde are thus held at the same constant potential. The magnitude of the I_0 current is then proportional to formation conductivity, or inversely proportional to formation resistivity (Serra, 1984).

The I_0 current sheet is constrained to the disk-shaped area. The thickness, O_1O_2 , of the current sheet of the Guard Log tool is known to be 12 inches, much thinner than for the Laterolog 7 tool. As a result, the Guard Log tool typically has a better vertical resolution and shows more details than does the Laterolog 7 tool.

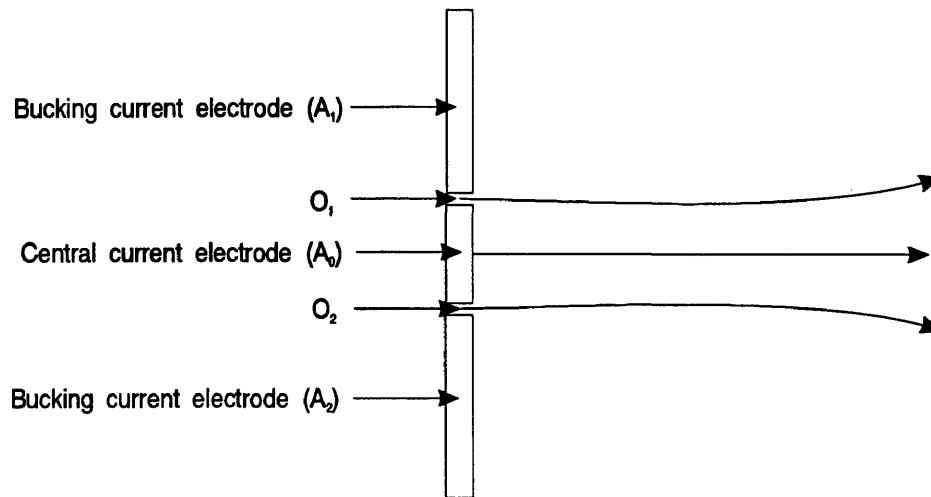


Figure 2.5: Current flow of the Guard Log

Furthermore, the influences of the borehole and of the invaded zone were slightly less.

2.2 Current Focusing in the Laterolog 7 Electrode

Basically, the Laterolog 7 and Guard Log electrode arrangements are designed to produce a situation where the central measuring current I_0 is confined between two horizontal and parallel surfaces out to a certain distance from the sonde. In so doing, they yield a better measurement than a small, or even a moderately large, mono-electrode or normal device, without sacrificing thin-bed resolution.

In the familiar Laterolog 7 (Figure 2.6), a seven-electrode device is used to focus the central measuring current by using the bucking-amplifier-balance system.

The Laterolog 7 device is comprised of a center electrode, A_0 , and three pairs of electrodes: two near-potential electrodes M_1 and M_2 ; two far-potential electrodes $M_{1'}$ and $M_{2'}$; and two current electrodes A_1 and A_2 (Figure 2.6). The electrodes of each pair of potential electrodes are symmetrically located with respect to A_0 and are electrically connected to each other by short-circuiting wires.

A constant current, I_0 , is emitted from A_0 . Through bucking electrodes, A_1 and A_2 , adjustable currents are emitted; the bucking current intensity is adjusted automatically by a dynamic feedback circuit so that the two pairs of monitoring electrodes, M_1 and M_2 and $M_{1'}$ and $M_{2'}$, are brought to the same potential. The potential is measured between one of the monitoring electrodes and an electrode at the surface (i.e., at infinity for practical purpose). With a constant I_0 current, this potential varies directly with formation resistivity (Serra, 1984).

Since the potential difference between the $M_1 - M_2$ pair and the $M_{1'} - M_{2'}$ pair is maintained at zero, no current from A_0 is flowing in the hole between M_1 and $M_{1'}$ or between M_2 and $M_{2'}$. Therefore, the current from A_0 must penetrate horizontally into the formations.

Figure 2.7 shows the distribution of current lines when the sonde is in a homogeneous isotropic medium; the sheet of I_0 current retains a fairly constant thickness up to a distance (about 3 feet from the borehole axis when A_0M_1 is equal to 12 inches). Experiments have shown that the sheet of I_0 current retains substantially

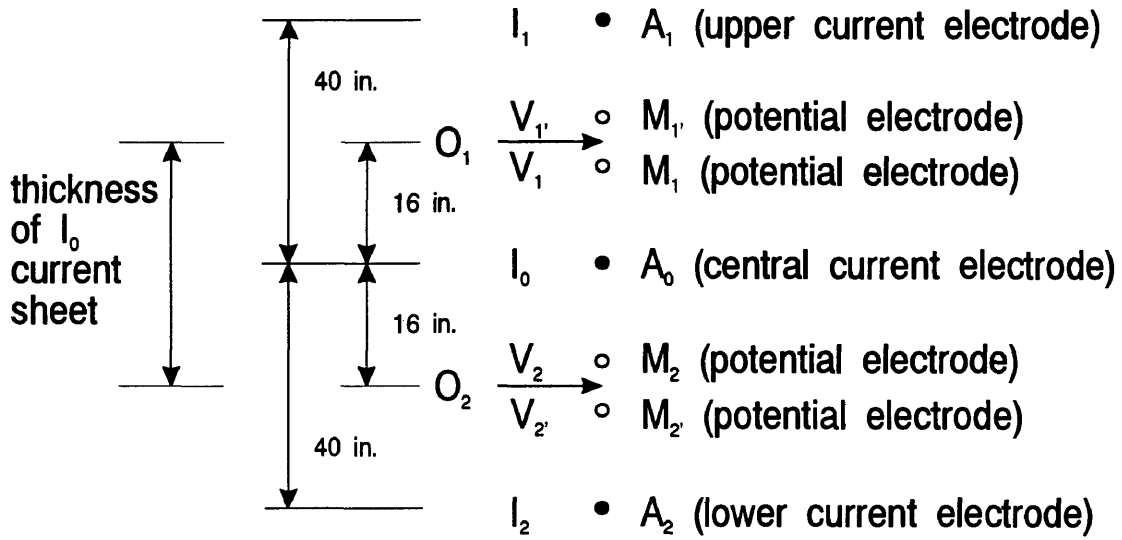


Figure 2.6: The Laterolog 7 electrode array (Schematic)

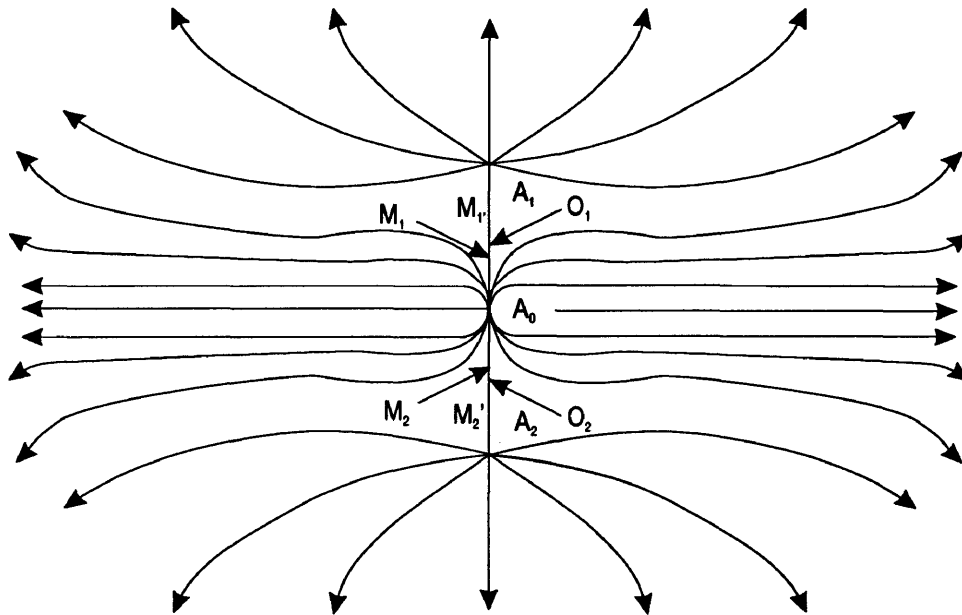


Figure 2.7: Current flow of the Laterolog 7

the same shape opposite thin (80 inches, that is, total length of the Laterolog 7 tool) resistive beds (Schlumberger, 1987).

In this study, the following Laterolog 7 tool is considered; the thickness of the I_0 current sheet is approximately 32 inches (distance O_1O_2 on Figure 2.6), and the length A_1A_2 of the sonde is 80 inches.

Chapter 3

FORWARD MODELING OF THE LATEROLOG 7 AND GUARD LOG

The forward model consists of the responses of the Laterolog 7 electrode configurations to an assumed earth model, which may have both vertical and lateral variations. As shown in Figure 3.1, for simplicity, the earth model allows only discrete resistivity changes in each direction (Kim, 1986) rather than allowing the possibility of gradual changes (Wang, 1991).

The responses of the Laterolog 7 tool to an earth model that has horizontal and radial boundaries are modeled with a finite difference method. Figure 3.1 shows a two dimensional logging environment that has axial symmetry about the borehole axis and has horizontal layers, borehole, invaded zones, and uninvaded zones. Invaded zones may have different resistivities and diameters.

Cylindrical symmetry is assumed and a cylindrical coordinate system is used. Three current electrodes of the Laterolog 7 tool are centered in the borehole and the potentials are measured along the borehole axis.

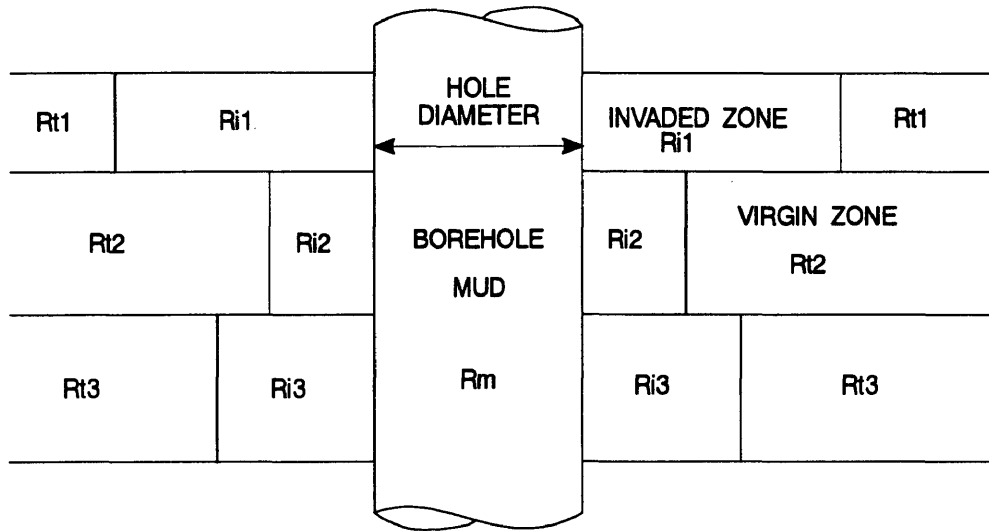


Figure 3.1: An axially symmetric logging environment

3.1 Potential Equation

The flow of steady state electric current in the medium is governed by the potential equation

$$\nabla \cdot \left(\frac{1}{\rho} \nabla U \right) + q = 0, \quad (3.1)$$

where ρ is the resistivity of the medium, U the potential, and q the intensity of the current source. In a cylindrical coordinate system, assuming axial symmetry about the borehole axis, equation 3.1 is expressed as

$$\frac{\partial}{\partial r} \left(\frac{1}{\rho} \frac{\partial U}{\partial r} \right) + \frac{\partial}{\partial z} \left(\frac{1}{\rho} \frac{\partial U}{\partial z} \right) + \frac{1}{r\rho} \frac{\partial U}{\partial r} + q = 0, \quad (3.2)$$

where $\rho = \rho(r, z)$ and $U = U(r, z)$. In the above equation, r and z represent the radial coordinate and the vertical coordinate, respectively. Equation 3.2 defines the electric potential due to a system of current sources in an extended medium.

Equation 3.2 has the following boundary conditions (Kim, 1986).

$$\left\{ \begin{array}{l} \frac{\partial U}{\partial r} \Big|_{r=0} = 0 \\ \lim_{r \rightarrow \infty} U = 0 \\ \lim_{z \rightarrow \pm\infty} U = 0, \end{array} \right. \quad (3.3)$$

or more generally, boundary conditions for the equation 3.2 are,

$$\left\{ \begin{array}{l} \frac{\partial U}{\partial r} \Big|_{r=0} = 0 \\ \lim_{r \rightarrow \infty} \left(pU + q \frac{\partial U}{\partial r} \right) = 0 \\ \lim_{z \rightarrow \pm\infty} \left(pU + q \frac{\partial U}{\partial r} \right) = 0. \end{array} \right. \quad (3.4)$$

where p and q are constant coefficients.

In general, the analytical solution of equation 3.2 is not easy to obtain with the above boundary conditions when the earth model is complex. A finite difference solution of the equation 3.2, however, can be found with the same boundary conditions even though the earth model is complex.

3.2 General Considerations for FD Algorithm of the Laterolog 7

The general considerations in the development of the finite difference algorithm from the above partial differential equation system (equation 3.2 and equation 3.3) are as follows (Towle, Whitman, and Kim, 1988):

1. the specific grid system,
2. the effective resistances across bed boundaries not coincident with the grid (vertically and horizontally),
3. the boundary conditions and how they drive the algorithm,
4. the compensation for a finite grid system,
5. an efficient numerical algorithm for inverting a large sparse matrix, and
6. the additional grid lines inserted at the Laterolog 7 current and potential electrode positions to reduce the interpolation effect.

The choice of the grid system is the main factor that affects the finite difference result. An appropriate rate of grid expansion can be determined by the competing factors of accuracy and computational efficiency. The accuracy is poor if the grid size expands too rapidly. On the other hand, excessive computer time is required if the grid size expands too slowly. The expansion rate should be determined by taking into account the size and the complexity of the earth model. In the case where

the earth model is intricate, a small expansion rate should be used. The expansion rates in the radial direction and the axial direction may be different from each other according to the earth model. Also the smallest grid spacings in both directions should be determined by taking into account the dimensional details of the earth model, especially near the current and potential electrodes.

For efficiency, the grid spacings increase exponentially as distance from the central current electrode (A_0) increases. Figure 3.2 represents the radial and vertical sections of the medium near the central current electrode (A_0). Only a finite portion of the medium is considered and is divided into a number of rectangular grids. Since the model is symmetrical about the borehole axis (z -axis), only one-half of the vertical section, $r \geq 0$, will be discretized. In this study, the distances between the central current electrode (A_0) and each grid boundary are 50 feet radially and vertically (upward and downward).

It is necessary that the grids be finely spaced near the A_0 , A_1 , and A_2 electrodes, especially the central current electrode A_0 , as this is usually the region of most rapid fluctuations in potential (Dakhnov, 1962). By contrast, at points far from the A_0 , A_1 , and A_2 electrodes, especially the central current electrode A_0 , where fluctuations in potential are typically relatively slow, the grid may be much coarser than the grid near the central current electrode area. As shown in Figure 3.2, near the central current electrode (A_0), vertical and horizontal grid spacings are the smallest

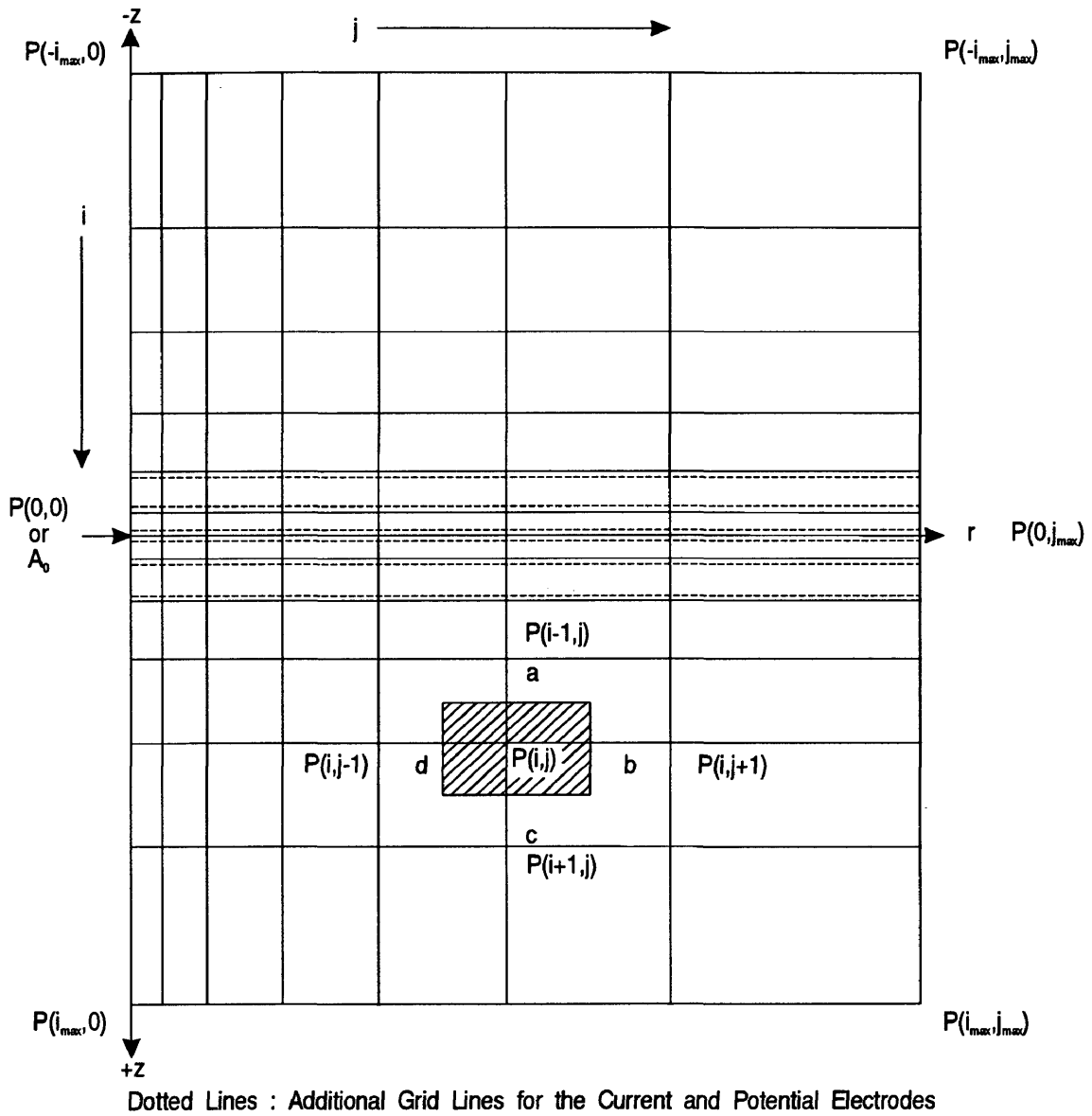


Figure 3.2: An exponentially expanding rectangular grid system in cylindrical coordinates

in both directions in this study. However, near the other six electrodes (two current electrodes which are above and below the central current electrode, and four potential electrodes), the vertical and horizontal grid spacings are larger. In order to compensate for the fluctuations in potential, six additional grid lines at those six electrodes are considered (see dotted lines in Figure 3.2). Using those six additional grid lines, the loss of accuracy in the numerical approximation can be minimized. In general, the grid system is designed to fit the shape of the potential, which varies rapidly near the borehole and becomes smaller with slower variations far from the borehole axis and from the source. It is convenient and systematic to increase the grid spacings exponentially as distance from the central current electrode (A_0) increases.

3.3 Development of the Basic FD Equation of the Laterolog 7

The following is a development of the basic finite difference equation used for the Laterolog 7 tool in this study (Kim, 1986).

The node corresponding to the i th row and the j th column in the grid of Figure 3.2 is denoted by $P(i, j)$ and its immediate four neighbors are denoted by $P(i - 1, j)$, $P(i, j + 1)$, $P(i + 1, j)$, and $P(i, j - 1)$ in the clockwise direction. The distances of $P(i, j)$ from the nodes $P(i - 1, j)$, $P(i, j + 1)$, $P(i + 1, j)$, and $P(i, j - 1)$ are defined to be a , b , c and d , respectively. In this grid system, the upper and lower sides of the vertical boundaries correspond to $i = -i_{max}$ and $i = i_{max}$, respectively.

The inner side of radial boundary, that is, borehole axis ($r = 0$), corresponds to $j = 0$, while the outer side of radial boundary corresponds to $j = j_{max}$. In this study, the distance between $i = -i_{max}$ and $i = i_{max}$ is about 100 feet, and the distance between $j = 0$ and $j = j_{max}$ is about 50 feet. The position of the central current electrode is denoted by $P(0,0)$.

The location of $P(i,j)$ in an exponentially expanding grid system can be expressed by

$$r(i,j) = \frac{\Delta r(1)(\alpha^{j-1} - 1)}{\alpha - 1}, \quad (3.5)$$

and

$$z(i,j) = \pm \frac{\Delta z(1)(\beta^{|i_0-i|} - 1)}{\beta - 1}, \quad (3.6)$$

where α and β denote the expanding ratio for the radial and axial directions, respectively, and j is from 0 to j_{max} , and i is from $-i_{max}$ to i_{max} . $\Delta r(1)$ represents the smallest radial spacing corresponding to the distance of $P(i,1)$ from the axis of symmetry, and $\Delta z(1)$ represents the smallest vertical spacing corresponding to the distance of $P(-1,j)$, or $P(1,j)$ from $P(0,j)$. The element associated with $P(i,j)$ represents the rectangular area bounded by $z(i - a/2, j)$, $r(i, j + b/2)$, $z(i + c/2, j)$, and $r(i, j - d/2)$, in the vertical cross section (hatched area in Figure 3.2).

By using the grid system and the notation as described in Figure 3.2, the finite

difference equivalent of equation 3.2 can be obtained as

$$\begin{aligned} & \frac{2}{b+d} \left[\frac{U(i,j+1) - U(i,j)}{\rho(i,j+b/2)b} - \frac{U(i,j) - U(i,j-1)}{\rho(i,j-d/2)d} \right] + \\ & \frac{2}{a+c} \left[\frac{U(i+1,j) - U(i,j)}{\rho(i+c/2,j)c} - \frac{U(i,j) - U(i-1,j)}{\rho(i-a/2,j)a} \right] + \\ & \frac{U(i,j+1) - U(i,j-1)}{r(i,j)\rho(i,j)(b+d)} + q_{ij} = 0, \end{aligned} \quad (3.7)$$

where $\rho(i-a/2,j)$, $\rho(i,j+b/2)$, $\rho(i+c/2,j)$, and $\rho(i,j-d/2)$ denote the average resistivities between the point $P(i,j)$ and its four corresponding neighbors $P(i-1,j)$, $P(i,j+1)$, $P(i+1,j)$, and $P(i,j-1)$, respectively.

Further details incorporated in the finite difference modeling scheme to provide for the more complex models are as follows (Towle et al., 1988):

1. Equation 3.7 represents only a slice of earth and must be rotated through 360 degrees about the borehole axis to represent the current flow in a rotationally symmetric earth.
2. For the radial component of current flow, if there are lateral (axial) variations within a given grid element, these are modeled with series resistances. Similarly, vertical (layered) variations are modeled with parallel resistances. In general, a combination of series and parallel resistances may be needed intra-grid, depending on the complexity of the model. A similar rationale applies to the vertical

component of current flow.

3. At the borehole axis, due to the boundary condition as expressed in equation 3.3, the governing potential equation 3.2 has no third term, and the finite difference equation 3.7 has no corresponding term.
4. Since by necessity we use a finite grid, the external model at i_{\max} and/or j_{\max} must be designed with care so that the potential is fictitiously allowed to approach a constant at "great distance" from the central current electrode (A_0). Realistic inhomogeneous models would indicate that the potential would not be uniform on the boundary. In this study, the Neumann boundary condition (Smith, 1985; Burden and Faires, 1989) is used for the outer boundaries. The characteristic of the Neumann boundary condition is that the slopes of potential in both radial and axial directions are very close to zero.
5. Finally, the system of linear finite difference equations represented in equation 3.7 is reorganized in the form of $Ax = b$, where A is a coefficient matrix of conductivities, x a vector of potentials, and b a vector of current. This system is solved using the Jacobian conjugate gradient method in the ITPACK 2C software package (Kincaid et al., 1982).

3.4 Theory of Current Focusing in the Laterolog 7 Tool

In this study, the synthetic focusing approach method (Shattuck et al., 1987; Bittar et al., 1990) was used. As shown in Figure 3.3, we can calculate the potentials at M_1 , $M_{1'}$, M_2 , and $M_{2'}$ caused by current I_0 which comes from central current electrode A_0 (case zero). For convenience, those potentials are called V_{10} , $V_{1'0}$, V_{20} , and $V_{2'0}$, respectively. The first subscript of the potential representations refers to the potential electrode position, and the second subscript to the source current electrode position. We can also calculate the potentials at four potential electrodes, M_1 , $M_{1'}$, M_2 , and $M_{2'}$, caused by current I_1 and I_2 which comes from upper current electrode A_1 (case one) and lower current electrode A_2 (case two), respectively. The potentials caused by I_1 are called V_{11} , $V_{1'1}$, V_{21} , and $V_{2'1}$, respectively, and the potentials caused by I_2 are called V_{12} , $V_{1'2}$, V_{22} , and $V_{2'2}$, respectively.

Assume that the intensities of I_1 and I_2 are equal to that of I_0 . To make the current I_0 flow laterally, it is required to make the potential difference between V_1 and $V_{1'}$ zero, and also make the potential difference between V_2 and $V_{2'}$, where V_1 , $V_{1'}$, V_2 , and $V_{2'}$ represent the total potential of at M_1 , $M_{1'}$, M_2 , and $M_{2'}$, respectively. Because V_{10} , V_{11} , and V_{12} are directly proportional to the intensities of I_0 , I_1 , and I_2 , respectively, the total potential V_1 at M_1 electrode can be expressed in terms of V_{10} , V_{11} , V_{12} , and two unknown coefficients α and β (principle of superposition). Here the reason why α and β are used is to determine the intensities of I_1 and I_2 in terms of I_0 .

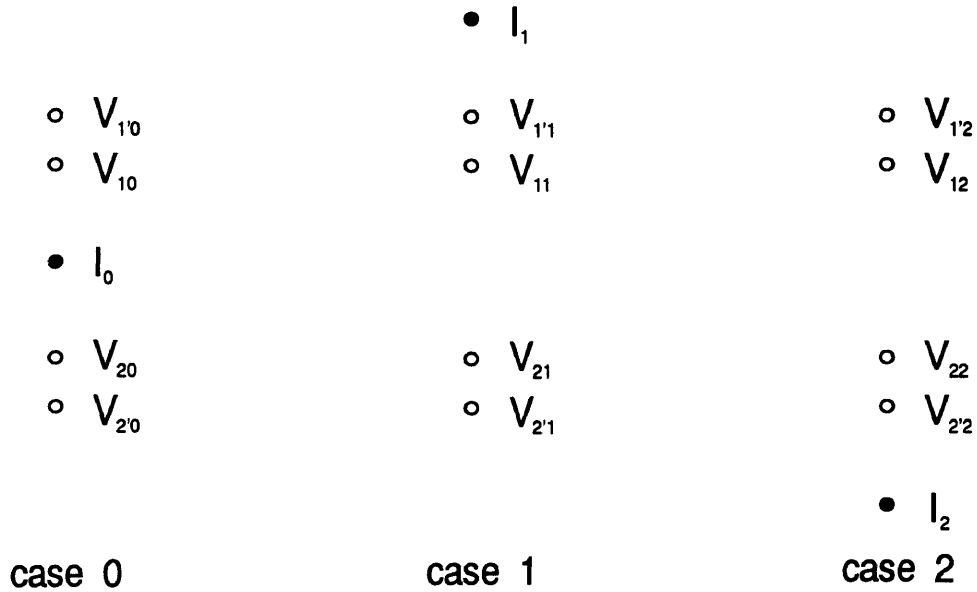


Figure 3.3: Principle of current focusing

This α will be multiplied by I_0 in order to determine the intensity of I_1 . Similarly, β will be multiplied by I_0 in order to determine the intensity of I_2 . These α and β are called the focusing coefficients. Total potential V_1 at M_1 electrode can be expressed as

$$V_1 = V_{10} + \alpha V_{11} + \beta V_{12} \quad (3.8)$$

Similarly, total potentials $V_{1'}$, V_2 , and $V_{2'}$ at $M_{1'}$, M_2 , and $M_{2'}$ electrodes, respectively, can also be expressed as

$$V_{1'} = V_{1'0} + \alpha V_{1'1} + \beta V_{1'2} \quad (3.9)$$

$$V_2 = V_{20} + \alpha V_{21} + \beta V_{22} \quad (3.10)$$

$$V_{2'} = V_{2'0} + \alpha V_{2'1} + \beta V_{2'2} \quad (3.11)$$

In the above four equations, there are four equations with twelve knowns and six unknowns (V_1 , $V_{1'}$, V_2 , $V_{2'}$, α , and β). The potential difference between V_1 and $V_{1'}$, and another potential difference between V_2 and $V_{2'}$ should be zero to make the current I_0 flow laterally. It is achieved to make the equation 3.8 and equation 3.9 same, and to make the equation 3.10 and equation 3.11 simultaneously.

$$V_{10} + \alpha V_{11} + \beta V_{12} = V_{20} + \alpha V_{21} + \beta V_{22} \quad (3.12)$$

$$V_{1'0} + \alpha V_{1'1} + \beta V_{1'2} = V_{2'0} + \alpha V_{2'1} + \beta V_{2'2} \quad (3.13)$$

Then, there are only two equations with two unknowns α and β . Using equation 3.12 and equation 3.13, two focusing coefficients α and β can be calculated. Once α and β are calculated, the intensities of I_1 at the upper current electrode and I_2 at the lower current electrode will be determined by the product of α and intensity of I_0 and by the product of β and intensity of I_0 , respectively. With I_0 and these newly determined current intensities I_1 and I_2 , the current I_0 from the central current electrode will

flow laterally (Shattuck et al., 1987; Bittar et al., 1990).

3.5 Calculations of the Apparent Resistivity of the Laterolog 7

In Figure 2.6, assume a homogeneous earth model. The potentials V_1 and $V_{1'}$ at M_1 and $M_{1'}$, respectively, will be

$$V_1 = \frac{\rho I_1}{4\pi A_1 M_1} + \frac{\rho I_0}{4\pi A_0 M_1} + \frac{\rho I_2}{4\pi A_2 M_1}, \quad (3.14)$$

$$V_{1'} = \frac{\rho I_1}{4\pi A_1 M_{1'}} + \frac{\rho I_0}{4\pi A_0 M_{1'}} + \frac{\rho I_2}{4\pi A_2 M_{1'}}. \quad (3.15)$$

Because the potentials V_1 and $V_{1'}$ are equal,

$$V_1 = V_{1'}, \quad (3.16)$$

$$\frac{\rho I_1}{4\pi A_1 M_1} + \frac{\rho I_0}{4\pi A_0 M_1} + \frac{\rho I_2}{4\pi A_2 M_1} = \frac{\rho I_1}{4\pi A_1 M_{1'}} + \frac{\rho I_0}{4\pi A_0 M_{1'}} + \frac{\rho I_2}{4\pi A_2 M_{1'}}. \quad (3.17)$$

Using $I_1 = I_2$, because the homogeneous earth model is assumed, equation 3.17 can be expressed in the following form,

$$I_1 = CI_0, \quad (3.18)$$

If equation 3.18 is inserted into equation 3.15,

$$V_{1'} = \frac{\rho I_0}{4\pi} \left(\frac{C}{A_1 M_{1'}} + \frac{1}{A_0 M_{1'}} + \frac{C}{A_2 M_{1'}} \right) = \rho I_0 G, \quad (3.19)$$

where G is defined as

$$G = \left(\frac{C}{A_1 M_{1'}} + \frac{1}{A_0 M_{1'}} + \frac{C}{A_2 M_{1'}} \right) \frac{1}{4\pi}, \quad (3.20)$$

Finally, the apparent resistivity ρ is obtained

$$\rho = \frac{V_{1'}}{I_0} \frac{1}{G}, \quad (3.21)$$

where $1/G$ is called the “geometric factor”.

3.6 Investigations of Optimal Laterolog 7 Tool Configuration

In this section, optimal Laterolog 7 electrode configuration will be investigated. Although several publications offer a description of the Laterolog 7 electrode configuration, what is not published are the tool spacings $A_0 M_1$ and $A_0 M_{1'}$ (and equivalently, $A_0 M_2$ and $A_0 M_{2'}$). The lack of a set of commonly known exact electrode configuration hinders quantitative comparisons between different simulation techniques. Without

knowing the exact electrode configuration of the Laterolog 7 tool, it is difficult to assess the accuracy of various computer codes which have been developed to simulate the Laterolog 7 devices for the purpose of log interpretations.

As shown in Figure 2.6, it is generally known that the thickness (O_1O_2) of the I_0 current sheet is approximately 32 inches, and the total tool length A_1A_2 is 80 inches. But the tool spacings A_0M_1 and A_0M_1' (and equivalently, A_0M_2 and A_0M_2') have not been published. Therefore, the lengths of A_0M_1 and A_0M_1' , with the condition that the length of O_1O_2 is 32 inches and the length of A_1A_2 is 80 inches can be changed in order to determine the best electrode configuration. Table 3.6 shows the apparent resistivity variations with the changes of the lengths A_0M_1 and A_0M_1' , in the homogeneous earth model. In this homogeneous earth model, borehole diameter is 8 inches, true resistivity is 100.0 ohm-m, and mud resistivity is 0.1 ohm-m.

Table 3.6 shows the apparent resistivity variations with the changes of the lengths A_0M_1 and A_0M_1' , in the three layer earth model. In this three layer earth model, as shown in Figure 3.4, borehole diameter is 8 inches, true resistivity is 100.0 ohm-m, shoulder layer resistivities are 3.0 ohm-m, and mud resistivity is 0.1 ohm-m. The central current electrode is located at the middle of the target bed (central layer).

From Table 3.6, when A_0M_1 is 0.900 feet, and A_0M_1' is 1.767 feet, apparent resistivity 101.533 ohm-m was obtained when true resistivity was 100.0 ohm-m. From Table 3.6, if A_0M_1 is 1.300 feet, and A_0M_1' is 1.367 feet, the apparent resistivity

Table 3.1: Apparent resistivity variations with the changes of the lengths A_0M_1 and A_0M_1' , in a homogeneous earth model with $d = 8$ inches, $R_t = 100.0$ ohm-m, and $R_m = 0.1$ ohm-m

A_1A_2 (feet)	O_1O_2 (feet)	A_0M_1 (feet)	A_0M_1' (feet)	R_{app} (ohm-m)
6.667	2.667	0.050	2.617	11.410
"	"	0.100	2.567	21.078
"	"	0.200	2.467	36.678
"	"	0.300	2.367	49.501
"	"	0.400	2.267	61.766
"	"	0.500	2.167	72.362
"	"	0.600	2.067	81.143
"	"	0.700	1.967	88.094
"	"	0.800	1.867	97.327
"	"	0.900	1.767	101.533
"	"	1.000	1.667	105.799
"	"	1.100	1.567	110.086
"	"	1.200	1.467	109.951
"	"	1.300	1.367	102.978
"	"	1.333	1.334	no-convergence

Table 3.2: Apparent resistivity variations with the changes of the lengths A_0M_1 and A_0M_1' in a three layer earth model with $d = 8$ inches, $R_t = 100.0$ ohm-m, $R_s = 3.0$ ohm-m, $R_m = 0.1$ ohm-m, and target bed thickness = 10 feet

A_1A_2 (feet)	O_1O_2 (feet)	A_0M_1 (feet)	A_0M_1' (feet)	R_{app} (ohm-m)
6.667	2.667	0.050	2.617	8.259
"	"	0.100	2.567	15.080
"	"	0.200	2.467	26.365
"	"	0.300	2.367	35.896
"	"	0.400	2.267	44.737
"	"	0.500	2.167	52.592
"	"	0.600	2.067	59.277
"	"	0.700	1.967	64.890
"	"	0.800	1.867	69.813
"	"	0.900	1.767	73.750
"	"	1.000	1.667	76.900
"	"	1.100	1.567	79.029
"	"	1.200	1.467	80.751
"	"	1.300	1.367	84.639
"	"	1.333	1.334	no-convergence

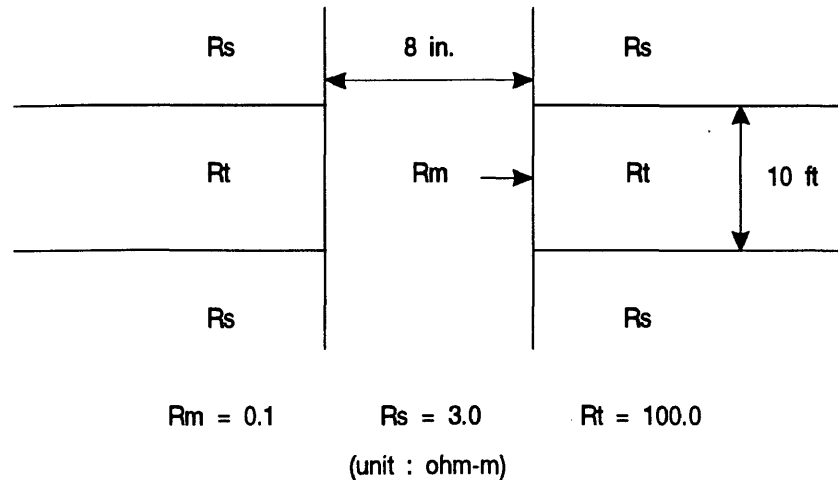


Figure 3.4: Three layer earth model for testing electrode configuration and apparent resistivity variations

was 84.639 ohm-m, while the true resistivity was 100.0 ohm-m. Those apparent resistivities are the closest values to the true resistivities in each case, respectively. From the above results, it is concluded that M_1 (and equivalently, M_2) electrode is in the range of 0.900 foot to 1.300 feet from the central current electrode A_0 , and M_1' (and equivalently, M_2') electrode is in the range of 1.367 feet to 1.767 feet from the central current electrode A_0 . Several other earth models which were tested in order to determine the optimal positions of the four potential electrodes of the Laterolog 7 tool of this study also show the same results. Through such trial-and-error attempts, the Laterolog 7 electrode configuration of this study was determined as follows: A_0M_1 (and equivalently, A_0M_2) is 1.000 feet (12 inches), and A_0M_1'

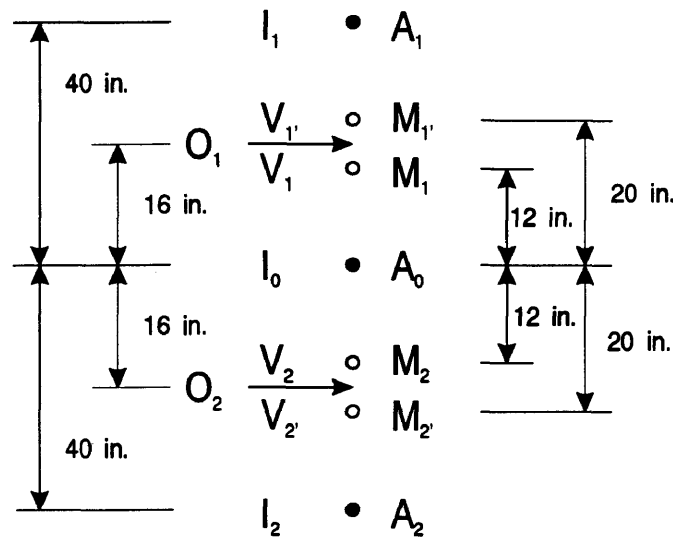


Figure 3.5: The Laterolog 7 electrode configuration in this study

(and equivalently, $A_0M_{2'}$) is 1.667 feet (20 inches). Figure 3.5 shows the Laterolog 7 electrode configuration in this study.

3.7 Computational Accuracy

The choice of the grid system is the main factor which affects the finite difference results. The rate of expansion can be determined by the competing factors of accuracy and computational efficiency. The accuracy will deteriorate if the grid size expands too rapidly. On the other hand, excessive computer time will be required if the grid size expands too slowly.

In this study, the expanding ratio in the range of 1.15-1.40 turned out to

provide a sufficiently fine grid spacing near the central current electrode. The ratio should be determined by considering the size and the complexity of the earth model. In the case where the earth model is small and complex, a small expanding ratio should be used. The expanding ratios of the radial direction (α) and the axial direction (β) may be different from each other according to the earth model.

Also, the smallest grid spacings, $\Delta r(1)$ and $\Delta z(1)$, which are in the radial and axial directions, respectively, should be determined by considering the earth model, especially the location of the borehole wall and the thickness of the earth model layers. $\Delta r(1)$ is smaller than the radius of the borehole automatically by using the additional vertical grid line at the middle of the borehole axis and borehole wall. $\Delta z(1)$ is determined by the relation between the predetermined $\Delta z(1)$ and the thickness of bed which includes $P(0,0)$. (The predetermined $\Delta z(1)$ is fixed as 0.25 feet in this study.) If the predetermined $\Delta z(1)$ is less than the distance between $P(0,0)$ and bed boundary, the predetermined $\Delta z(1)$ will be used as $\Delta z(1)$. If the predetermined $\Delta z(1)$ is greater than the distance between $P(0,0)$ and bed boundary, the distance between $P(0,0)$ and bed boundary will be used as $\Delta z(1)$. Potential near $P(0,0)$ shows rapid change, while potential far away from $P(0,0)$ shows slow change. Therefore, these small values of $\Delta r(1)$ and $\Delta z(1)$ provide even and uniform distribution of current near the central current electrode A_0 , yielding more accurate determinations of the potential in this vicinity.

To minimize the interpolation effect, additional grid lines are considered. There are six additional horizontal grid lines for four potential electrodes (M_1 , M_1' , M_2 , and M_2') and two current electrodes (A_1 and A_2). Four additional horizontal grid lines are always placed at corresponding potential electrodes, and the remaining two additional horizontal grid lines are also placed at the upper and lower current electrodes, respectively. These additional grid lines are very effective in decreasing the interpolation effect.

To minimize the interpolation effect from the discrete grid for the Laterolog 7 electrode arrangement, $i_{max} = 15$, and $j_{max} = 15$ are used for "Production" purposes. For "Quality" purposes, $i_{max} = 25$ and $j_{max} = 25$ are used. "Production" runs several times as fast as "Quality" , but is mildly less accurate. These sizes of grid system provided sufficient accuracy for the Laterolog 7 electrode configuration, and it took about 2.5-3.0 and 6.5-7.5 seconds of CPU time per sampling point on the RISC 6000 computer when "Production" and "Quality" were chosen, respectively. The size of the grid system depends on the required detail and the actual size of the simulation earth model.

3.8 Faster FD Algorithm of the Laterolog 7

In the above indicated CPU times, most of the computing time is spent when a large sparse matrix is inverted. In the forward modeling of the Laterolog 7 tool in this

study, the large sparse matrix inversion is performed three times per sampling point in order to focus the current from the central current electrode. If it is possible to use the large sparse matrix inversion only one time per sampling point, the speed of the forward modeling program will be three times faster than it is. This idea is applied to make the forward modeling program of the Laterolog 7 tool faster in this study. In Figure 3.3, we need the first matrix inversion at A_0 in case 0 to obtain V_{10} , $V_{1'0}$, V_{20} , and $V_{2'0}$, the second matrix inversion at A_1 in case 1 to obtain V_{11} , $V_{1'1}$, V_{21} , and $V_{2'1}$, and the last matrix inversion at A_2 in case 2 to obtain V_{12} , $V_{1'2}$, V_{22} , and $V_{2'2}$. In the notation, the first subscript of the potential representations refers to the potential electrode position, and the second subscript to the source current electrode position. Through these three matrix inversions, three groups of potential distributions from three current sources will be calculated, respectively, and then they will be combined properly in order to focus the current from A_0 and calculate the apparent resistivity. After the calculation of the apparent resistivity at a certain sampling point, three current source positions will be moved simultaneously for the calculations of the next sampling point. These procedures will be continued from the beginning of sampling points to the end of sampling points. This is the conventional numerical approach for the Laterolog 7 tool. (The line 2 in Figure 3.6 is the prototype for the conventional approach.)

The procedure which uses a large sparse matrix inversion only one time per

sampling point is illustrated in Figure 3.6. Suppose that the four potentials V_{10} , $V_{1'0}$, V_{20} , and $V_{2'0}$ are calculated from the central current electrode at a certain point (point A_0 in line 2). In order to obtain the focusing effect, two more current electrodes can be considered, one is point A_1 in line 2 and the other is point A_2 in line 2. Here, assume that there are line 1 and line 3 as shown in Figure 3.4. The distance between line 1 (or line 3) and line 2 is half of the tool length (40 inches in this study). Instead of calculating the potentials V_{11} , $V_{1'1}$, V_{21} , and $V_{2'1}$ caused by I_1 in line 2, it is possible to use four equivalent potentials caused by I_0 in line 1 as shown in Figure 3.6. Similarly, instead of calculating the potentials V_{12} , $V_{1'2}$, V_{22} , and $V_{2'2}$ caused by I_2 in line 2, it is also possible to use four equivalent potentials caused by I_0 in line 3 as shown in Figure 3.6. (Of course, in both cases, the potential electrode positions are quite different from the original Laterolog 7 tool arrangement.) If those potentials are combined properly, the total potential at each potential electrode in line 2 will be obtained under the condition that the current is focused. Apparent resistivity will be calculated using these four total potentials (V_1 , $V_{1'}$, V_2 , and $V_{2'}$) in line 2. This new approach is exactly the same as the conventional numerical approach except the number of matrix inversion per sampling point. This procedure is applied to the Laterolog 7 forward modeling program in this study.

The new program takes about one third of computing time when compared with computing time of the conventional program in this study. Here, the reason why

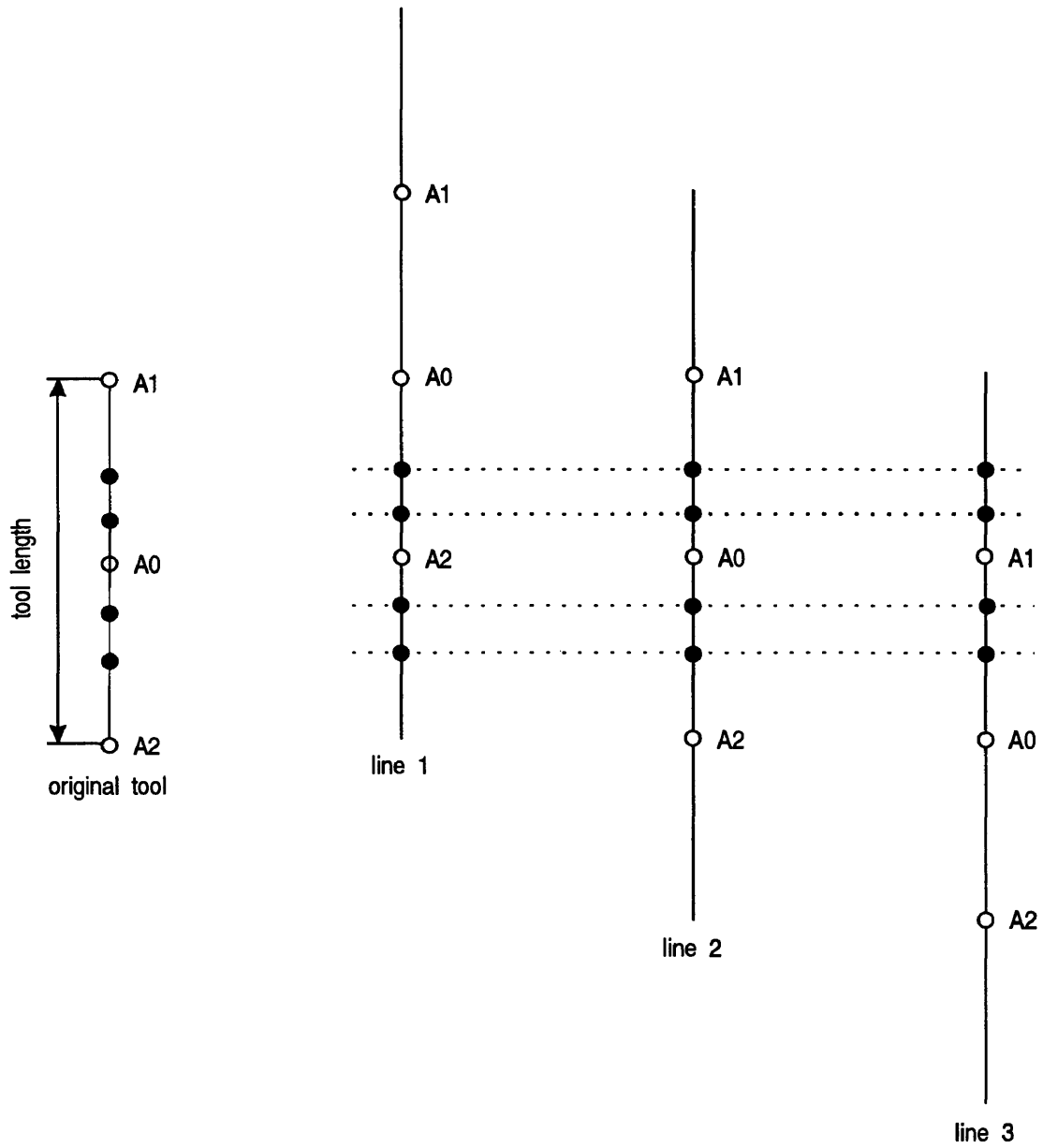


Figure 3.6: Principle of faster finite difference algorithm of the Laterolog 7

it takes “about one third” instead of “exactly one third” is that for the beginning and final parts of sampling points, several imaginary additional sampling points in line 1 and 3 are needed to focus the current from the central current electrode.

3.9 Verifications of Current Focusing

In order to verify the current focusing in the finite difference forward modeling approach for the Laterolog 7 tool, equipotential lines are considered. The equipotential line is always perpendicular to the current flow. Therefore, by drawing the equipotential lines around the three current sources in many cases, the flow of current I_0 of the Laterolog 7 tool can be inferred in this study. To draw the equipotential lines, forward modeling program is changed to give the potential distribution inside the grid system used. Radial position, vertical position, and potential value are required to draw the equipotential lines.

Figure 3.7 through Figure 3.18 show the earth models and their equipotential lines. In these figures, the borehole diameter is set to 8 inches, and the dotted line represents the location of the bed boundary. Figure 3.7 shows the homogeneous earth model without borehole. Using this earth model, equipotential lines are obtained in Figure 3.8. As indicated in Figure 3.8, the current from the central current electrode A_0 flows laterally. Figure 3.9 shows the homogeneous earth model with borehole. Using this earth model, equipotential lines are displayed in Figure 3.10. As indicated

in Figure 3.10, the current from the central current electrode A_0 also flows laterally. Figure 3.11 shows a three layer earth model with borehole. In this earth model, the central current electrode A_0 is located at the center of the target bed. Using this earth model, equipotential lines are displayed in Figure 3.12. The equipotential lines in the right and left hand sides of the dotted lines show the different shapes. As indicated in Figure 3.12, the current from the central current electrode A_0 also flows laterally and is symmetrical about the central current electrode A_0 . Figure 3.13 shows a three layer earth model with borehole. In this earth model, the central current electrode A_0 is located at the upper boundary of the target bed. Using this earth model, equipotential lines are displayed in Figure 3.14. The equipotential lines in the right and left hand sides of the dotted lines show the different shapes. Figure 3.14 indicates a lateral flow of current which is from the central current electrode at depth 995 feet. Figure 3.15 shows a five layer earth model with borehole. In this earth model, the central current electrode A_0 is located at depth 1015 feet. Using this earth model, equipotential lines are obtained in Figure 3.16. Figure 3.16 indicates a lateral flow of current I_0 . Figure 3.17 shows a nine layer earth model with borehole. In this earth model, the central current electrode A_0 is located at depth 1095 feet. Using this earth model, equipotential lines are displayed in Figure 3.18. Figure 3.18 also indicates a lateral flow of current I_0 . In all cases, the current from the central current electrode flows laterally.

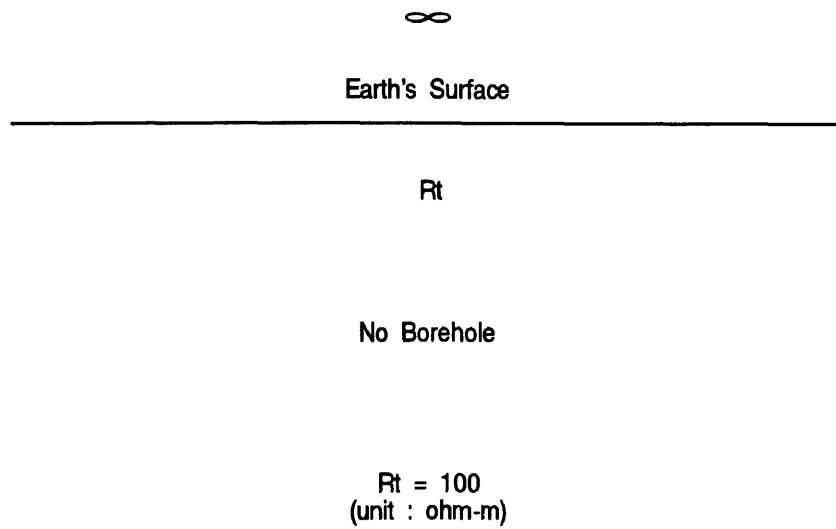


Figure 3.7: Homogeneous earth model without borehole

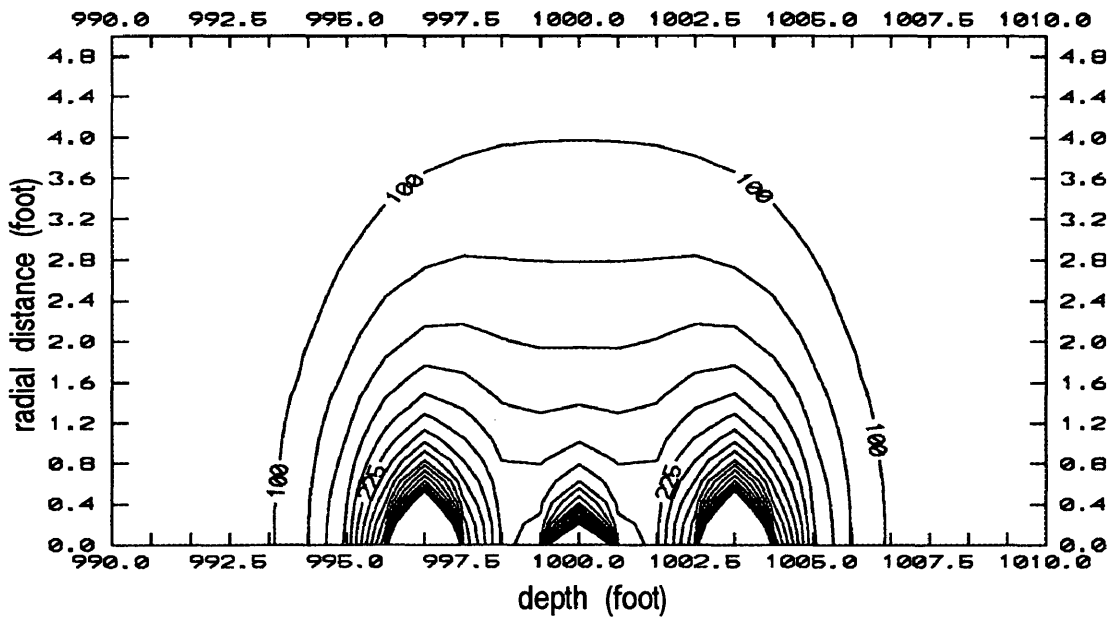


Figure 3.8: Equipotential lines of homogeneous earth model without borehole

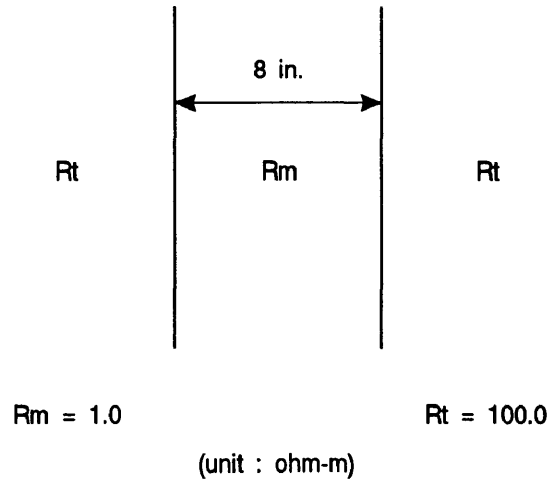


Figure 3.9: Homogeneous earth model with borehole

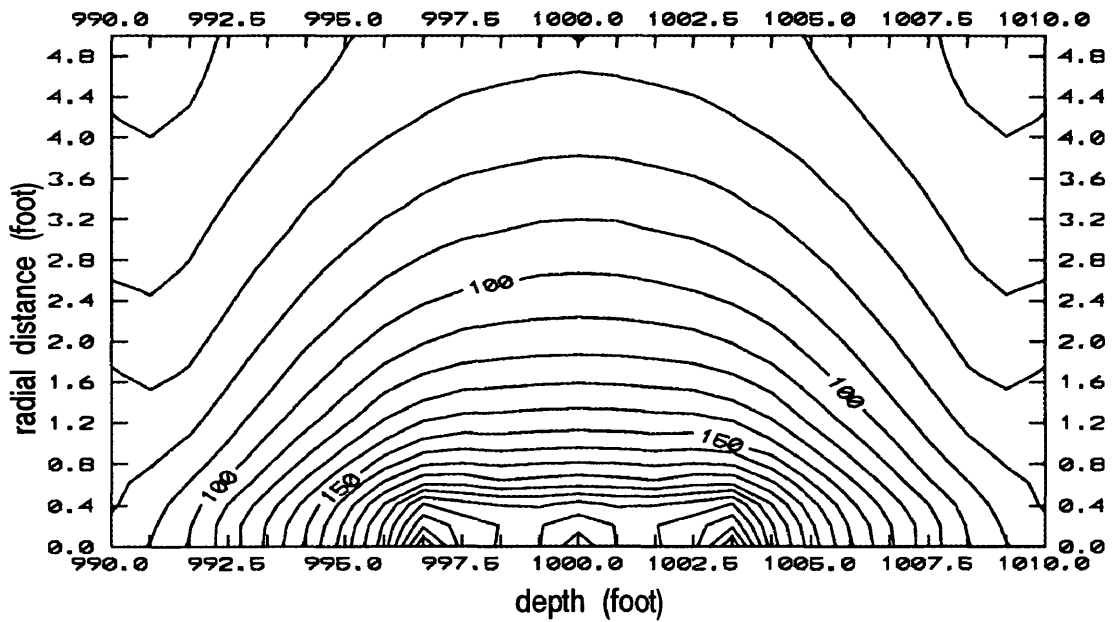


Figure 3.10: Equipotential lines of homogeneous earth model with borehole

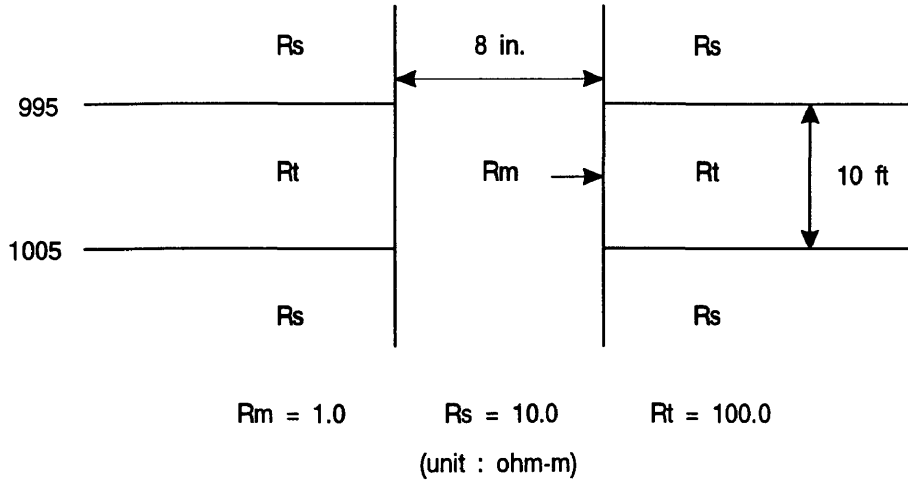


Figure 3.11: Three layer earth model when the central current electrode is in the middle of the resistive layer

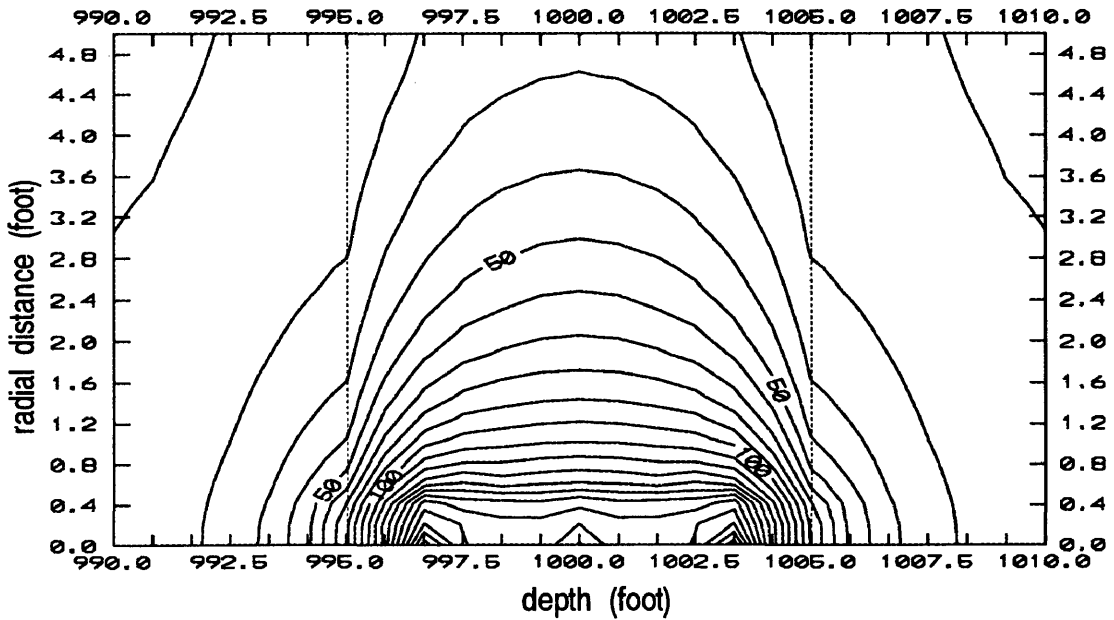


Figure 3.12: Equipotential lines of three layer earth model when the central current electrode is in the middle of the resistive layer

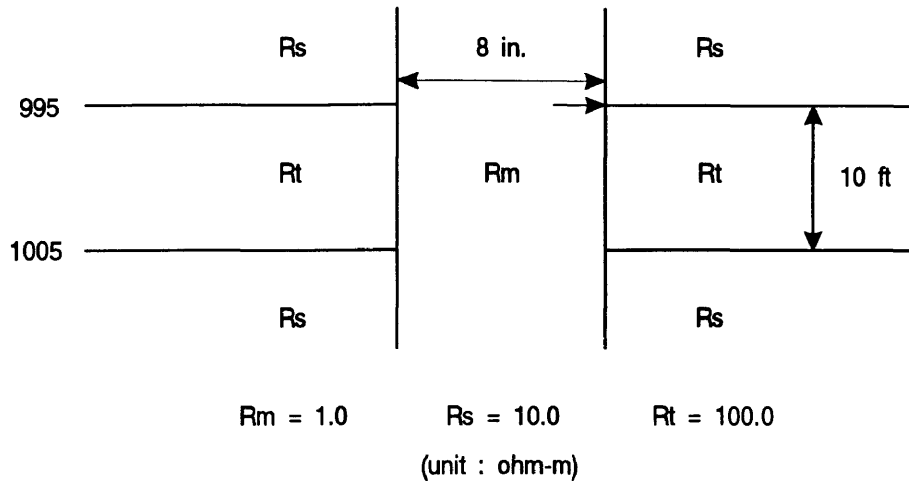


Figure 3.13: Three layer earth model when central current electrode is at the boundary between resistive and conductive beds

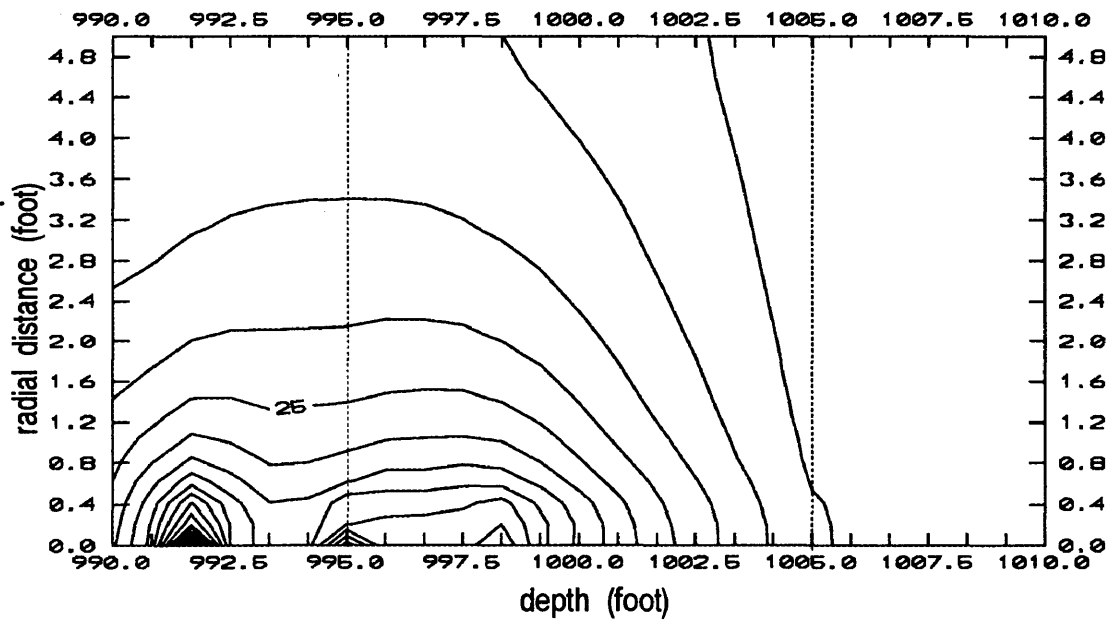


Figure 3.14: Equipotential lines of three layer earth model when central current electrode is at the boundary between resistive and conductive beds

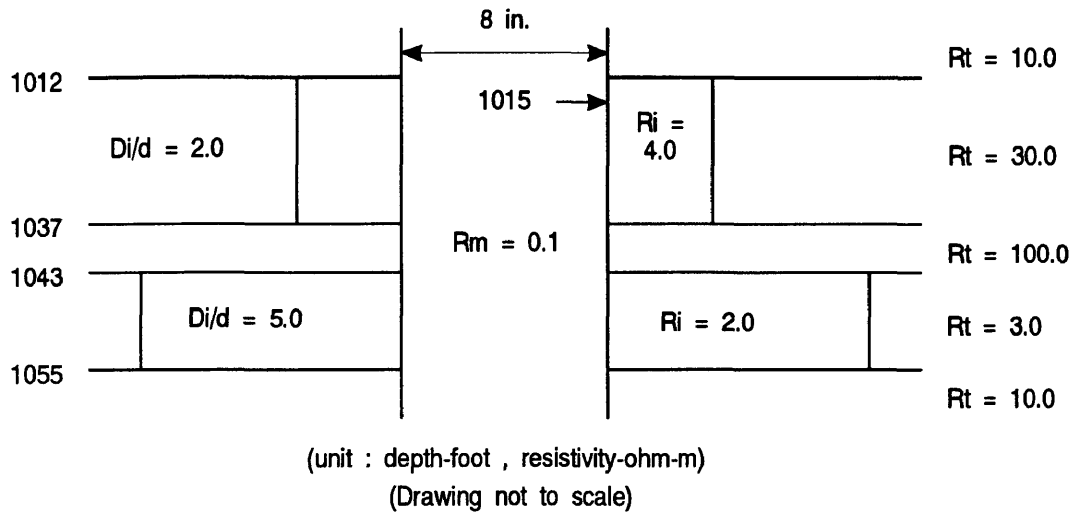


Figure 3.15: Five layer earth model when the central current source is at depth 1015 feet

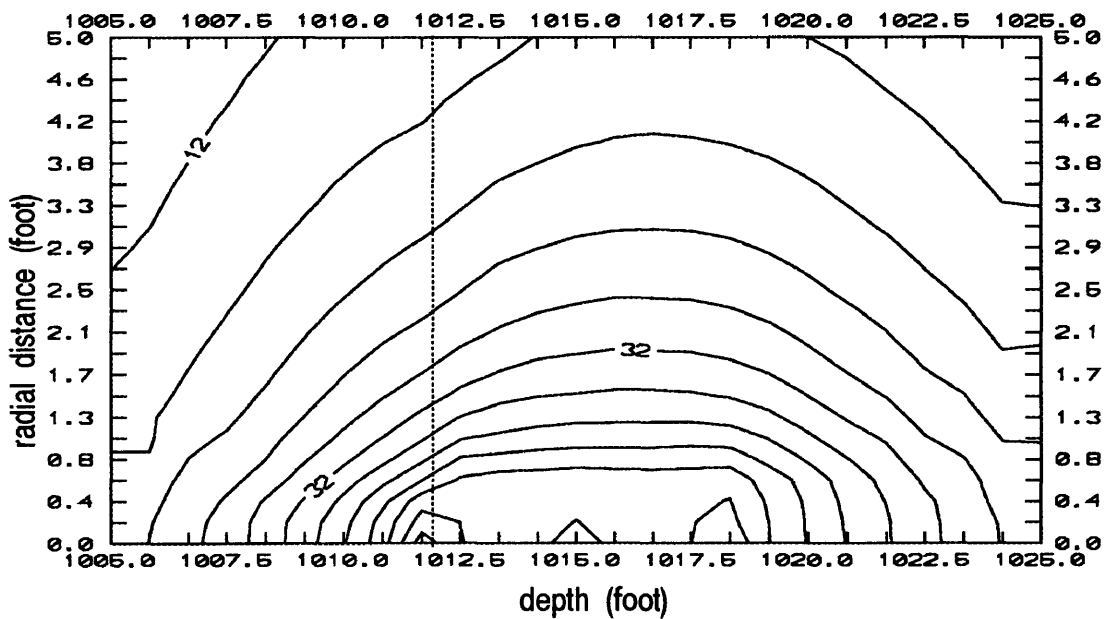


Figure 3.16: Equipotential lines of five layer earth model

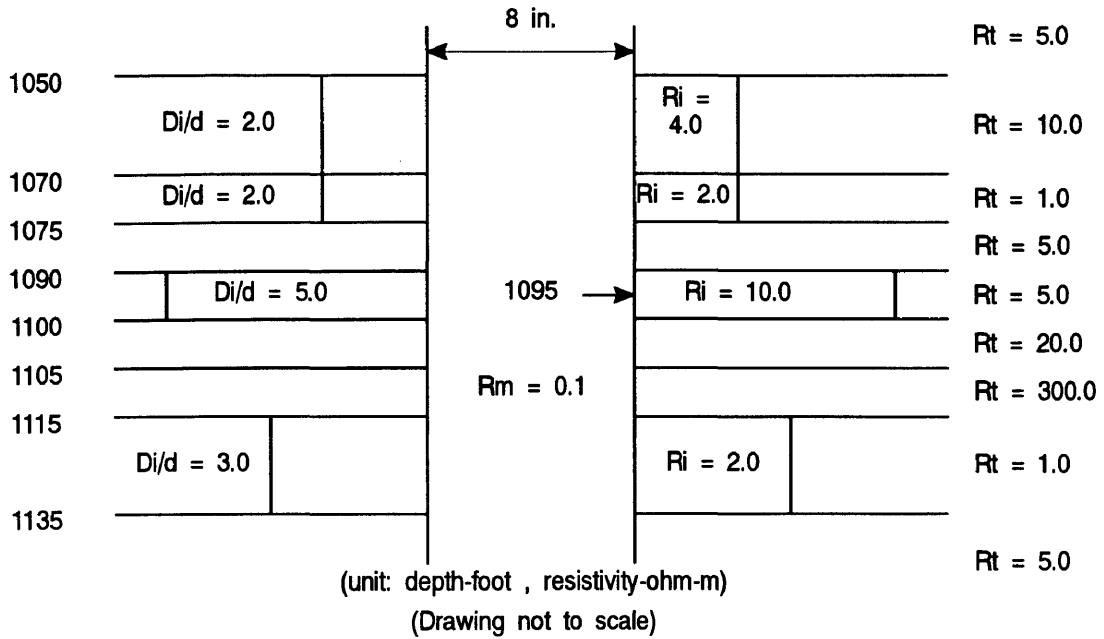


Figure 3.17: Nine layer earth model when the central current source is at depth 1095 feet

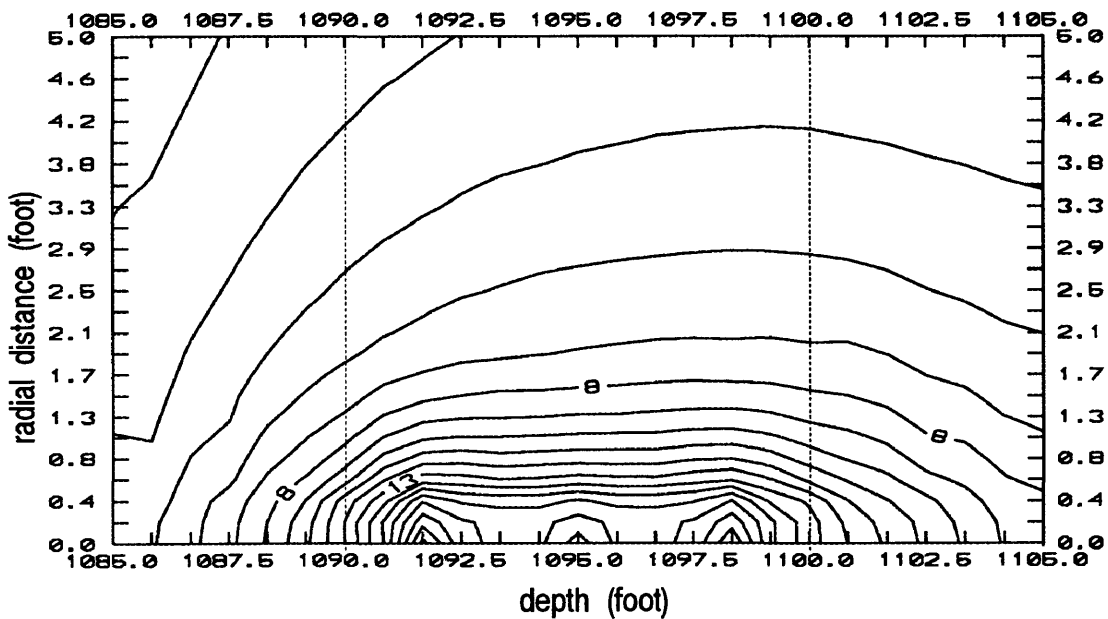


Figure 3.18: Equipotential lines of nine layer earth model

3.10 Verifications of the Results

The numerical results obtained from the finite difference method for the Laterolog 7 electrode configuration have been checked against other available solutions in limiting cases. These include the analytical solutions for the horizontally layered earth model and the cylindrically layered earth model (Gianzero and Anderson, 1982), and the physical scale modeling results (Shattuck et al., 1987; Bittar et al., 1990). The comparisons of the analytical solution with the finite difference solutions show good agreement. Comparisons of the physical scale modeling with the finite difference solution also show good agreement. Therefore, the forward modeling of the Laterolog 7 tool configuration using the finite difference method appears to be credibly accurate, computationally efficient, and versatile.

3.10.1 Comparisons with the Analytical Solutions

In this section, the finite difference method is compared with the analytical solution in limiting test models. These selected test models which are two dimensional have two characteristics. One is that R_m has much lower resistivity value than R_t , and the other is that R_s (resistivity of the shoulder layer) has also lower resistivity value than R_t .

In the analytical method, the solutions for the potential induced by a constant current source are formulated in terms of both Fourier cosine and Fourier sine

transforms with unknown coefficients. A suitable matching of the necessary boundary conditions results in a system of singular integral equations. An iterative solution is obtained for these transform coefficients which, in turn, are used to determine the potential at an arbitrary point of measurement (Gianzero and Anderson, 1982).

First, a synthetic log for the Laterolog 7 tool configuration in the two layer earth model is presented in Figure 3.19. In Figure 3.19, the resistivities of the beds are 1.0, 100.0 ohm-m from top to bottom, R_m is 0.1 ohm-m, and the borehole diameter is 8 inches. As shown in Figure 3.19, the departure of the finite difference solution from the analytical solution is very small. The relative error involved in the finite difference solution with "Production" is less than two percent.

The second test model consists of three horizontally parallel layers with no invaded zone (Figure 3.20). The resistivities of two shoulder layers are 1.0 ohm-m, the resistivity and the thickness of the target bed are 10.0 ohm-m and 40 inches, respectively, R_m is 0.1 ohm-m, and borehole diameter is 8 inches. In Figure 3.20, good agreement is also displayed between the finite difference solution and analytical solution.

The next two test models (Figure 3.21 and Figure 3.22) show three horizontally parallel layers with an invaded zone. The resistivities of two shoulder layers are 1.0 ohm-m, the resistivity and the thickness of target bed are 10.0 ohm-m and 40 inches, respectively, R_m is 0.1 ohm-m, and borehole diameter is 8 inches. The resistivity of

the invaded zone is 2.0 ohm-m in both models. The difference is that in Figure 3.21 the invasion diameter (D_i) is 35 inches (i.e., $D_i/d = 4.375$), and in Figure 3.22 D_i is 140 inches (i.e., $D_i/d = 17.5$), respectively. The apparent resistivity curves in the resistive bed shows the difference. This difference indicates the forward modeling program for the Laterolog 7 is sensitive to the depth of invasion and resistivity of the invaded zone. These comparisons of the finite difference solutions with analytical solutions also show good agreement.

One of the advantages of the finite difference method is that it can provide apparent resistivities which are extremely difficult, if not impossible, to compute by the analytical method. Another limitation of the analytical method is that the numerical integration sometimes diverges. From the above results, it is seen that the finite difference solution consistently agrees well with the analytical solution whenever these methods are able to be applied in a simple model. Having established credibility for the finite difference algorithm for the Laterolog 7 tool, we will proceed to analyze models for which analytical solutions are not available.

3.10.2 Comparisons with the Physical Scale Modeling

Physical scale modeling is a useful technique for studying the responses of well logging tools. Due to the large size and the deep investigation of some of the tools, it is very difficult and expensive to construct full scale environments with known electrical properties for those tools. Such measurements in known geometries are of

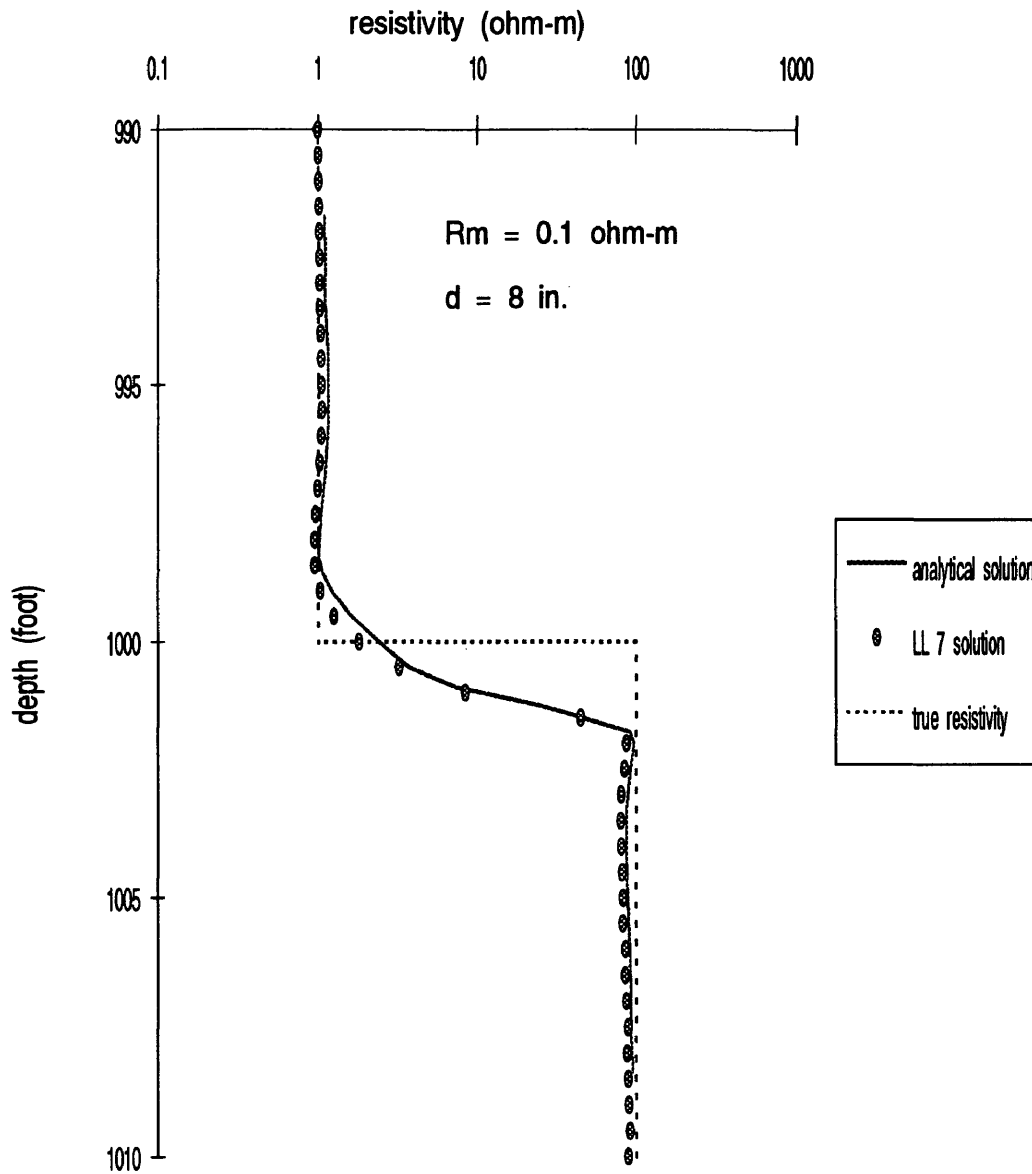


Figure 3.19: Comparison of finite difference solution with analytical solution for the Laterolog 7 (Thick beds)

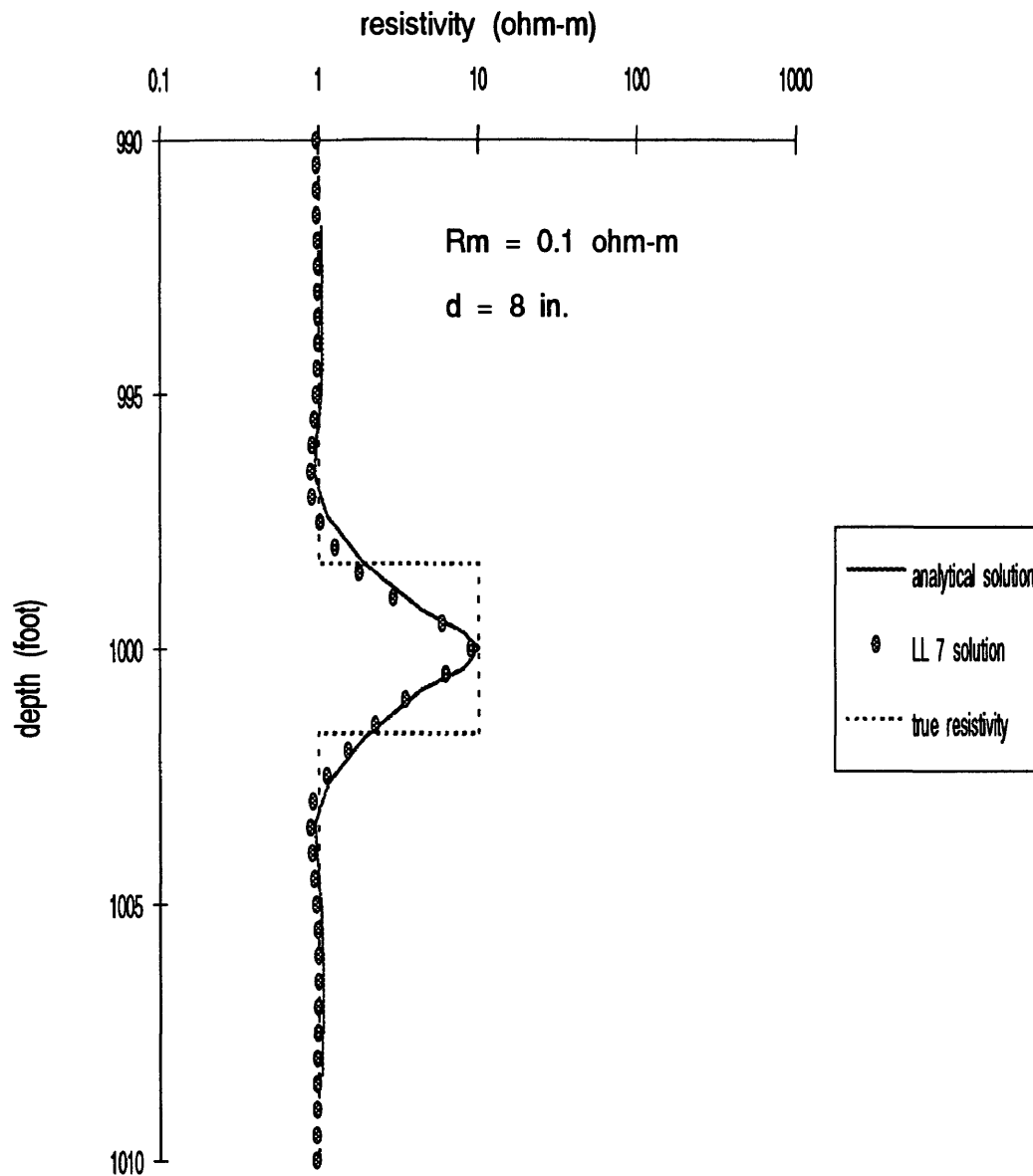


Figure 3.20: Comparison of finite difference solution with analytical solution for the Laterolog 7 (Thin beds)

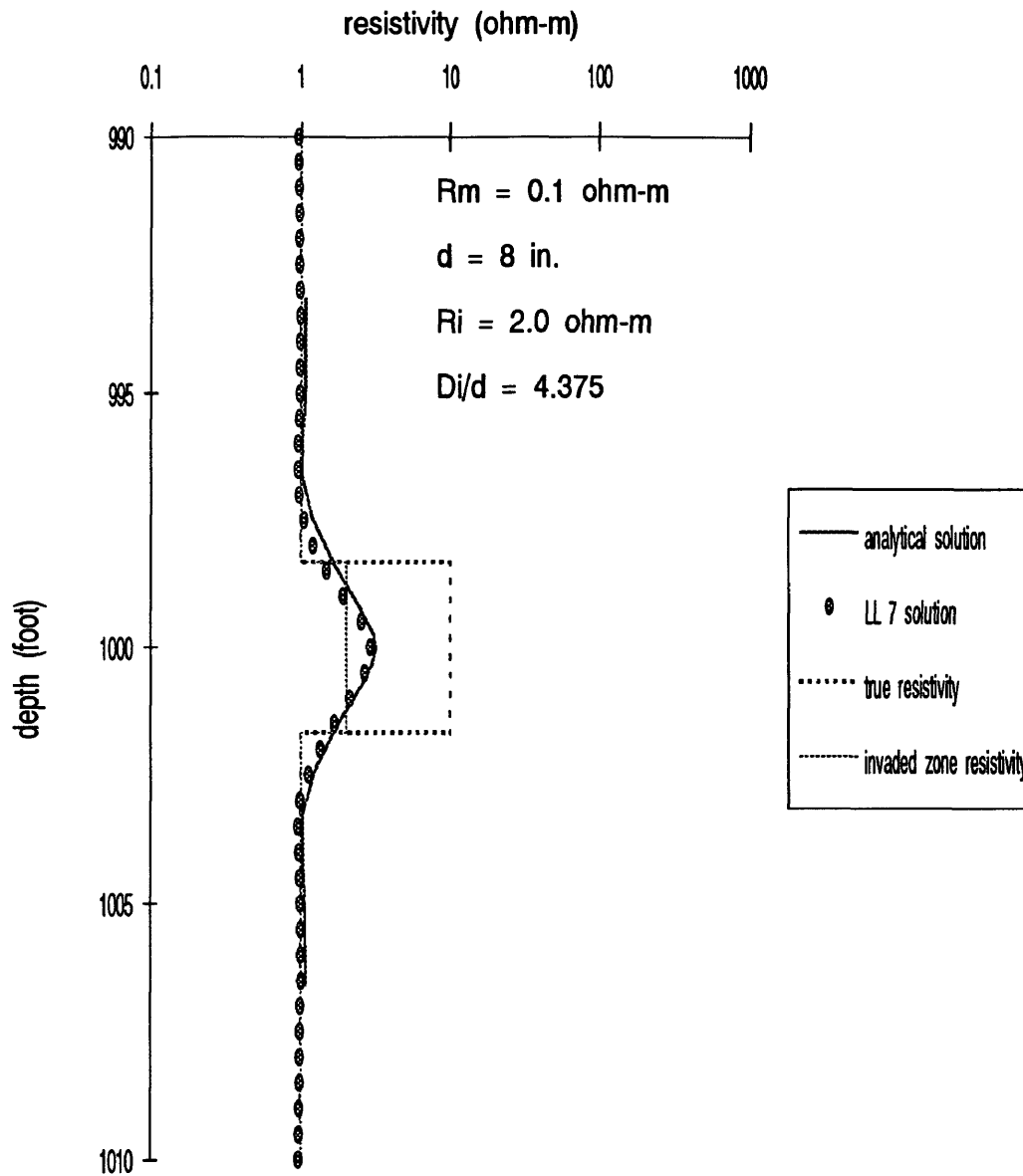


Figure 3.21: Comparison of finite difference solution with analytical solution for the Laterolog 7 (Thin-invaded beds, $D_i/d = 4.375$)

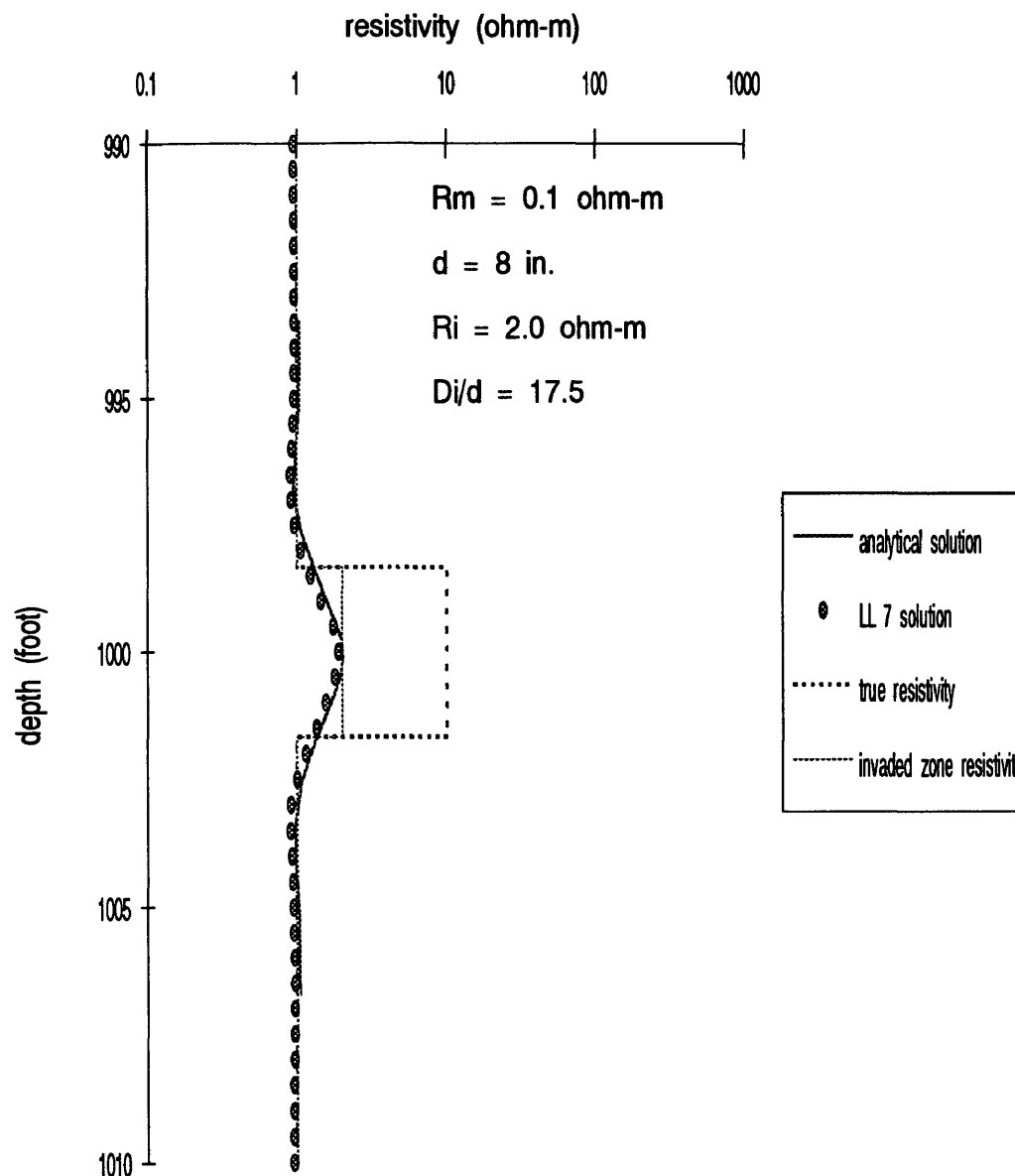


Figure 3.22: Comparison of finite difference solution with analytical solution for the Laterolog 7 (Thin-invaded beds, $D_i/d = 17.5$)

potential benefit in two ways. First, they can be used to verify calculations that have been made of a tool's responses by some theoretical method. Second, measurements can be made in situations where the theoretical methods are difficult to apply. In either situation, the measurements provide data that can be used to help interpret the response of the tool, which in turn improves the basic understanding of data obtained from well logging tools.

The University of Houston Well Logging Laboratory performed a Laterolog 7 physical scale modeling in 1987 and 1990 (Shattuck et al., 1987; Bittar et al., 1990). Every tool length and borehole diameter is scaled down about 25 times. In other words, in the physical scale modeling experiments the total tool length is 3.1750 inches, A_0M_1 (and equivalently A_0M_2) length is 0.4625 inches, and A_0M_1' (and equivalently A_0M_2') length is 0.7875 inches.

In this subsection, a two dimensional finite difference solution is compared with the physical scale modeling result. In order to compare the solution of this study with the physical scale modeling results, the physical scale modeling is scaled up 25 times. Fig 3.23 shows the comparison of the finite difference solution with the physical scale modeling result. In this comparison, the value of R_m is 0.1 ohm-m. (In fact, it is not possible to obtain the value of R_m in physical scale modeling experiments.) In Figure 3.23 good agreement of the physical scale modeling result with the finite difference solution is indicated. But in this finite difference solution approach point

current electrodes are modeled, while in the physical scale modeling approach point current electrodes were not used. Hence, the different shape of the curve in the range of depths between 1020 feet and 1030 feet in Figure 3.23 showed that physical scale modeling did not detect the change of the apparent resistivity curve correctly. In other words, when there is a resistive bed between conductive layers, the apparent resistivity curve of the Laterolog 7 tool should have a little lower value at the center of the resistive bed than near the edges of the resistive bed (Chemali et al., 1988; Schlumberger, 1987).

3.11 Response of Synthetic Laterolog 7 for Various Earth Models

In this section, the synthetic Laterolog 7 responses in some earth models for which analytic solutions do not exist are determined. Two model types are considered:

1. relatively resistive object beds and,
2. relatively conductive object beds.

Three bed thicknesses are included for each type to include thick bed, critically thick bed, and thin bed. In this section, the thick bed is 12 feet thick, the critically thick bed is 6.67 feet (80 inches) thick, and the thin bed is 4 feet thick, respectively. The critically thick bed has a thickness which is equal to the total length of the Laterolog 7. The effects due to the variations in earth parameters are also considered. The earth parameters include mud resistivity (R_m), borehole diameter (d), invasion

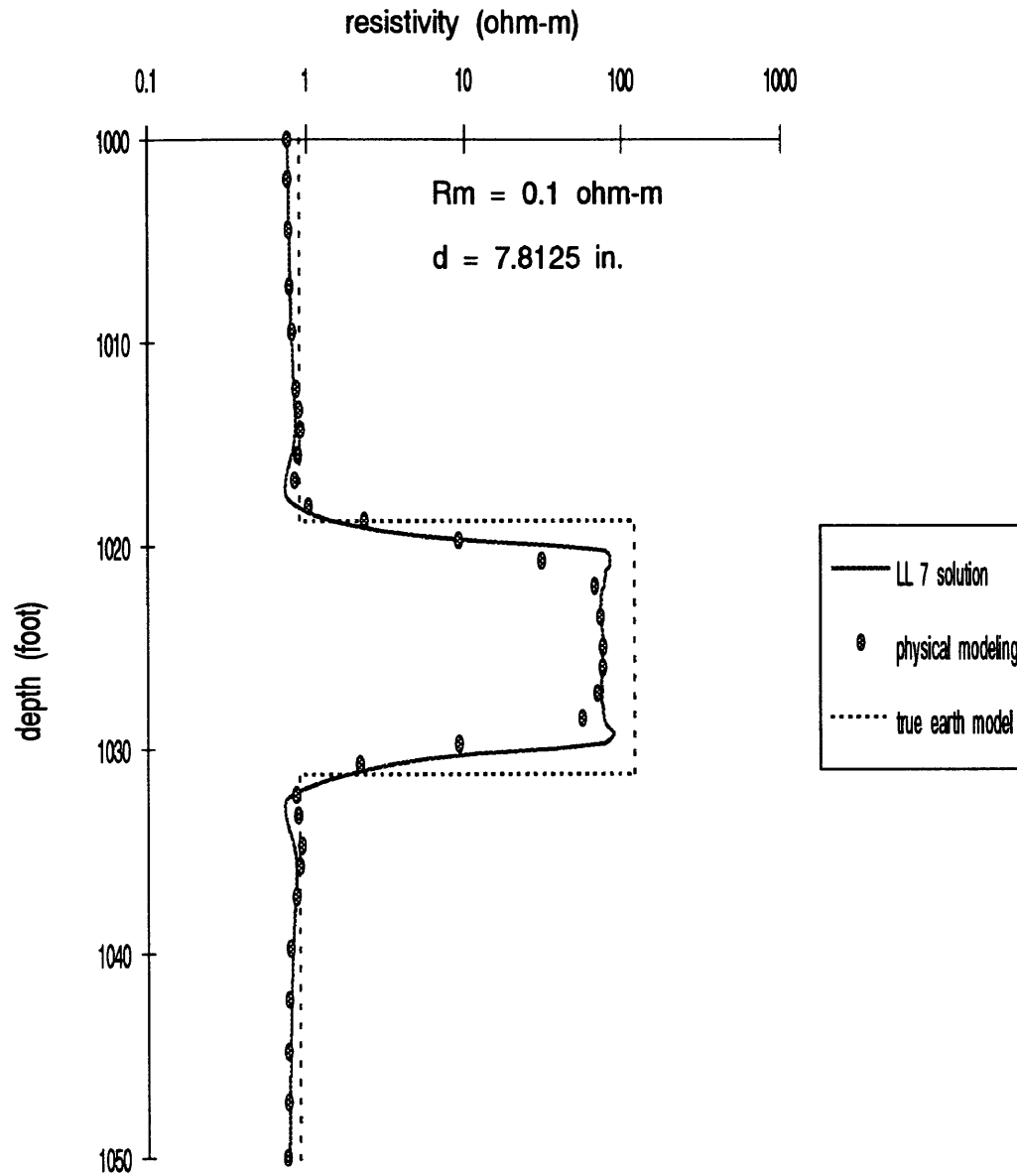


Figure 3.23: Comparison of finite difference solution with physical scale modeling for the Laterolog 7

diameter (D_i), resistivity of the invaded zone (R_i), and true resistivity of the formation (R_t). The complete sets of the forward modeling responses for the Laterolog 7 are included in Appendix A for the conductive bed and in Appendix B for the resistive bed.

3.11.1 The Responses of the Laterolog 7 Tool in a Conductive Bed

R_a versus R_m

First, the responses of the Laterolog 7 tool with variations of the mud resistivity are investigated. Figure A.1 (or Figure 3.24), Figure A.2, and Figure A.3 show the responses of the Laterolog 7 tool in the cases of thick, critically thick, and thin bed, respectively. The resistivities of the conductive bed and the shoulder layer are 10.0 and 100.0 ohm-m, respectively, and the borehole diameter is 8 inches. Mud resistivities of 0.1, 1.0, and 10.0 ohm-m are considered. No invasion is considered. The responses show:

1. There is no appreciable difference between curves; that is, the mud resistivity has very little effect on the log responses when there is no invasion.
2. The minimum value of the apparent resistivity curves in the conductive bed is slightly greater than the true resistivity.
3. The apparent resistivity in the shoulder layer is slightly less than the true resistivity, when the mud resistivity is low.

4. The apparent resistivity in the case of conductive bed is slightly greater than the true resistivity in the case of the thick and critically thick conductive beds regardless of mud resistivity (Figure A.1 and Figure A.2). In the case of a thin conductive bed there is a good agreement between R_a and R_t in the conductive bed when R_m is intermediate to high, and R_a is greater than R_t when R_m is low (Figure A.3).
5. The apparent resistivity curves have the same shapes in thick and critically thick conductive layer cases. However, the apparent resistivity curve for the thin conductive layer case has a different shape from that for the thick and critically thick cases.

R_a versus d

Second, the responses of the Laterolog 7 tool with variations of the borehole diameter are investigated. Figure A.4 (or Figure 3.25), Figure A.5, and Figure A.6 show the responses of the Laterolog 7 tool in the cases of thick, critically thick, and thin bed, respectively. The resistivities of the conductive bed and shoulder layer are 10.0 and 100.0 ohm-m, respectively. The mud resistivity is 0.1 ohm-m, and borehole diameters of 8, 10, and 12 inches are considered. No invasion is considered. The responses show:

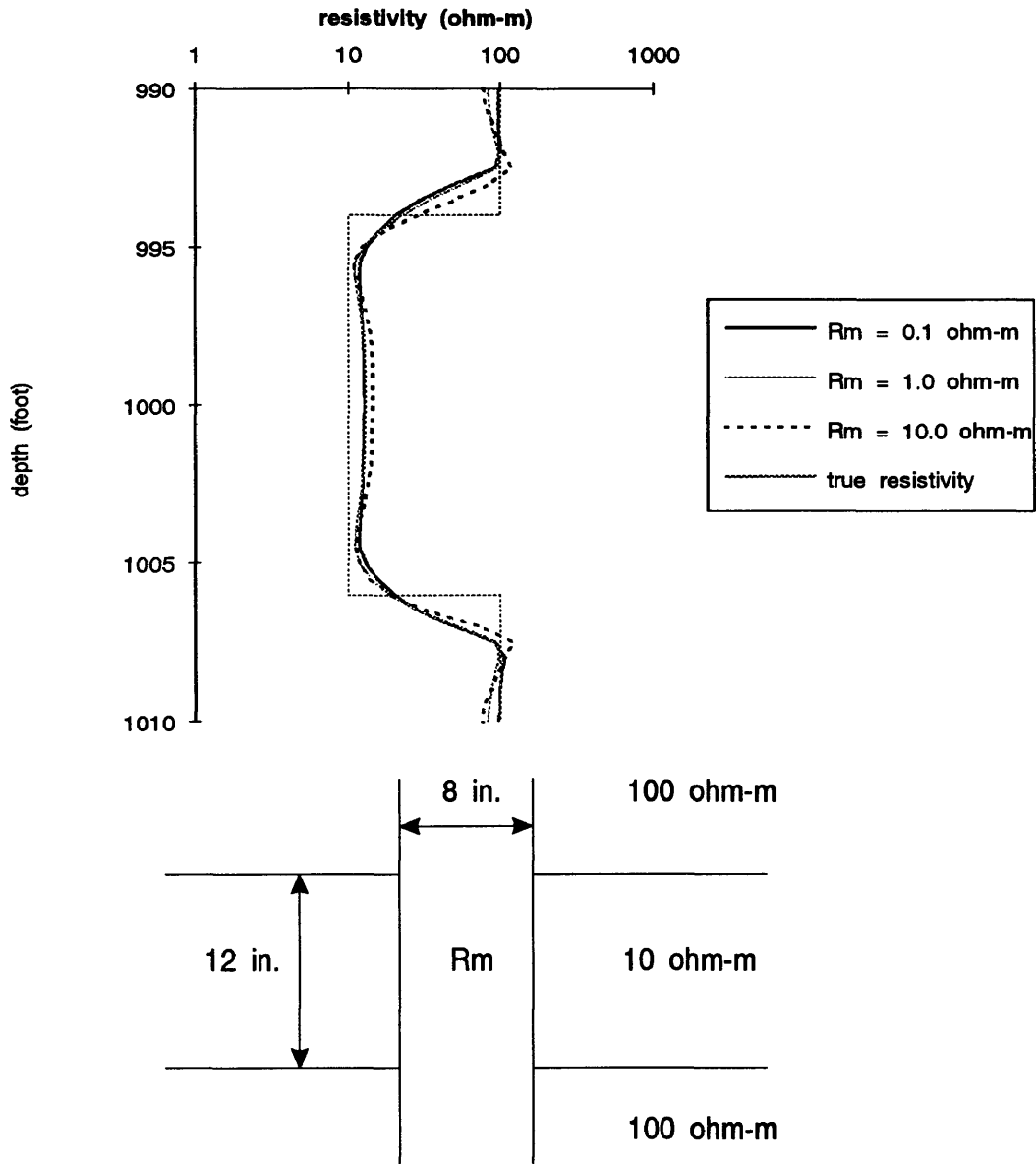


Figure 3.24: Variations in R_m (Thick - Conductive)

1. There is no appreciable difference between curves; that is, the borehole diameter has very little effect on the log responses when there is no invasion.
2. The apparent resistivity in the conductive bed is slightly greater than the true resistivity regardless of the thickness of the conductive bed.
3. The apparent resistivity in the shoulder layer is close to the true resistivity regardless of the borehole diameter.
4. The apparent resistivity curves have the same shape regardless of the thickness of the conductive bed.

R_a versus D_i

Third, the responses of the Laterolog 7 tool with variations of the extent of invasion are investigated. Figure A.7 (or Figure 3.26), Figure A.8, and Figure A.9 show the responses of the Laterolog 7 tool in the cases of thick, critically thick, and thin bed, respectively. The resistivities of the conductive bed and shoulder layer are 10.0 and 100.0 ohm-m, respectively. The resistivities of the mud and invaded zone are 0.1 ohm-m and 20.0 ohm-m, respectively. Invasion diameters of $2d$ (16 inches), $5d$ (40 inches), and $10d$ (80 inches) are considered, where borehole diameter d is 8 inches. The responses show:

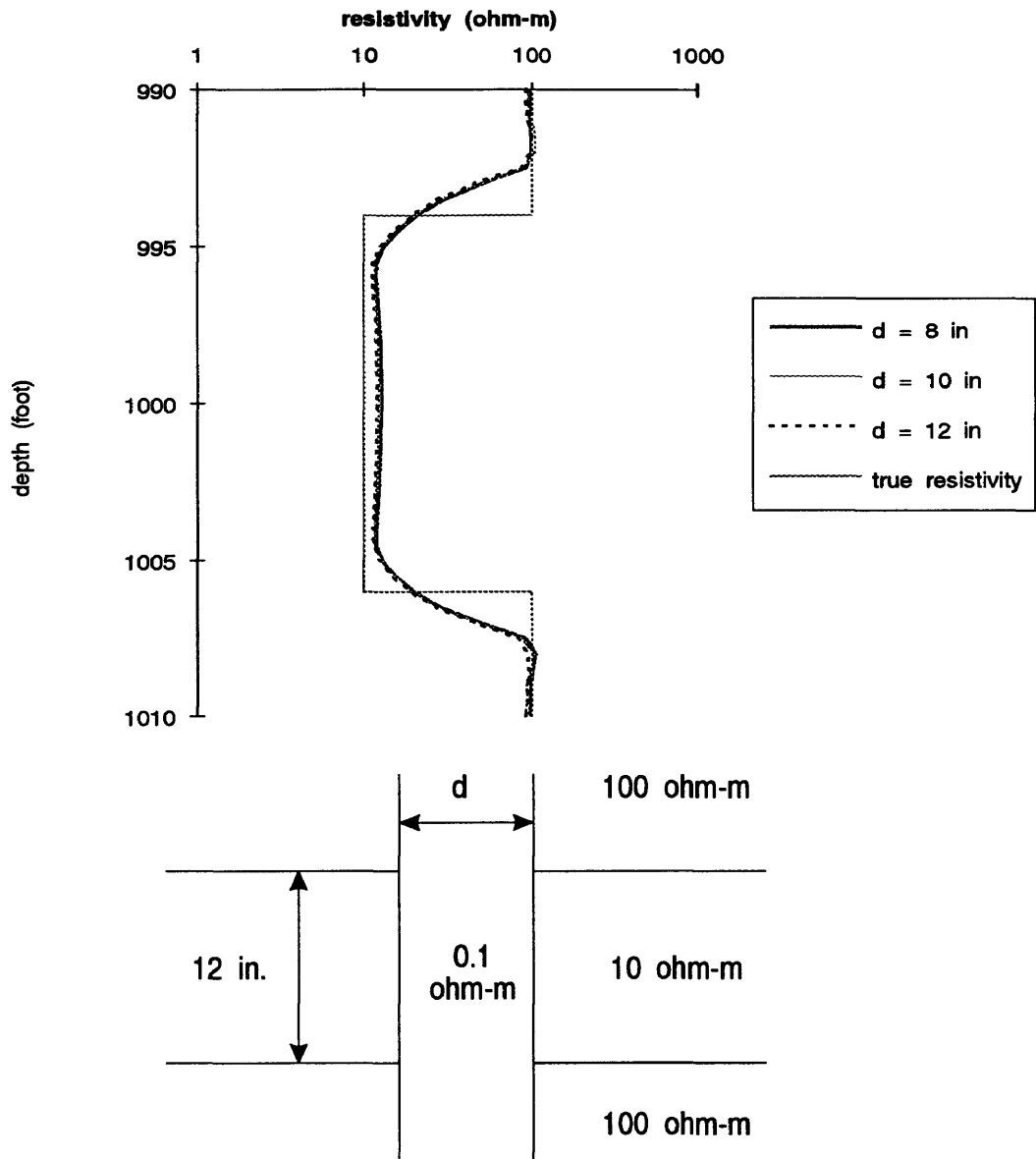


Figure 3.25: Variations in d (Thick - Conductive)

1. The apparent resistivity of the conductive bed is substantially affected by the extent of invasion.
2. The apparent resistivity in the conductive bed is farther from the true resistivity, as the invasion diameter increases.
3. The apparent resistivity in the shoulder layer is not appreciably affected by the invasion. Hence, the tails of the curves are merged into one at the shoulder beds, and conform with the apparent resistivity curve which is obtained without consideration of the invasion.
4. The apparent resistivity curves have the same shapes regardless of the conductive bed thickness.

R_a versus R_i

Fourth, the responses of the Laterolog 7 tool with variations of the invasion zone resistivity are investigated. Figure A.10 (or Figure 3.27), Figure A.11, and Figure A.12 show the responses of the Laterolog 7 tool in the cases of thick, critically thick, and thin bed, respectively. The resistivities of the conductive bed and shoulder layer are 10.0 and 100.0 ohm-m, respectively. The resistivity of the mud is 0.1 ohm-m. The invasion diameter is $5d$ (40 inches). Resistivities of the invaded zone of 20.0, 50.0, and 100.0 ohm-m are considered. The responses show:

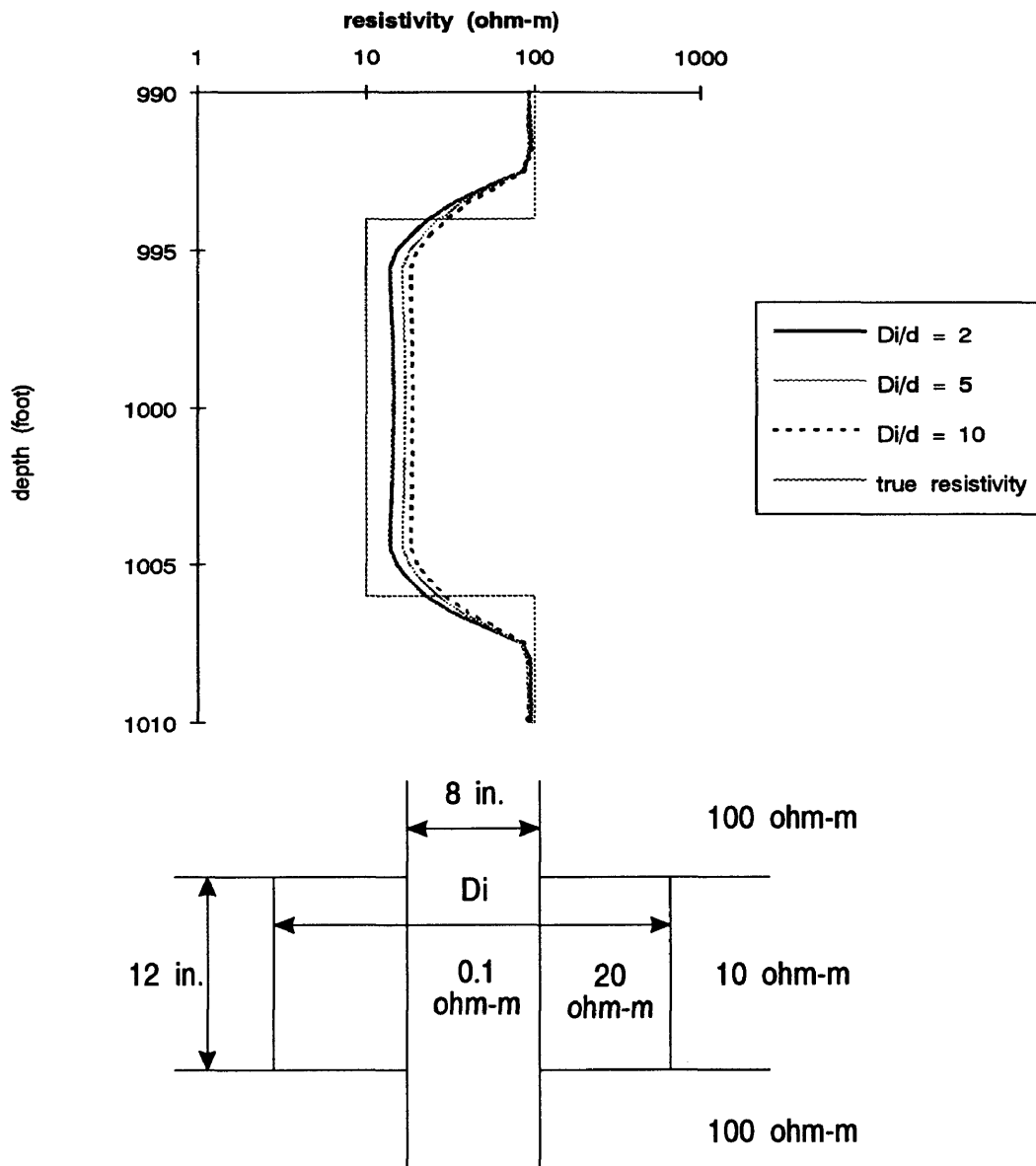


Figure 3.26: Variations in D_i (Thick - Conductive)

1. The apparent resistivity of the conductive bed is considerably affected by the resistivity variations of the invaded zone. The apparent resistivity increases, as the resistivity of the invaded zone increases.
2. The apparent resistivity in the shoulder layer is not affected appreciably regardless of either the thickness of the conductive bed or the resistivity of the invaded zone.
3. The apparent resistivity in the conductive bed is not affected appreciably regardless of the thickness of conductive bed.
4. The apparent resistivity curves have the same shapes regardless of the conductive bed thickness.

R_a versus R_t

Finally, the responses of the Laterolog 7 tool with variations of the true resistivity are investigated. Figure A.13 (or Figure 3.28), Figure A.14, and Figure A.15 show the responses of the Laterolog 7 tool in the cases of thick, critically thick, and thin bed, respectively. The resistivities of the shoulder layers are 20.0 ohm-m. The mud resistivity and the resistivity of the invaded zone are 0.1 and 10.0 ohm-m, respectively. True resistivities of 1.0, 2.0, 5.0, and 10.0 ohm-m are considered. This model can be encountered in nature when the borehole is filled with salty mud and

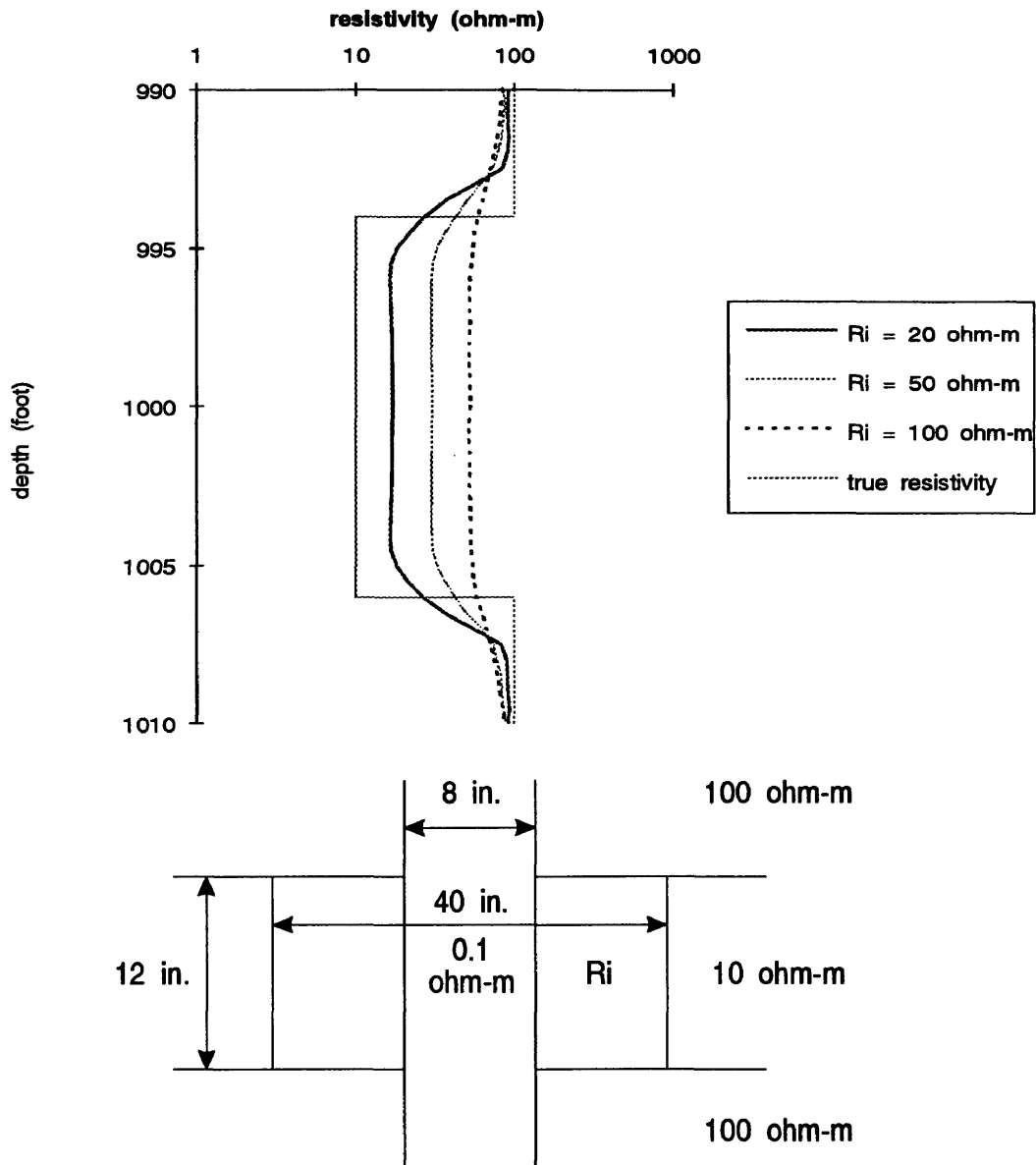


Figure 3.27: Variations in R_i (Thick - Conductive)

a formation is saturated with the formation water of low resistivity. The responses show:

1. The apparent resistivity of the conductive bed is considerably affected by the resistivity variations of the conductive bed. The apparent resistivity increases, as the resistivity of the conductive bed increases.
2. The apparent resistivity in the shoulder layer is not affected appreciably regardless of either the thickness of conductive bed or the resistivity of the conductive bed.
3. The apparent resistivity in the conductive bed is not affected appreciably regardless of the thickness of the conductive bed.
4. The apparent resistivity curves have the same shapes regardless of the conductive bed thickness.

Conclusions regarding Conductive Layers

From the analyses of the apparent resistivity curves for the Laterolog 7 tool in conductive beds, it can be concluded as follows:

1. The mud resistivity has very little effect on the apparent resistivity curve.
2. The apparent resistivities are greatly affected by the variations in the invaded zone resistivity.

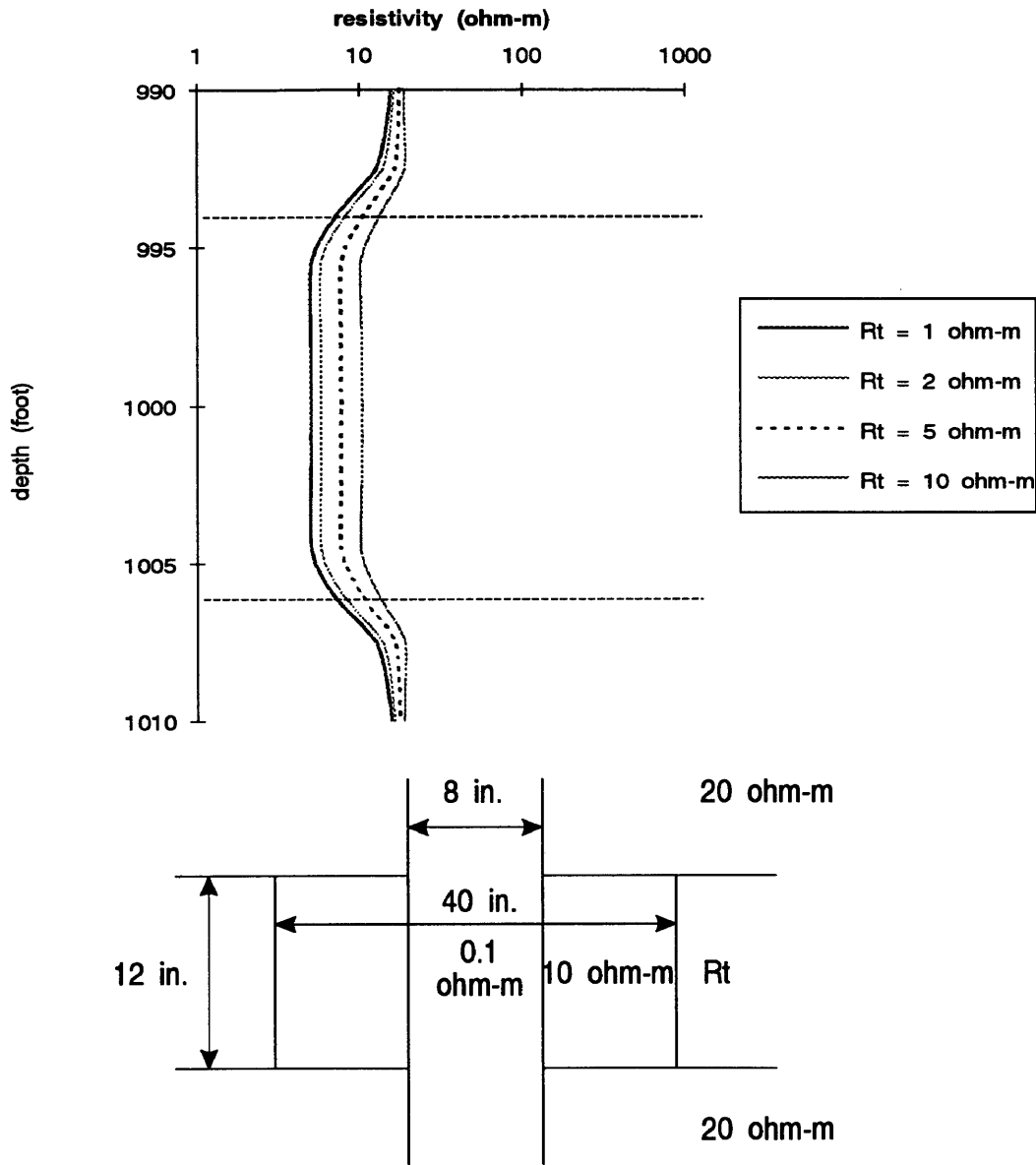


Figure 3.28: Variations in R_t (Thick - Conductive)

3. From the change of apparent resistivity curves in the cases of thick, critically thick, and thin bed with variations of any earth parameter, it is considered to be difficult to identify the true resistivity and the boundary of a conductive bed if its thickness is less than the thickness of current sheet (O_1O_2 in Figure 2.6).
4. The large diameter hole adversely affects the apparent resistivity responses in conductive beds.

3.11.2 The Responses of the Laterolog 7 Tool in a Resistive Bed

R_a versus R_m

First, the responses of the Laterolog 7 tool with variations of the mud resistivity are investigated. Figure B.1 (or Figure 3.29), Figure B.2, and Figure B.3 show the responses of the Laterolog 7 tool in the cases of thick, critically thick, and thin bed, respectively. The resistivities of the resistive bed and the shoulder layer are 100.0 and 10.0 ohm-m, respectively, and the borehole diameter is 8 inches. Mud resistivities of 0.1, 1.0, and 10.0 ohm-m are considered. No invasion is considered. The responses show:

1. There is no appreciable difference between curves; that is, the mud resistivity has very little effect on the log responses when there is no invasion.
2. The maximum value of the apparent resistivity curves in the resistive bed is slightly smaller than the true resistivity.

3. The apparent resistivity in the shoulder layer is slightly greater than the true resistivity, when the mud resistivity is low.
4. The apparent resistivity in the case of a resistive bed is slightly less than the true resistivity in the case of thick and critically thick resistive beds regardless of mud resistivity (Figure B.1 and Figure B.2). In the case of a thin resistive bed there is a good agreement between R_a and R_t in the resistive bed when R_m is intermediate to high, and R_a is less than R_t when R_m is low (Figure B.3).
5. The apparent resistivity curves have the same shapes in thick and critically thick resistive layer cases. However, the apparent resistivity curve for the thin resistive layer case has a different shape from that for the thick and critically thick cases.

R_a versus d

Second, the responses of the Laterolog 7 tool with variations in the borehole diameter are investigated. Figure B.4 (or Figure 3.30), Figure B.5, and Figure B.6 show the responses of the Laterolog 7 tool in the cases of thick, critically thick, and thin bed, respectively. The resistivities of the resistive bed and shoulder layer are 100.0 and 10.0 ohm-m, respectively. The mud resistivity is 0.1 ohm-m, and borehole diameters of 8, 10, and 12 inches are considered. No invasion is considered. The responses show:

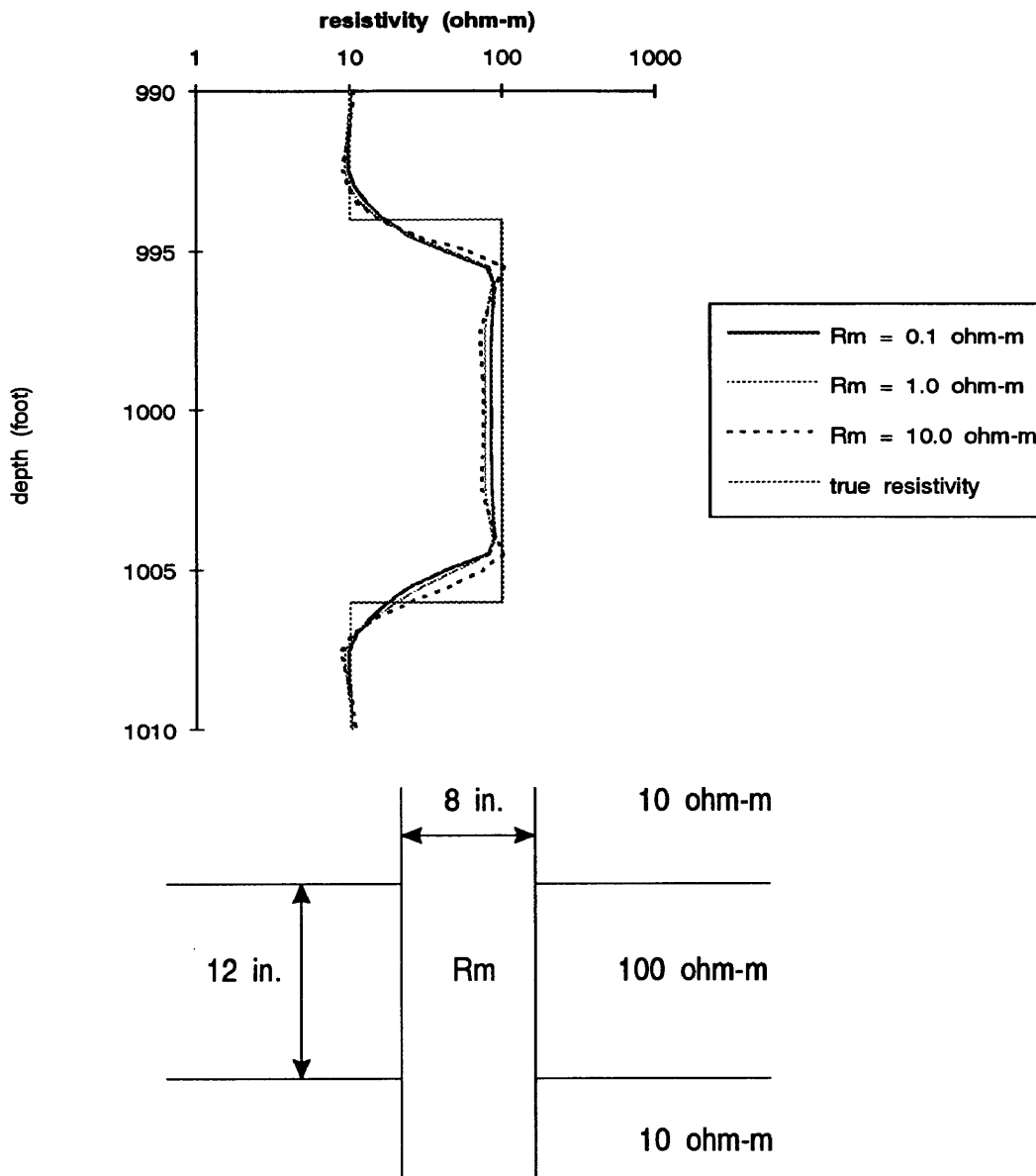


Figure 3.29: Variations in R_m (Thick - Resistive)

1. There is no appreciable difference between curves; that is, the borehole diameter has very little effect on the log responses when there is no invasion.
2. The apparent resistivity in the resistive bed is slightly less than the true resistivity regardless of the thickness of the resistive bed.
3. The apparent resistivity in the shoulder layer is close to the true resistivity regardless of the borehole diameter.
4. The apparent resistivity curves have the same shape regardless of the thickness of the resistive bed.

R_a versus D_i

Third, the responses of the Laterolog 7 tool with the variations in the extent of invasion are investigated. Figure B.7 (or Figure 3.31), Figure B.8, and Figure B.9 show the responses of the Laterolog 7 tool in the cases of thick, critically thick, and thin bed, respectively. The resistivities of the resistive bed and shoulder layer are 100.0 and 10.0 ohm-m, respectively. The resistivities of the mud and the invaded zone are 0.1 ohm-m and 20.0 ohm-m, respectively. Invasion diameters of $2d$ (16 inches), $5d$ (40 inches), and $10d$ (80 inches) are considered, where the borehole diameter d is 8 inches. The responses show:

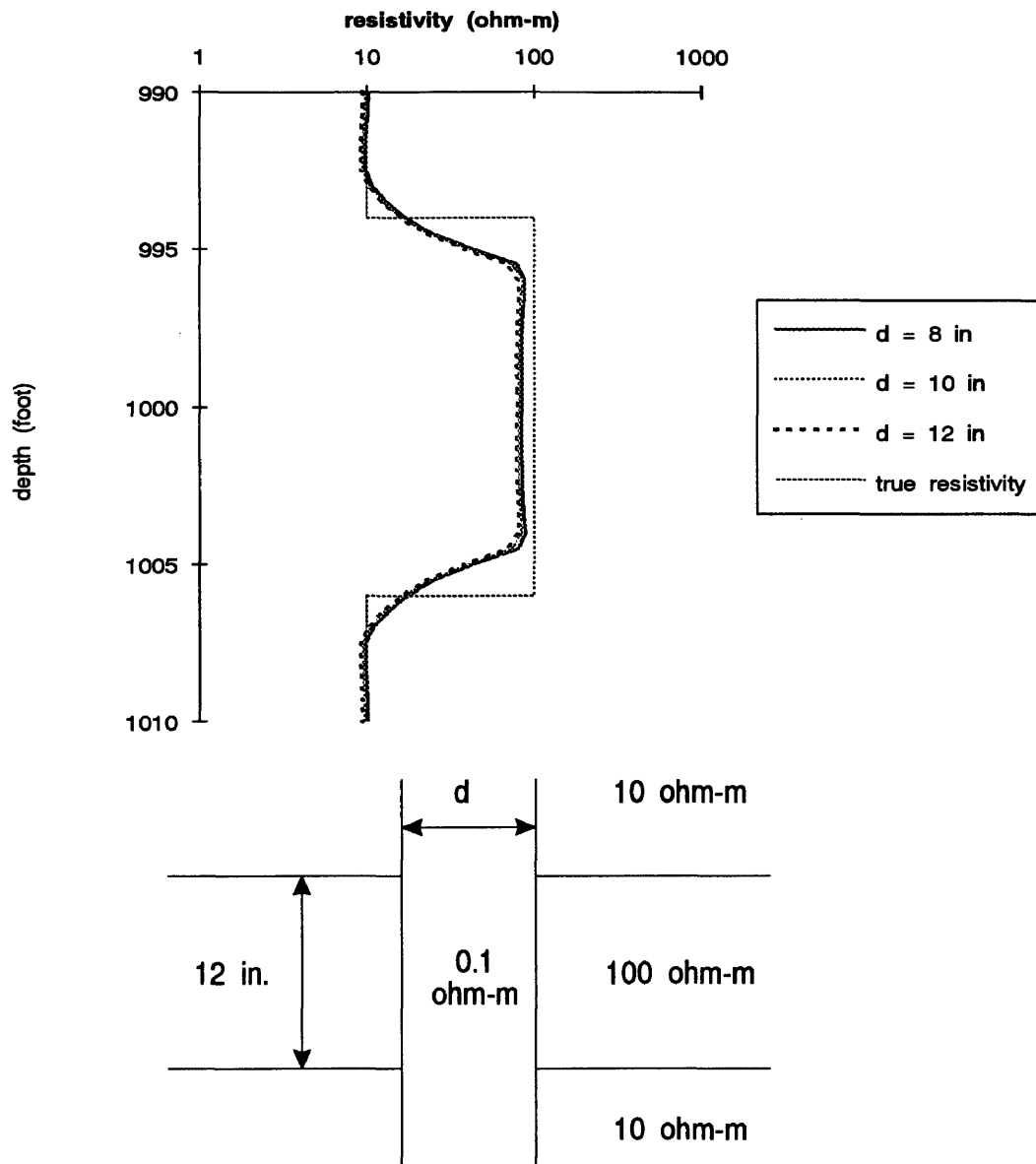


Figure 3.30: Variations in d (Thick - Resistive)

1. The apparent resistivity of the resistive bed is greatly affected by the extent of invasion.
2. The apparent resistivity in the resistive bed is farther from the true resistivity, as the invasion diameter increases.
3. The apparent resistivity in the shoulder layer is not appreciably affected by the invasion. Hence, the tails of the curves are merged into one at the shoulder beds, and conform with the apparent resistivity curve which is obtained without a consideration of the invasion.
4. The apparent resistivity curves have the same shapes regardless of the resistive bed thickness.

R_a versus R_i

Fourth, the responses of the Laterolog 7 tool with the variations of the invasion zone resistivity are investigated. Figure B.10 (or Figure 3.32), Figure B.11, and Figure B.12 show the responses of the Laterolog 7 tool in the cases of thick, critically thick, and thin bed, respectively. The resistivities of the resistive bed and shoulder layer are 100.0 and 10.0 ohm-m, respectively. The resistivity of the mud is 0.1 ohm-m. The invasion diameter is 40 inches ($5d$). Resistivities of the invaded zone of 10.0, 20.0, and 50.0 ohm-m are considered. The responses show:

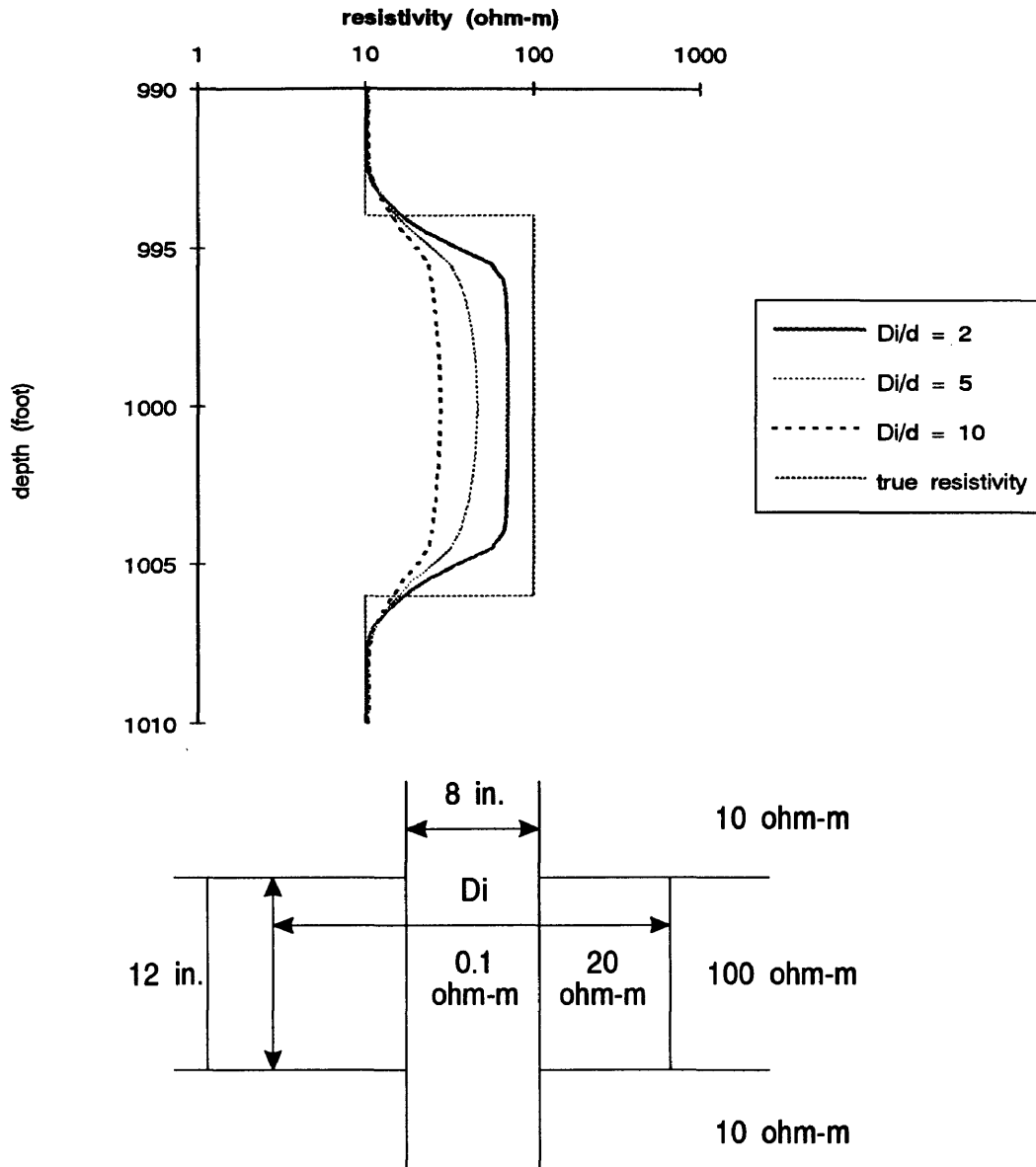


Figure 3.31: Variations in D_i (Thick - Resistive)

1. The apparent resistivity of the resistive bed is considerably affected by the resistivity variations of the invaded zone. The apparent resistivity increases as the resistivity of the invaded zone increases.
2. The apparent resistivity in the shoulder layer is not affected appreciably regardless of either the thickness of resistive bed or the resistivity of invaded zone.
3. The apparent resistivity in the resistive bed is not affected appreciably regardless of the thickness of resistive bed.
4. The apparent resistivity curves have the same shapes regardless of the resistive bed thickness.

R_a versus R_t

Finally, the responses of the Laterolog 7 tool with the variations of the true resistivity are investigated. Figure B.13 (or Figure 3.33), Figure B.14, and Figure B.15 show the responses of the Laterolog 7 tool in the cases of thick, critically thick, and thin bed, respectively. The resistivities of the shoulder layers are 5.0 ohm-m. The mud resistivity and the resistivity of the invaded zone are 0.1 and 10.0 ohm-m, respectively. True resistivities of 10.0, 20.0, 50.0, and 100.0 ohm-m are considered. For example, in the case where the formation resistivity factor (F) of the target bed is 20, the resistivity index (I) is 25, and the resistivity of the formation water is 0.1 ohm-m,

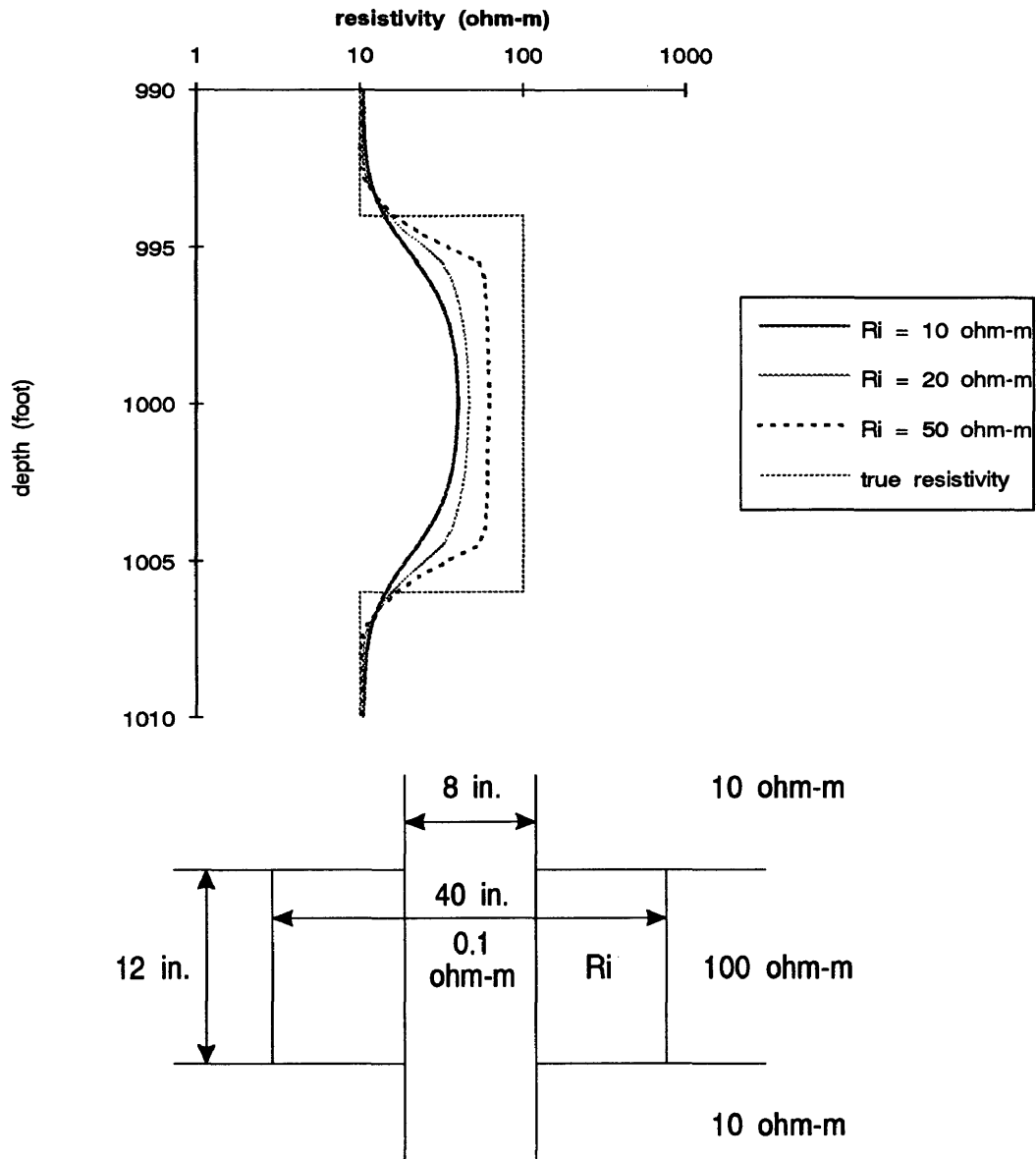


Figure 3.32: Variations in R_i (Thick - Resistive)

then the true resistivity of the formation will be 50.0 ohm-m. Also, the resistivity of the invaded zone will be 10.0 ohm-m, if the invaded zone is filled with a 0.5 ohm-m mud filtrate. The responses show:

1. The apparent resistivity of the resistive bed is considerably affected by the resistivity variations of the resistive bed. The apparent resistivity increases, as the resistivity of the resistive bed increases.
2. The apparent resistivity in the shoulder layer is not affected appreciably regardless of either the thickness of resistive bed or the resistivity of the resistive bed.
3. The apparent resistivity in the resistive bed is not affected appreciably regardless of the thickness of the resistive bed.
4. The apparent resistivity curves have the same shapes regardless of the resistive bed thickness.

Conclusions regarding Resistive Layers

From the analyses of the apparent resistivity curves for the Laterolog 7 tool in the resistive beds, it can be concluded as follows:

1. The mud resistivity and the borehole diameter have very little effect on the apparent resistivity curve.

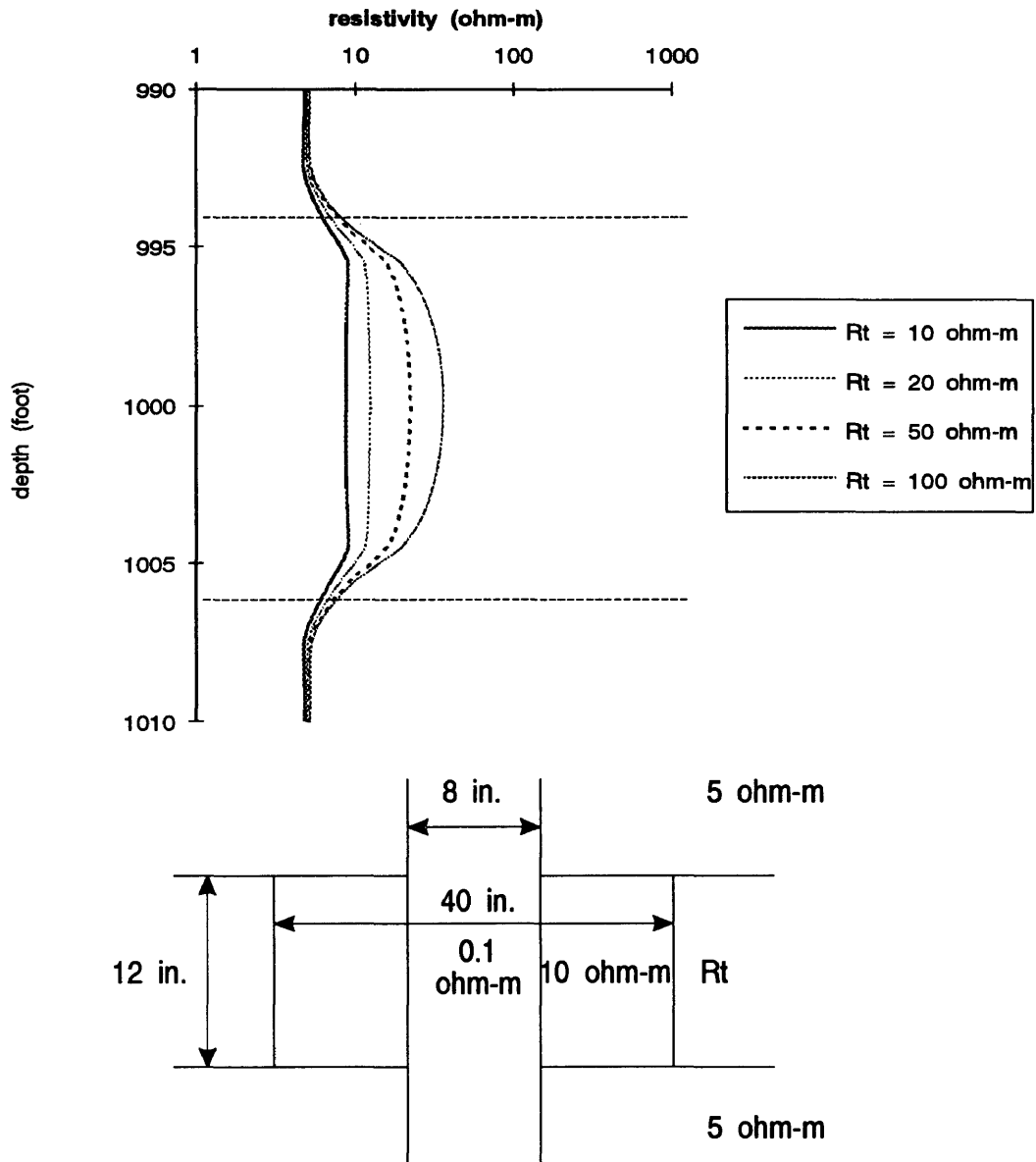


Figure 3.33: Variations in R_t (Thick - Resistive)

2. The apparent resistivities are greatly affected by the variations in the invaded zone resistivity.
3. From the change of apparent resistivity curves in the cases of thick, critically thick, and thin bed with variations of any earth parameter, it is considered to be difficult to identify the true resistivity and the boundary of a resistive bed if its thickness is less than the thickness of current sheet (O_1O_2 in Figure 2.6).

General Conclusions

In general, the logging environment which affects the response of the Laterolog 7 arrangement can be summarized as follows:

1. Borehole effect : While a large borehole diameter and a low resistivity mud increase the departure from the true resistivity in the conventional ES arrangements (Kim, 1986), in the Laterolog 7 arrangement a large diameter hole affects adversely the apparent resistivity responses only in a conductive bed, not in a resistive bed, and a low resistivity mud does not affect the departure from the true resistivity much in the Laterolog 7 arrangement. This is one of the main advantages of the Laterolog 7 tool compared with the conventional ES tools.
2. Invasion effects : The apparent resistivity is very sensitive to the invasion diameter and the invaded zone resistivity.

3. If bed thickness is less than the thickness of current sheet (O_1O_2 in Figure 2.6), it is considered to be difficult to identify the true resistivity and the boundary of a resistive bed.

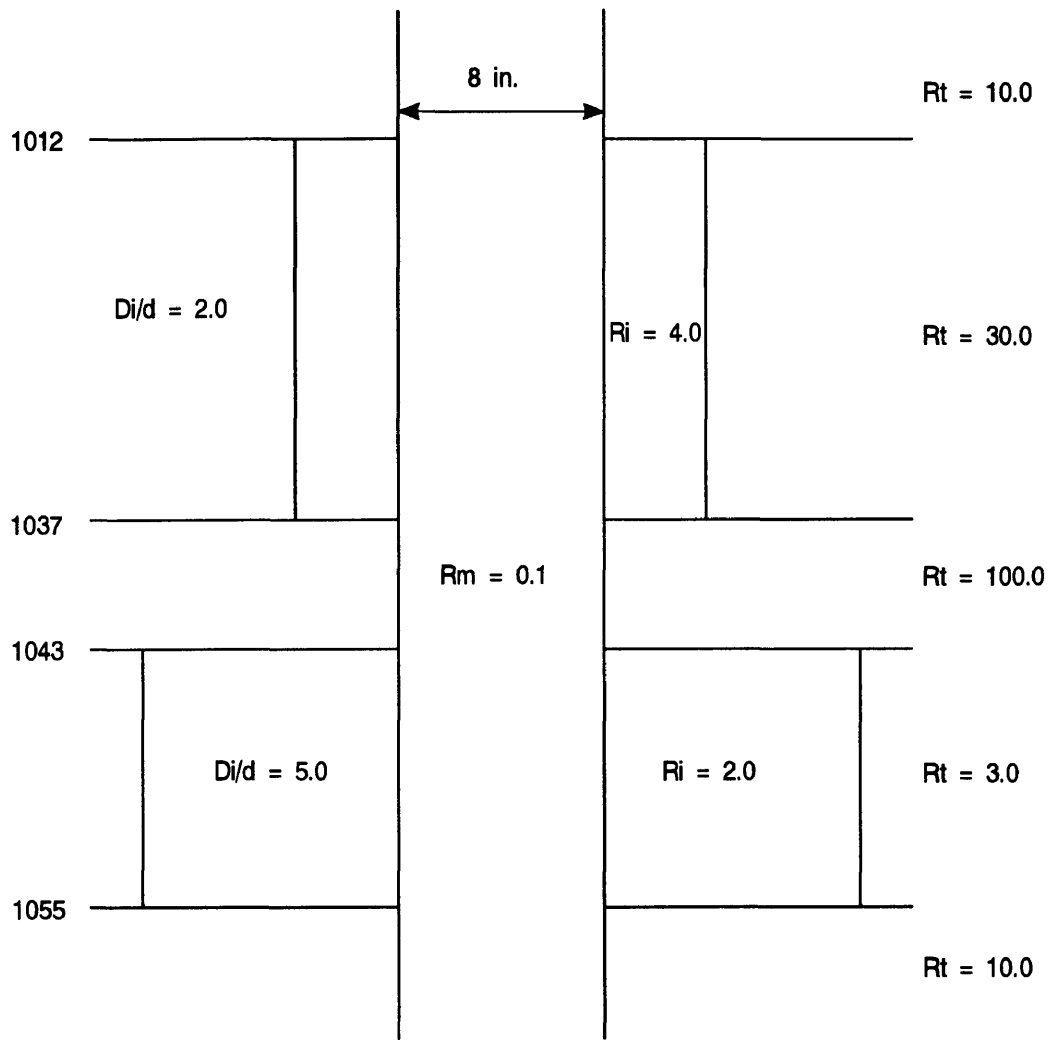
3.11.3 Multiple Invaded Layers

Finally, multiple layer earth models with invasion are investigated. Figure 3.34 and Figure 3.35 show a five layer earth model and its apparent resistivity curve, respectively. The resistivity of the shoulder layer is 10.0 ohm-m, and the resistivities of the other layers are 30.0, 100.0, and 3.0 ohm-m from top to bottom. The mud resistivity is 0.1 ohm-m and the borehole diameter is 8 inches. The invaded zone resistivities are 4.0 and 2.0 ohm-m and the invasion diameters are 16 and 40 inches from top to bottom, respectively. The bed thickness are 25, 6, and 12 feet from top to bottom of the model. Figure 3.35 indicates that the apparent resistivities of the finite difference method of the Laterolog 7 tool matches the true resistivities relatively well. In the layer from 1012 feet to 1037 feet, the apparent resistivity curves shows the fairly large departure from the true resistivity. This departure is because in this layer there is a large resistivity contrast between the true resistivity ($R_t = 30.0$ ohm-m) and the invasion resistivity ($R_i = 4.0$ ohm-m), and invasion diameter is significant at 16 inches ($D_i/d = 2$). However, in the layer from 1043 feet to 1055 feet, the apparent resistivity curve is very close to the true resistivity. This correlation is because in this layer there is a small resistivity contrast between the true resistivity ($R_t = 3.0$

ohm-m) and the invasion resistivity ($R_i = 2.0$ ohm-m), even though invasion diameter is significant at i 40 inches ($D_i/d = 5$).

Figure 3.36 and Figure 3.37 shows a nine layer earth model and its apparent resistivity curve for the Laterolog 7 tool. All physical parameters are indicated in Figure 3.36. In Figure 3.37, good agreement between the true resistivity and the apparent resistivity curves is indicated. However, in the layer from 1090 feet to 1100 feet, a departure from true resistivity is indicated. This departure is because in this layer a significant 40 inch invasion depth affects the apparent resistivity curve much more than the true resistivity does.

Figure 3.38 and Figure 3.39 show the apparent resistivity curves of Oklahoma benchmark for the 6FF40 (from the Center for Well-Logging, University of Houston) tool and for the Laterolog 7 tool of this study, respectively. There are 27 layers. While the apparent resistivity curve for the 6FF40 tool did not detect several thin layers in the range of 4990 feet to 5010 feet, the apparent resistivity curve for the Laterolog 7 tool of this study did detect the thin layers down to two-foot thickness. Figure 3.40 shows the comparison of apparent resistivity curves from 6FF40 tool and the Laterolog 7 tool in this study for Oklahoma benchmark.



(unit : depth-foot , resistivity-ohm-m)
 (Drawing not to scale)

Figure 3.34: Five layer earth model

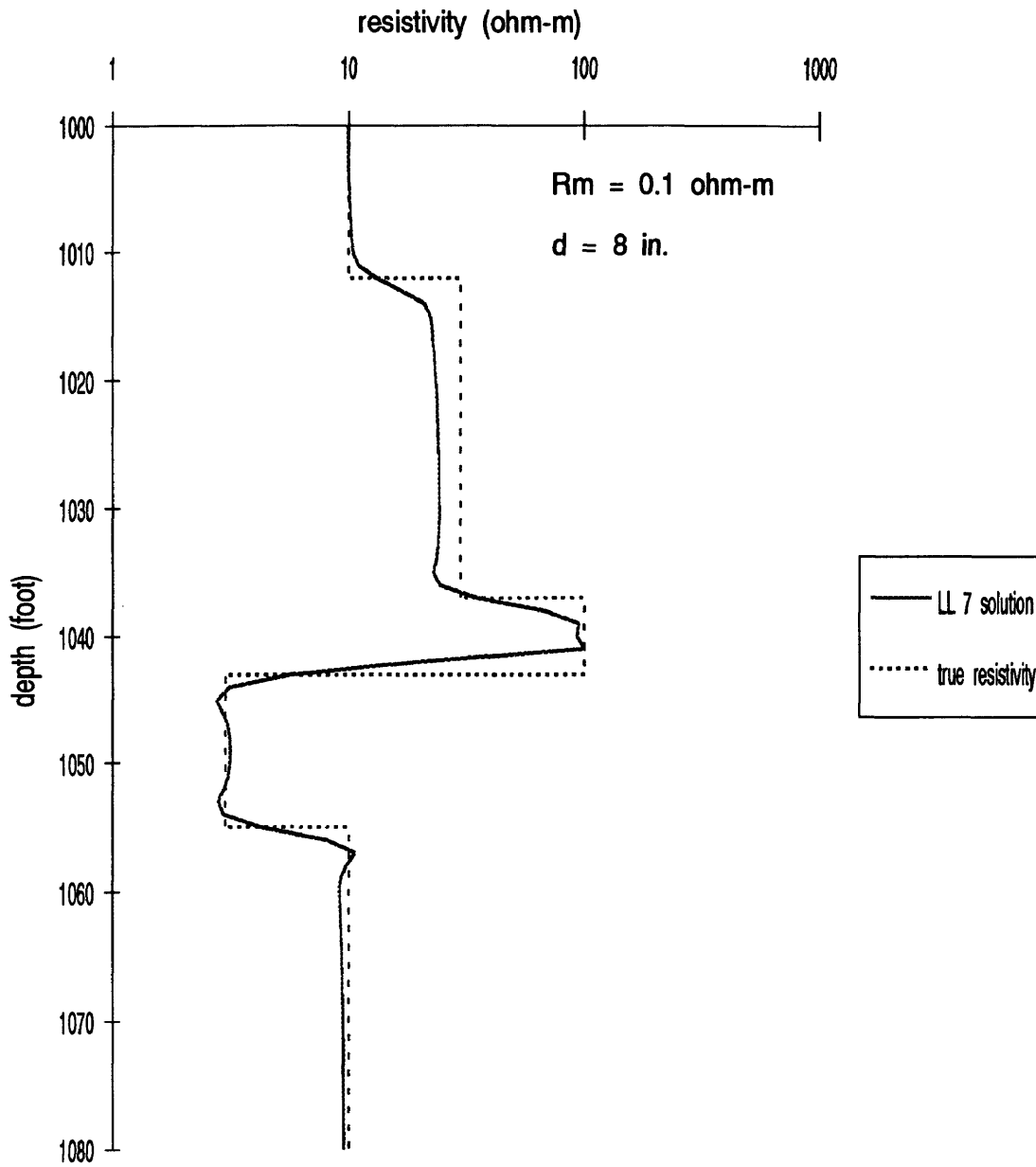


Figure 3.35: The synthetic Laterolog 7 in five layer earth model

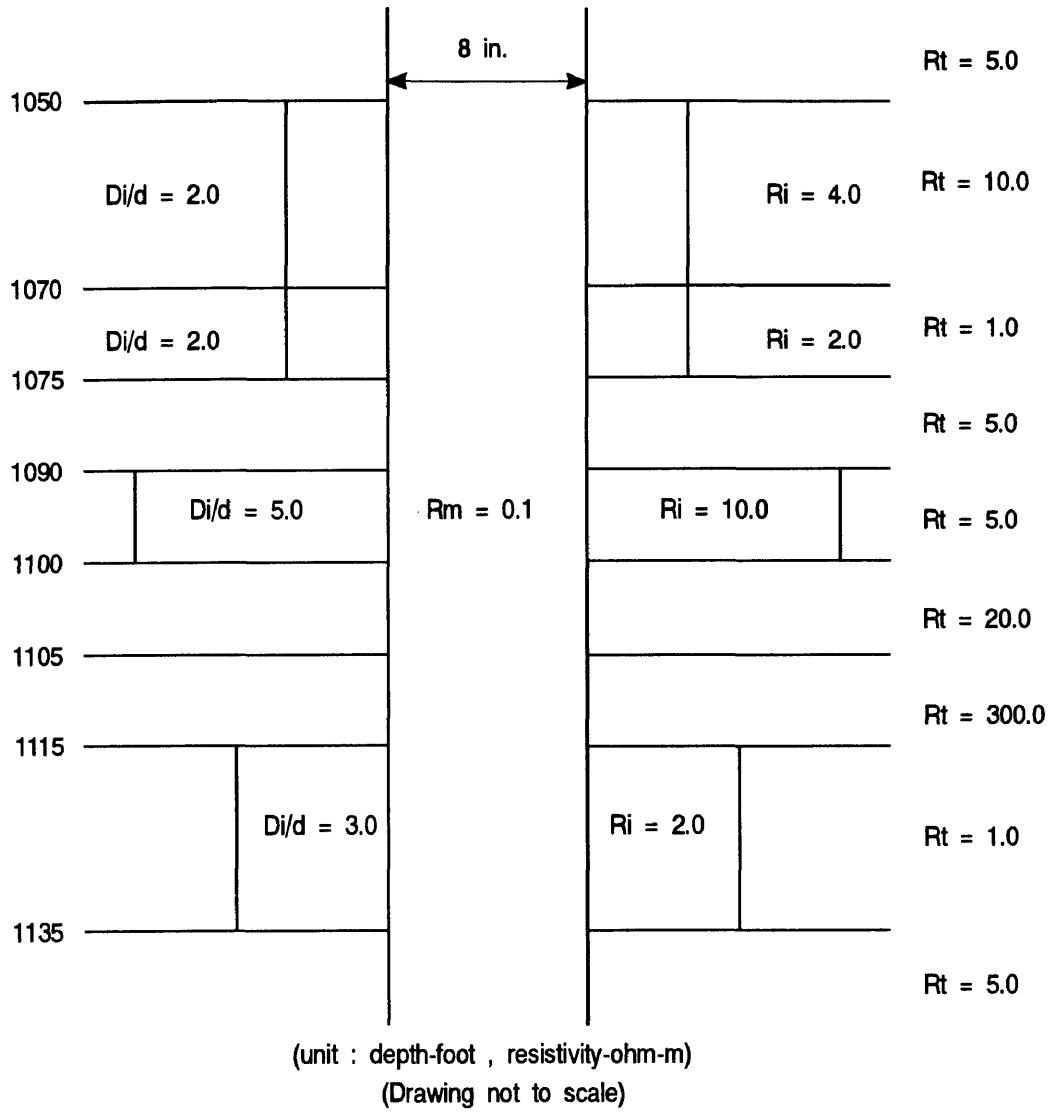


Figure 3.36: Nine layer earth model

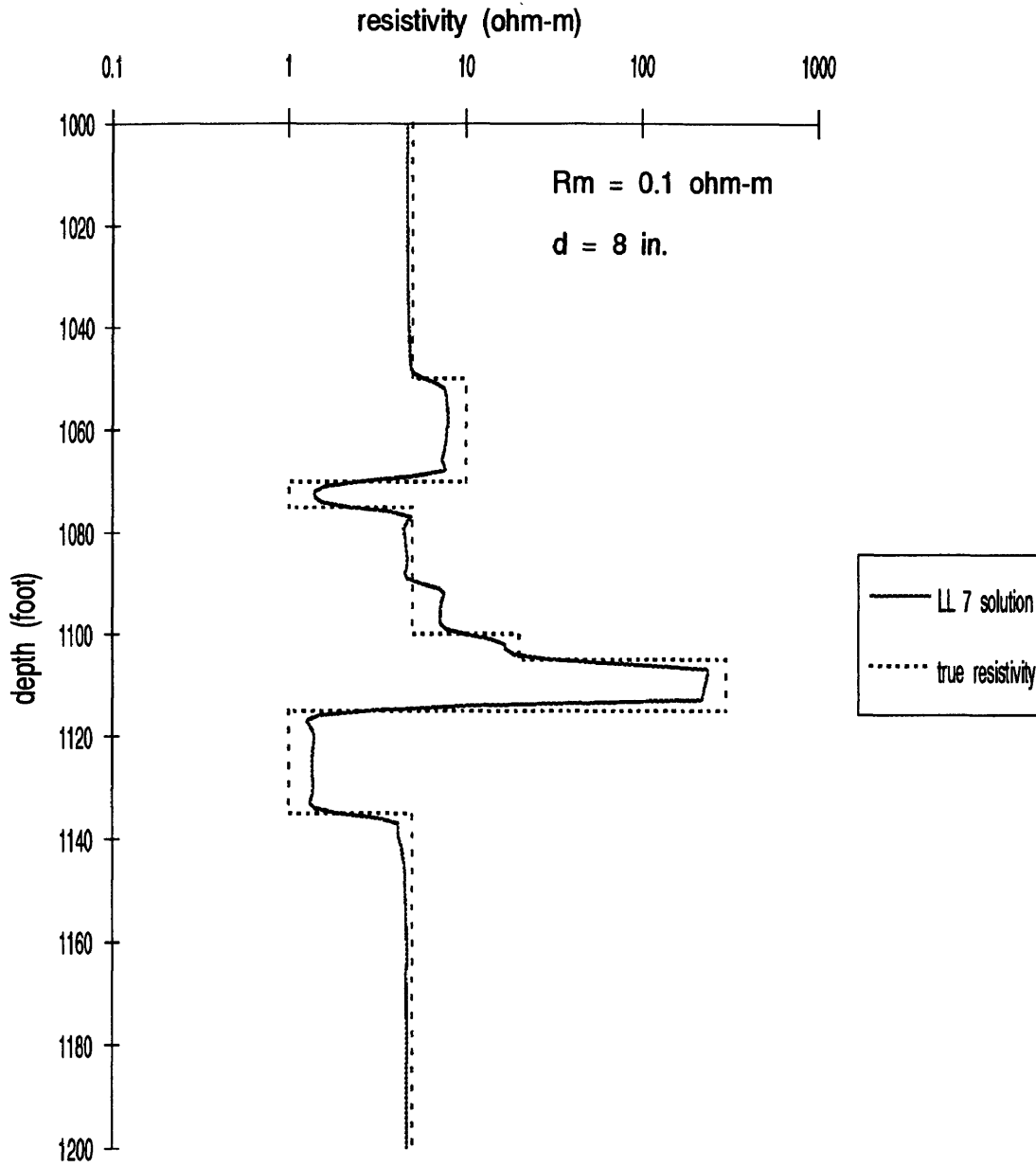


Figure 3.37: The synthetic Laterolog 7 in nine layer earth model

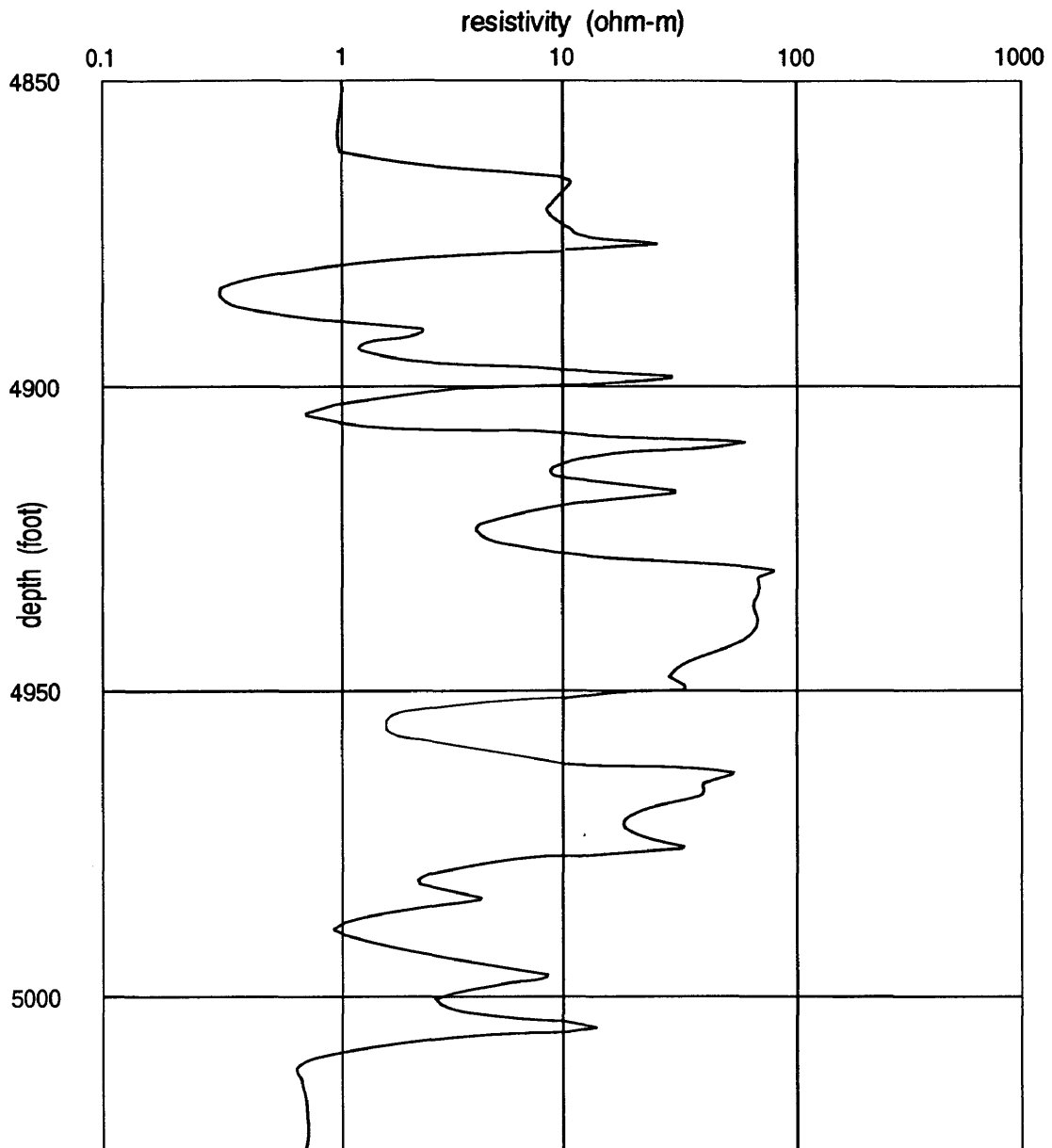


Figure 3.38: A synthetic 6FF40 in 27 layer earth model (from Center for Well-Logging, University of Houston)

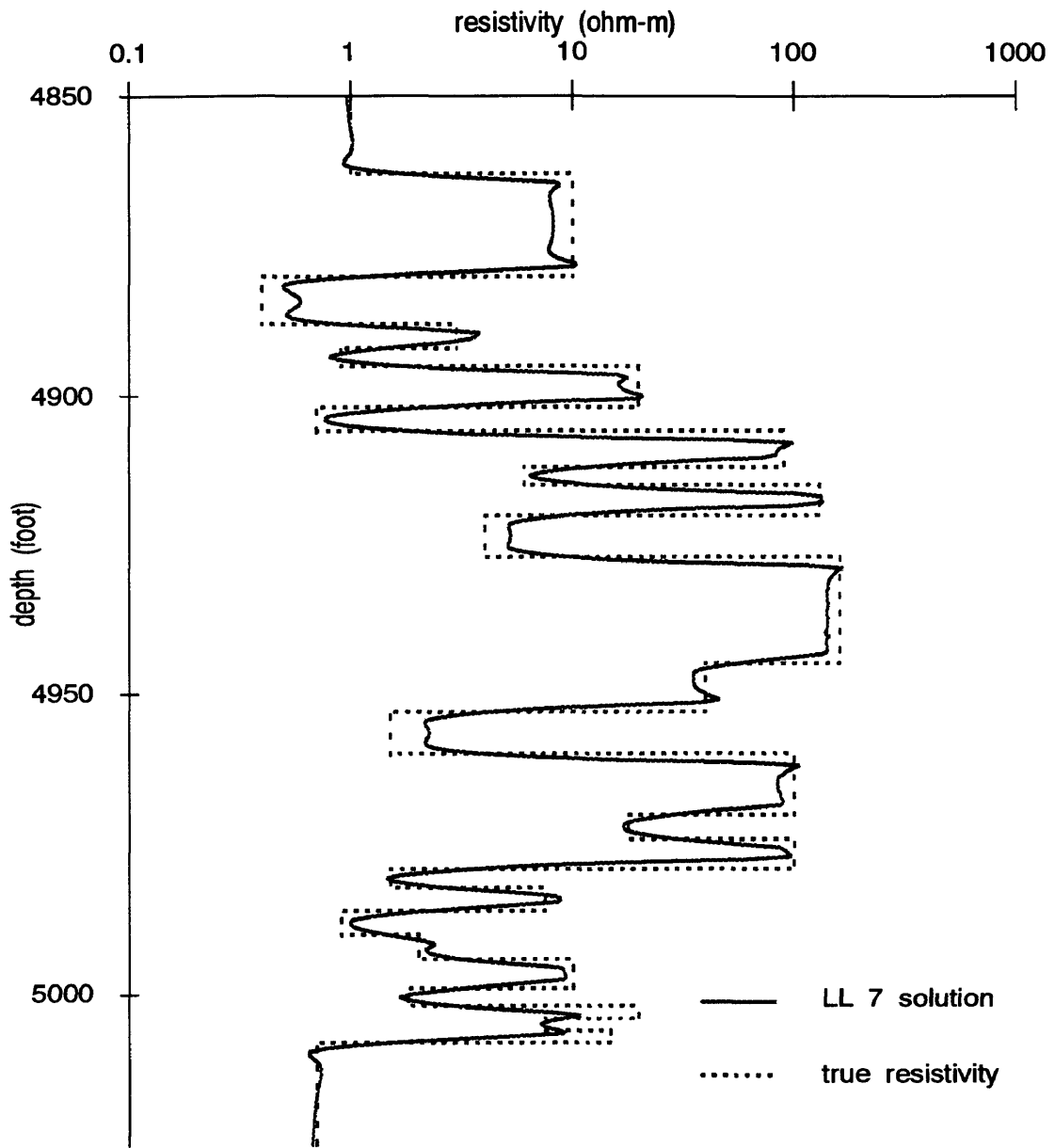


Figure 3.39: The synthetic Laterolog 7 in 27 layer earth model

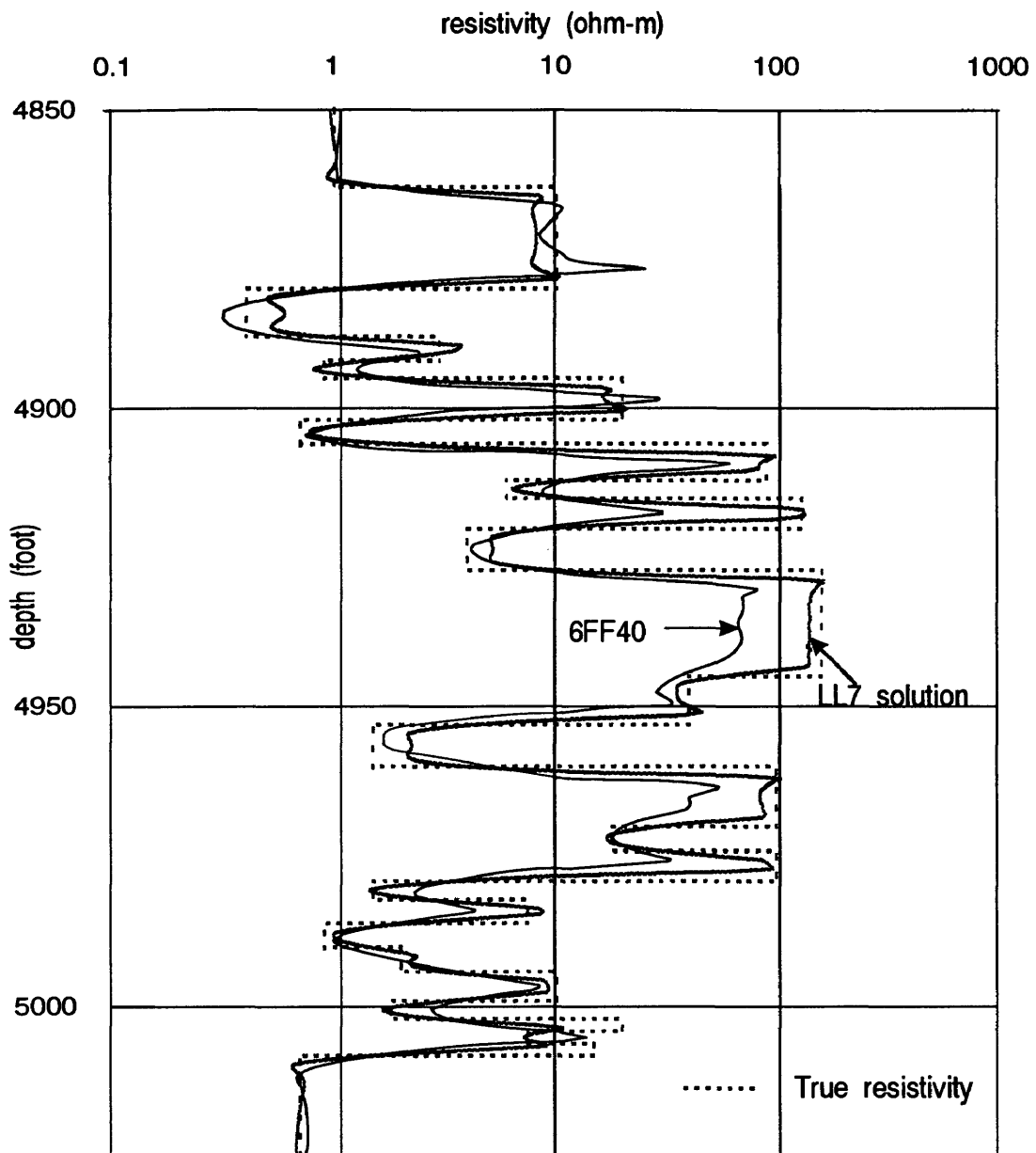


Figure 3.40: Comparison of apparent resistivity curves from 6FF40 tool and the Laterolog 7 tool in this study for Oklahoma benchmark

3.12 Basis of Forward Modeling of the Guard Log

In this section, the basis of forward modeling of the Guard Log will be considered for further studies.

One approach to model the Guard Log electrode approximates the cylindrical tool as a prolate spheroid (Owen and Greer, 1951; Guyod 1964). All equipotential surfaces are assumed to be concentric prolate spheroids and the flow of current is bounded by hyperboloids. This approach ignores the refraction of current at the borehole wall and at the boundaries of invaded zones.

The approach for the Guard Log electrode response in this study is based on a series of electrodes having the same diameter as the electrode (deWitte, L., Fournier, K.P., and Tejada-Flores, H., 1957) . The borehole wall and boundaries of the invaded zones are considered to be cylindrical. The current from each electrode can be calculated from the condition that all electrodes must be at the same potential and the potential distribution can be found by superposition of the fields due to the individual current sources.

In the Laterolog 7 the current from the adjacent electrode is regulated so as to focus the central current essentially into the form of a horizontal current sheet. In the Guard Log there is no such artificial regulation of the current from the adjacent electrodes (guards). Here, the focusing is achieved by maintaining all electrodes at the same potential which is done by simple short circuiting. There will be no tendency

for current to flow from one electrode to the other in the surrounding medium and, therefore, the current must flow laterally in the region of the midpoint of the tool. The longer the guards the farther out the tendency of lateral focusing will be maintained. It is possible to represent the guards by a series of adjacent electrodes and calculate the current that flows from each electrode in order to maintain the same potential at all the electrodes.

To derive the expression for the potential distribution, assume that the cylindrical guard system of length $2L$ and diameter $2a$ is approximated by a series of $2n + 1$ electrodes of radius a . Let the electrodes be equally spaced along the axis of the borehole so that the centers of the two outer electrodes coincide with the intersection of the end planes of the guards and the borehole axis. The centers of two adjacent electrodes are then a distance $s = 2L/2n$ apart (Figure 3.41). Let the current from the central electrode be I_0 , that from each one of the immediately adjacent pair I_1 , that from each one of the following pair I_2 , and so on.

The synthetic focusing method described in Chapter 3.4 can be used to model the Guard Log. Figure 3.42 shows the potential distribution caused by current source I_i in the earth model. The potential distribution curve in Figure 3.42 can be expressed as

$$V_i = a_1 I_i + a_2 I_i + \cdots + a_m I_i = \sum_{k=1}^m a_k I_i \quad (3.22)$$

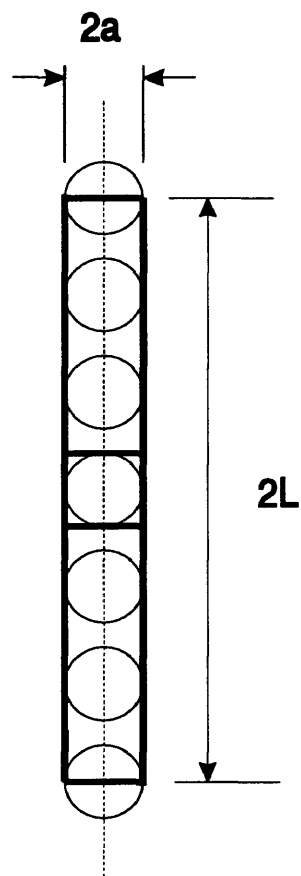


Figure 3.41: Approximation guard electrode by $2n + 1$ electrodes. (In this figure $n = 3$, ratio of diameter to length is exaggerated)

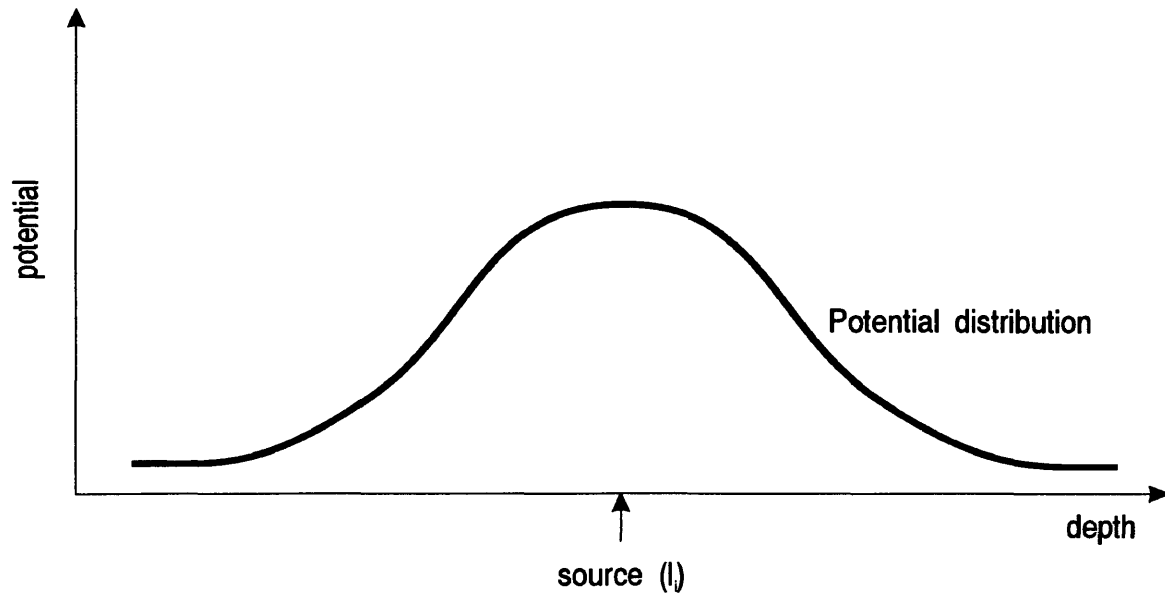


Figure 3.42: Potential distribution caused by I_i

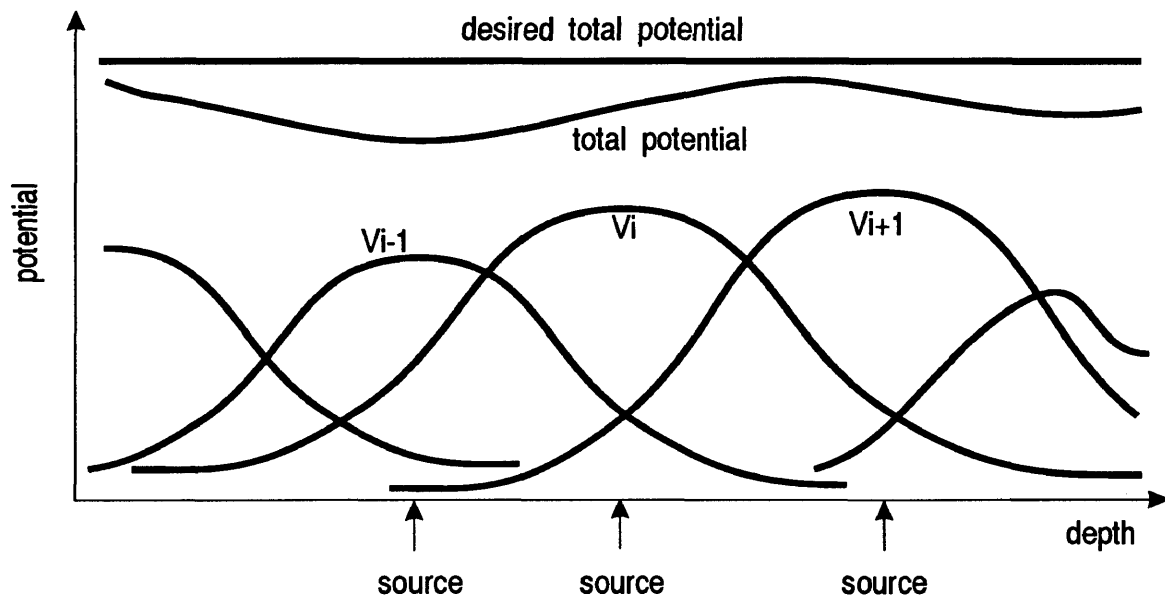


Figure 3.43: Total potential distribution caused by I_0, I_1, \dots, I_n

where $i = 0, \dots, n$, and a_1, a_2, \dots, a_m are the coefficients which have both resistivity information and geometric information of each layer. m represents the m th node position in the vertical axis ($r = 0$) of the grid system.

Figure 3.43 shows the potential distribution caused by current sources I_0, I_1, \dots, I_n in the earth model. The total potential distribution curve can be expressed as

$$V_j = V_0 + c_1 V_1 + \dots + c_n V_n \quad (3.23)$$

where $j = 0, \dots, n$, and c_1, c_2, \dots, c_n are the weighting factors for V_1, V_2, \dots, V_n , respectively, to make the “desired total potential” curve in Figure 3.43.

The condition $V_0 = V_1 = \dots = V_n$ leads to n simultaneous equations with n unknowns c_1, c_2, \dots, c_n . After the n simultaneous equations are solved, the intensities of current $c_1 I_0, c_2 I_0, \dots, c_n I_0$ will be used instead of I_1, I_2, \dots, I_n , respectively. This will satisfy the condition $V_0 = V_1 = \dots = V_n$. This procedure will cause the current to flow laterally from the tool in the region of the central electrode. This is the desired current focusing effect.

Chapter 4

INVERSION OF THE LATEROLOG 7

The purpose of the borehole resistivity data inversion in this study is to determine earth parameters, such as resistivity and boundary of the earth layers, and resistivity and diameter of the invaded zones, from Laterolog 7 log data or from DLL Dual Laterolog-MicroSFL log data. A two dimensional inversion scheme is considered. The two dimensional earth model in this chapter consists of layers separated by plane-parallel boundaries without invaded zones. In other words, the inversion scheme used in this study will yield two earth parameters: resistivity and boundary of earth layer. In order to obtain the resistivity and diameter of invaded zones using an inversion scheme, two more focused logging tools or a multiple-array Laterolog tools are needed.

This two dimensional horizontally layered earth model can be applied to the case where a drill-hole penetrates beds of finite thickness. Once the model is chosen and the earth geometry is defined, apparent resistivities are calculated from the forward modeling program and compared with the observed data. The root-mean-

squares (**rms**) error between the calculated data and the observed data is then found. Then the earth parameters are changed to minimize the **rms** error and new apparent resistivities are calculated from the forward modeling program and compared with the observed data again. This procedure will be repeated for a number of iterations until the desired accuracy is obtained.

Depending on the source and exact procedure, the general inversion process is known variously as *Generalized Linear Inversion*, *Marquardt Inversion*, or *Ridge Regression Analysis*. Mathematically the process is described in detail in Marquardt (1970) and applied to resistivity inversion problems in Inman, Ryu, and Ward (1973) and Inman (1975).

An outline of the general inversion scheme is as follows (Kim, 1986; Whitman, Towle, and Kim, 1989; Whitman, Schön, Towle, and Kim, 1990):

1. define a forward earth model;
2. make an initial guess of earth parameters;
3. minimize the difference between the earth model and available data, which proceeds as follows:
 - (a) approximate earth model with a linear version - use the first two terms of a Taylor series;
 - (b) determine relative sensitivity of the earth model to the various parameters

- take partial derivatives with respect to the earth parameters;
- (c) using the approximate linear model, compute an improved parameter set, making sure that the new earth parameter guess is not “too far” from the preceding, so the Taylor series approximation will be valid;
- (d) check to see if the earth model with the new earth parameters fits the data “adequately”;
- (e) if not, then cycle back to 3(a).

Inman et al. (1973) discussed a problem of direct interpretation of surface resistivity sounding curves for a horizontally layered earth model by using the generalized linear inverse theory. They also discussed the resolution of the model parameters to be determined. Then Inman (1975) applied a ridge regression estimator to the resistivity inversion problem, and discussed a statistical analysis for the estimated parameters. Hoversten, Dey, and Morrison (1982) compared five least-squares inversion techniques in resistivity sounding and found that the ridge regression algorithm required the fewest number of forward calculations to reach the desired convergence criteria. Moreover, Inman (1975) pointed out that the ridge regression estimator is more stable than the generalized linear inversion estimator.

In this study, the Marquardt inversion scheme is used to invert the Laterolog 7 log data. This study investigates a two dimensional inversion of the Laterolog 7 responses for both hypothetical log data and field log data.

4.1 Ridge Regression Estimator

The apparent resistivity of the Laterolog 7 can be evaluated for a given earth model. The M unknown earth parameters \mathbf{P} (vertical and radial boundaries and resistivities of each layer) are related to the measurable quantity C (modeled log responses, see equation 4.1), which is generally a nonlinear functional.

$$C = C(\mathbf{P}, \mathbf{X}), \quad (4.1)$$

where the current estimated values for the model parameters are contained in the vector \mathbf{P} . The vector \mathbf{X} contains the N depth reference points at which the apparent resistivities are measured.

The apparent resistivity, calculated from equation 4.1 is iteratively improved in an attempt to fit the observed data O . The fitting is usually carried out in a least-square sense, which is in turn imposed on a linearized version of the governing model, C .

The basic modeling assumption is that

$$O = C + \epsilon, \quad (4.2)$$

where O represents the observations (actual log), C is the modeled response and ϵ represents all errors (modeling and observational inaccuracies).

The generally nonlinear apparent resistivity model, equation 4.1, is linearized by expansion to reexpress the modeling equation 4.2 in a Taylor series about an initial estimate \mathbf{P}^0 in the parameter space at an earth depth point, resulting in equation 4.3 below. Using a truncated Taylor series in equation 4.2 (neglecting second and higher order terms), yields

$$O(\mathbf{X}, \mathbf{P})_i = C(\mathbf{X}, \mathbf{P}^0)_i + \sum_{j=1}^N \frac{\partial}{\partial P_j} [C(\mathbf{X}, \mathbf{P}^0)_i] (P_j - P_j^0) + \epsilon, \quad (4.3)$$

where $O(\mathbf{X}, \mathbf{P})_i$ is the i th observation, $C(\mathbf{X}, \mathbf{P}^0)_i$ is the modeled value at observation point i for the current estimate of the unknown parameter set \mathbf{P} , $(P_j - P_j^0)$ is the linear estimate of the correction needed in the j th unknown parameter for $j = 1, M$ and $i = 1, N$. Now ϵ represents all errors with the addition of the Taylor series truncation. Rewriting equation 4.3 in matrix notation, we have

$$\Delta \mathbf{G} = \mathbf{A} \Delta \mathbf{P}, \quad (4.4)$$

where

$$\Delta \mathbf{G}_i = O(\mathbf{X}, \mathbf{P})_i - C(\mathbf{X}, \mathbf{P}^0)_i, \quad (4.5)$$

$$A_{ij} = \left. \frac{\partial C(\mathbf{X}, \mathbf{P})_i}{\partial P_j} \right|_{\mathbf{x}=\mathbf{x}_i, \mathbf{P}=\mathbf{P}^0}, \quad (4.6)$$

and

$$\Delta P_j = P_j - P_j^0. \quad (4.7)$$

Equation 4.4 through equation 4.7 represent a system of N linear equations in M unknowns. The \mathbf{A} in equation 4.4 is known as the system matrix and it represents the sensitivities of the calculated values with respect to the small changes in the current estimate of the parameters (Whitman et al, 1989). In the borehole resistivity problem, the system matrix \mathbf{A} is comprised of partial derivatives of the apparent resistivity with respect to the resistivity and thickness (or boundary position) of each vertical and horizontal layer in the current model.

Because the problem is nonlinear and is linearized by expansion in a Taylor series, the solution of equation 4.4 provides only a linear estimate of $\Delta \mathbf{P}$; thus, equation 4.3 is only approximately true for small values of $\Delta \mathbf{P}$.

The ridge regression estimator, $\Delta \mathbf{P}'$, of $\Delta \mathbf{P}$ is

$$\Delta \mathbf{P}' = (\mathbf{A}^T \mathbf{A} + k\mathbf{I})^{-1} \mathbf{A}^T \Delta \mathbf{G}, \quad (4.8)$$

where \mathbf{I} is the identity matrix and $k \geq 0$ (Marquardt, 1970). Equation 4.8 implies that the diagonal elements of $\mathbf{A}^T \mathbf{A}$ are increased in the ridge regression estimator by an amount k . Hence, the inversion of the matrix $(\mathbf{A}^T \mathbf{A} + k\mathbf{I})$, which is frequently ill-conditioned, is more stable than the inversion of matrix $\mathbf{A}^T \mathbf{A}$, the corresponding

matrix in the least-squares solution. It should be noted that, even when $\mathbf{A}^T\mathbf{A}$ is not ill-conditioned, that is, when it is readily invertible, it is necessary to limit the size of $\Delta\mathbf{P}'$ due to the Taylor series approximation. In fact, k provides the limiting effect, where larger k 's correspond to smaller $\Delta\mathbf{P}'$. The underlying idea of the ridge regression estimator is that the $\Delta\mathbf{P}'$ minimizes the sum of squares of residuals (disparities between the model and observations)

$$\Phi(\Delta\mathbf{P}') = (\Delta\mathbf{G} - \mathbf{A}\Delta\mathbf{P}')^T(\Delta\mathbf{G} - \mathbf{A}\Delta\mathbf{P}') \quad (4.9)$$

on the sphere whose squared radius is $\Delta\mathbf{P}'^T\Delta\mathbf{P}'$. The best vector direction for efficiently finding a minimum residual sum of squares on the least-squares loss surface lies somewhere between the direction given by the Taylor series increment ($k = 0$) and the direction of the steepest descent ($k = \infty$).

An important consideration in the ridge regression estimator is the choice of suitable values of k , so that the residual sum of squares is minimized. This damping factor k can be obtained by inserting various values of k into equation 4.9, plotting the residual sum of squares versus k , and using the k corresponding to the minimum (Marquardt, 1970). The current earth parameters are then replaced by the new parameters corresponding to the value of k which yields a minimum error between the observed and the calculated data. The new parameter set \mathbf{P} is obtained from the relation.

$$\mathbf{P} = \mathbf{P}^0 + \Delta\mathbf{P}. \quad (4.10)$$

In this way, the new earth parameter \mathbf{P} yields a new apparent resistivity curve that presumably better fits the field data. The parameter \mathbf{P} obtained in equation 4.10 now replaces the old parameter \mathbf{P}^0 and the procedure continues until a solution is obtained. Generally, with each iteration the value of k is reduced. At the initial stage of the inversion process, k has a relatively large value; this corresponds to fitting the broad aspects of the data, and as the iterations goes on, the smaller values of k allow the finer details to be fit. The process of choosing k is automated.

4.2 Parameter Resolution and Statistics

The ridge regression estimator of the unknown parameter changes $\Delta\mathbf{P}$ is obtained from equation 4.8, and the new parameter estimates are calculated by using equation 4.10. Once the final estimates are obtained, earth parameters can be analyzed qualitatively through the resolution matrix (Inman et al., 1973). The accuracy of the final model fit can be analyzed by using χ^2 goodness of fit statistics.

Multiplying equation 4.4 by \mathbf{A}^T , the substitution for $\mathbf{A}^T\Delta\mathbf{G}$ in equation 4.8 yields

$$\Delta\mathbf{P}' = (\mathbf{A}^T\mathbf{A} + k\mathbf{I})^{-1}\mathbf{A}^T\mathbf{A}\Delta\mathbf{P} = \mathbf{R}\Delta\mathbf{P}, \quad (4.11)$$

where the matrix \mathbf{R} is referred to as the resolution matrix. Equation 4.11 shows that the estimated parameter changes $\Delta P'_j$ are linearly related to the unknown parameter changes ΔP_j . If the model is overconstrained ($N > M$), as is almost always the case, and the rank of the system matrix \mathbf{A} is near the number of unknown parameters, then the resolution matrix will approximate the identity matrix (Inman et al., 1973). This would imply that the parameters are “well resolved.” If on the other hand a diagonal element of the resolution matrix is substantially less than one (also implying that there are non-diagonal elements in the same row significantly greater than zero), then the parameter corresponding to that row will be relatively poorly resolved. More specifically, the resolution of a particular parameter, \mathbf{P}_j , is seen by the “delta-likeness” of the j th row of \mathbf{R} . Thus, if only the diagonal element jj is sizable, the parameter is well resolved, whereas a spread of numbers indicates that \mathbf{P}_j is “confused” with those parameters corresponding to columns having significant off-diagonal size; for example, if the ij th position is significant in size, \mathbf{P}_j is confused with \mathbf{P}_i . The interpretation of this is that the data are inadequate to decide whether an effect is due to \mathbf{P}_j or \mathbf{P}_i .

Convergence of the general algorithm is usually within a few iterations, depending on the complexity of the model. Due to the nonuniqueness of the inverse problems, the estimated earth model generally may be different from the true earth. However, if the interpreter makes a decent initial guess consistent with local geologic style, then it can be expected that the estimated earth model will also be reasonable.

4.3 Particulars for the Log Inversion

In the problem of borehole resistivity data inversion for the Laterolog 7, a weighted least-squares scheme is used. Recognizing the tendency of absolute error for a resistivity log to increase with absolute instrument reading, a logarithmic weighting (Rijo, Peltonm Feitosa, and Ward, 1977) is used. In this weighting scheme, the function to be minimized in the least-squares sense is

$$(\Delta G)^2 = \sum_{i=1}^N [\log O_i - \log C_i]^2. \quad (4.12)$$

This scheme weights the data unequally, reducing the normally strong emphasis on large deviations of the model from the data. With the logarithmic weighting the system matrix \mathbf{A} and the perturbing equation 4.10 are then replaced by

$$A_{ij} = \left. \frac{\partial \log C(\mathbf{X}, \mathbf{P})_i}{\partial \log P_j} \right|_{\mathbf{x}=\mathbf{x}_i, \mathbf{P}=\mathbf{P}^0}, \quad (4.13)$$

and $\mathbf{P} = \mathbf{P}^0 \times 10^{\Delta \mathbf{P}'}$.

The rms log error is derived from

$$E(\text{rmslog}) = [(\Delta G)^2 / N]^{0.5}, \quad (4.14)$$

and the percent error can be calculated by using the relation

$$E(\%) = 100 \times 10^{(E(\text{rmslog})-1)}. \quad (4.15)$$

The estimation of data variance for the logarithmically weighted least-squares fit can be obtained from the reduced chi square (χ^2) (Hoversten et al., 1982; Yang and Ward, 1984)

$$\chi^2 = \frac{\Delta \mathbf{G}^T \mathbf{W}^T \mathbf{W} \Delta \mathbf{G}}{N - M}, \quad (4.16)$$

where

$$W_{ij} = \begin{cases} \log O_i - \log C_i & \text{for } i = j \\ 0 & \text{for } i \neq j \end{cases} \quad (4.17)$$

and $(N - M)$ represents the degrees of freedom.

The inversion algorithm will be repeated for a predetermined number of iterations, or until the difference between the minimum error of the two successive iterations is less than a desired value, or until the new error is less than a predetermined error tolerance.

4.4 Test Results

In this section, two dimensional inversion schemes are tested for both hypothetical and field log data. In the case of hypothetical log data, two model types are

considered:

1. relatively resistive object beds and,
2. relatively conductive object beds.

Three bed thicknesses are investigated with each type to include thick bed, critically thick bed, and thin bed. In this section, the thick bed is 12 feet thick, the critically thick bed is 6.67 feet (80 inches) thick, and the thin bed is 3.33 feet (40 inches) thick, respectively. The critically thick bed has the thickness which is equal to the Laterolog 7 electrode spacing.

In the hypothetical approach, Figure C.1 through Figure C.6 in Appendix C are related to relatively conductive beds, and Figure C.7 through Figure C.12 in Appendix C are related to relatively resistive beds. In the field approach, one field log data is inverted.

Using an initial guess earth model, both the hypothetical and the field log data are inverted. The inverted solution which is the output of the inversion program is called the best fit earth model. The best fit earth model is used to produce the best fit log data using the forward modeling program. Then the hypothetical and the field log data and the best fit log data are compared in order to check the accuracy of the Laterolog 7 inversion program of this study.

4.4.1 Two Dimensional Inversion of Hypothetical Log Data

In general, from the results of the forward modeling scheme, it is more difficult to guess the depth of a bed boundary than to guess the resistivity value, especially if there are several thin layers in the earth model. Hence, the initial guess resistivity values which are used in this study deviate approximately 10 percent from the true resistivity values, and the initial guess boundary depths deviate more than 10 percent from the true boundary depths.

In order to terminate the program after achieving good results, there are three criteria for stopping the inversion program.

1. If the inversion program reaches a predetermined number of iteration, the inversion program will stop. In this study, the predetermined number is set to ten.
2. At the end of an iteration if the new root-mean-square error is greater than the old root-mean-square error, the inversion program will stop.
3. If the ϵ is less than 5×10^{-2} , the inversion program will stop. This ϵ value is obtained by a trial-and error method and is related to the root-mean-square ohm-m disparity between the inverted log and the actual log.

Figure C.1 through Figure C.12 (or Figure 4.1 through Figure 4.6) show the results for thick, critically thick, thin hypothetical conductive and resistive earth

models.

Thick Conductive Case

Figure 4.1 (or Figure C.1) illustrates the hypothetical earth model, the initial guess earth model, and the best fit earth model resulting from inversion for the thick conductive case. Table 4.4.1 shows the changes of depth of bed boundary and resistivity of each layer at each iteration in the inversion process. Table 4.4.1 also shows the values of the hypothetical model and the diagonal elements of the resolution matrix, which indicates a good fit. Figure C.2 also shows good agreement between the hypothetical log data and the best fit log data.

Critically Thick Conductive Case

Figure 4.2 (or Figure C.3) illustrates the hypothetical earth model, the initial guess earth model, and the best fit earth model resulting from inversion for the critically thick conductive case. Table 4.4.1 shows the changes of depth of bed boundary and resistivity of each layer at each iteration in the inversion process. Table 4.4.1 also shows the values of the hypothetical model and the diagonal elements of the resolution matrix, which indicates a good fit. Figure C.4 also shows good agreement between the hypothetical log data and the best fit log data.

Table 4.1: The change of depth and resistivity at each iteration in the inversion process (Thick - Conductive Case)

# of iteration	depth		resistivity			rms error
	Boundary 1	Boundary 2	Bed 1	Bed 2	Bed 3	
0	992.00	1008.00	110.00	9.00	110.00	
1	992.76	1007.62	109.99	9.25	105.01	27.2
2	993.50	1007.19	109.36	9.42	105.08	18.9
3	993.92	1006.75	106.04	9.44	101.36	12.1
4	993.90	1006.38	93.34	10.85	92.76	3.0
5	993.95	1006.00	96.52	11.05	93.72	2.5
6	993.94	1006.00	96.84	11.05	96.24	1.9
7	993.97	1006.02	96.33	10.77	98.75	1.2
8	993.96	1006.05	96.68	10.82	99.10	0.9
9	993.96	1006.05	97.14	10.82	99.00	1.0
hypothetical	994.00	1006.00	100.00	10.00	100.00	
resolution diagonal	0.98	0.98	0.99	0.99	0.99	

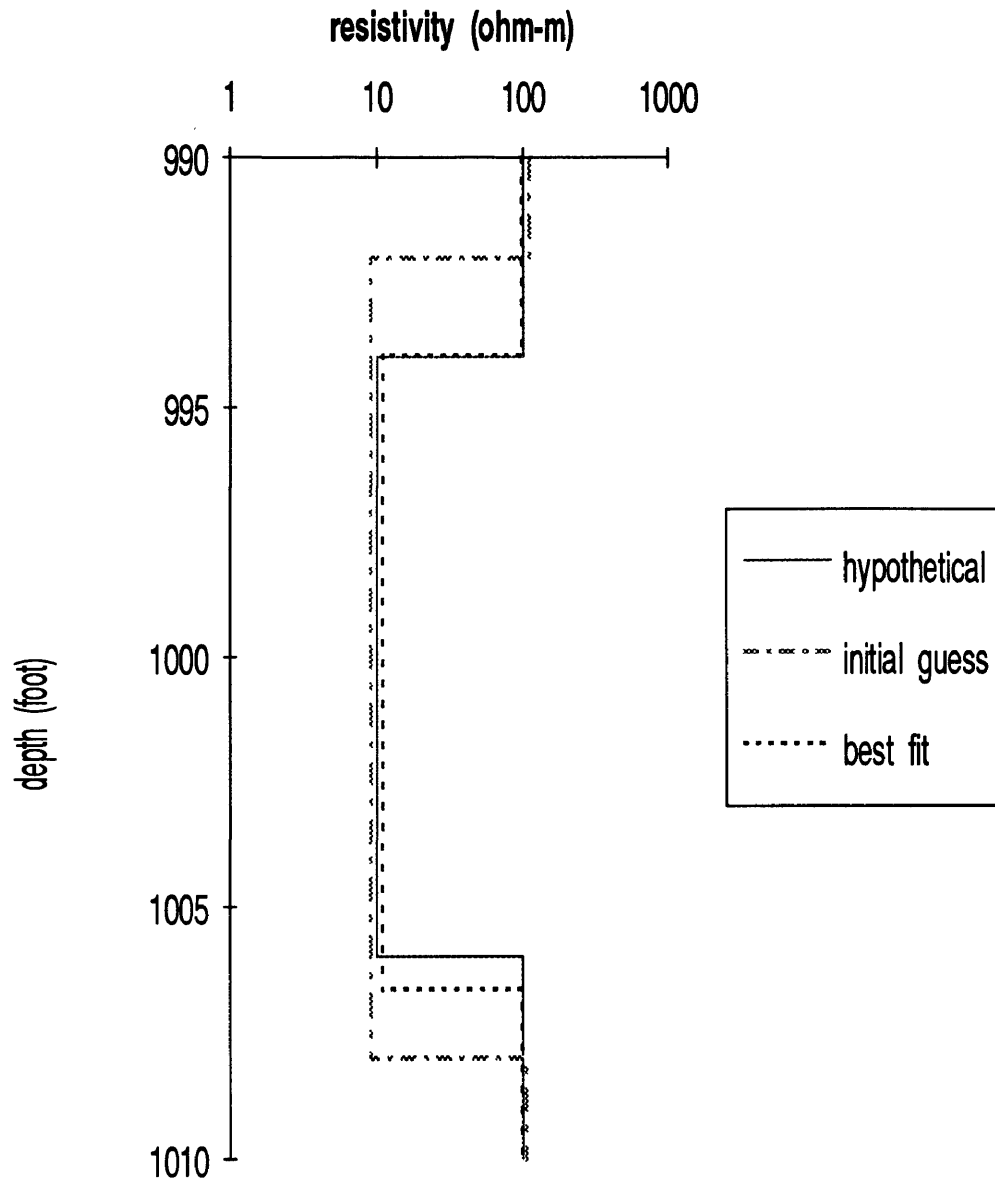


Figure 4.1: Comparison of hypothetical earth model, initial guess earth model, and best fit earth model (Thick - Conductive Case)

Table 4.2: The change of depth and resistivity at each iteration in the inversion process (Critically Thick - Conductive Case)

# of iteration	depth		resistivity			rms error
	Boundary 1	Boundary 2	Bed 1	Bed 2	Bed 3	
0	995.00	1005.00	110.00	9.00	105.00	
1	995.64	1004.56	109.86	8.75	104.84	24.5
2	996.21	1004.17	109.04	9.25	104.37	15.9
3	996.61	1003.83	108.24	9.18	102.94	9.8
4	996.65	1003.64	107.15	9.26	103.81	7.7
5	996.64	1003.54	103.66	9.75	102.84	5.2
6	996.65	1003.48	100.52	9.99	102.39	3.6
7	996.69	1003.40	100.37	9.71	102.63	4.0
8	996.68	1003.46	100.10	9.71	102.29	4.0
9	996.66	1003.48	99.73	9.74	102.73	3.9
hypothetical	996.67	1003.33	100.00	10.00	100.00	
resolution diagonal	0.98	0.97	0.99	0.98	0.99	

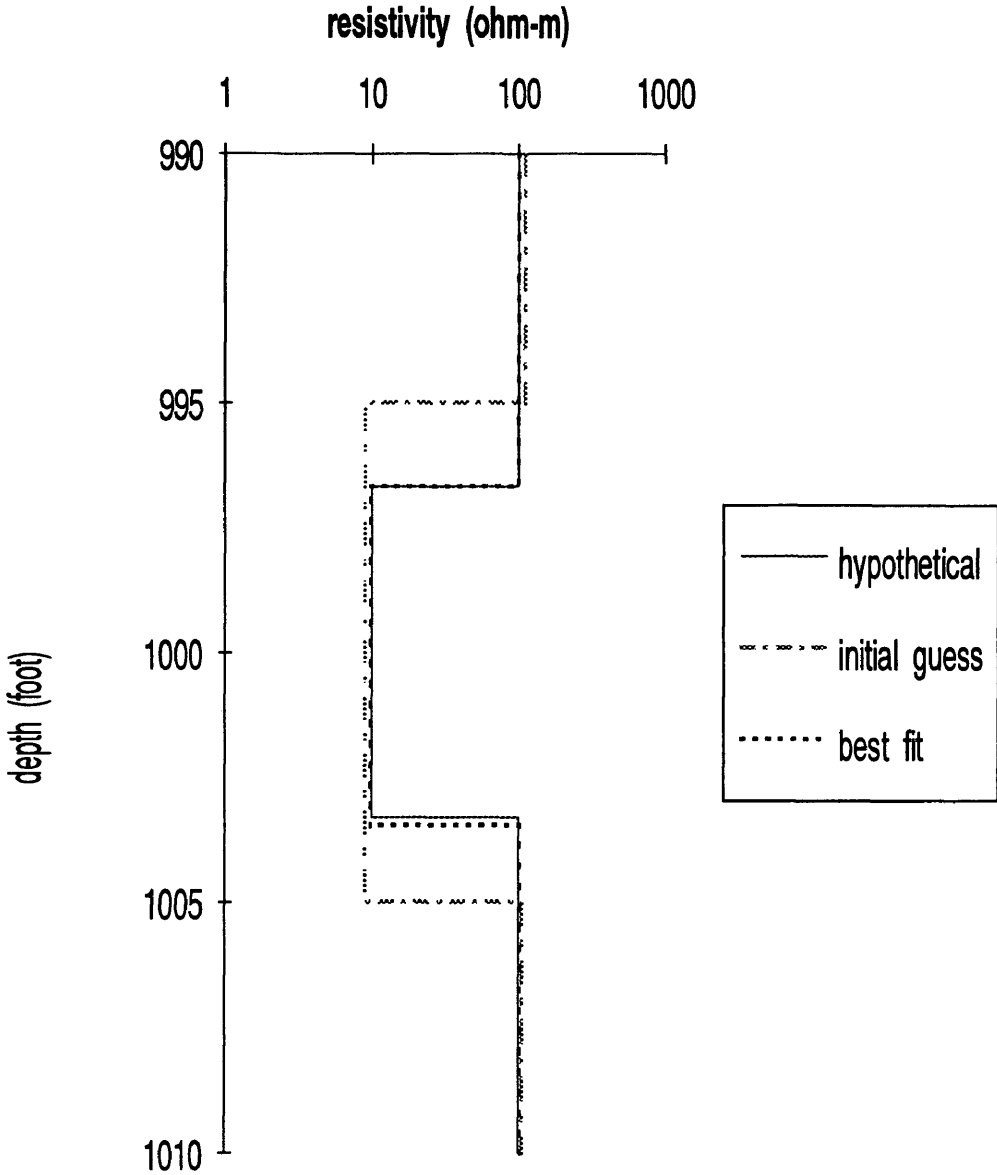


Figure 4.2: Comparison of hypothetical earth model, initial guess earth model, and best fit earth model (Critically Thick - Conductive Case)

Table 4.3: The change of depth and resistivity at each iteration in the inversion process (Thin - Conductive Case)

# of iteration	depth		resistivity			rms error
	Boundary 1	Boundary 2	Bed 1	Bed 2	Bed 3	
0	997.00	1003.00	110.00	9.00	105.00	
1	997.67	1002.67	109.84	9.26	104.77	20.4
2	998.11	1002.27	109.34	9.69	104.13	12.8
3	998.26	1002.01	108.80	9.57	104.03	9.8
4	998.29	1001.94	105.34	9.66	103.88	8.0
5	998.31	1001.80	102.99	9.98	101.26	5.2
6	998.28	1001.78	102.05	10.19	100.80	4.2
7	998.30	1001.70	99.71	10.54	100.62	3.0
8	998.29	1001.72	99.70	10.59	100.77	3.2
9	998.28	1001.74	99.80	10.69	100.79	3.2
hypothetical	998.33	1001.67	100.00	10.00	100.00	
resolution diagonal	0.97	0.98	0.98	0.99	0.99	

Thin Conductive Case

Figure 4.3 (or Figure C.5) illustrates the hypothetical earth model, the initial guess earth model, and the best fit earth model resulting from inversion for the thin conductive case. Table 4.4.1 shows the changes of depth of bed boundary and resistivity of each layer at each iteration in the inversion process. Table 4.4.1 also shows the values of the hypothetical model and the diagonal elements of the resolution matrix, which indicates a good fit. Figure C.6 also shows good agreement between the hypothetical log data and the best fit log data.

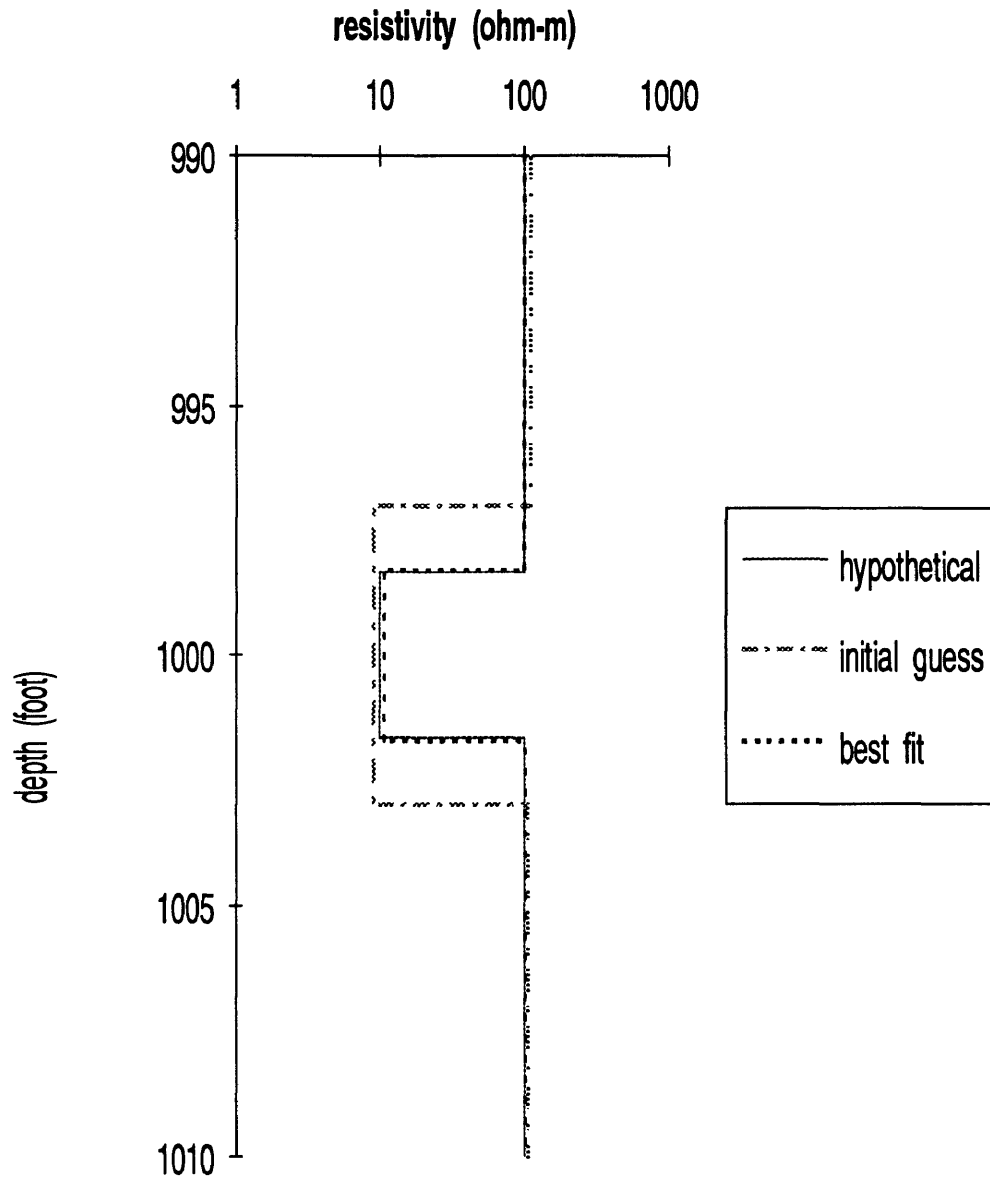


Figure 4.3: Comparison of hypothetical earth model, initial guess earth model, and best fit earth model (Thin - Conductive Case)

Table 4.4: The change of depth and resistivity at each iteration in the inversion process (Thick - Resistive Case)

# of iteration	depth		resistivity			rms error
	Boundary 1	Boundary 2	Bed 1	Bed 2	Bed 3	
0	992.00	1008.00	9.00	105.00	11.00	
1	992.97	1007.45	8.40	104.04	9.50	22.4
2	993.67	1006.96	8.69	98.61	8.93	12.4
3	993.97	1006.53	9.76	94.27	9.11	6.9
4	993.91	1006.18	8.74	96.38	10.61	3.0
5	993.97	1005.99	8.62	97.97	10.43	0.9
6	993.99	1005.98	8.82	98.36	10.35	0.7
7	993.99	1005.98	9.02	98.53	10.11	0.6
8	994.00	1005.98	9.14	98.60	10.10	0.6
9	994.01	1005.98	9.32	98.36	10.11	0.5
hypothetical	994.00	1006.00	10.00	100.00	10.00	
resolution diagonal	0.99	0.99	1.00	0.99	1.00	

Thick Resistive Case

Figure 4.4 (or Figure C.7) illustrates the hypothetical earth model, the initial guess earth model, and the best fit earth model resulting from inversion for the thick resistive case. Table 4.4.1 shows the changes of depth of bed boundary and resistivity of each layer at each iteration in the inversion process. Table 4.4.1 also shows the values of the hypothetical model and the diagonal elements of the resolution matrix, which indicates a good fit. Figure C.8 also shows good agreement between the hypothetical log data and the best fit log data.

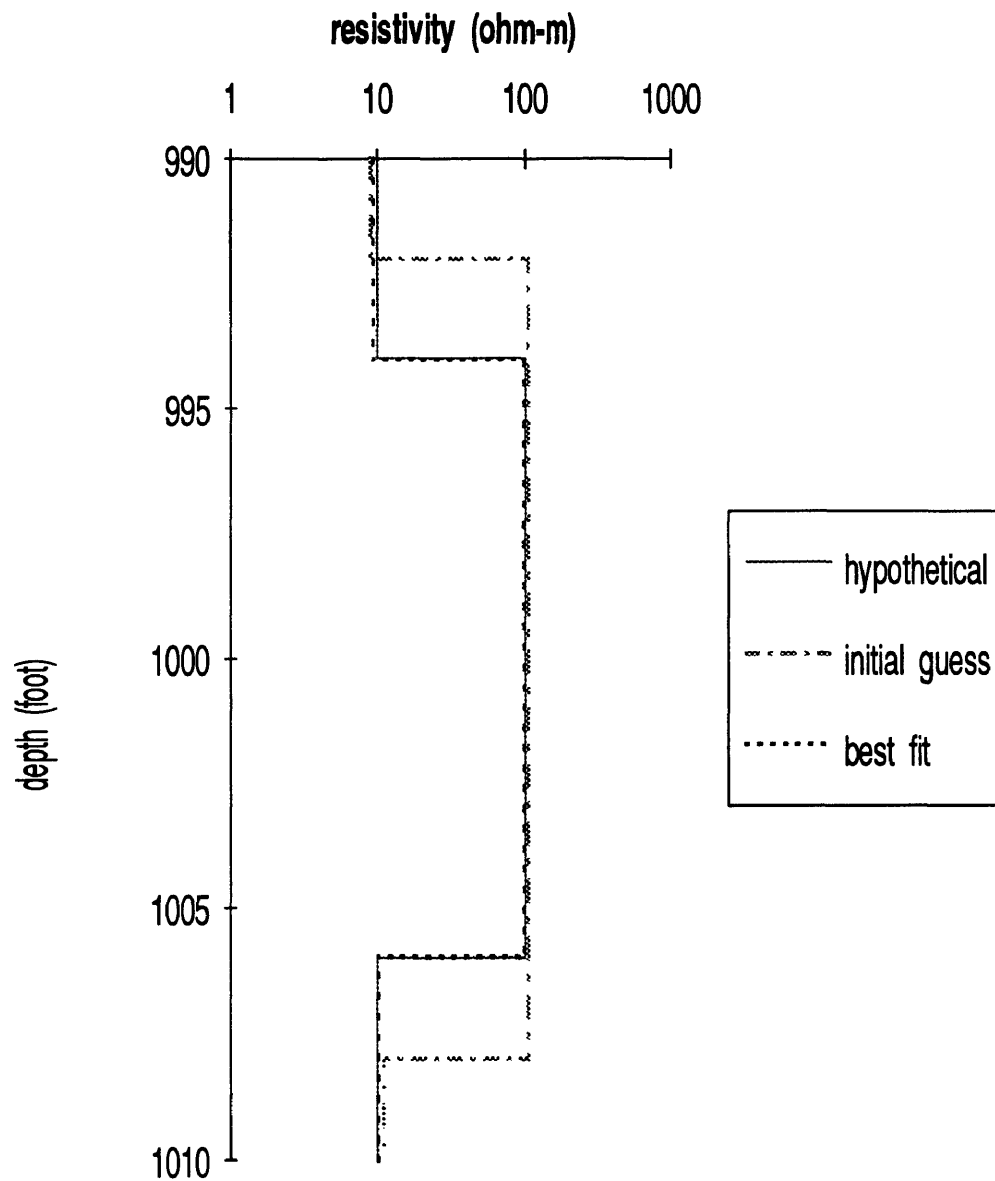


Figure 4.4: Comparison of hypothetical earth model, initial guess earth model, and best fit earth model (Thick - Resistive Case)

# of iteration	depth		resistivity			rms error
	Boundary 1	Boundary 2	Bed 1	Bed 2	Bed 3	
0	995.00	1005.00	9.00	105.00	11.00	
1	995.87	1004.48	8.71	104.26	11.45	18.8
2	996.65	1004.05	11.39	100.86	8.66	9.4
3	996.56	1003.85	8.80	93.75	7.03	5.8
4	996.62	1003.49	9.07	92.21	9.25	2.9
5	996.64	1003.38	8.93	97.57	9.27	1.0
6	996.68	1003.34	9.27	99.50	9.56	0.6
7	996.66	1003.33	9.64	98.33	9.57	0.3
8	996.68	1003.33	9.63	98.88	9.74	0.3
9	996.67	1003.33	9.74	98.26	9.73	0.2
hypothetical	996.67	1003.33	10.00	100.00	10.00	
diagonal coefficient	0.98	0.99	0.99	0.99	0.99	

Table 4.5: The change of depth and resistivity at each iteration in the inversion process (Critically Thick - Resistive Case)

Critically Thick Resistive Case

Figure 4.5 (or Figure C.9) illustrates the hypothetical earth model, the initial guess earth model, and the best fit earth model resulting from inversion for the critically thick resistive case. Table 4.5 shows the changes of depth of bed boundary and resistivity of each layer at each iteration in the inversion process. Table 4.5 also shows the values of the hypothetical model and the diagonal elements of the resolution matrix, which indicates a good fit. Figure C.10 also shows good agreement between the hypothetical log data and the best fit log data.

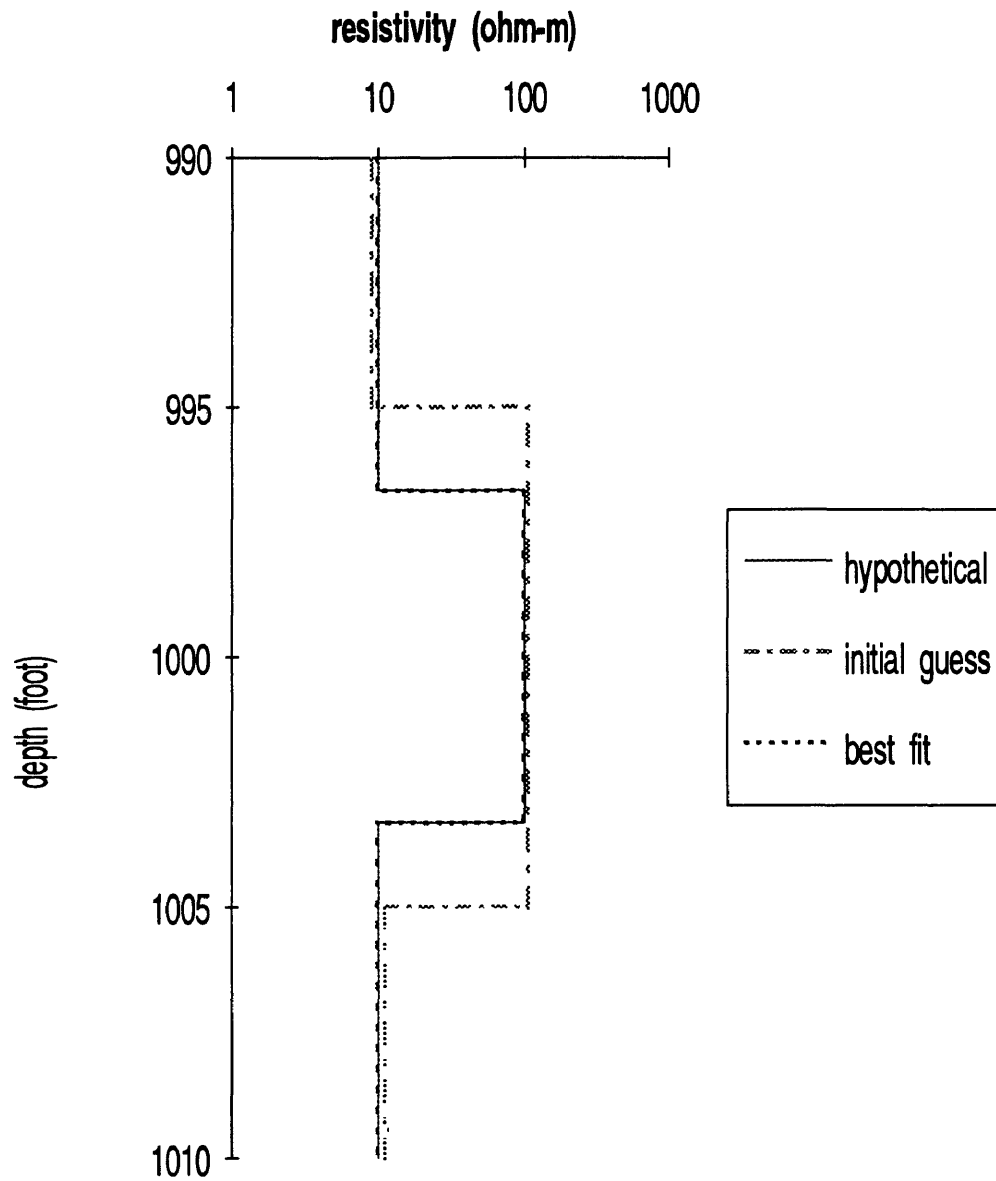


Figure 4.5: Comparison of hypothetical earth model, initial guess earth model, and best fit earth model (Critically Thick - Resistive Case)

# of iteration	depth		resistivity			rms error
	Boundary 1	Boundary 2	Bed 1	Bed 2	Bed 3	
0	997.00	1003.00	9.00	105.00	11.00	
1	997.75	1002.51	8.98	104.40	10.93	14.8
2	998.24	1002.04	6.54	102.03	11.01	8.0
3	998.34	1001.66	9.41	94.58	11.11	2.3
4	998.42	1001.51	10.40	94.38	10.26	0.6
5	998.40	1001.53	10.51	94.34	10.01	0.6
6	998.42	1001.52	10.51	96.00	10.03	0.6
7	998.40	1001.53	10.52	94.04	10.02	0.6
8	998.42	1001.52	10.51	96.14	10.04	0.6
9	998.39	1001.53	10.49	93.31	10.01	0.6
hypothetical	998.33	1001.67	10.00	100.00	10.00	
diagonal coefficient	0.98	0.98	0.99	0.98	0.99	

Table 4.6: The change of depth and resistivity at each iteration in the inversion process (Thin - Resistive Case)

Thin Resistive Case

Figure 4.6 (or Figure C.11) illustrates the hypothetical earth model, the initial guess earth model, and the best fit earth model resulting from inversion for the thin resistive case. Table 4.6 shows the changes of depth of bed boundary and resistivity of each layer at each iteration in the inversion process. Table 4.6 also shows the values of the hypothetical model and the diagonal element of the resolution matrix, which indicates a good fit. Figure C.12 also shows good agreement between the hypothetical log data and the best fit log data.

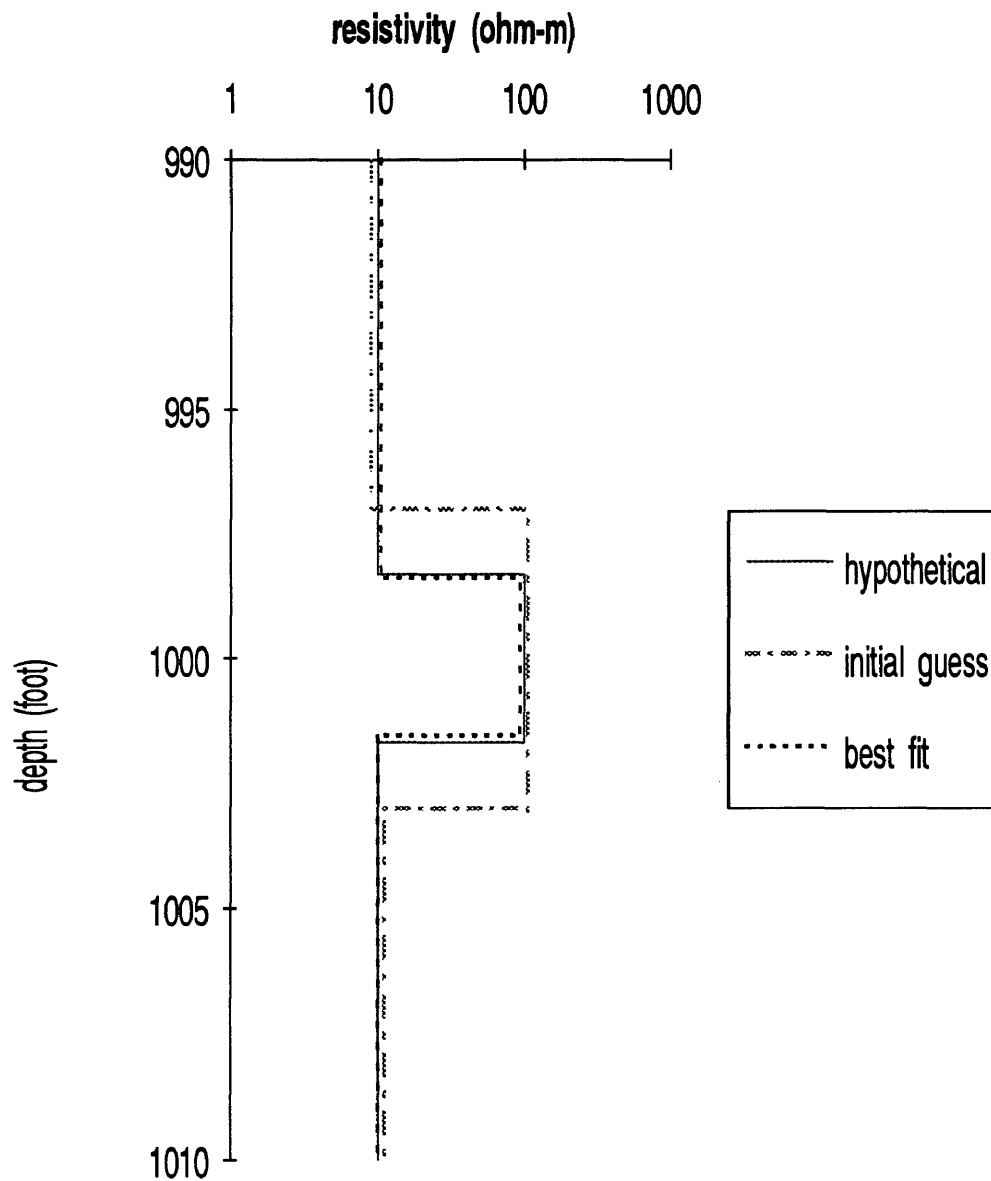


Figure 4.6: Comparison of hypothetical earth model, initial guess earth model, and best fit earth model (Thin - Resistive Case)

General Conclusions for Hypothetical Earth Model Inversion

From the Figure 4.1 through Figure 4.6, the depths of the bed boundary and the resistivities of each layer in the best fit earth model are very close to the those of the hypothetical earth model with the given initial guess earth model. Moreover, for all even numbered Figures between Figure C.2 and Figure C.12 in Appendix C, the hypothetical log shows the good agreement with the best fit log in all cases.

The rms errors in conductive bed cases are usually greater than those in resistive bed cases as shown in Table 4.4.1 through Table 4.6. This means that the forward modeling and inverse modeling programs for the Laterolog 7 work somewhat better in the resistive cases than in the conductive cases.

4.4.2 Two Dimensional Inversion of Field Log Data

A segment of a field log to be inverted for an earth model is shown in Figure 4.7 (Asquith, 1983). The digitized log, the initial earth model, and the best fit earth model are shown in Figure 4.8. The digitized log and the best fit log are shown in an expanded depth scale in Figure 4.9. The segment from 4000 feet to 4020 feet is chosen and an eight-layer initial guess model is considered. The borehole diameter is 7.875 inches, and the mud resistivity is 0.11 ohm-m.

In Figure 4.8, the initial guess earth model has one layer between 4008 feet and 4010 feet. But after inversion, this layer has almost disappeared. Two logs over

this interval from 4000 to 4020 feet in Figure 4.9 show good agreement. From the above observations, the inversion program of this study works well.

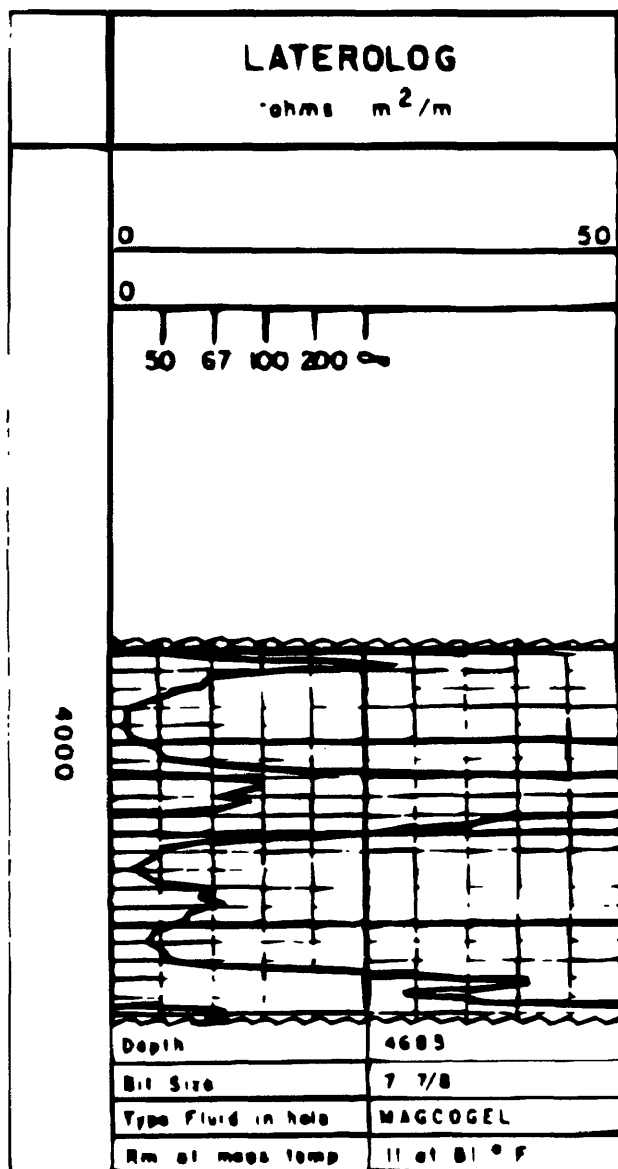


Figure 4.7: A segment of the Laterolog 7 log to be inverted to a one dimensional model (after George Asquith, 1983)

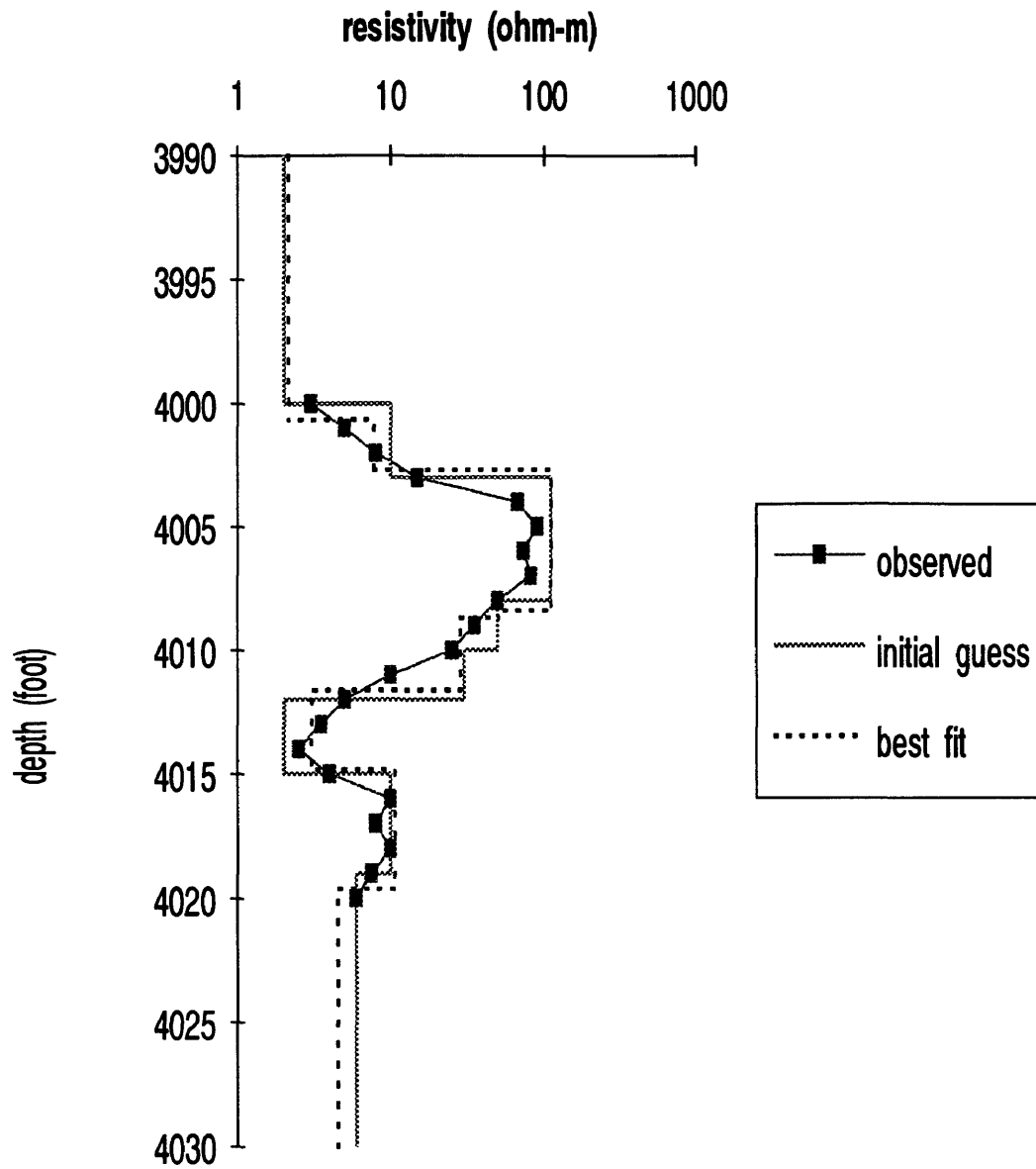


Figure 4.8: Comparison of observed data, initial guess earth model, and best fit earth model

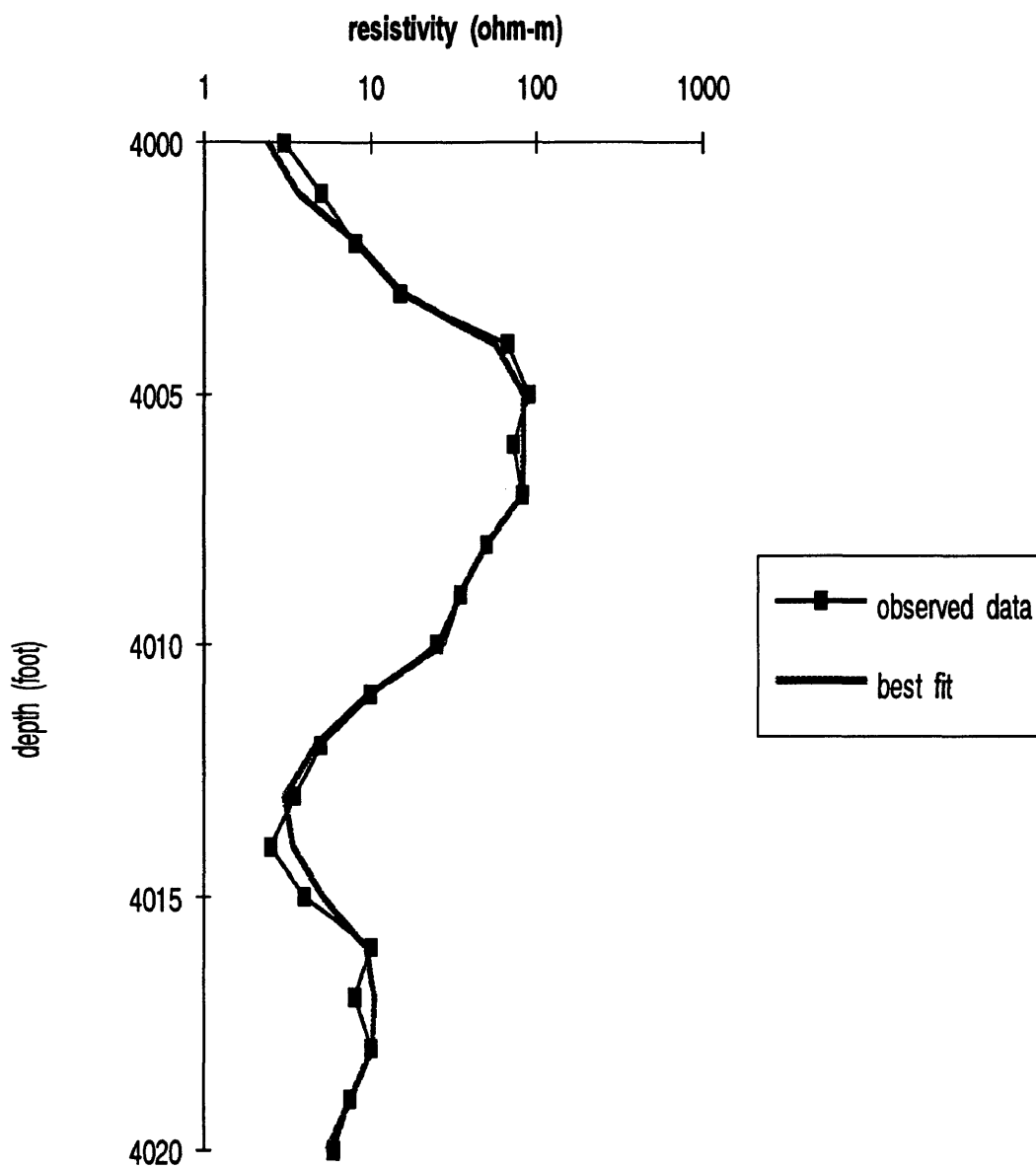


Figure 4.9: Comparison of observed data with best fit log

Chapter 5

CONCLUSIONS

The finite difference method was used to simulate the response of the Laterolog 7 tool configuration in a combined boundary earth model with axial symmetry about the borehole axis. In particular, the apparent resistivities for an earth model with borehole mud, invaded zone(s), and horizontal bed boundaries can be obtained.

Utilization of an exponentially expanding grid system reduced the size of the grid required for a given model and reduced the computation time. The accuracy of the forward modeling calculation was improved by a two dimensional average resistivity calculation and a Neumann boundary condition. Estimation of the electrical potentials at the exact position of the measuring electrodes by insertion of additional grid lines also improved the accuracy of the forward model.

Comparison with analytical solutions for horizontally and cylindrically layered earth models has shown that the finite difference method is a relatively accurate, fast, and flexible method for computation of apparent resistivities. Good agreement was also obtained between the finite difference solution and the physical scale modeling

results of Shattuck et al. (1987) and Bittar et al. (1990), respectively. The flexibility of the finite difference method was demonstrated by the synthetic resistivity logs calculated for multiple, invaded layer earth model.

A more efficient forward modeling method was also developed. Most of the computing time is spent on inverting a large sparse matrix. In the old forward scheme, three large sparse matrix inversions were performed per sampling point to focus the central current. But with the new forward scheme, only one large sparse matrix inversion is performed per sampling point to achieve the condition that the central current is focused. That means the new scheme is roughly three times faster than the old scheme.

A study of the effects of earth parameter variations with various two dimensional models shows the followings:

1. A large diameter hole adversely affects the apparent resistivity responses only in conductive beds, not in resistive beds in the Laterolog 7 arrangement.
2. A low resistivity mud does not significantly affect the departure from the true resistivity in the Laterolog 7 arrangement.
3. Apparent resistivity is significantly affected by the invasion diameter and the invaded zone resistivity.
4. If bed thickness is less than the thickness of current sheet (O_1O_2 in Figure 2.6),

it is considered to be difficult to identify the true resistivity and the boundary of a resistive bed.

Forward modeling of the Laterolog 7 for a two dimensional earth model has many possible applications. These include:

1. basis of the resistivity inversion scheme;
2. better interpretation of resistivity logs;
3. study of the effects of invasion diameter and invaded zone resistivity;
4. better calibration of resistivity tools; and
5. correction for the borehole environmental effect.

Inversion of the Laterolog 7 log data is accomplished by the Marquardt inversion process. Two dimensional earth models without invaded zones were tested. The test results indicated that the thickness and the true resistivity of each layer could be determined simultaneously. The hypothetical earth model and the best fit earth model showed good agreement. And the hypothetical log and the best fit log also showed good agreement. Inversion of field log data provides a seemingly realistic earth model.

Chapter 6

FURTHER STUDIES

Forward modeling of the Laterolog 7 tool for the combined boundary earth model, especially for the complicated axis-symmetrical logging environment, has many possible applications: the design of new electrode resistivity tools, the calibration of the existing tools, and the prediction of the apparent resistivity for a given geometry to improve the interpretation of the log data of the Laterolog 7 tool.

This study has been restricted to the finite difference forward modeling and inverse modeling of the Laterolog 7 tool. Conceptually, the principles of most focused tools are similar to each other. Therefore, the approach in this study can be used for the other focused tools. If axial symmetry about the borehole axis is not assumed, this finite difference method becomes meaningless. In this case, finite element method should be considered. This study can be the basis of a finite element forward modeling and inverse modeling for the Laterolog 7 and other focused tools.

Other possible applications include:

1. forward modeling for the Guard Log, Dual Laterolog, and a multiple-array Laterolog,
2. development of approximate forward solutions for faster inversion,
3. inverse modeling for the Guard Log, Dual Laterolog, and a multiple-array Laterolog,
4. resistivity data interpretation in a two dimensional earth model with an invaded zone, and
5. resistivity data interpretation in a three dimensional earth model.

References

- Anderson, B. and Barber, T.D., 1988, Using computer modeling to provide missing information for interpreting resistivity logs, SPWLA 29th Annual Logging Symposium, Paper H.
- Archie, G.E., 1942, The electrical resistivity log as an aid in determining some reservoir characteristics, J. Pet. Tech., 5, No. 1.
- Asquith, G.M., 1983, Basic well log analysis for geologists: The American Association of Petroleum Geologists, Tulsa.
- Barber, T.D., 1985, Introduction to the phasor dual induction tool, SPE 44, 1699-1706.
- Bateman, R.M., 1985, Open-hole log analysis and formation evaluation: International Human Resources Development Corporation, Boston.
- Bittar, M.S., Shattuck, D.P., and Shen, L.C., 1990, Laboratory study of the shallow laterolog in high and low contrast zones, The Log Analyst, 31, 189-197.
- Burden, L.B. and Faires, J.D., 1989, Numerical analysis: PWS-KENT Publishing Company, Boston.
- Chemali, R., Gianzero, S., and Strickland, R., 1983, The shoulder bed effect on the dual laterolog and its variation with the resistivity of the borehole fluid, SPWLA 24th Annual Logging Symposium, Paper UU.
- Chemali, R., Gianzero, S., and Su, S.M., 1988, The dual laterolog in common complex situations, SPWLA 29th Annual Logging Symposium, paper N.
- Dakhnov, V.N., 1962, Quarterly of Colorado School of Mines, translated by G.V. Keller, 445.
- Daniel, J.J., 1978, Interpretation of buried electrode resistivity data using a layered earth model, Geophysics, 43, 988-1001.

- deWitte, L., Fournier, K.P., and Tejada-Flores, H., 1957, Calculation of Guard electrode response curves, *Geophysics*, **22**, 67-74.
- Desbrandes, R., 1985, *Encyclopedia of well logging*: Gulf Publishing Company, Paris.
- Dewan, J.T., 1983, *Essentials of modern open hole log interpretation*: PennWell Publishing Company, Tulsa.
- Doll, H.G., 1950, The microlog - A new electrical logging method for detailed determination of permeable beds, *J. Pet. Tech.*, **2**, No. 6; *Pet. Trans., AIME* **189**, 70-79.
- Doll, H.G., 1951, The laterolog - A new resistivity logging method with electrodes using an automatic focusing system, *J. Pet. Tech.*, **3**, No. 11; *Pet. Trans., AIME*, **192**, 111-122.
- Doll, H.G., 1953, The microlaterolog, *J. Pet. Tech.*, **5**, No. 1; *Pet. Trans., AIME*, **198**, 80-95.
- Drahos, D., 1984, Electrical modeling of the inhomogeneous invaded zone, *Geophysics*, **49**, 1580-1585.
- Ellis, D.V., 1987, *Well logging for the earth scientists*: Elsevier, New York.
- García, G., 1991, Inversion of a lateral log using neural networks, Master's thesis T-3265, Colorado School of Mines, Golden, Colorado.
- Gianzero, S. and Rau, R., 1977, The effect of sonde position in the hole on responses of resistivity logging tools, *Geophysics*, **42**, 642-654.
- Gianzero, S. and Anderson, B., 1982, An integral transform solution to the fundamental problem in resistivity logging, *Geophysics*, **47**, 946-956.
- Gianzero, S., Lin, Y., and Chemali, R., 1985, The effect of sonde eccentricity on resistivity tools: An exact theoretical model, *SPWLA 26th Annual Logging Symposium*, Paper GG.
- Golub, G.H. and Van Loan, C.F., 1989, *Matrix computations*: The Johns Hopkins University Press, Baltimore and London.
- Guyod, H., 1955, Electrical analogue of resistivity logging, *Geophysics*, **20**, 615-629.

- Guyod, H., 1964, Factors affecting the responses of Laterolog-type logging systems (LL3 and LL7), *J. Pet. Tech.*, **16**, No. 2; *Pet. Trans. AIME*, **231**, 211-219.
- Hearst, J.R. and Nelson, P.H., 1985, *Well logging for physical properties*: McGraw-Hill Book Company, New York.
- Hilchie, D.W., 1978, *Applied openhole log interpretation*: Douglas W. Hilchie Inc., Golden, Colorado.
- Hoversten, G.M., Dey, A., and Morrison, H.F., 1982, Comparison of five least-squares inversion techniques in resistivity sounding, *Geophysical Prospecting*, **30**, 688-715.
- Inman, J.R., Ryu, J., and Ward, S.H., 1973, Resistivity inversion, *Geophysics*, **38**, 1088-1108.
- Inman, J.R., 1975, Resistivity inversion with ridge regression, *Geophysics*, **40**, 1088-1108.
- Johnson, H.M., 1962, Review article : A history of well logging, *Geophysics*, **27**, 507-527.
- Kim, J.H., 1986, *Forward modeling and inversion of responses for borehole normal and lateral electrode arrangements*, Ph.D. thesis T-3265, Colorado School of Mines, Golden, Colorado.
- Kincaid, D., Grimes, R., and John, R., 1982, ITPACK 2C: A Fortran package for solving large sparse linear systems by adaptive accelerated iterative methods: *ACM Trans. on Math. Software*, **8**, 302-322.
- Labo, J., 1986, *A practical introduction to borehole geophysics*: Society of Exploration Geophysicists, Tulsa.
- Marquardt, D.W., 1970, Generalized inverse, ridge regression, biased linear estimation, and nonlinear estimation, *Technometrics*, **12**, 592-612.
- Moran, J.H. and Chemali, R.E., 1979, More on the laterolog device, *Geophysical Prospecting*, **27**, 902-930.
- Mufti, I.R., 1978, A practical approach to finite-difference resistivity modeling, *Geophysics*, **43**, 930-942.
- Mufti, I.R., 1980, Finite-difference evaluation of apparent resistivity curves, *Geophys-*

- ical Prospecting, **28**, 146-166.
- Owen, J.E. and Greer, W.J., 1951, The Guard electrode logging system, *J. Pet. Tech.*, **3**, No. 12; *Pet. Trans. AIME*, **192**, 347-356.
- Rijo, L., Pelton, W.H., Feitosa, E.C., and Ward, S.H., 1977, Interpretation of apparent resistivity data from Apodi Valley, Rio Grande de Norte, Brasil, *Geophysics*, **42**, 811-822.
- Schlumberger, 1987. Log interpretation principles and applications: Schlumberger educational services.
- Serra, O., 1984, Fundamentals of well log interpretation: Elsevier, Amsterdam.
- Shattuck, D.P., Bittar M.S., and Shen, L.C., 1987, Scale modelling of the laterolog using synthetic focusing methods, *The Log Analyst*, **28**, 357-369.
- Shen, L.C. and Hardman, R.H., 1986, Effect of formation dip or hole deviation on induction logs, SPWLA **27th** Annual Symposium, Paper I.
- Simpson, R.S., Shang, H.C., and Shen, L.C., 1983, A laboratory study of induction logs using physical modeling, SPWLA **24th** Annual Logging Symposium, Paper M.
- Smith, G.D., 1985, Numerical solution of partial differential equations: finite difference methods, Oxford Applied Mathematics and Computing Science Series: Clarendon Press, Oxford.
- Strickland, R., Sinclair, P., Harber, J., and DeBrecht, J., 1987, Introduction to the high resolution induction tool, SPWLA **28th** Annual Logging Symposium, Paper M.
- Telford, W.M., Geldart, L.P., and Sheriff, R.E., 1990, Applied geophysics: Cambridge University Press, Cambridge.
- Tittman, J., 1986, Geophysical well logging: Academic Press, Inc., Orlando.
- Towle, G.H., Whitman, W.W., and Kim, J.H., 1988, Electric log modeling with a finite difference method, *The Log Analyst*, **29**, 184-195.
- Tsang, L., Chan, A.K., and Gianzero, S., 1984, Solution of the fundamental problem in resistivity logging with a hybrid method, *Geophysics*, **49**, 1596-1604.

- Wang, Z, 1991, Multiple-electrode logging tool and its applications, Ph.D. thesis T-4098, Colorado School of Mines, Golden, Colorado.
- Whitman, W.W., Towle, G.H., and Kim, J.H., 1989, Inversion of normal and lateral well logs with borehole compensation, *The Log Analyst*, **30**, 1-11.
- Whitman, W.W., Schön, J., Towle, G.H., and Kim, J.H., 1990, An automatic inversion of normal resistivity logs, *The log Analyst*, **31**, 10-19.
- Yang, F.W. and Ward, S.H., 1984, Inversion of borehole normal resistivity logs, *Geophysics*, **49**, 1541-1548.
- Yuratich, M.A. and Meger, W.J., 1984, The application of finite difference methods to normal resistivity logs, SPWLA 25th Annual Logging Symposium, Paper V.
- Zhang, G.J. and Shen, L.C., 1984, Response of a normal resistivity tool in a borehole crossing a bed boundary, *Geophysics*, **49**, 142-149.

Appendix A

Synthetic Laterolog 7 for Conductive Bed

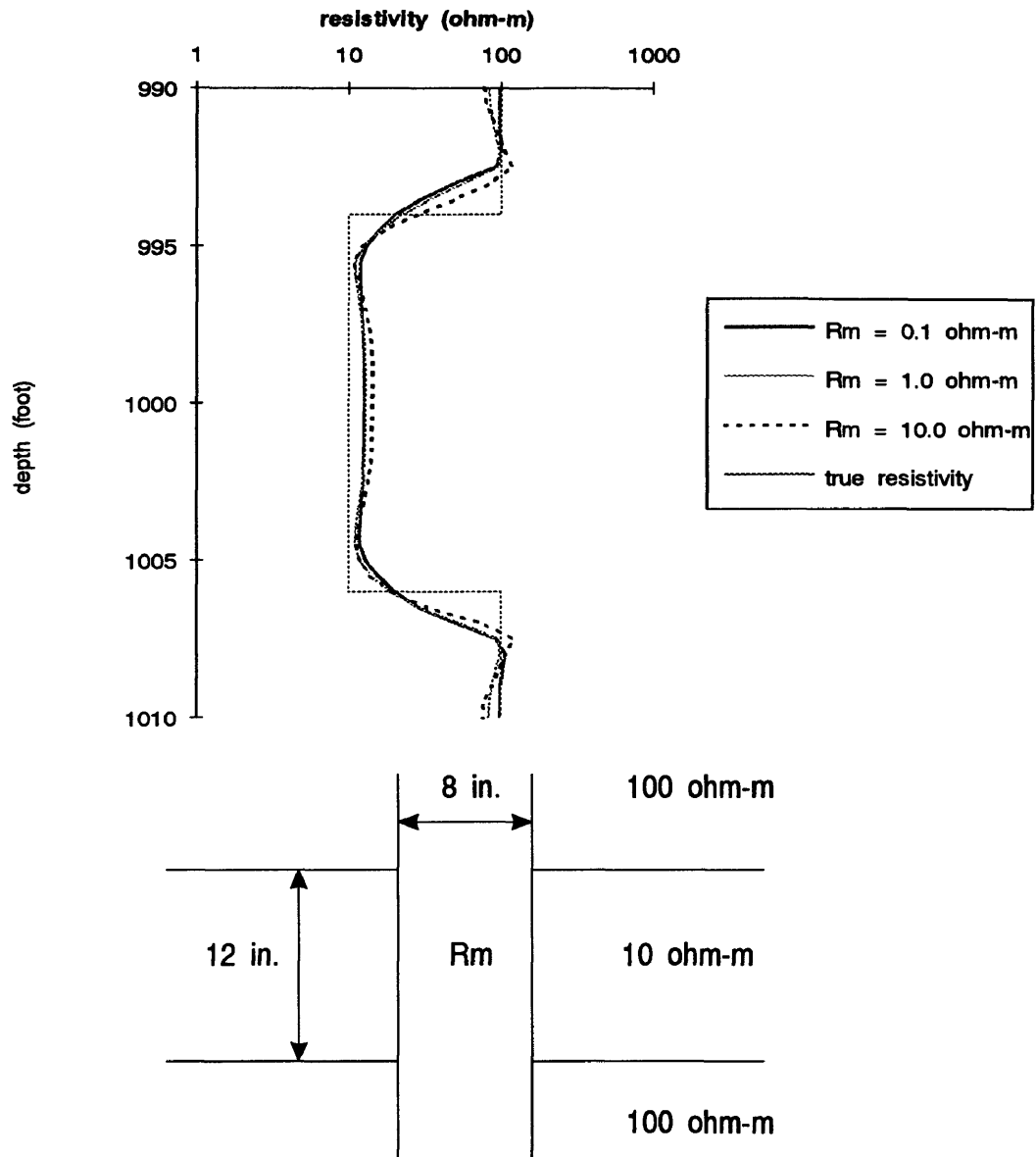


Figure A.1: Variation in R_m (Thick - Conductive)

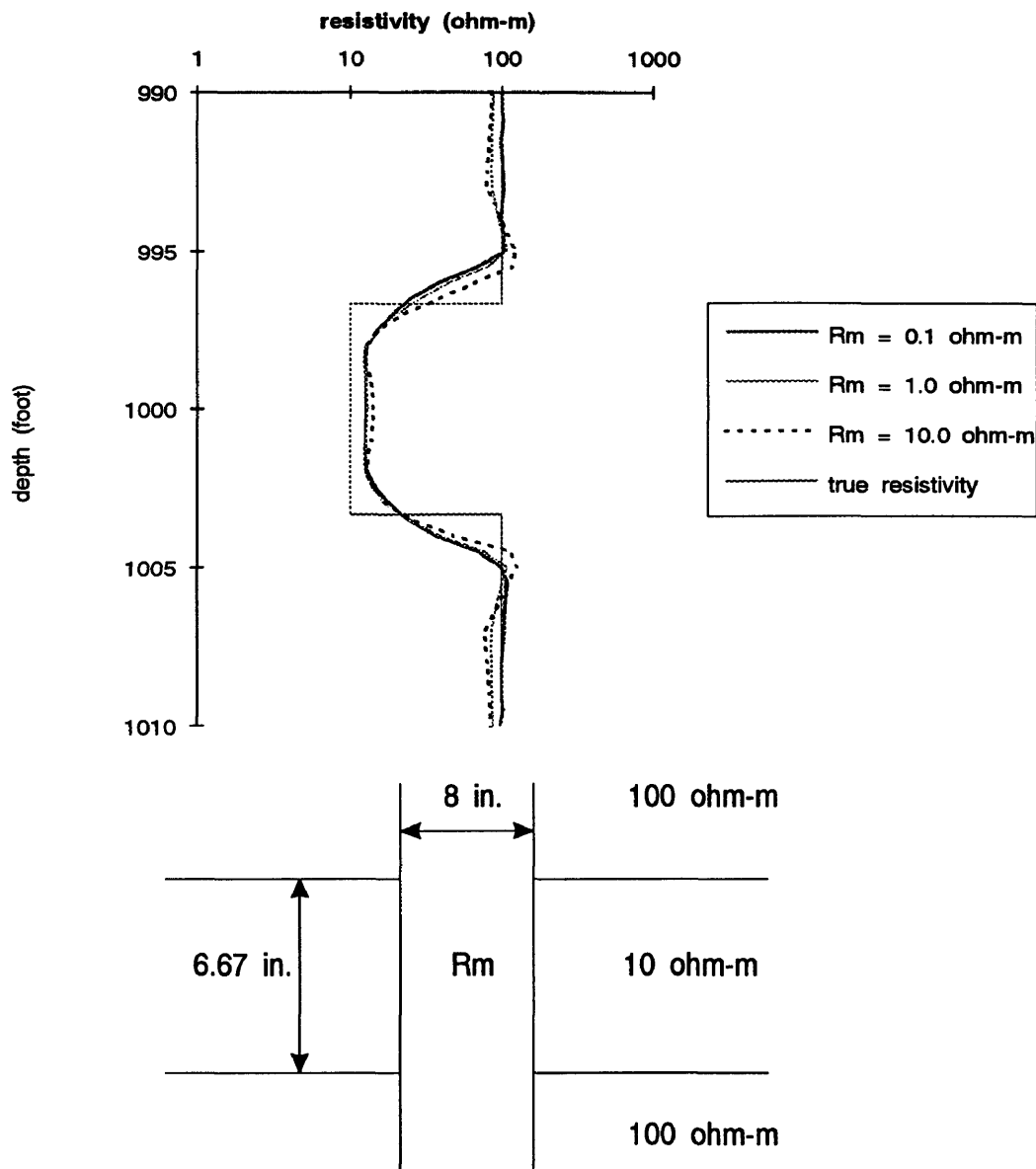


Figure A.2: Variation in R_m (Critically Thick - Conductive)

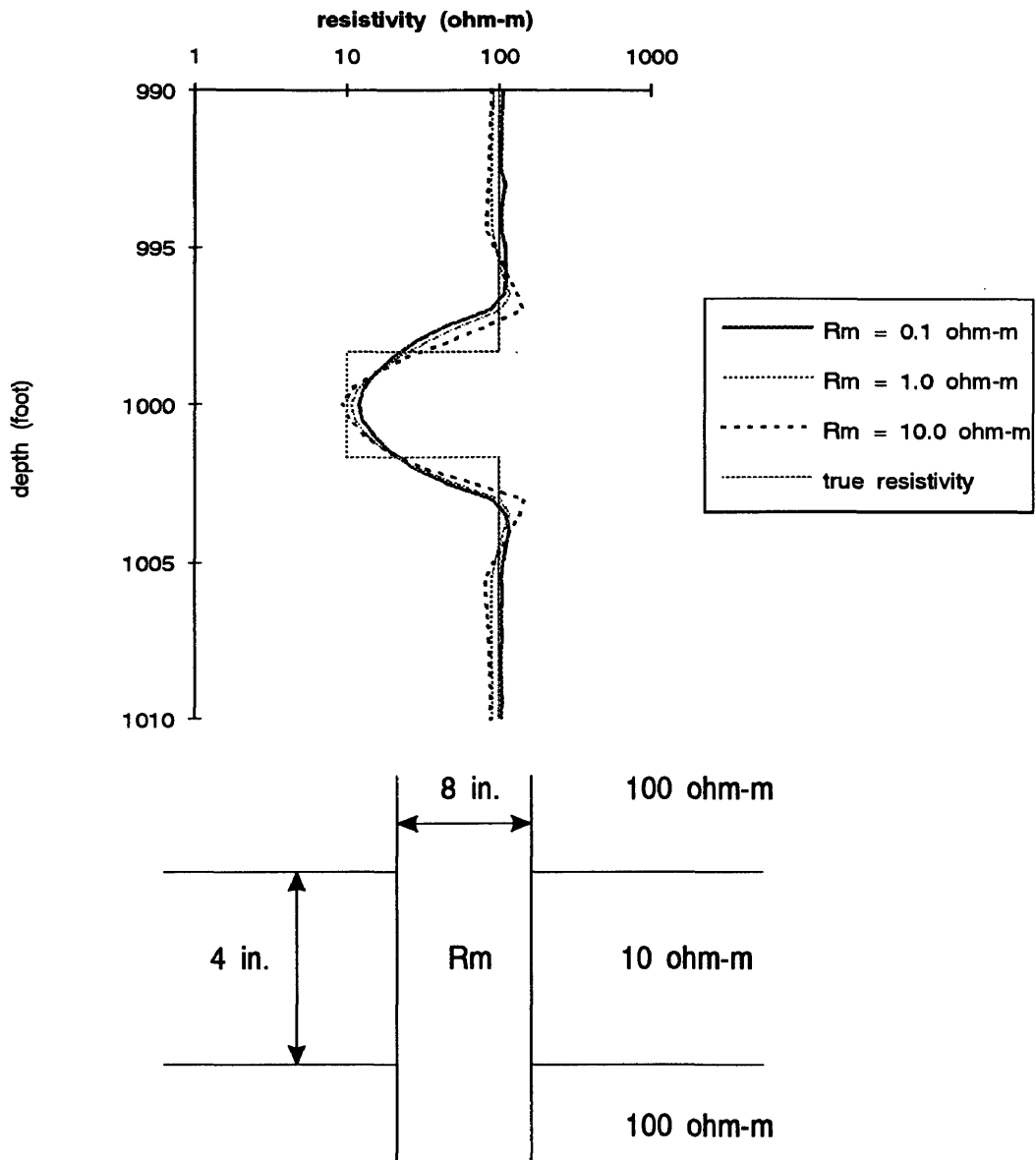


Figure A.3: Variation in R_m (Thin - Conductive)

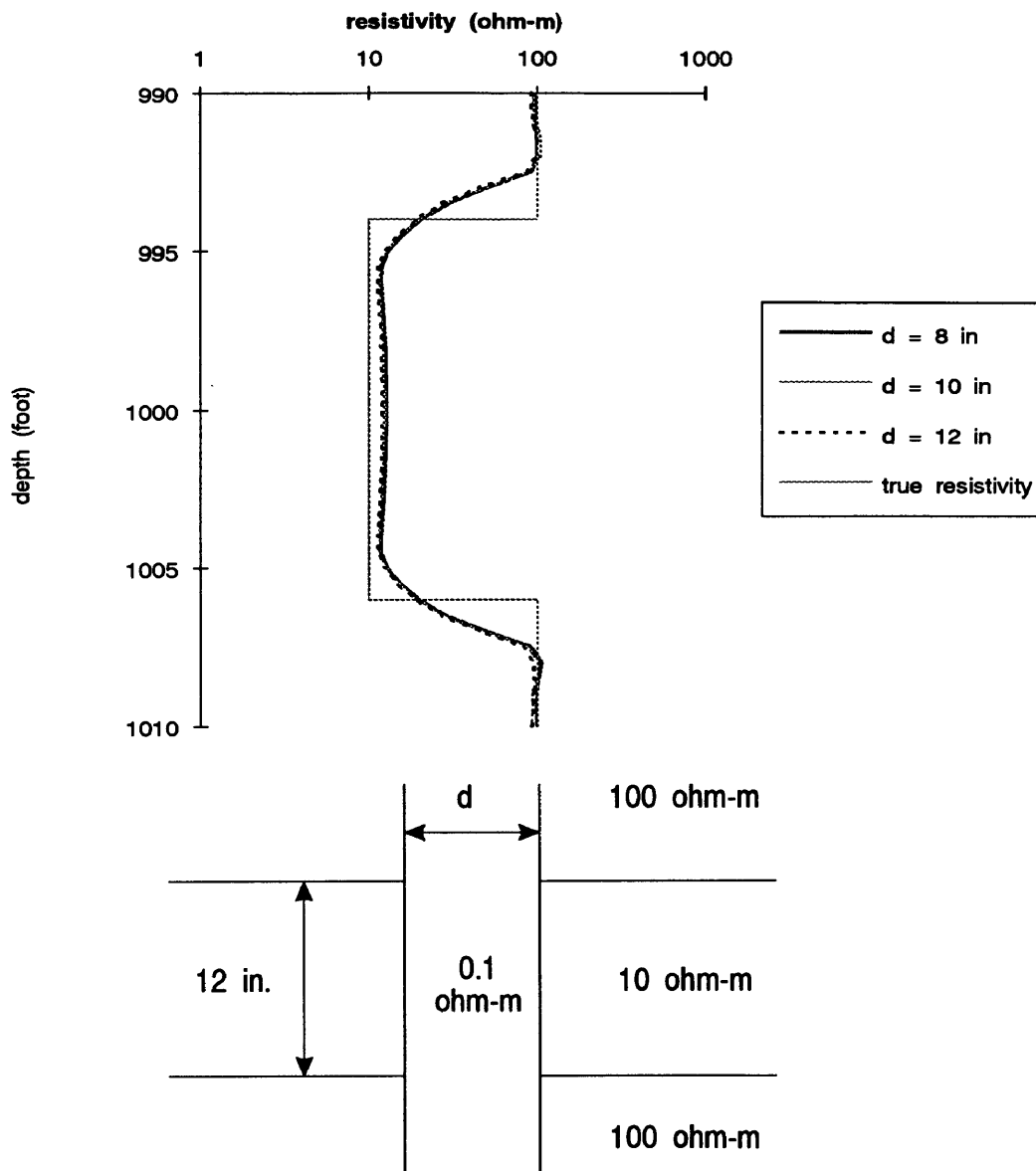


Figure A.4: Variation in d (Thick - Conductive)

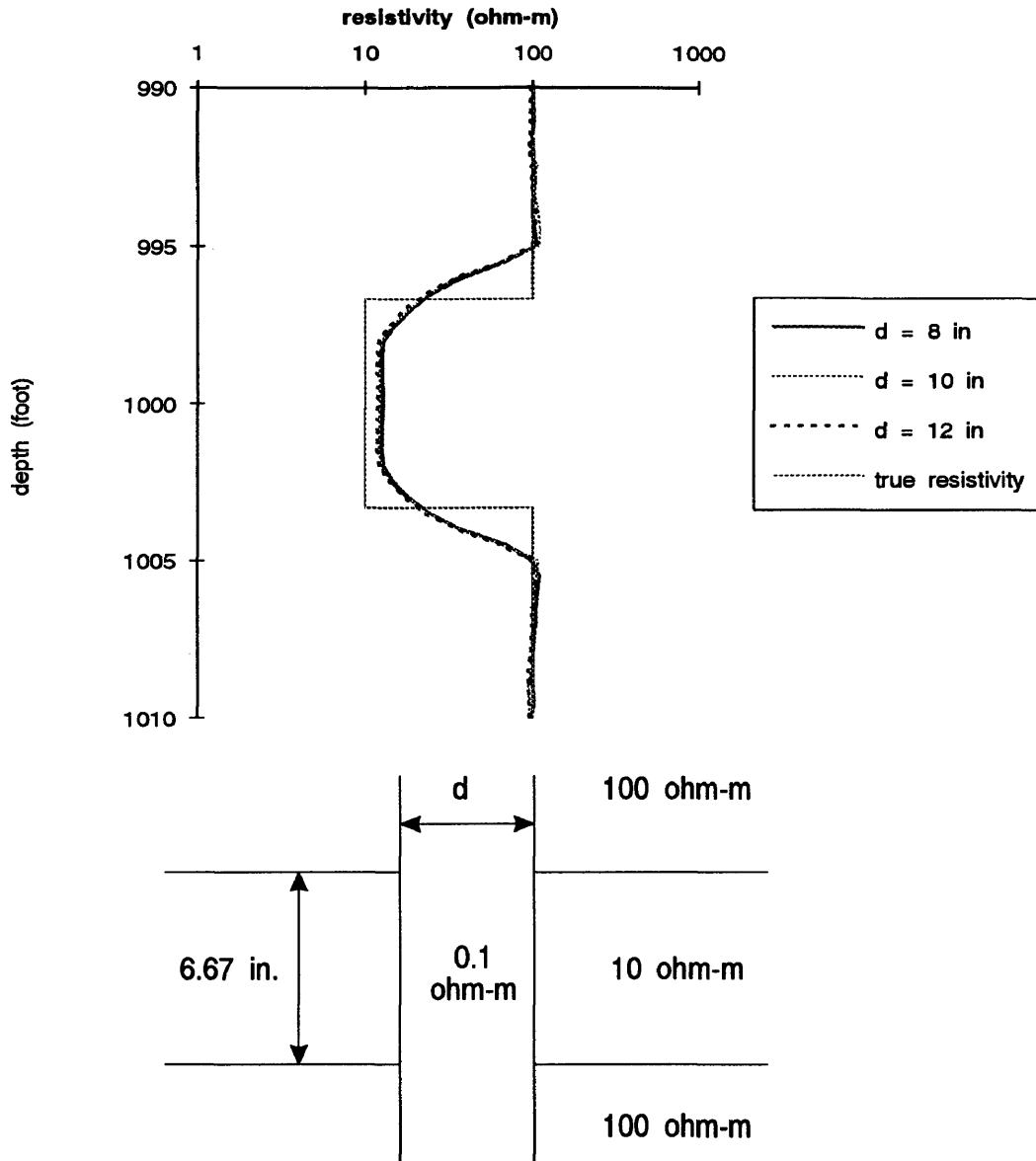


Figure A.5: Variation in d (Critically Thick - Conductive)

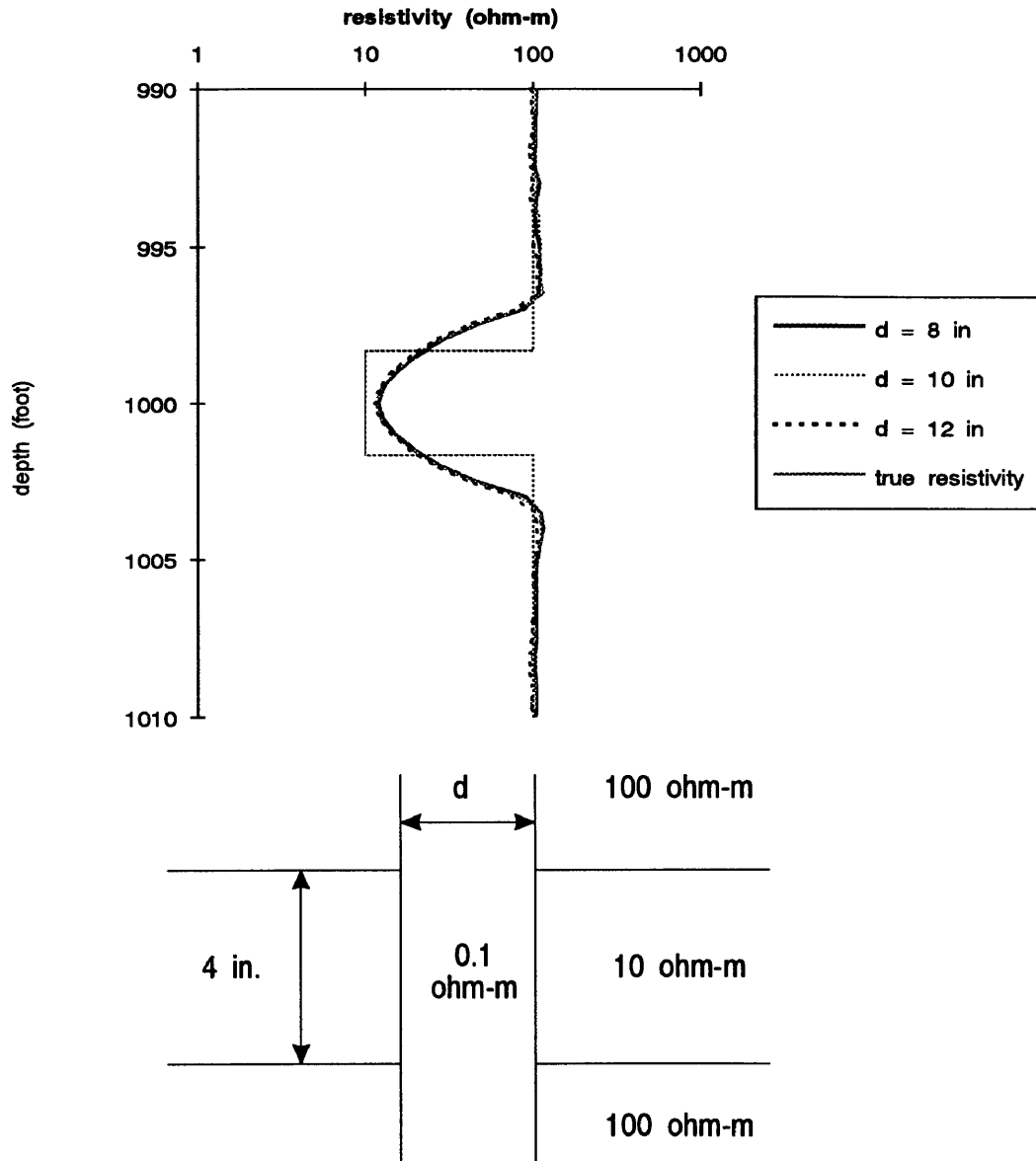


Figure A.6: Variation in d (Thin - Conductive)

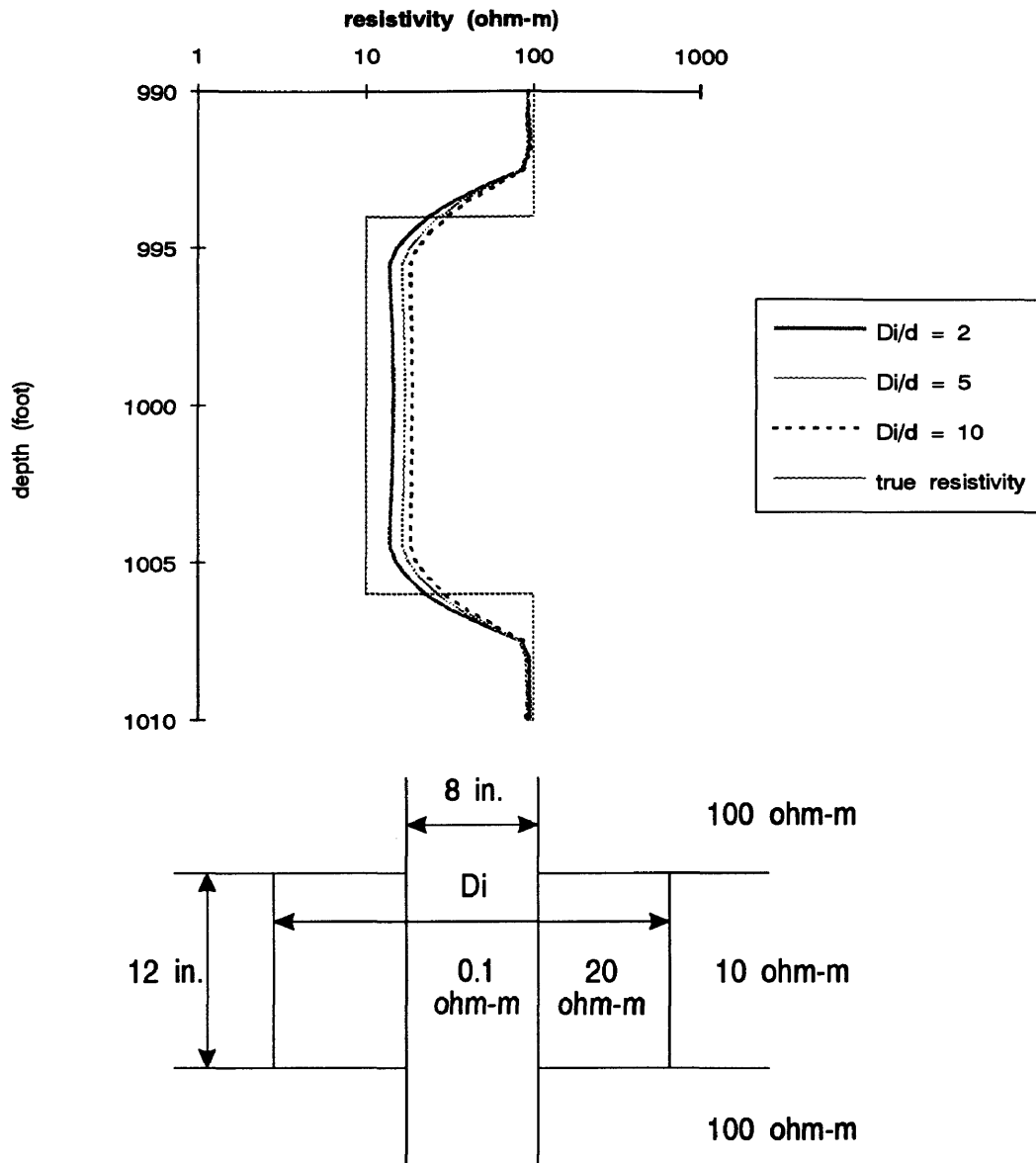


Figure A.7: Variation in D_i (Thick - Conductive)

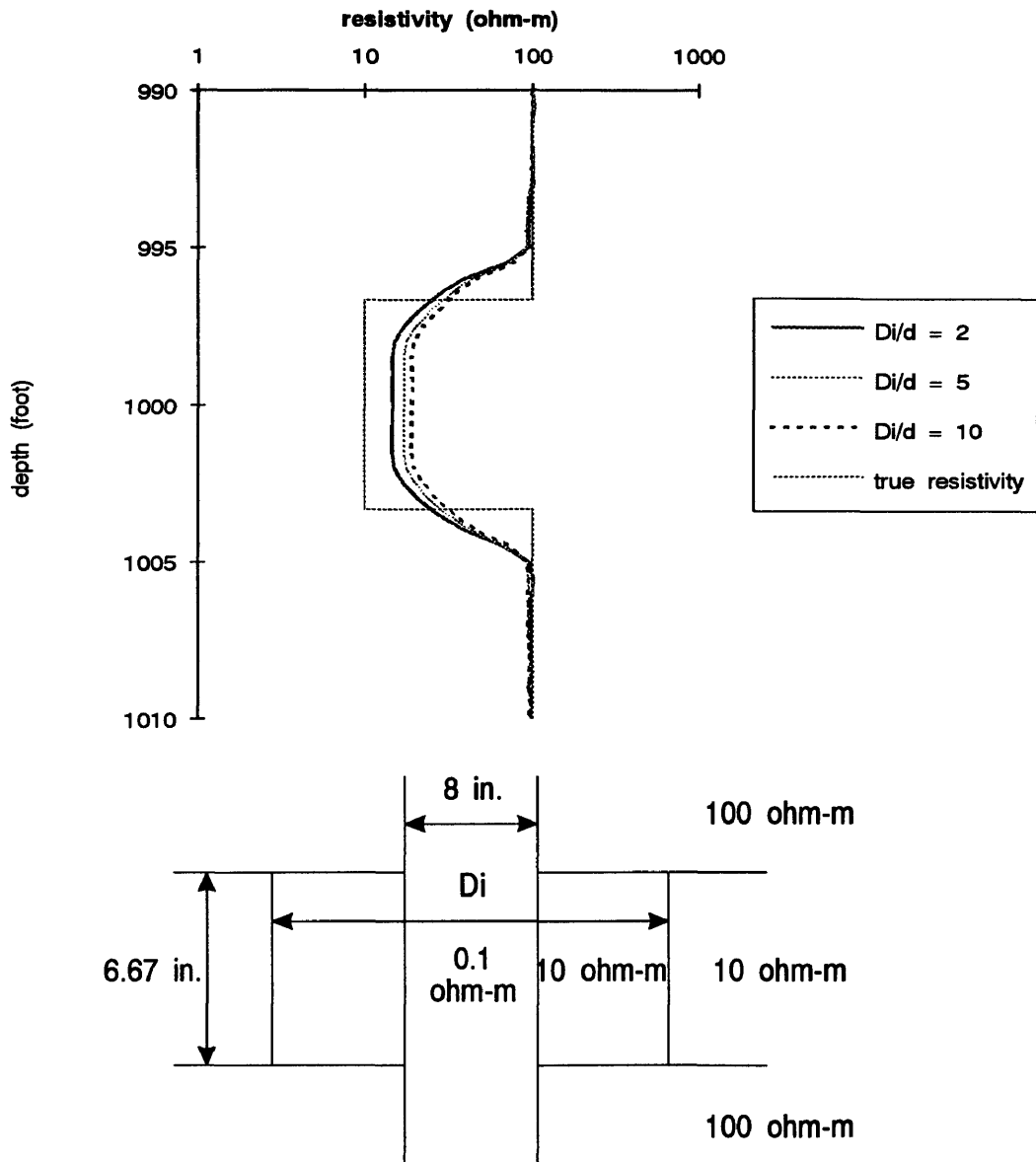


Figure A.8: Variation in D_i (Critically Thick - Conductive)

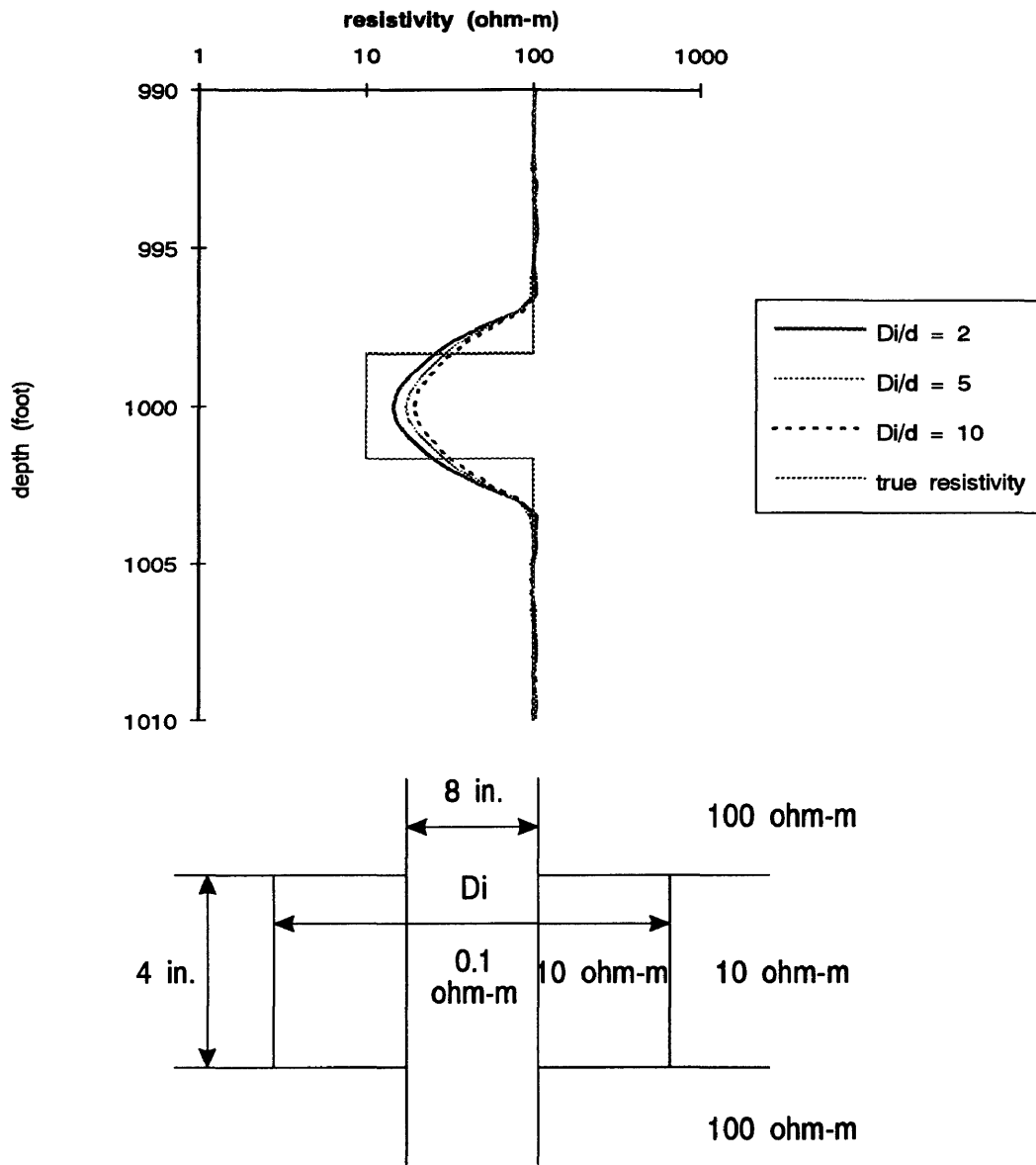


Figure A.9: Variation in D_i (Thin - Conductive)

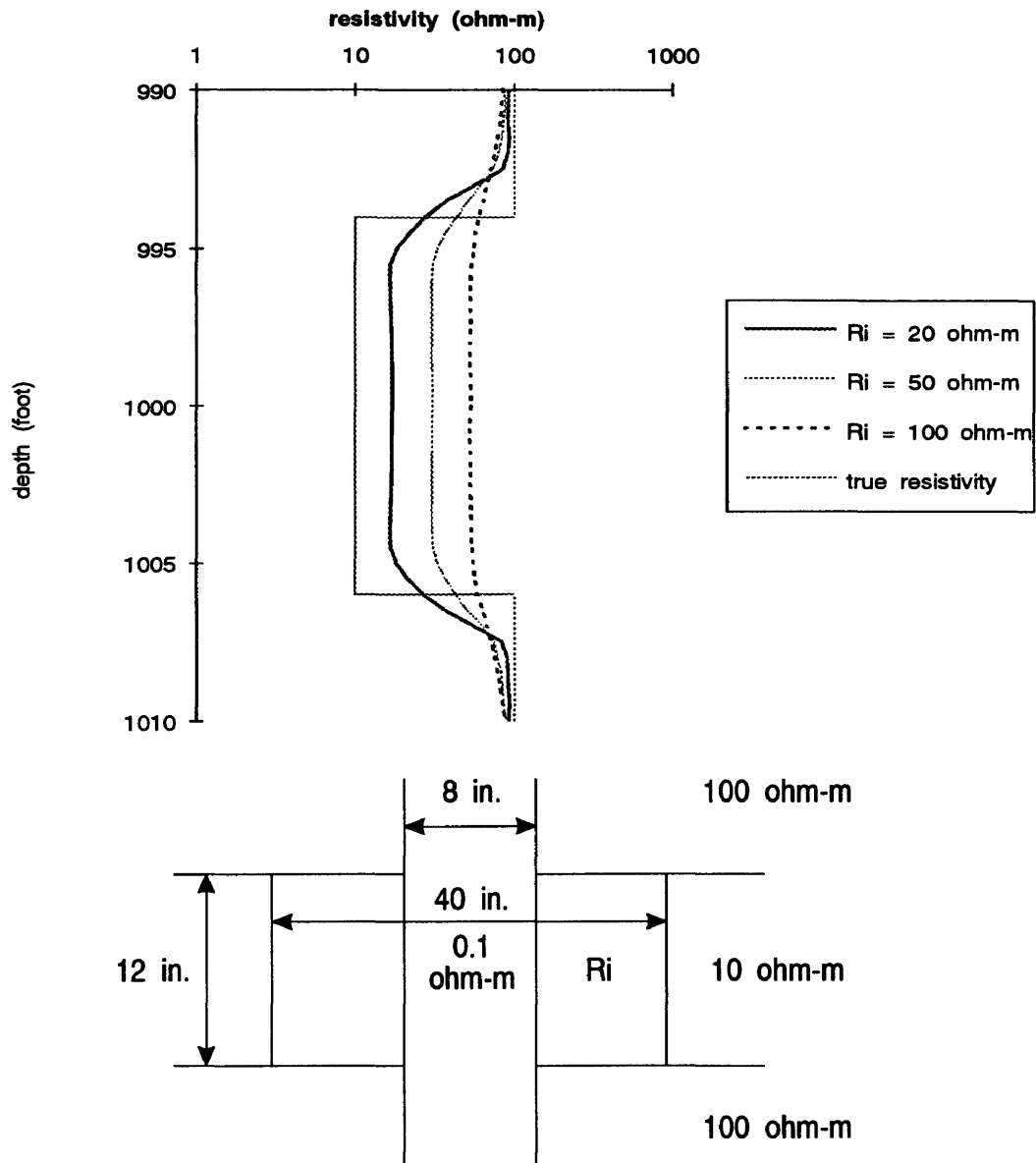


Figure A.10: Variation in R_i (Thick - Conductive)

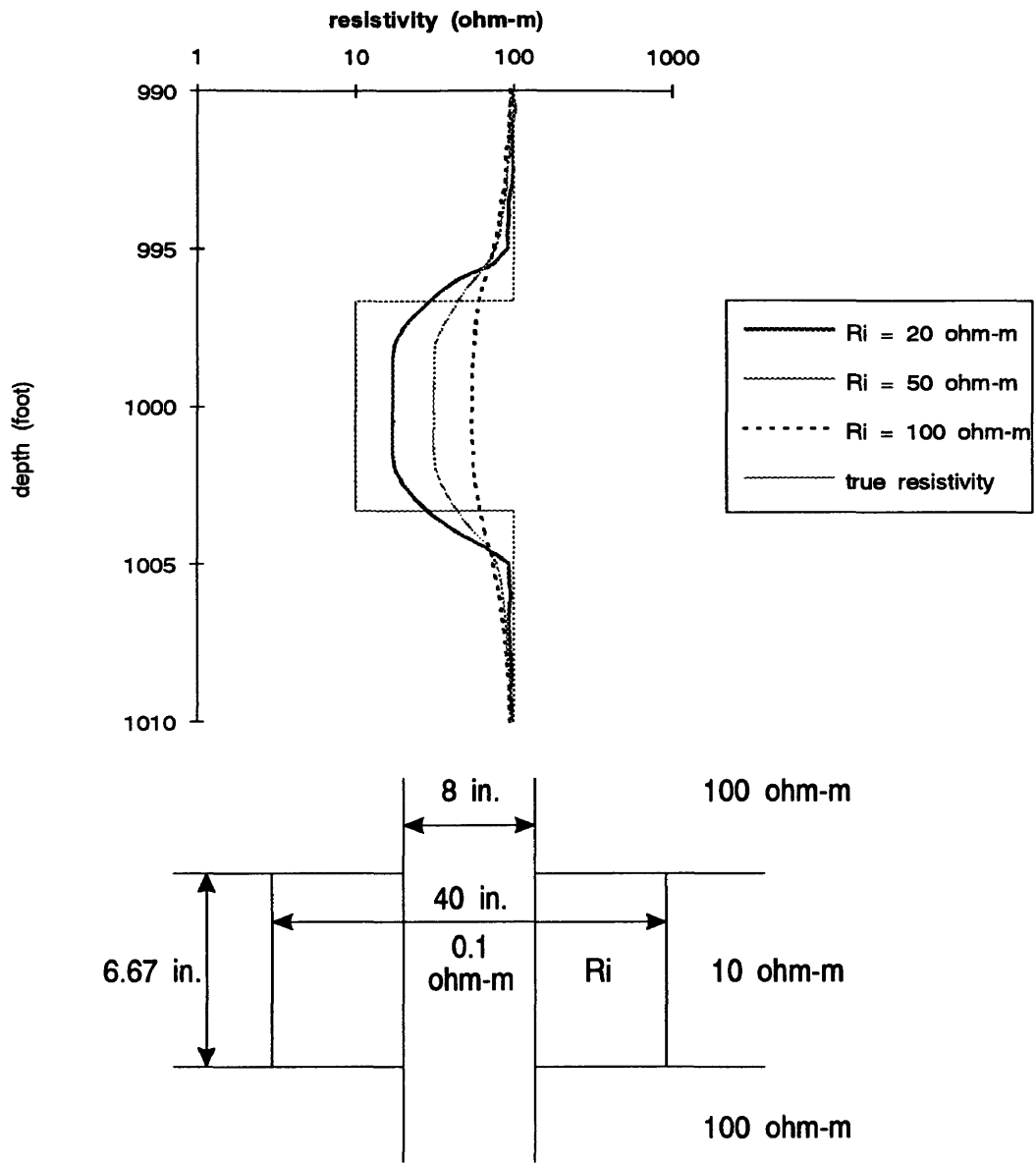


Figure A.11: Variation in R_i (Critically Thick - Conductive)

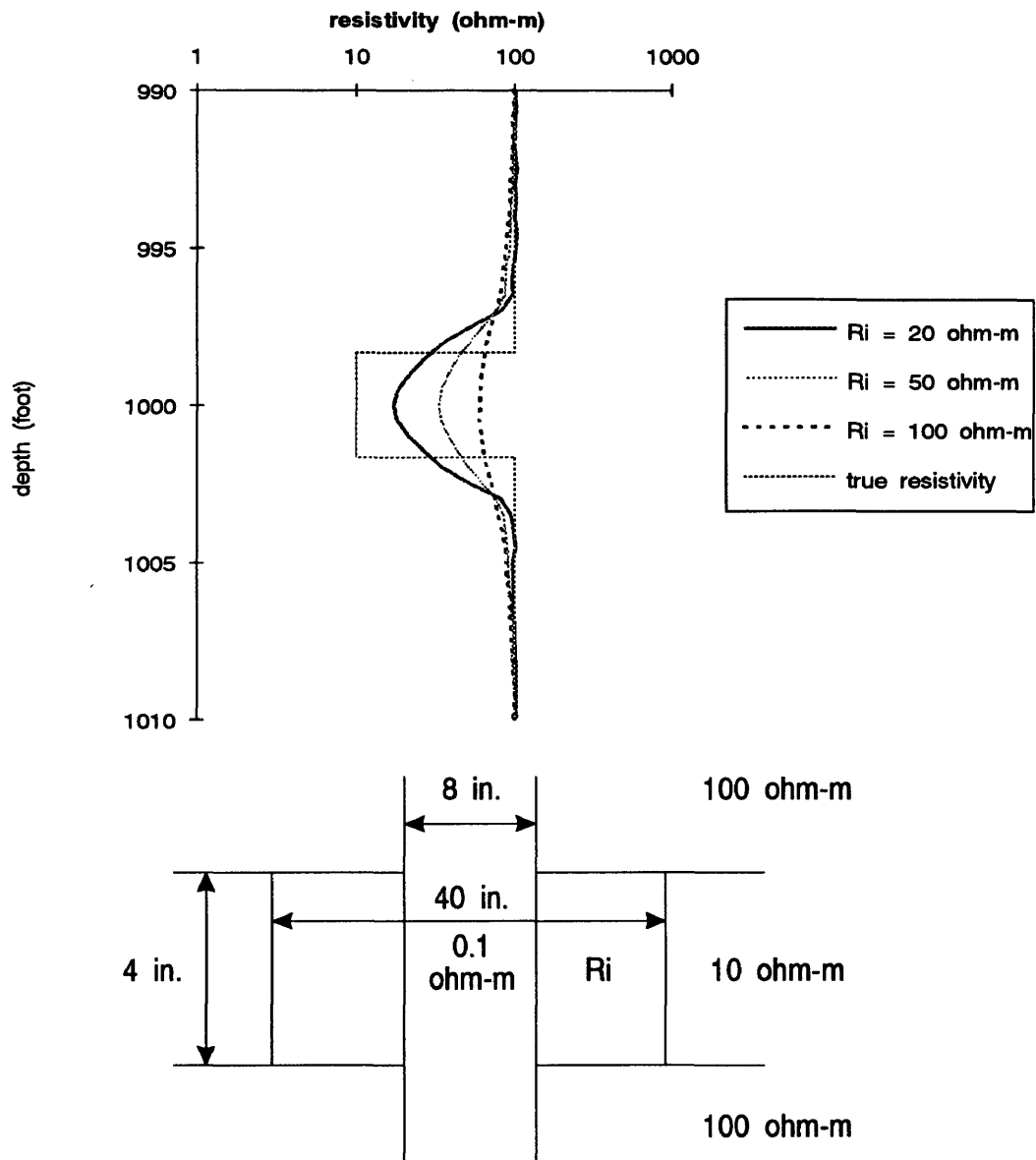


Figure A.12: Variation in R_i (Thin - Conductive)

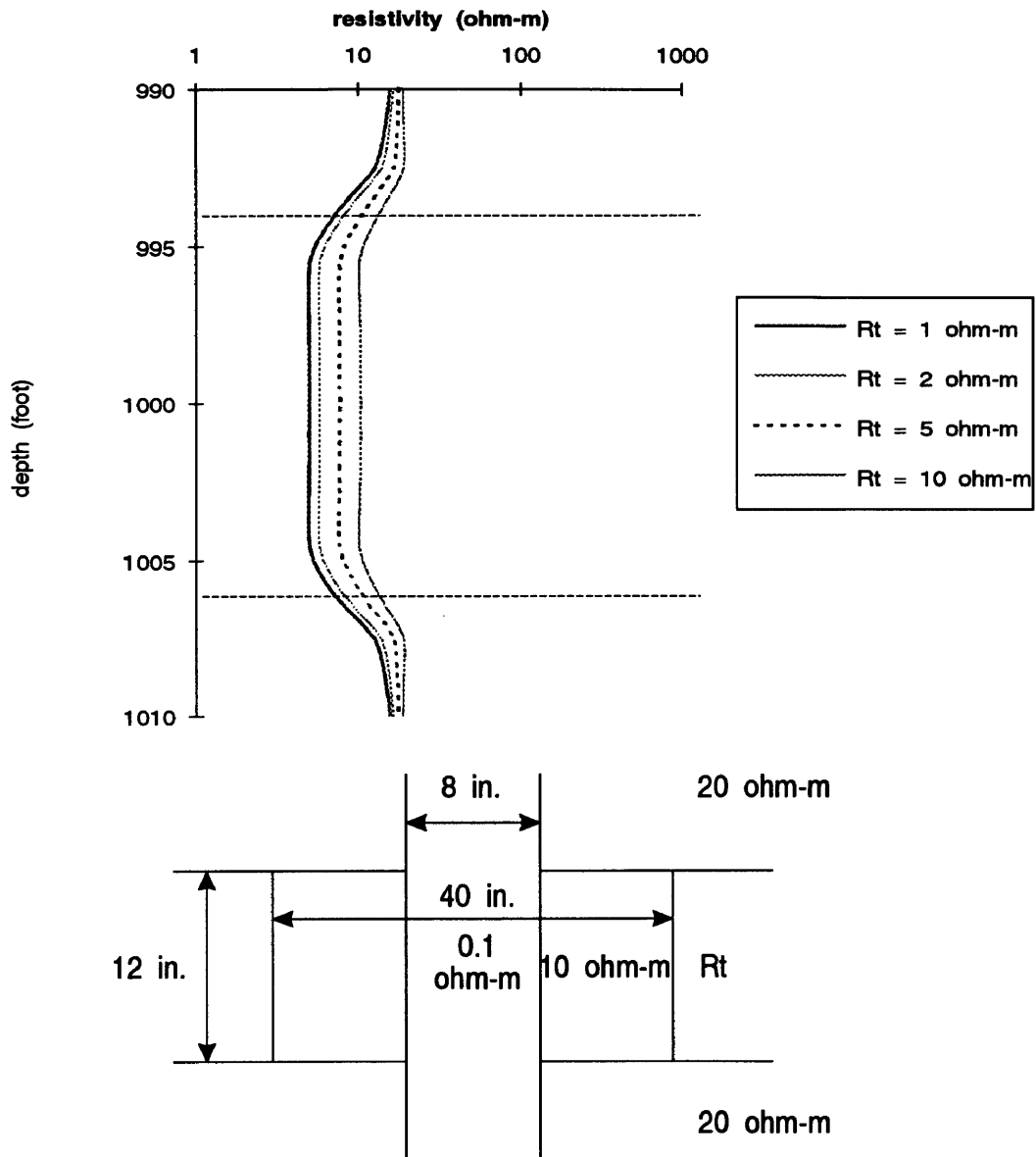


Figure A.13: Variation in R_t (Thick - Conductive)

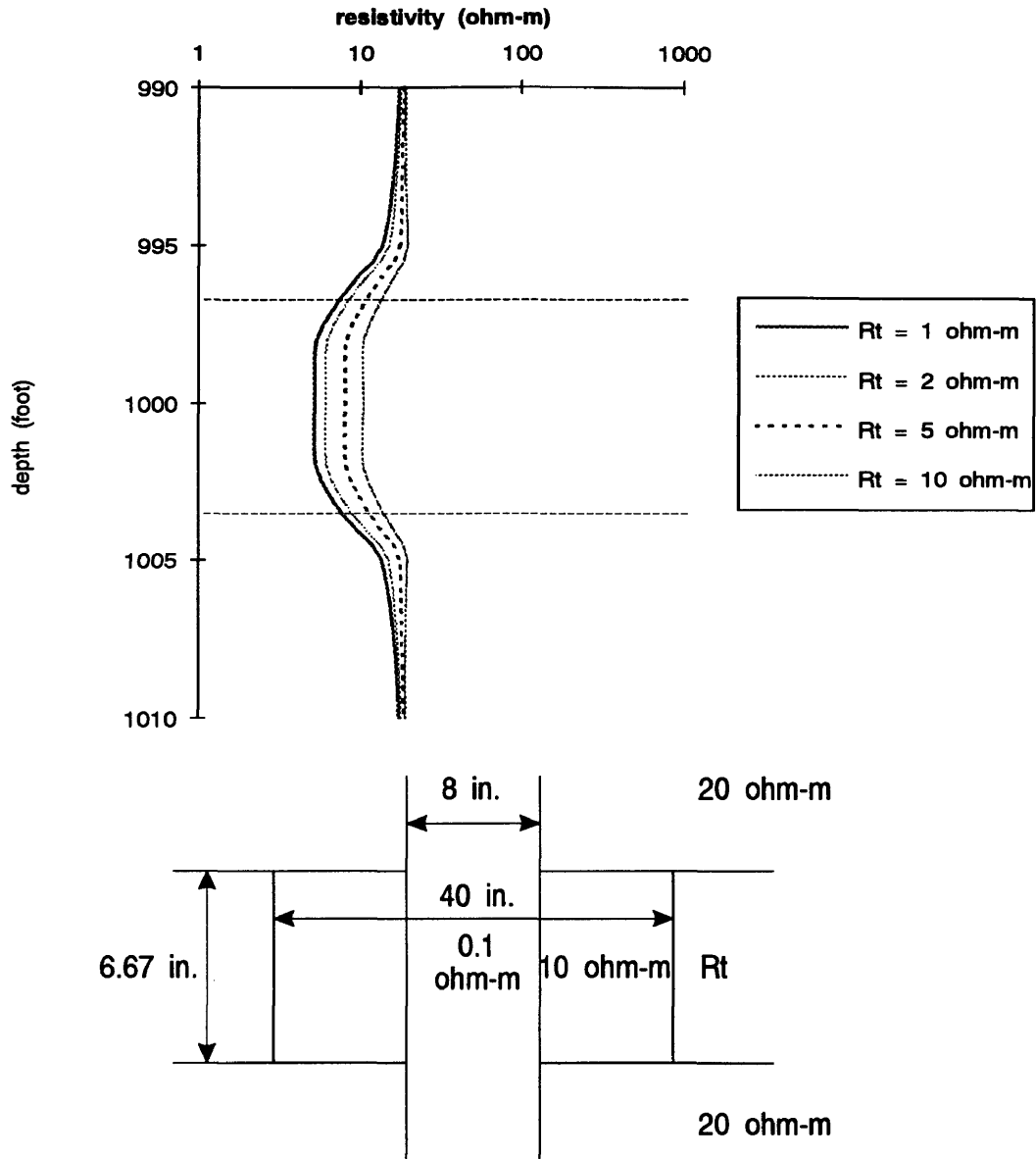


Figure A.14: Variation in R_t (Critically Thick - Conductive)

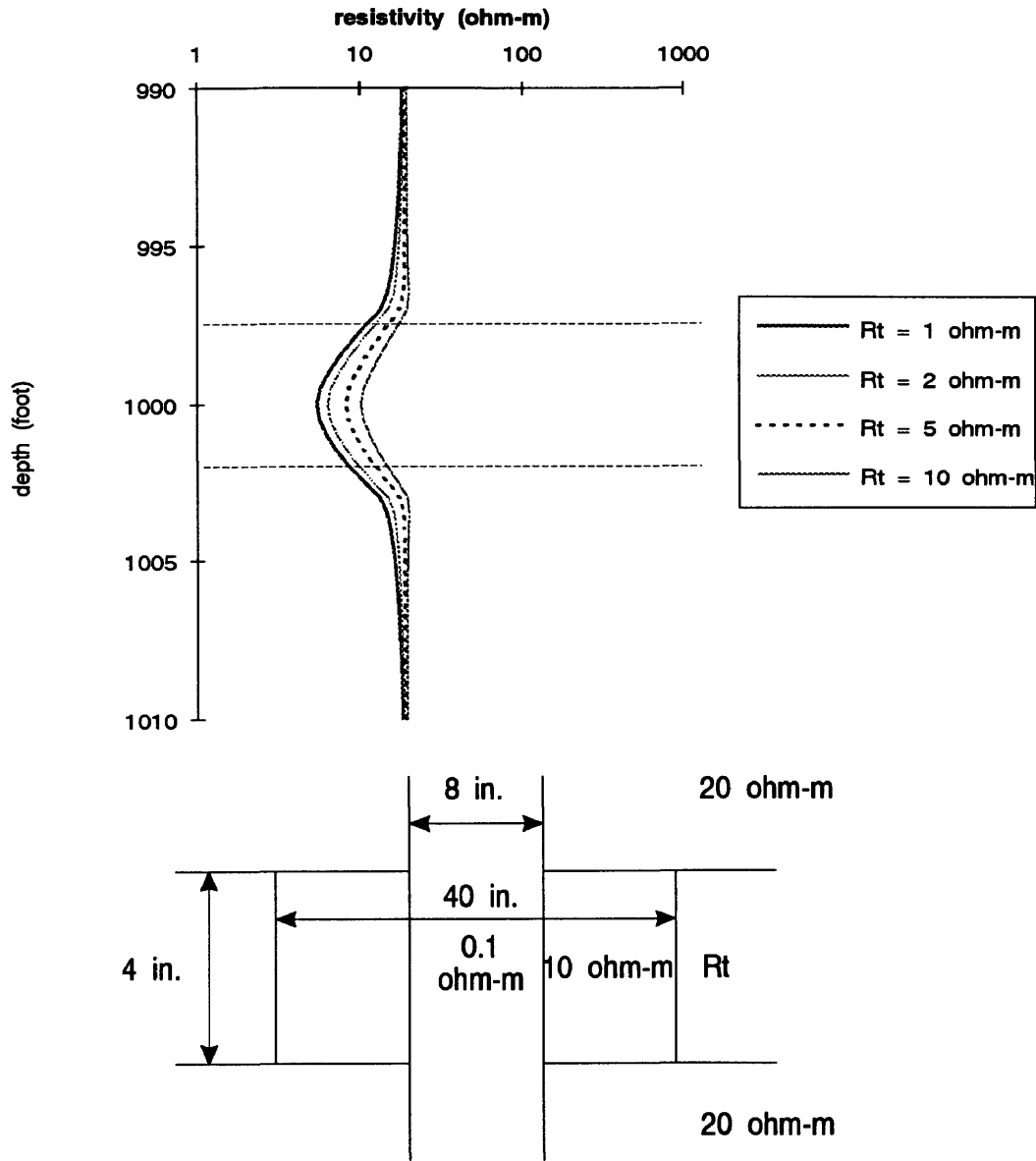


Figure A.15: Variation in R_t (Thin - Conductive)

Appendix B

Synthetic Laterolog 7 for Resistive Bed

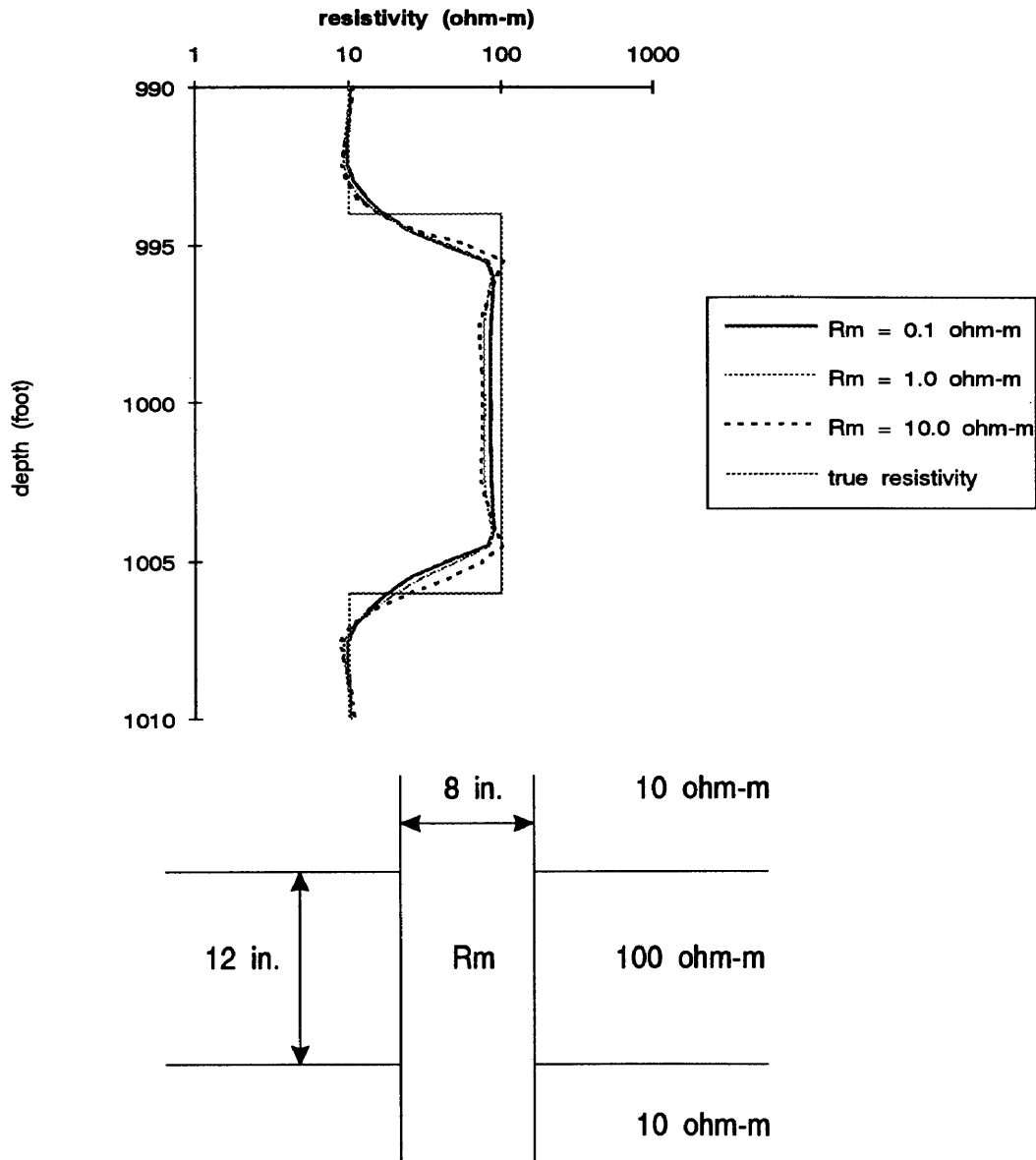


Figure B.1: Variation in R_m (Thick - Resistive)

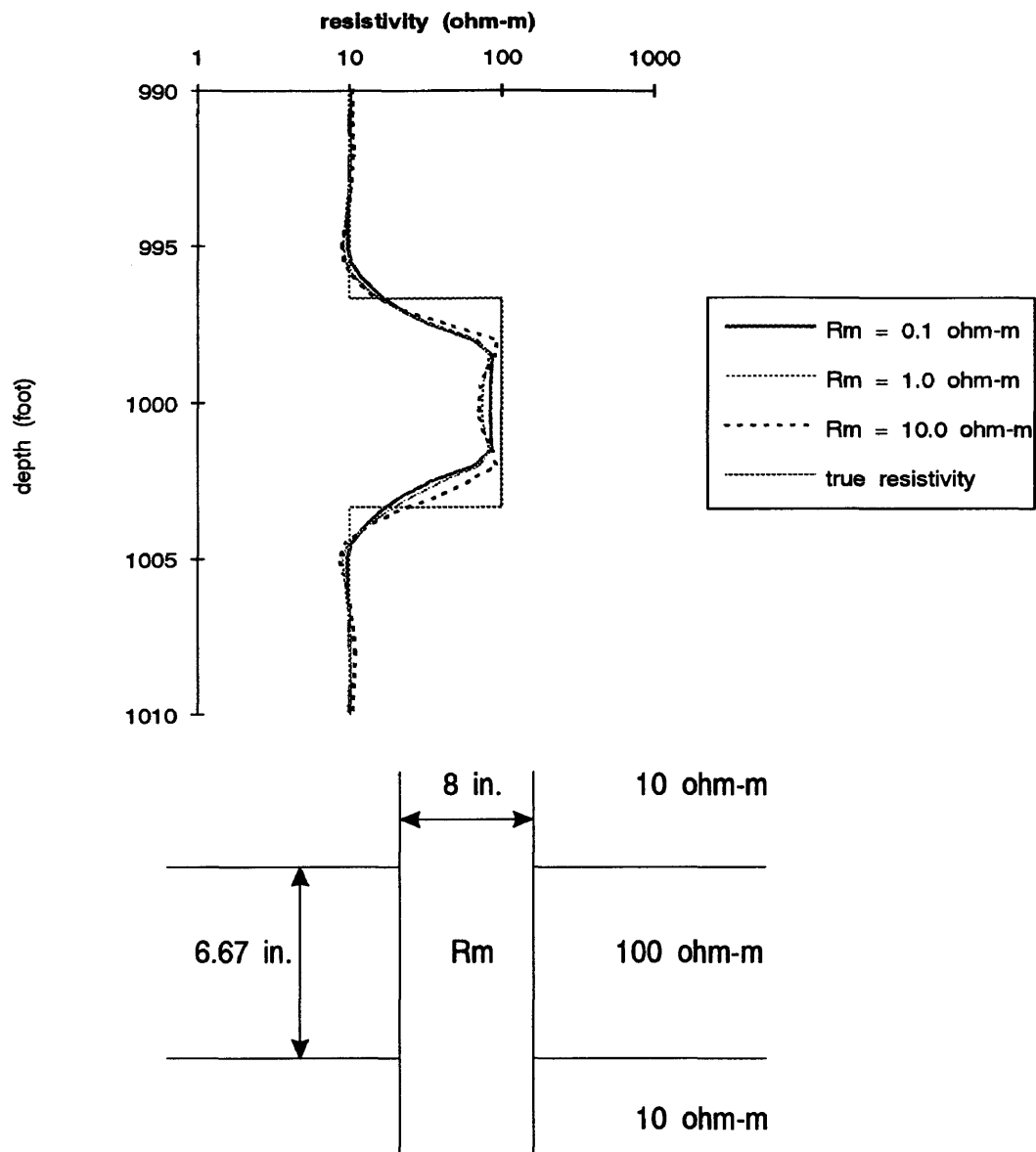


Figure B.2: Variation in R_m (Critically Thick - Resistive)

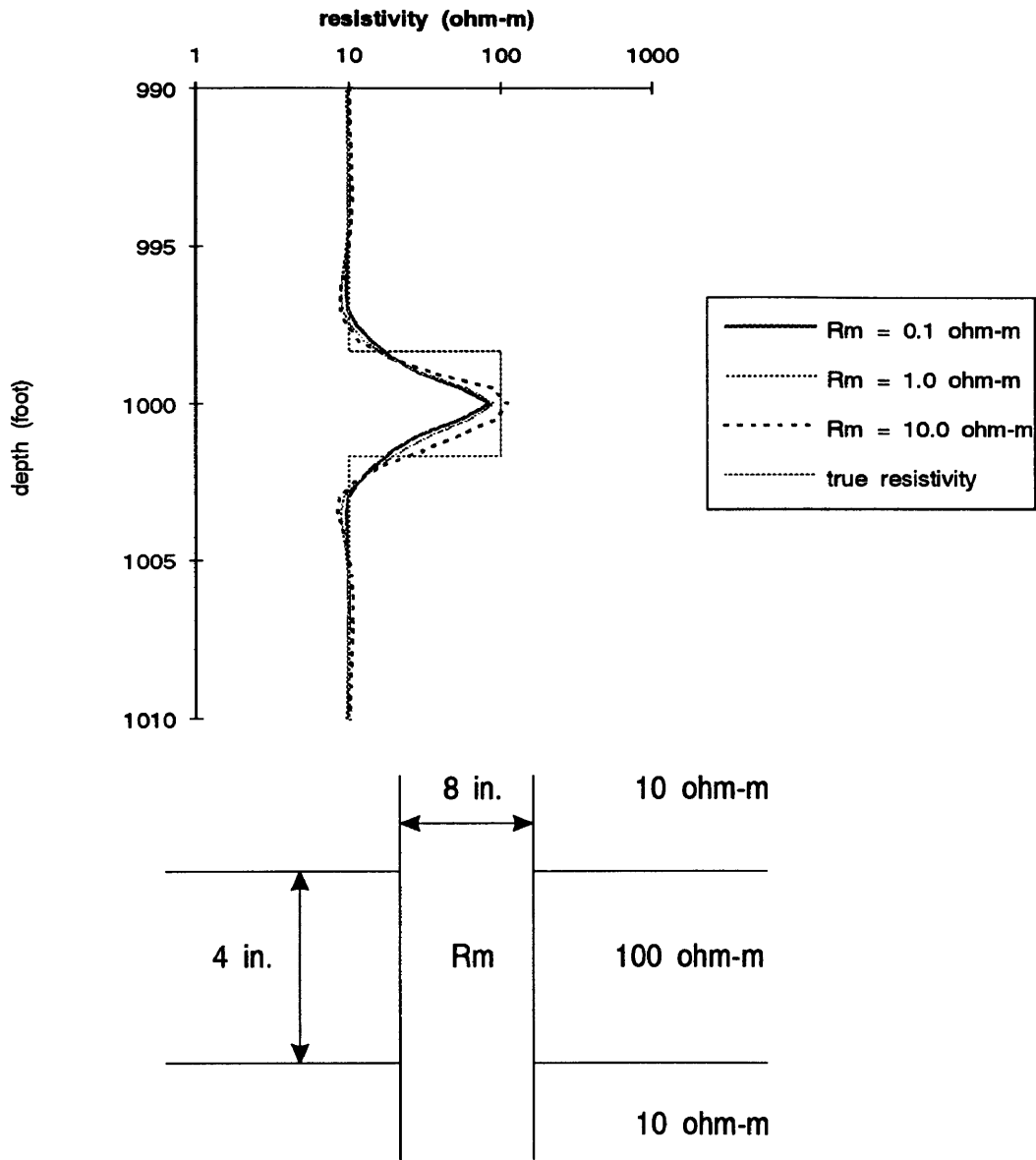


Figure B.3: Variation in R_m (Thin - Resistive)

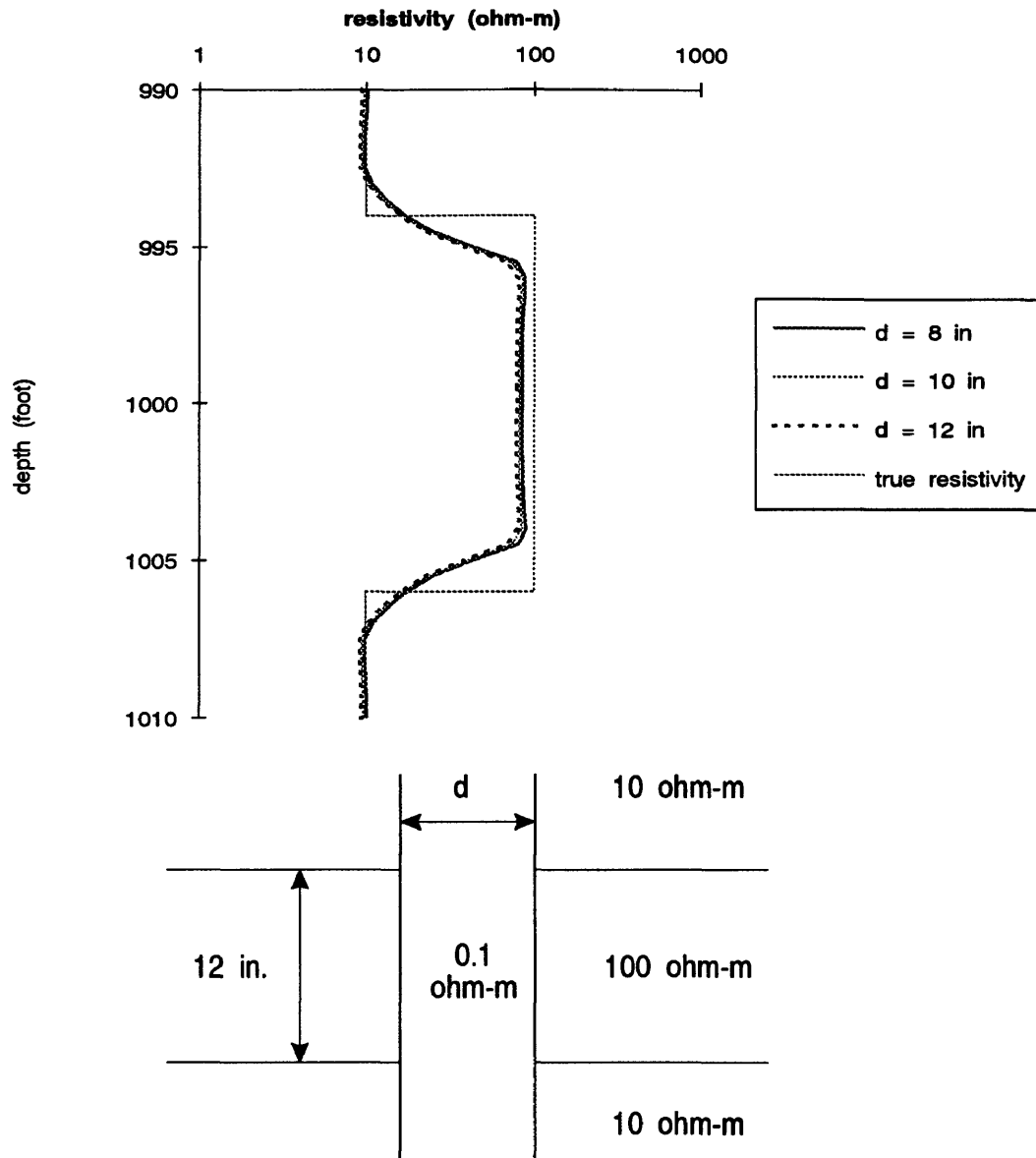


Figure B.4: Variation in d (Thick - Resistive)

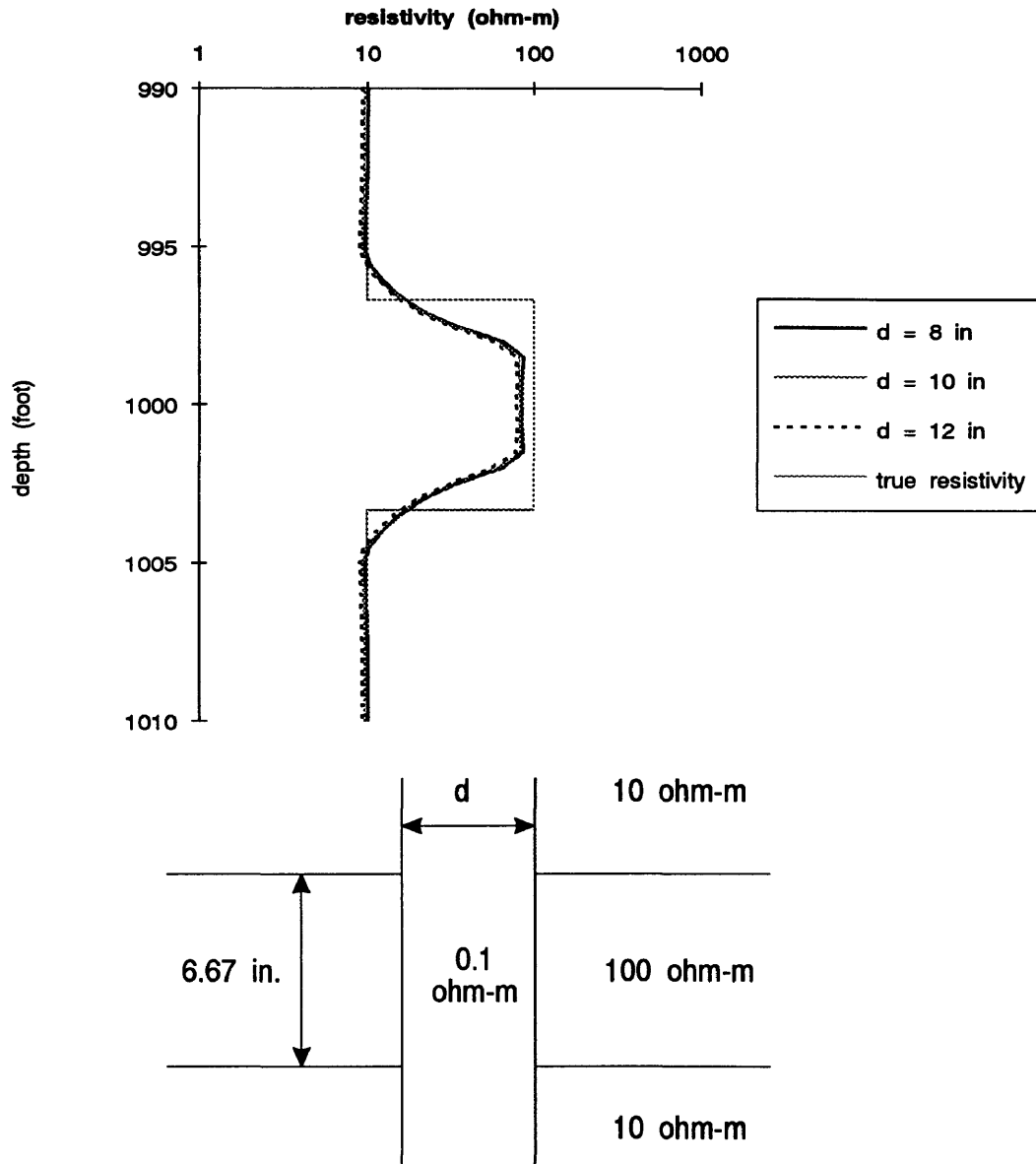


Figure B.5: Variation in d (Critically Thick - Resistive)

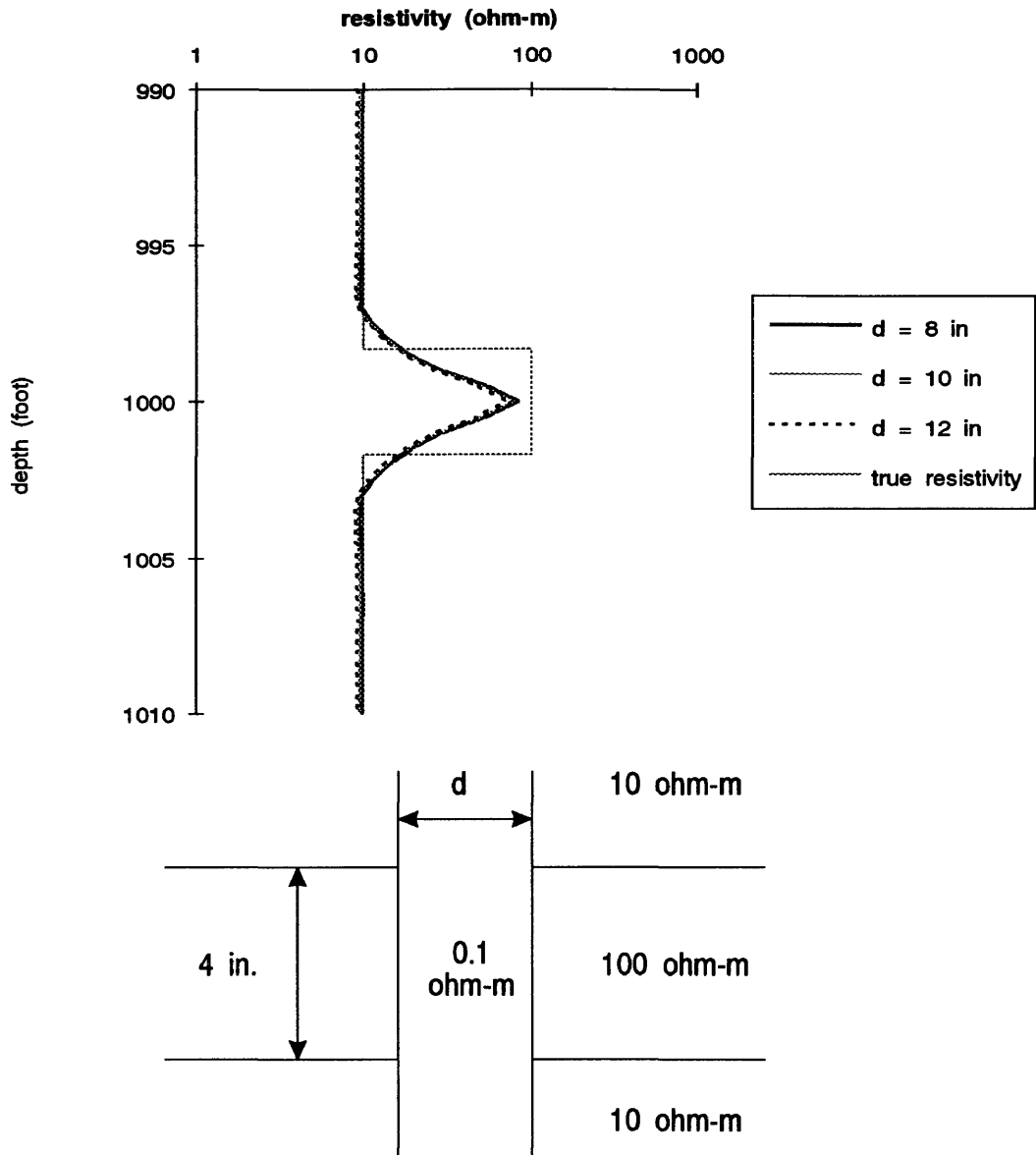


Figure B.6: Variation in d (Thin - Resistive)

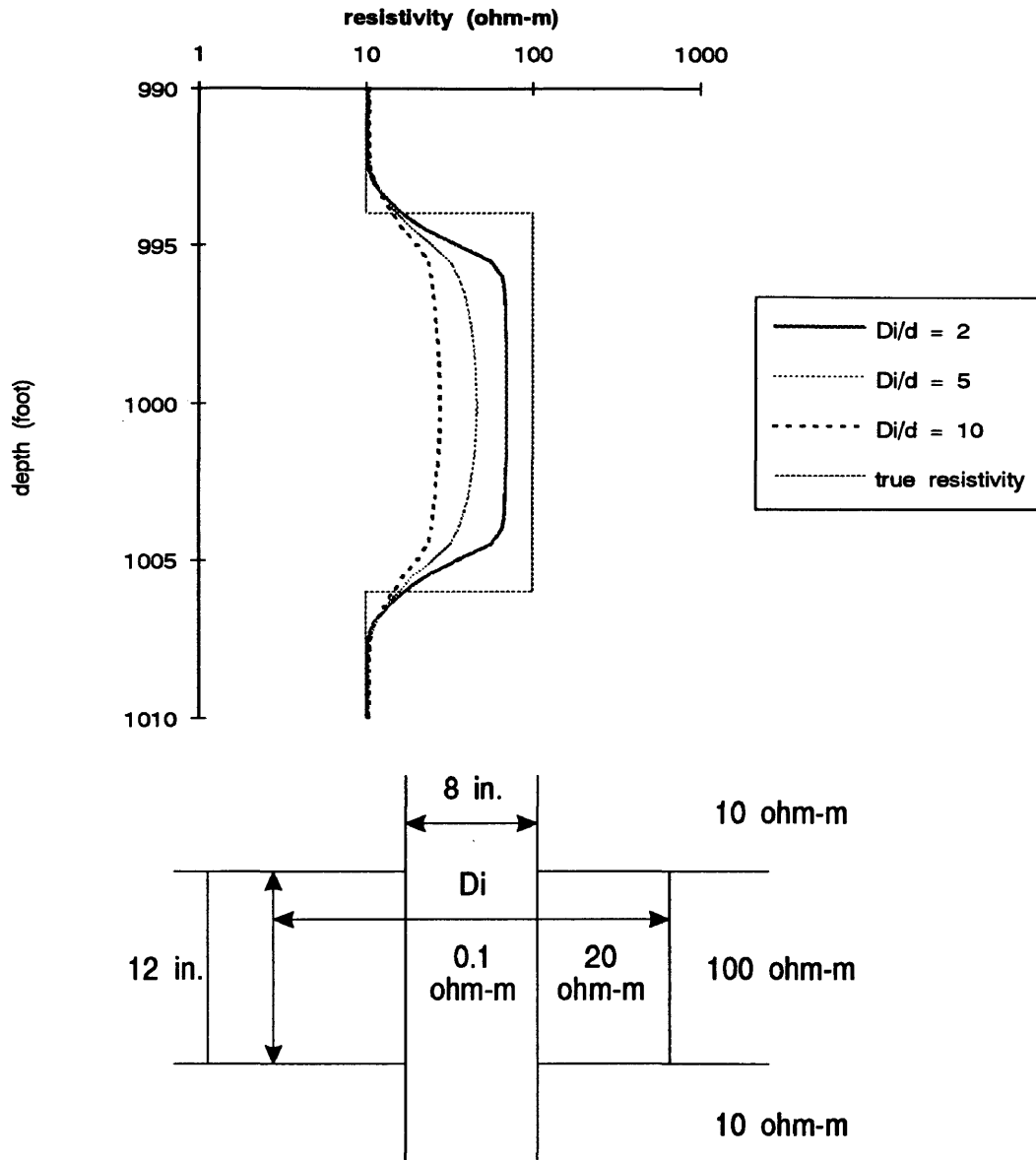


Figure B.7: Variation in D_i (Thick - Resistive)

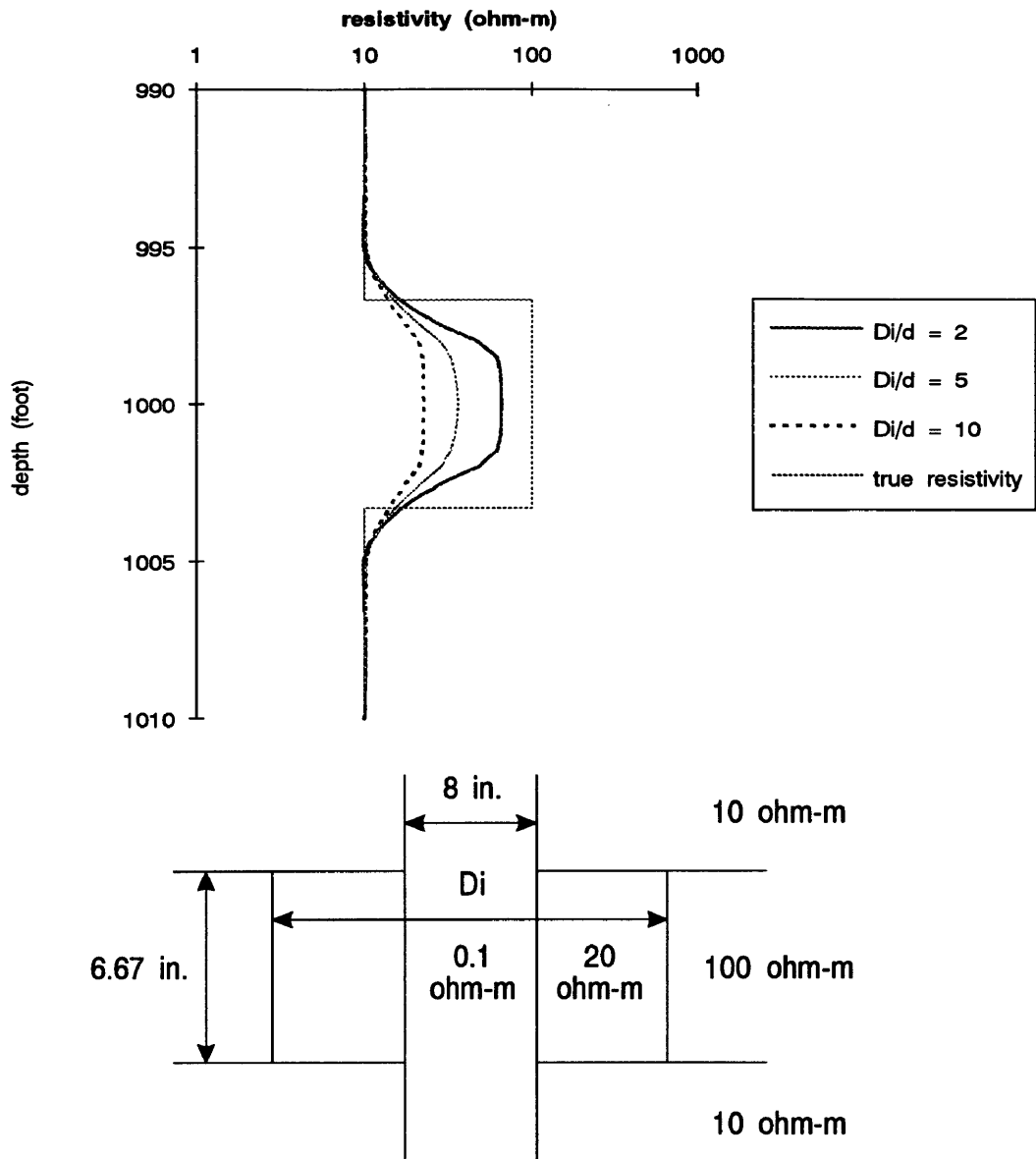


Figure B.8: Variation in D_i (Critically Thick - Resistive)

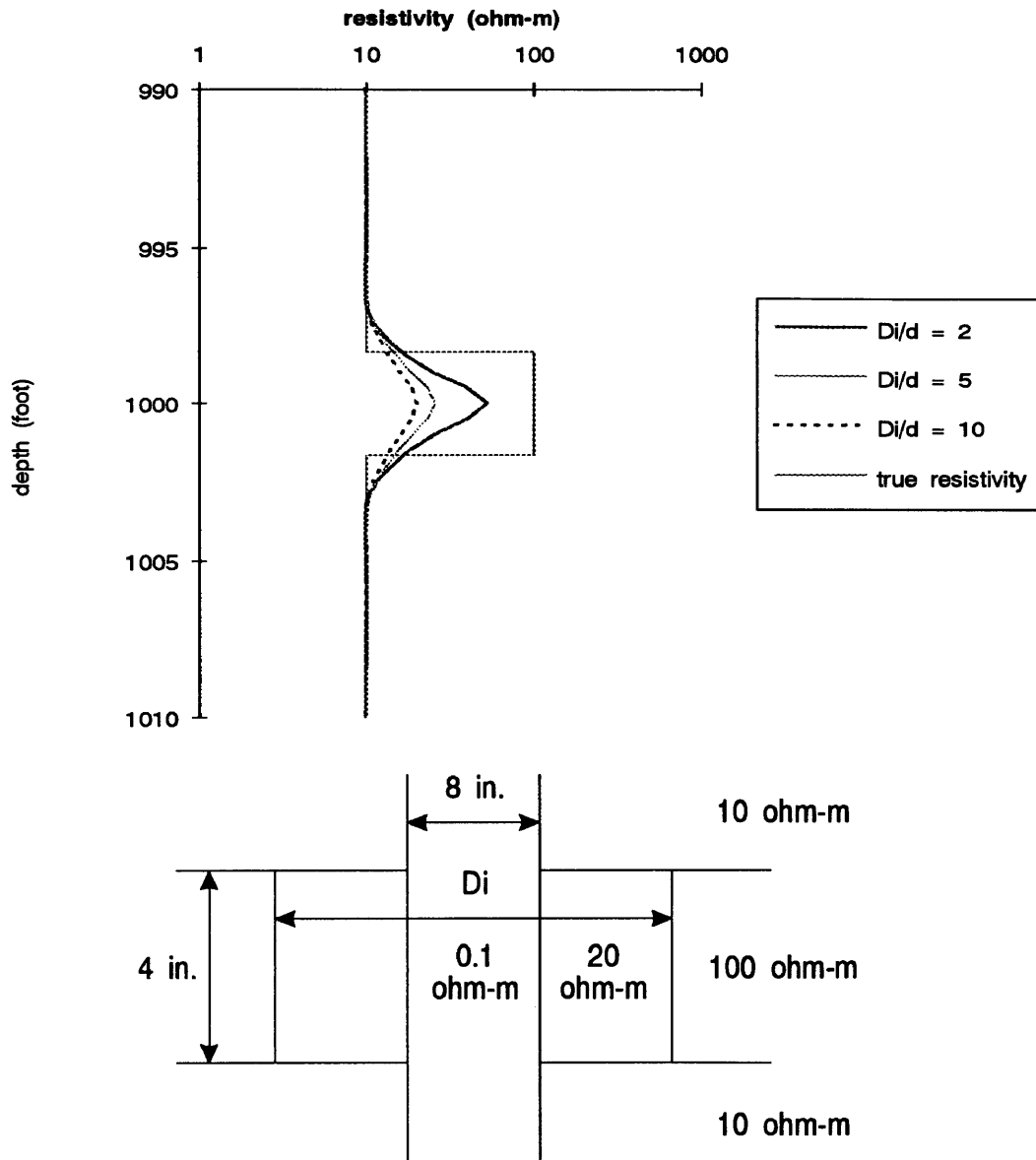


Figure B.9: Variation in D_i (Thin - Resistive)

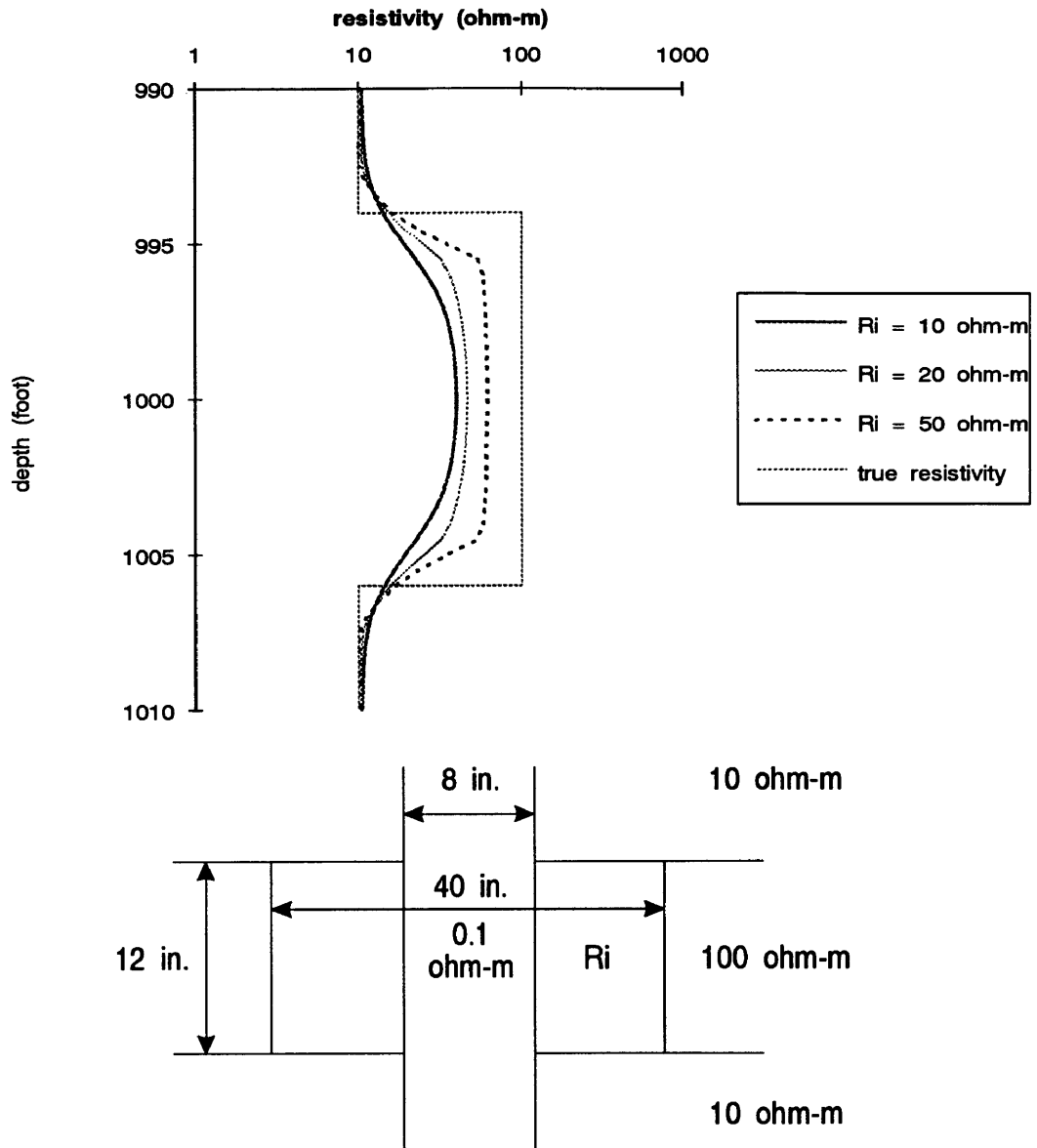


Figure B.10: Variation in R_i (Thick - Resistive)

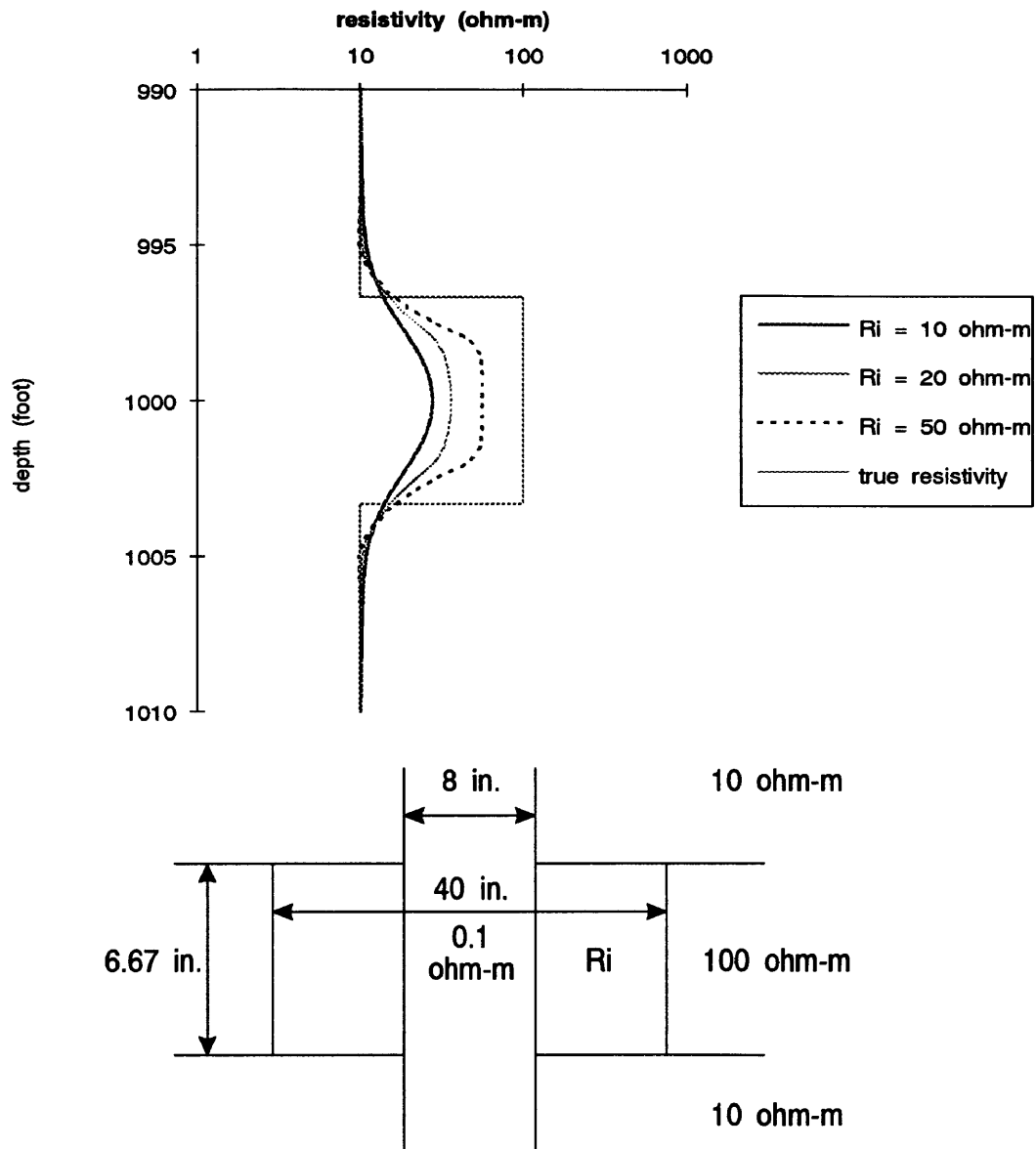


Figure B.11: Variation in R_i (Critically Thick - Resistive)

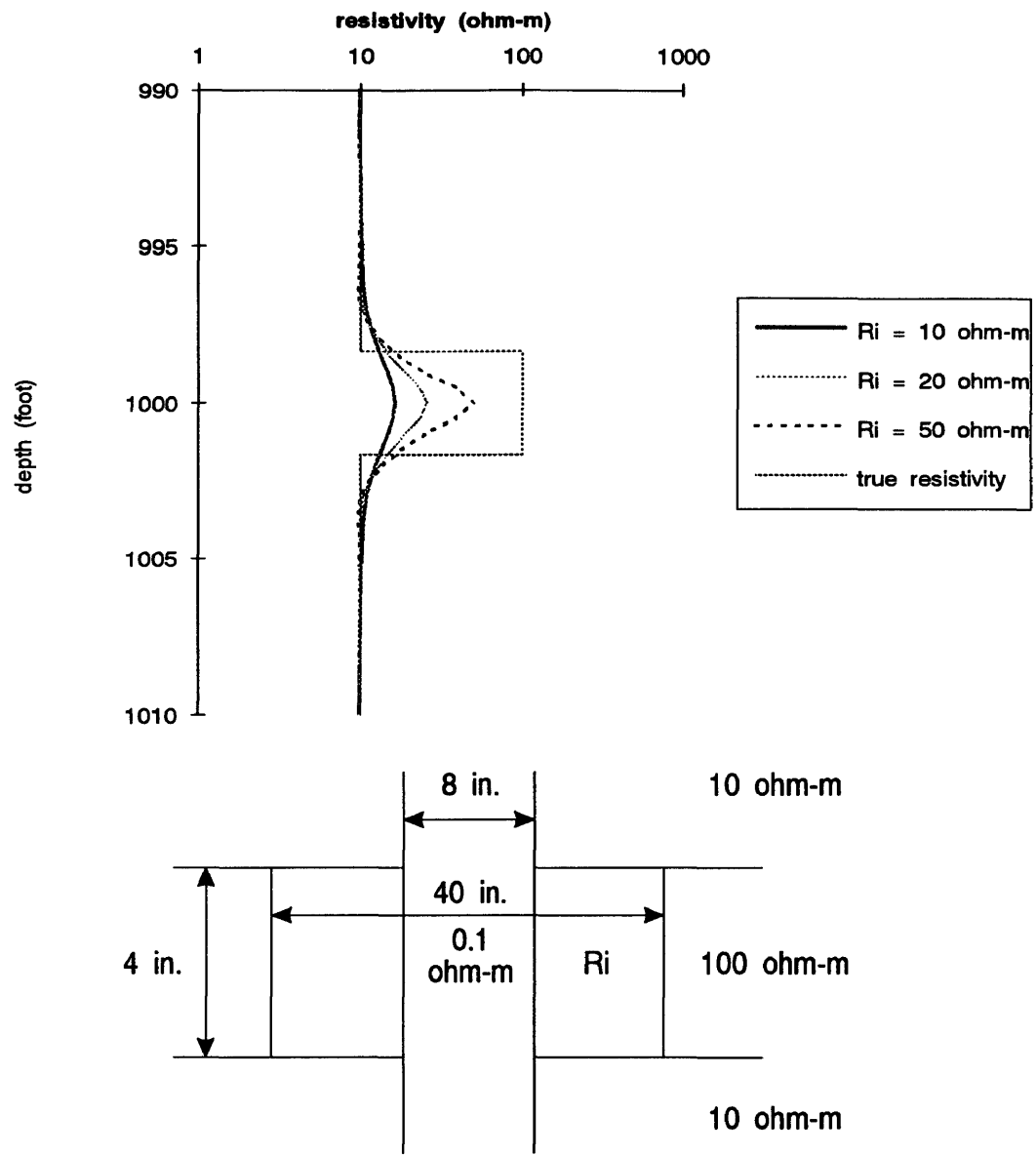


Figure B.12: Variation in R_i (Thin - Resistive)

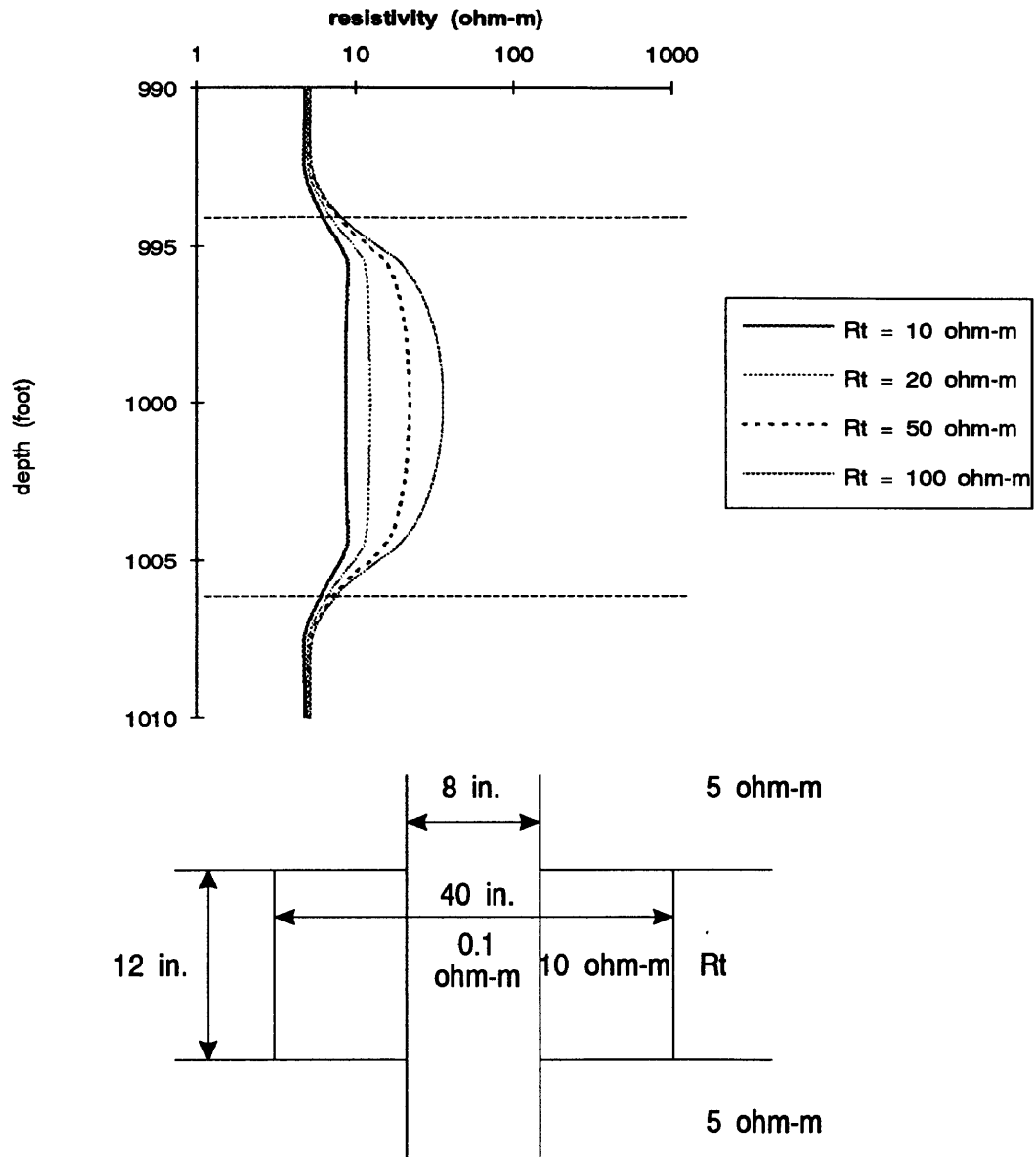


Figure B.13: Variation in R_t (Thick - Resistive)

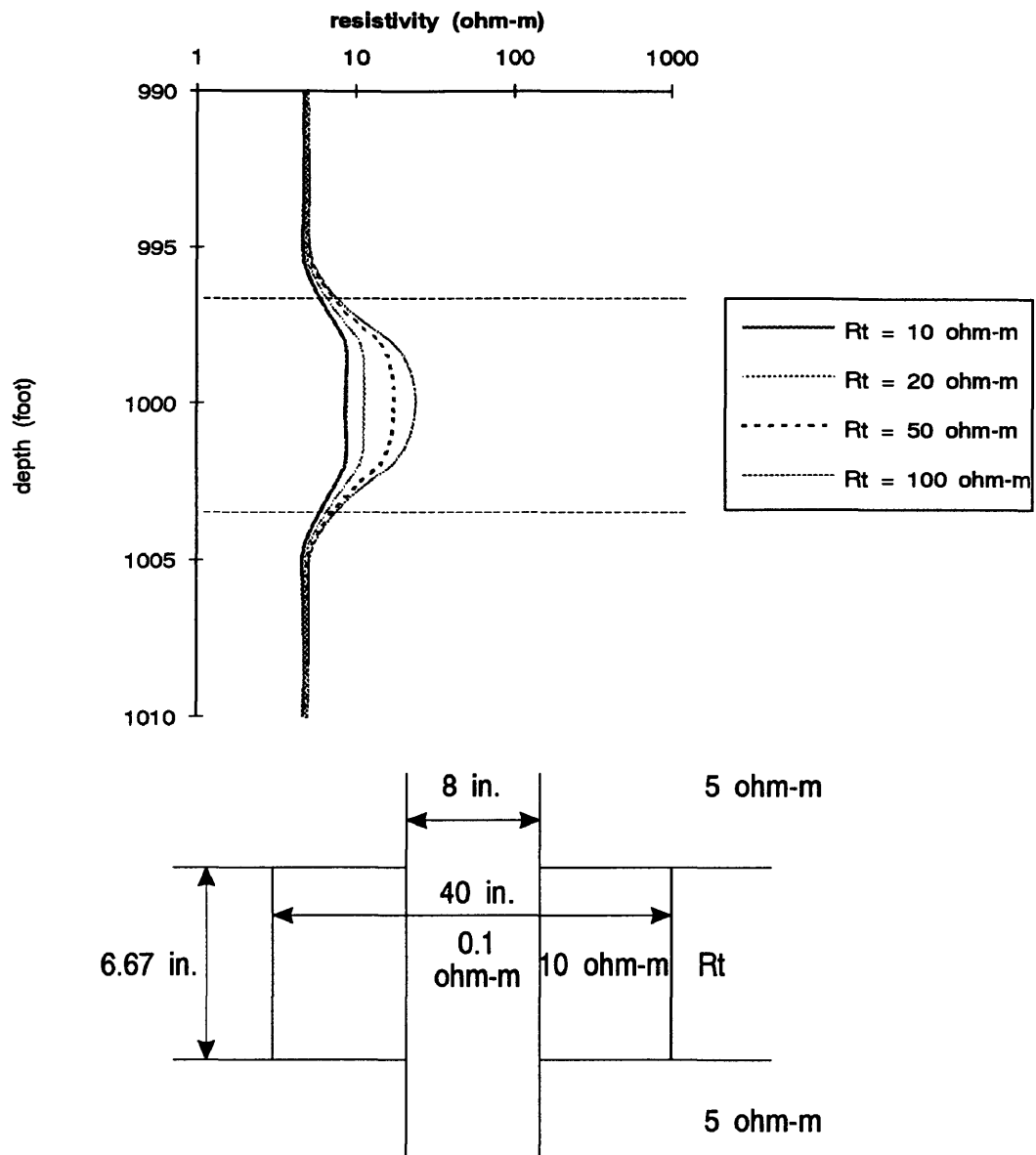


Figure B.14: Variation in R_t (Critically Thick - Resistive)

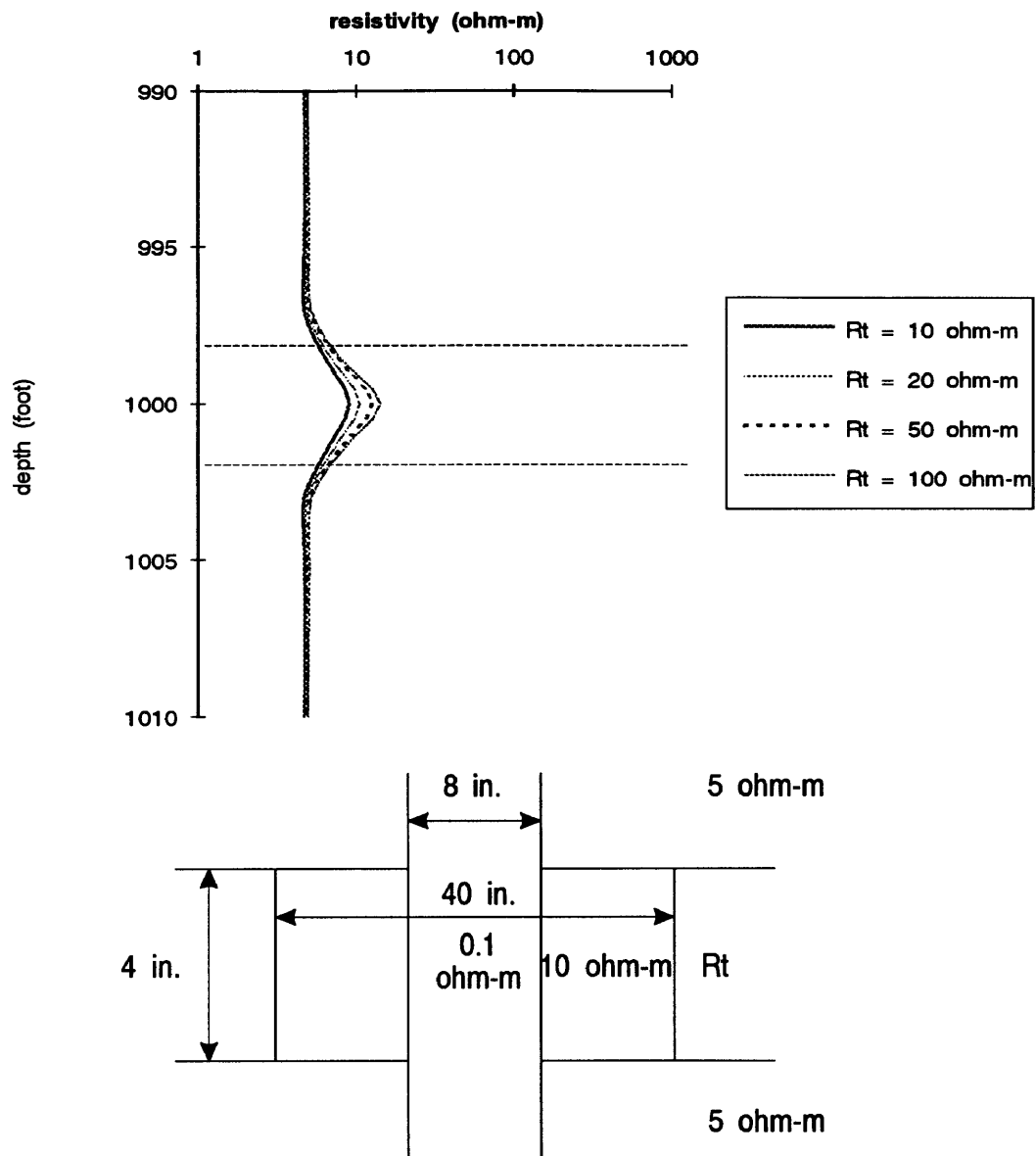


Figure B.15: Variation in R_t (Thin - Resistive)

Appendix C

Inversion of Laterolog 7

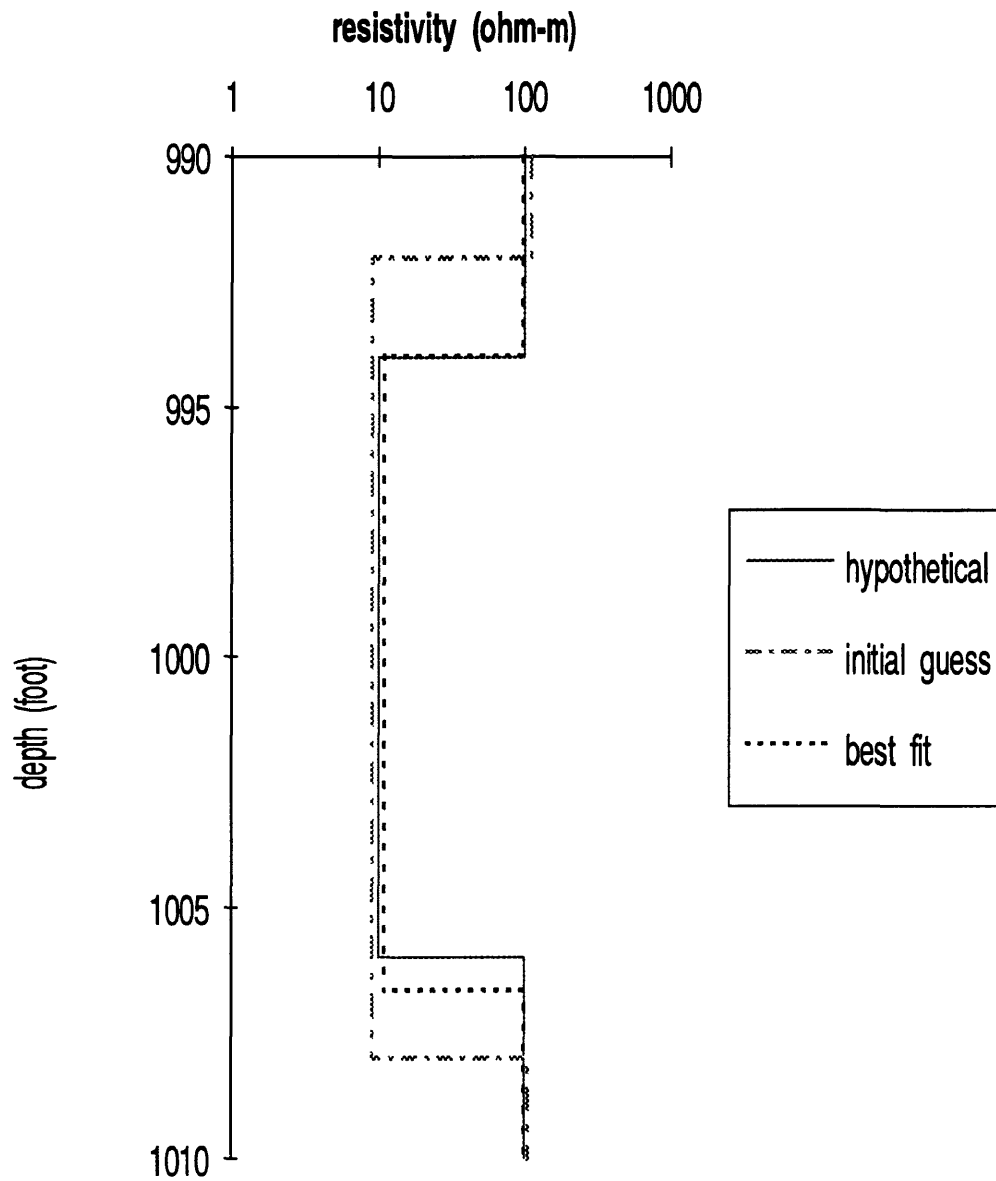


Figure C.1: Comparison of hypothetical earth model, initial guess earth model, and best fit earth model (Thick - Conductive Case)

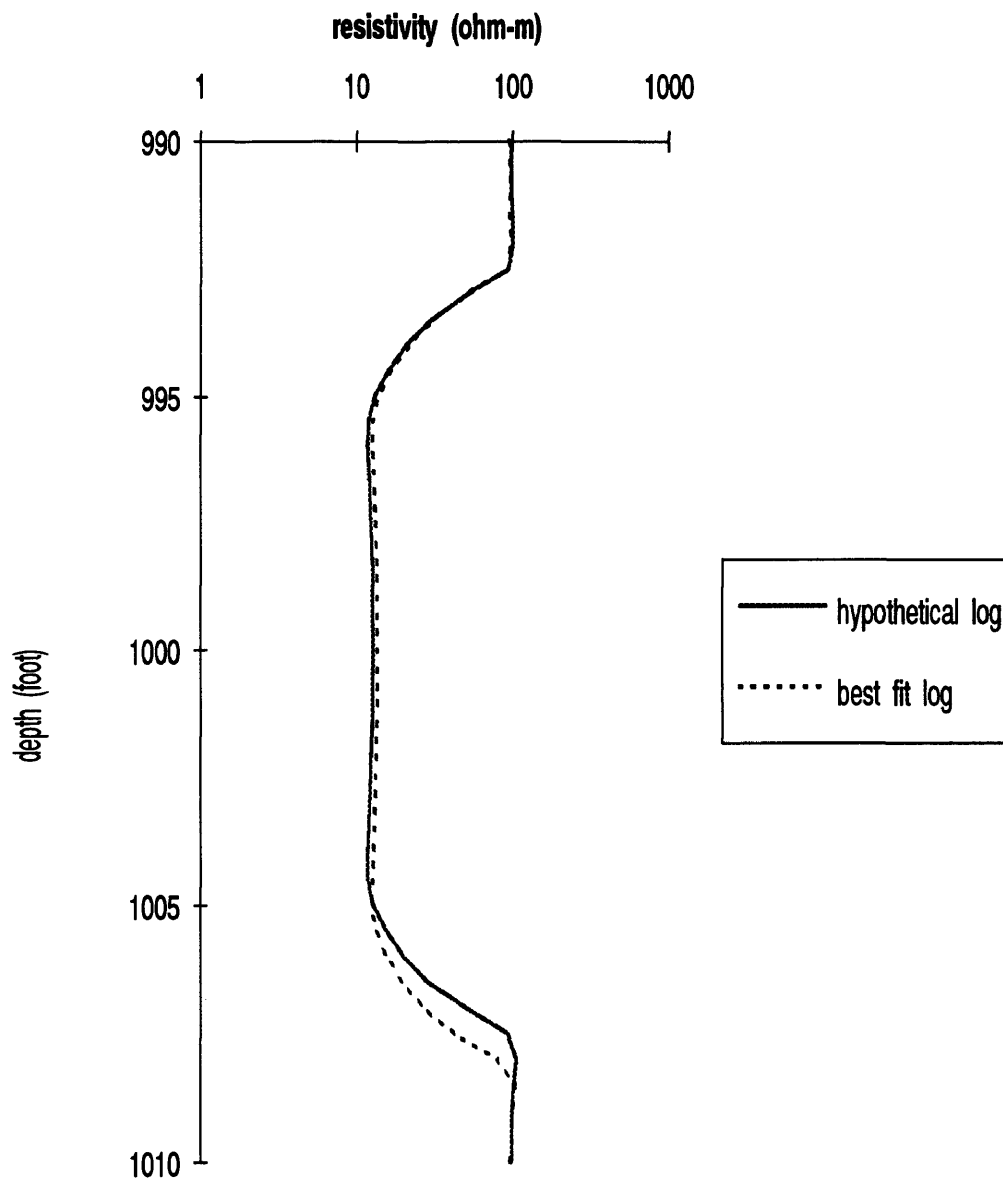


Figure C.2: Comparison of hypothetical log data with best fit log data (Thick - Conductive Case)

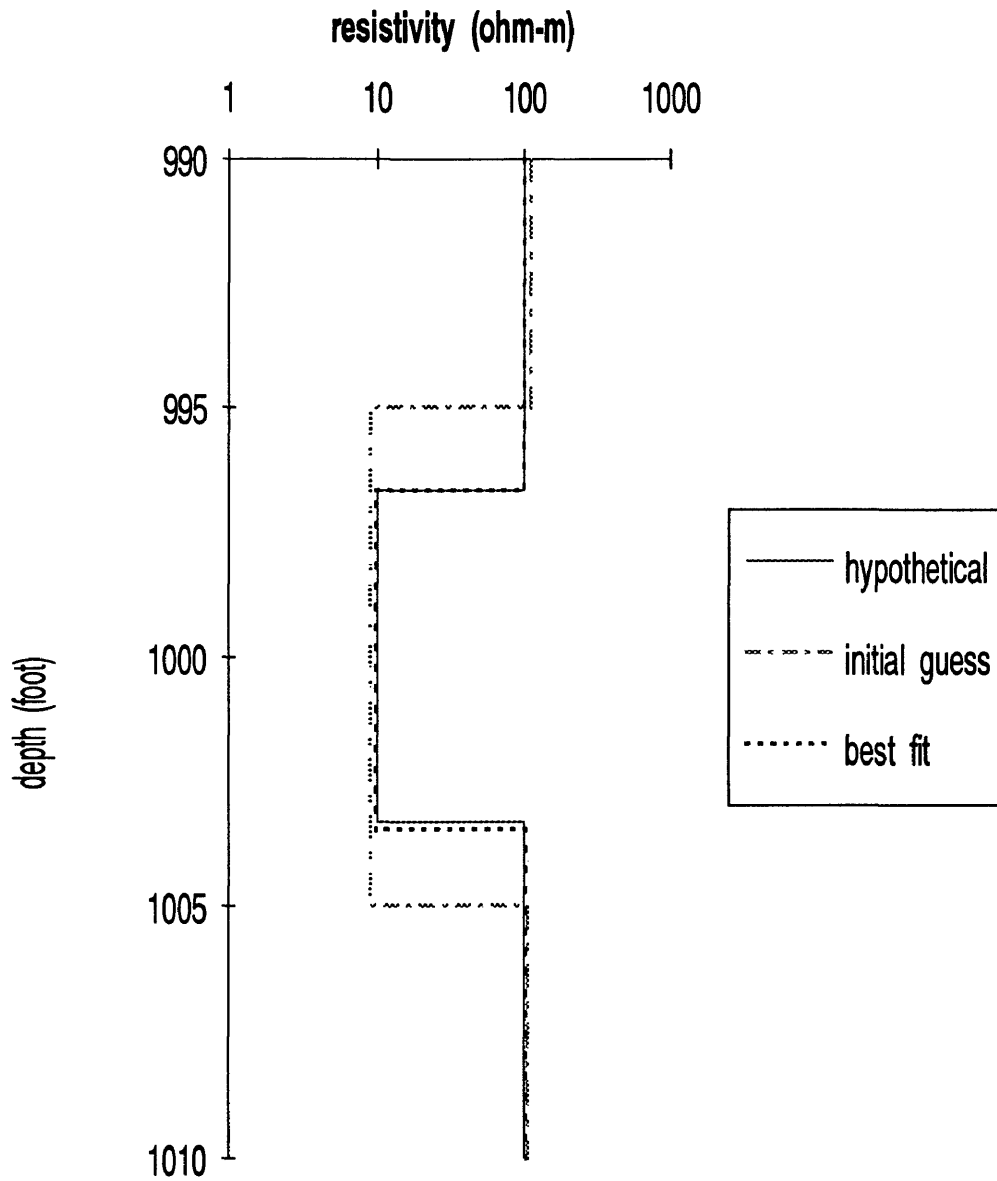


Figure C.3: Comparison of hypothetical earth model, initial guess earth model, and best fit earth model (Critically Thick - Conductive Case)

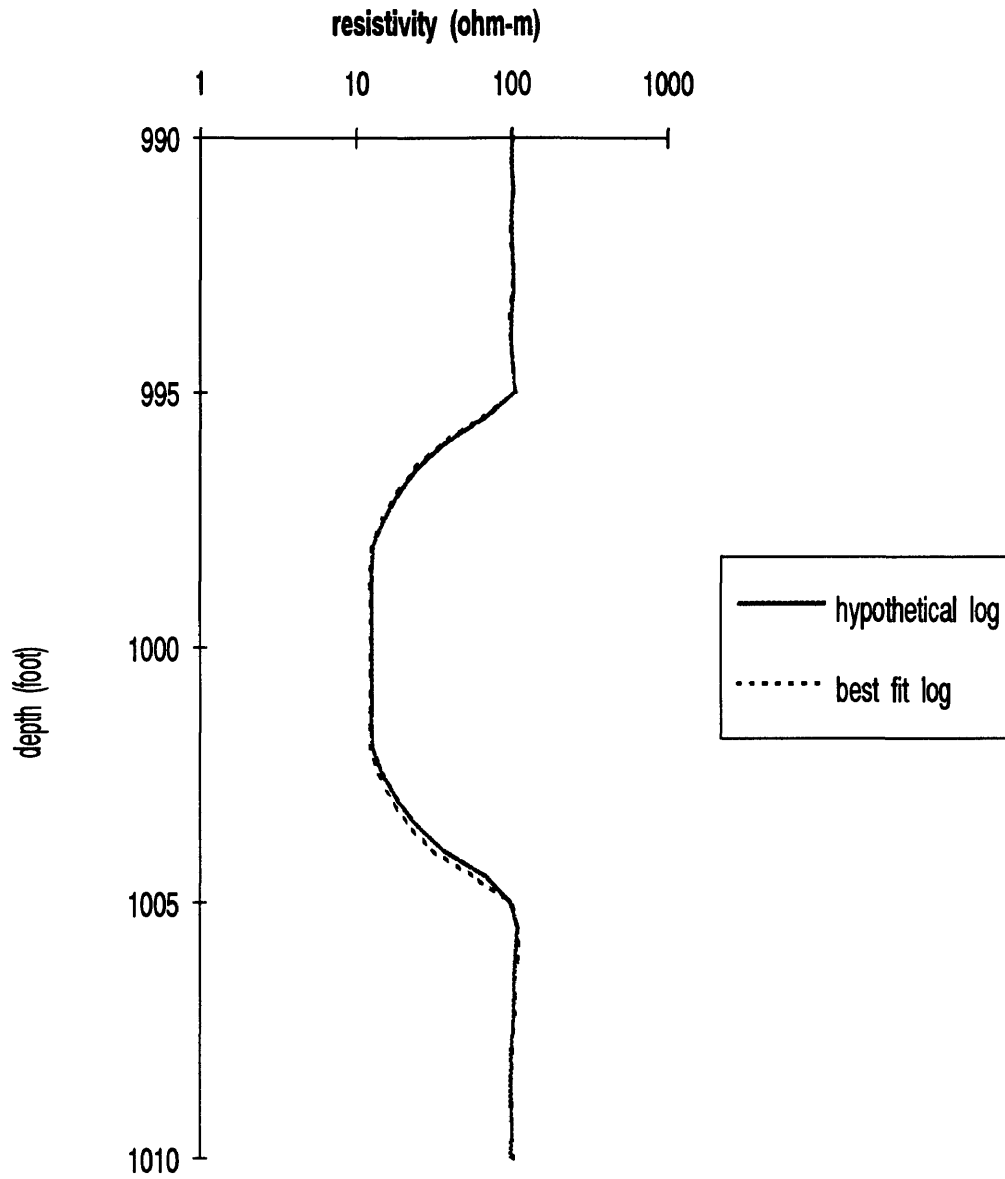


Figure C.4: Comparison of hypothetical log data with best fit log data (Critically Thick - Conductive Case)

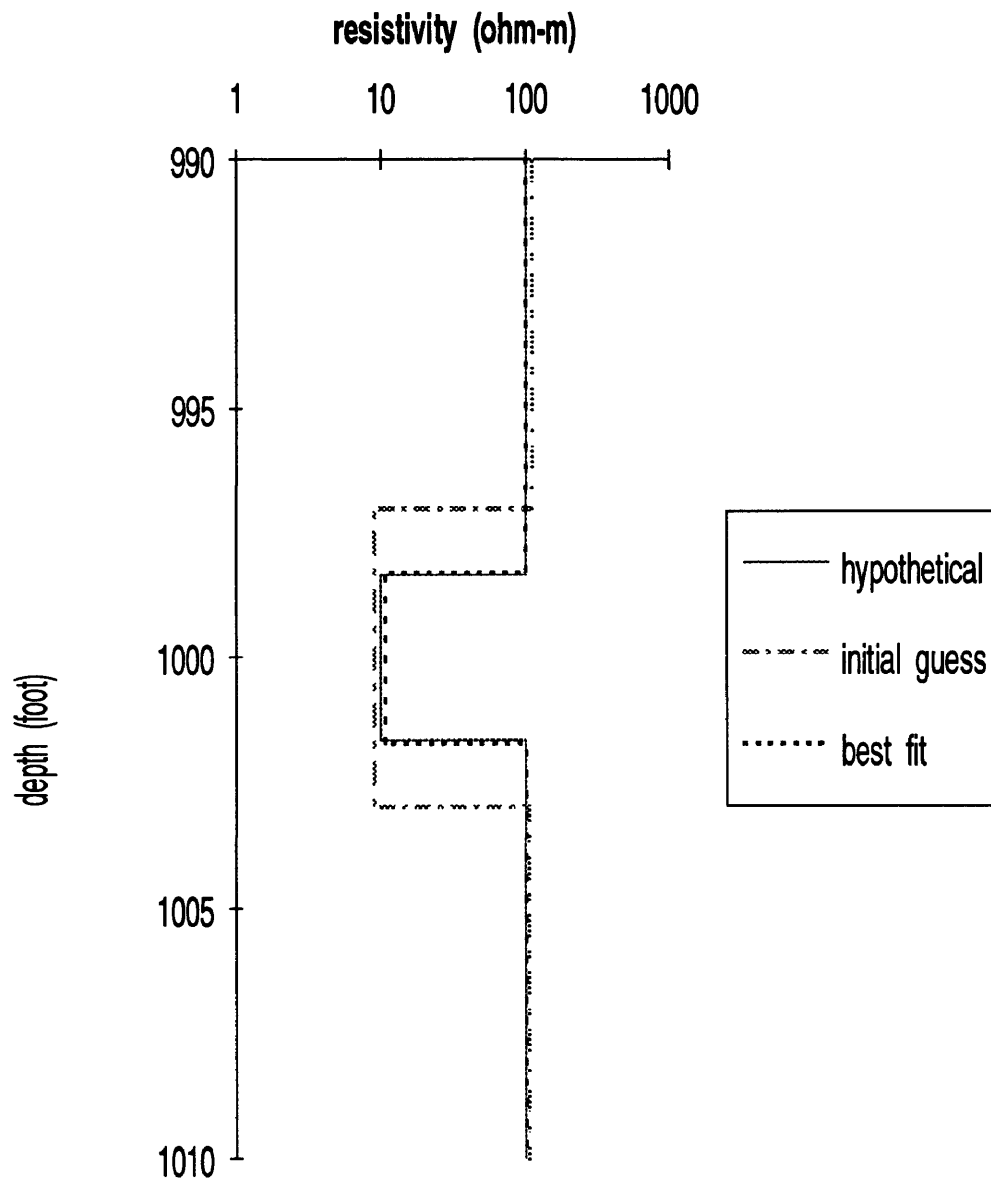


Figure C.5: Comparison of hypothetical earth model, initial guess earth model, and best fit earth model (Thin - Conductive Case)

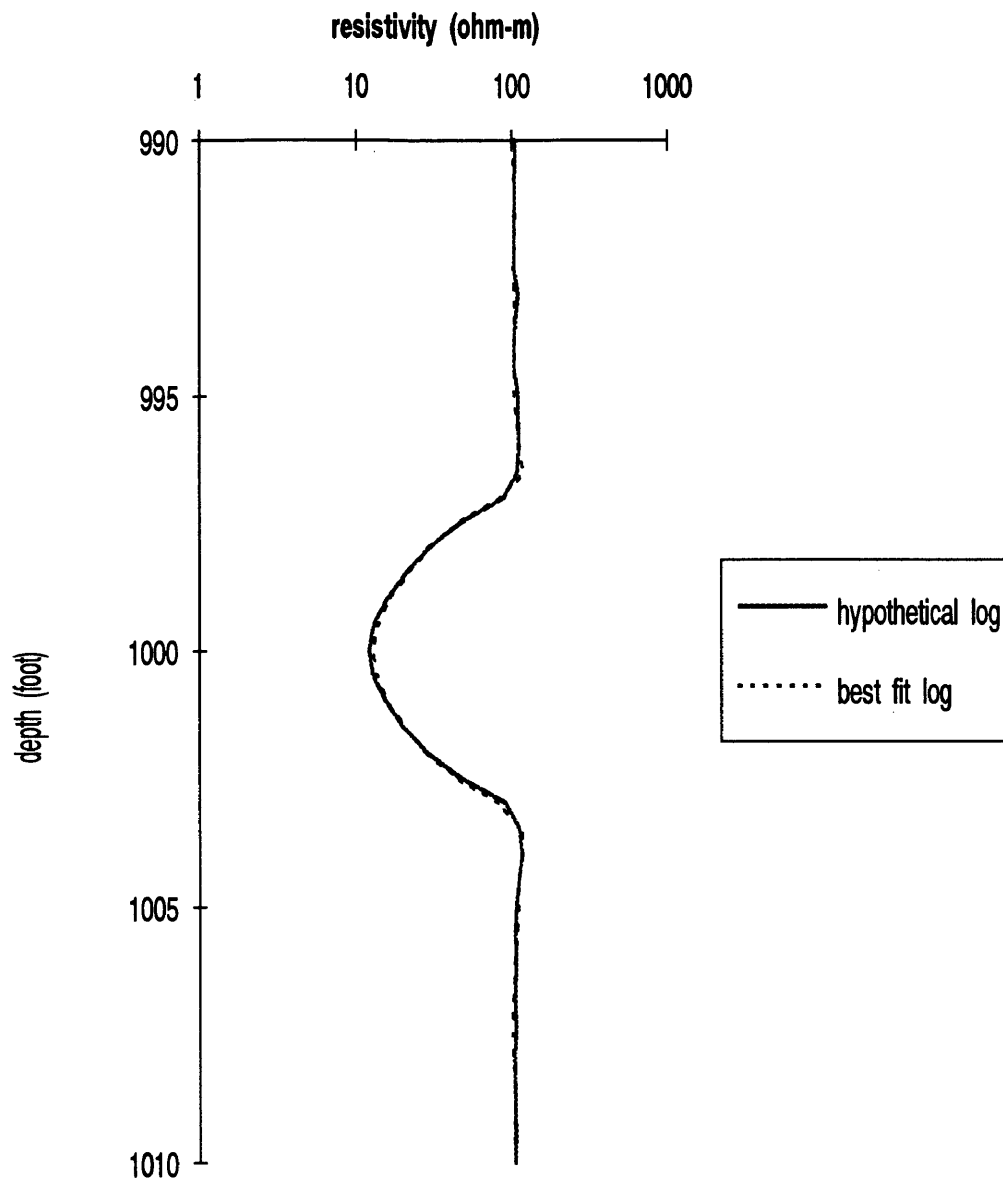


Figure C.6: Comparison of hypothetical log data with best fit log data (Thin - Conductive Case)

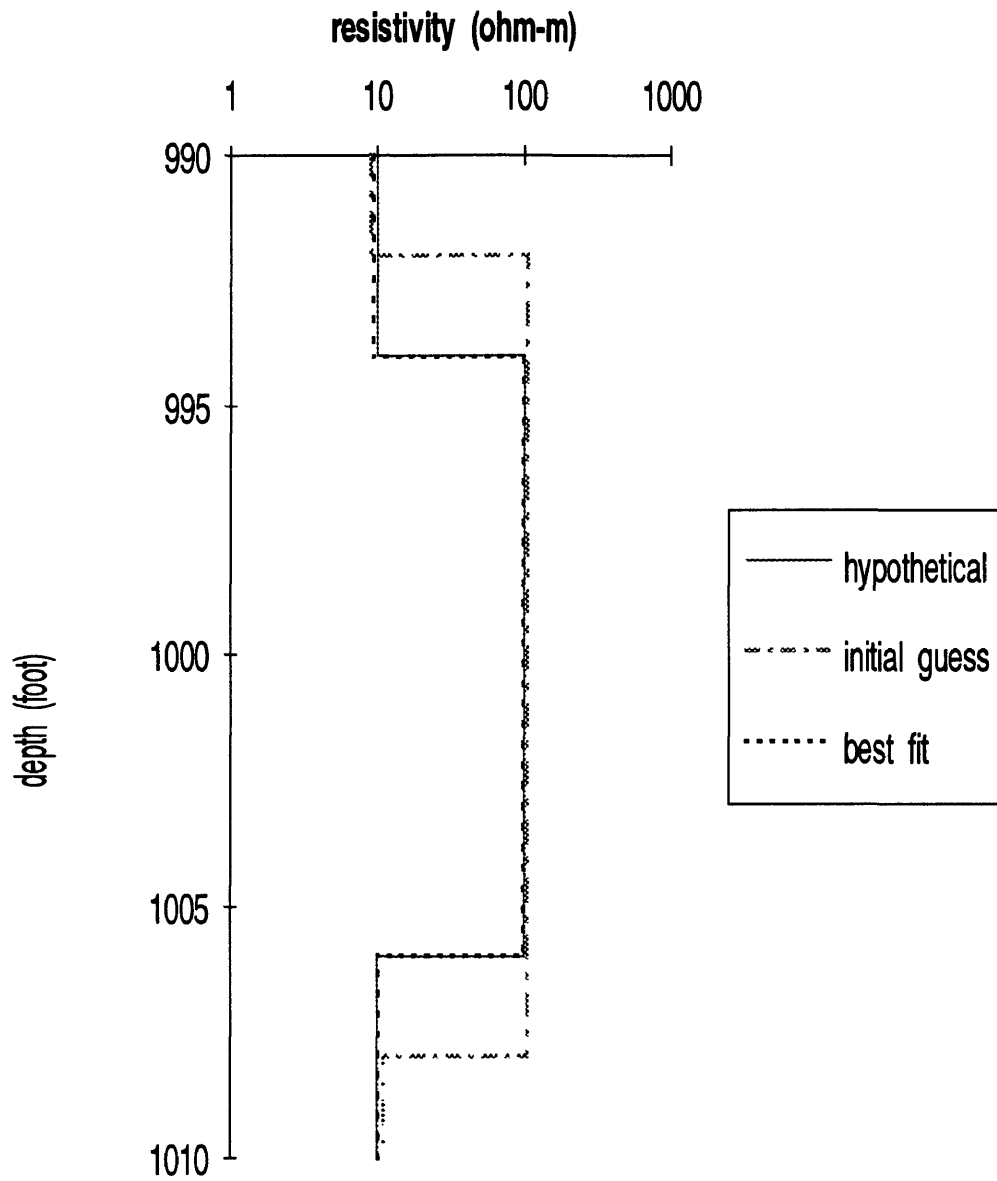


Figure C.7: Comparison of hypothetical earth model, initial guess earth model, and best fit earth model (Thick - Resistive Case)

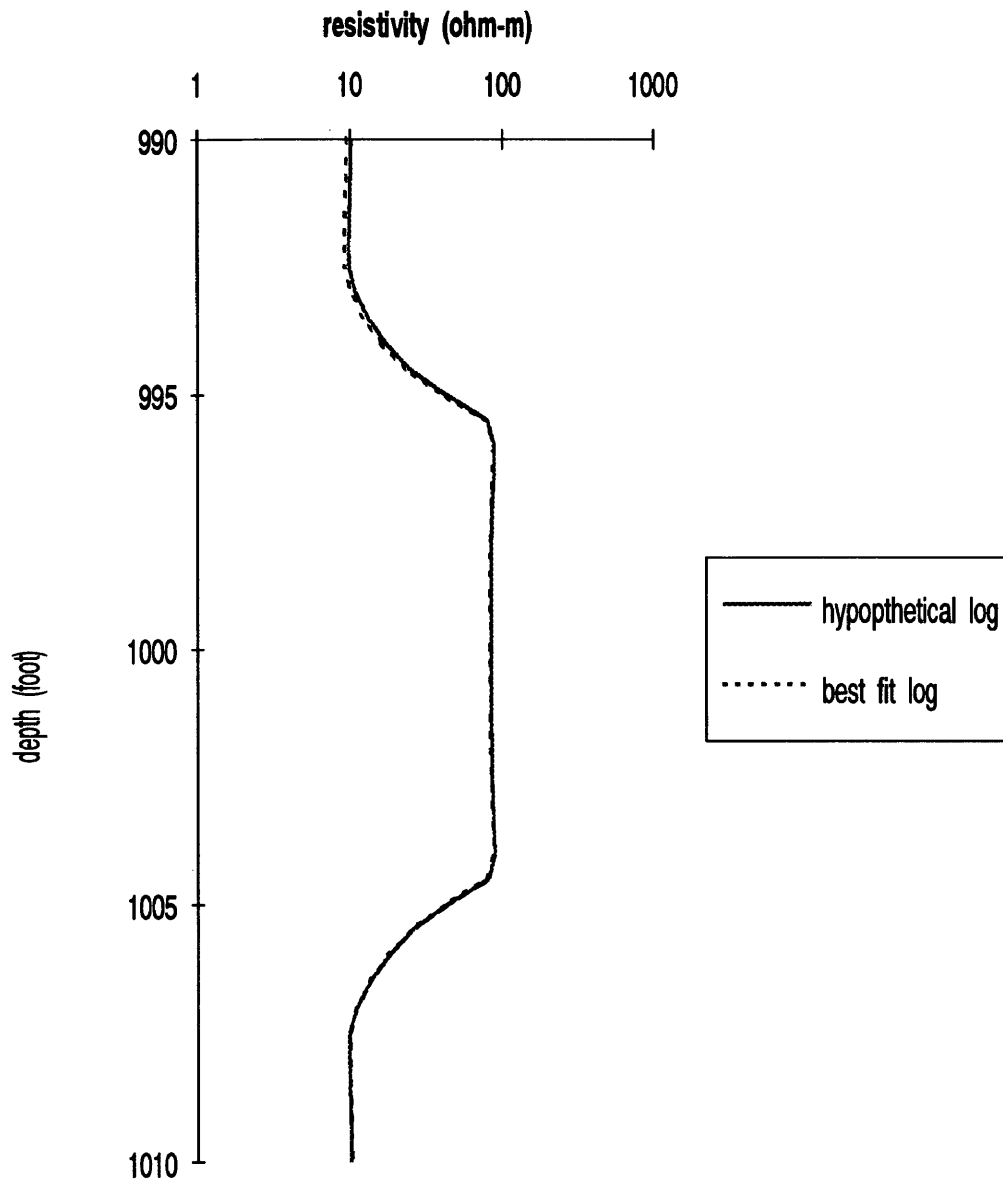


Figure C.8: Comparison of hypothetical log data with best fit log data (Thick - Resistive Case)

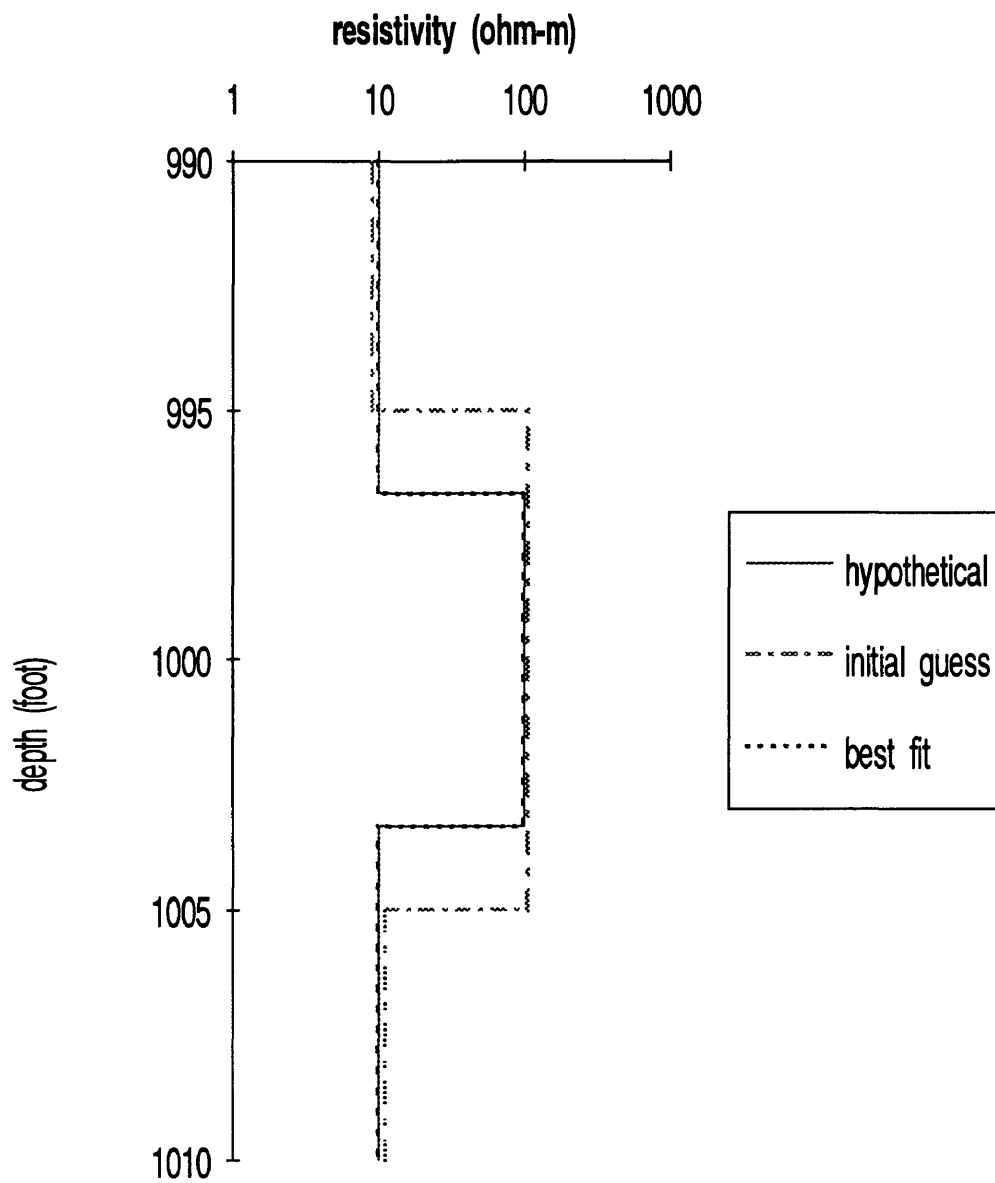


Figure C.9: Comparison of hypothetical earth model, initial guess earth model, and best fit earth model (Critically Thick - Resistive Case)

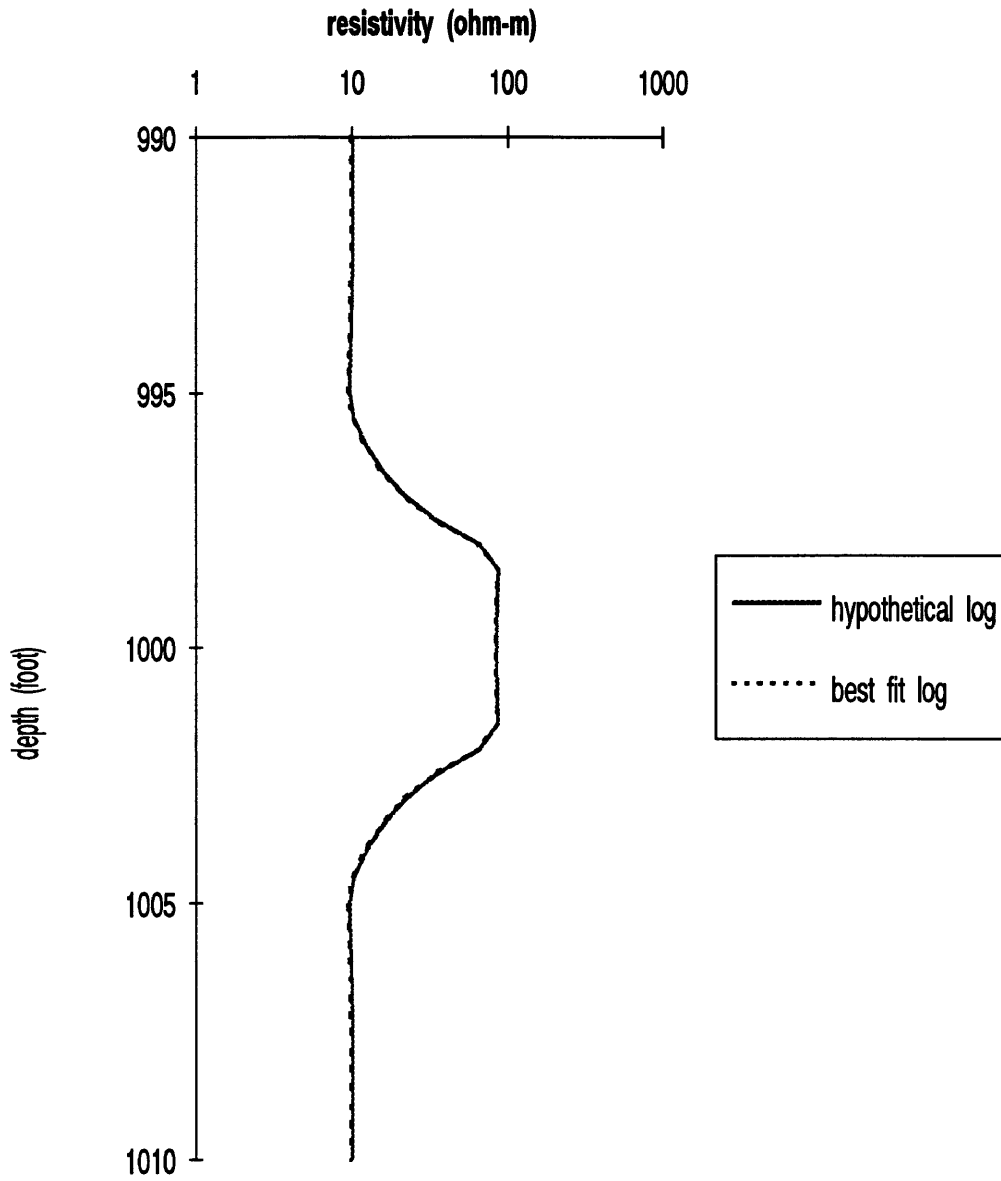


Figure C.10: Comparison of hypothetical log data with best fit log data (Critically Thick - Resistive Case)

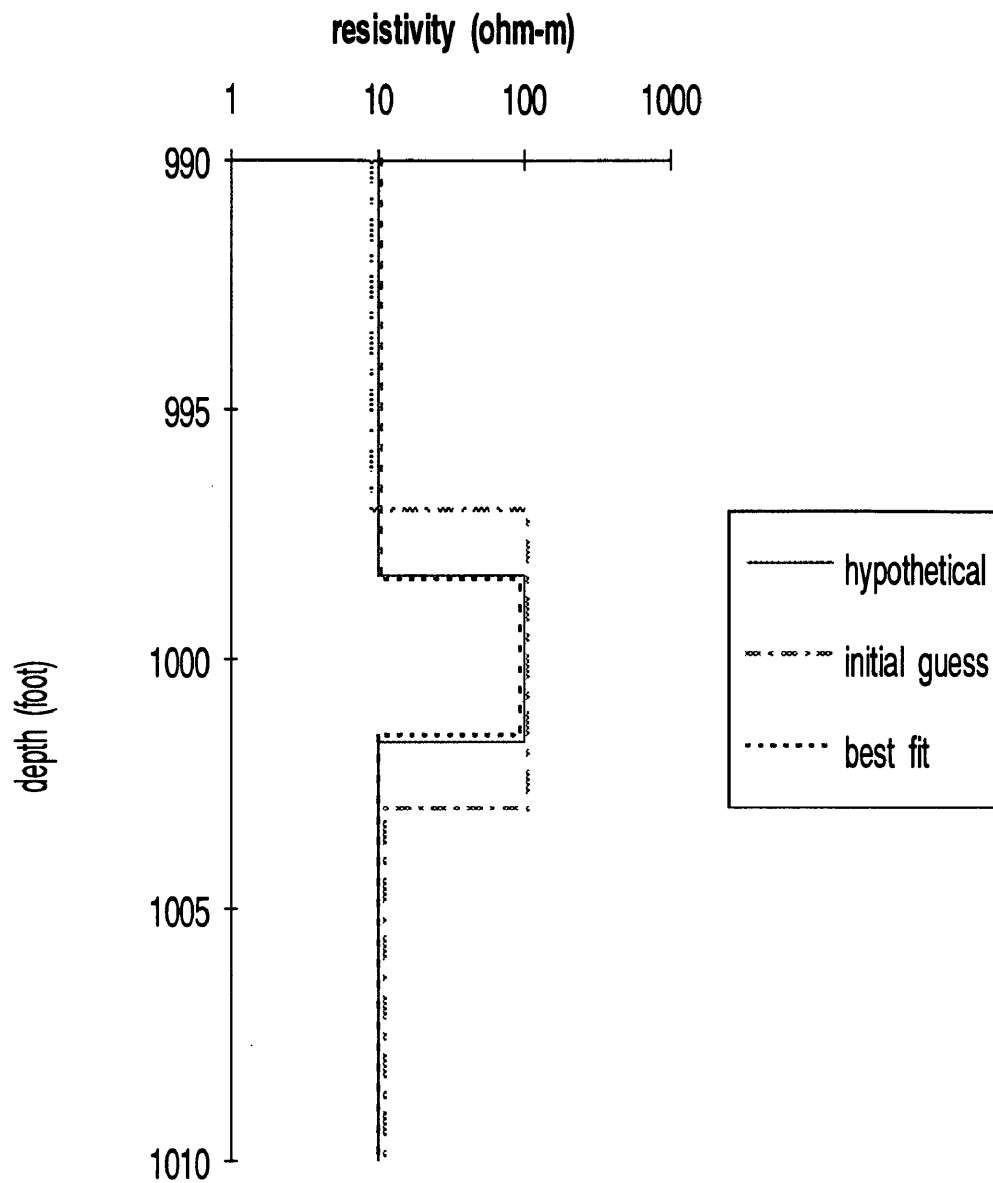


Figure C.11: Comparison of hypothetical earth model, initial guess earth model, and best fit earth model (Thin - Resistive Case)

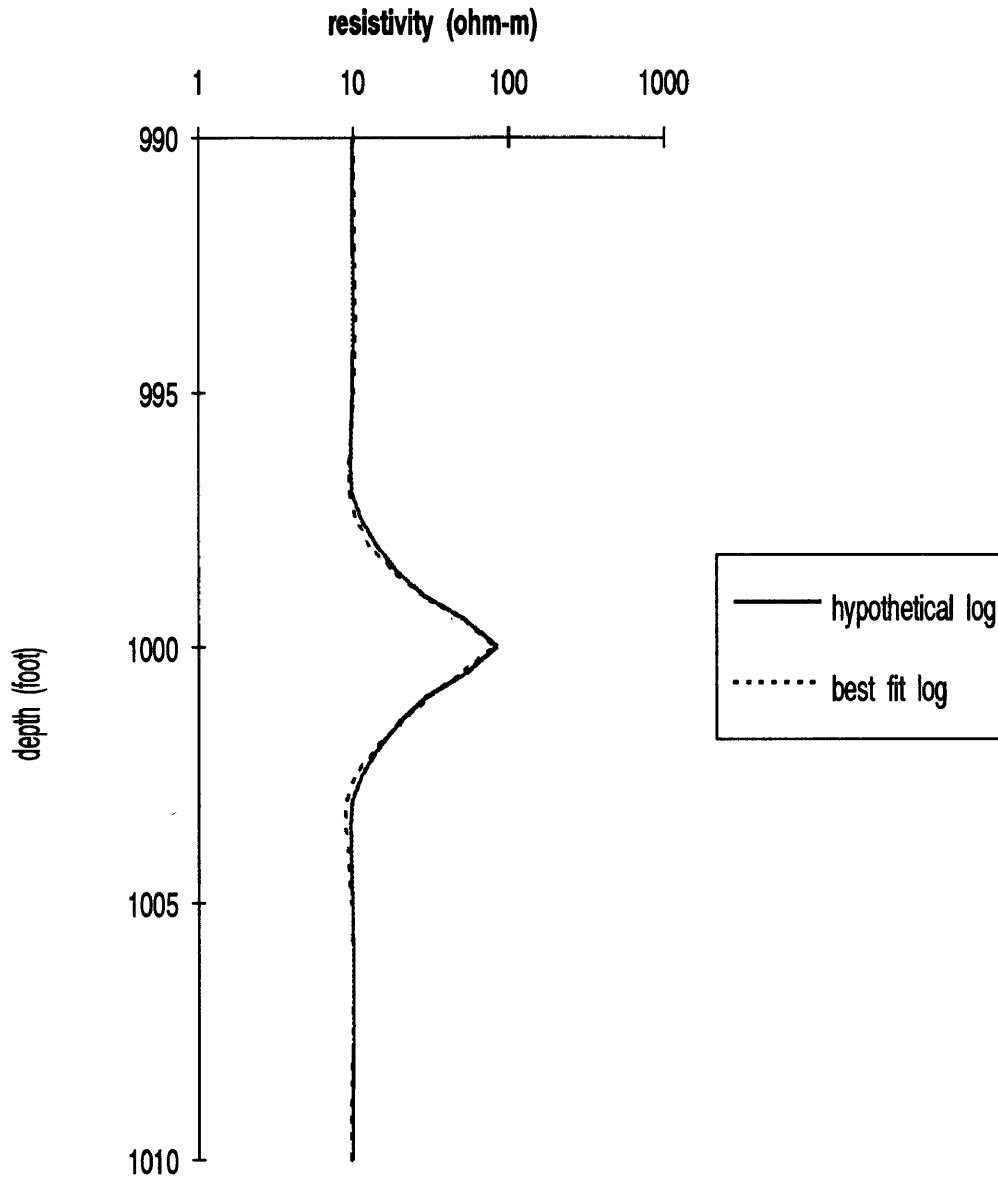


Figure C.12: Comparison of hypothetical log data with best fit log data (Thin - Resistive Case)